Dielectric characterizations, ex vivo experiments and multiphysics simulations of microwave hyperthermia of biological tissues

Guoyan Chen

HAL Id: tel-01373638

https://tel.archives-ouvertes.fr/tel-01373638

Submitted on 29 Sep 2016

A dissertation submitted for the degree of

Doctor of Philosophy (PhD)

of

Université Pierre et Marie Curie

in

École Doctorale de Sciences Mécanique, Acoustique, Électronique et Robotique de

Paris (SMAER)

Laboratory of Electronic and Electromagnetism (L2E)

presented by

CHEN Guoyan

Dielectric characterizations, ex vivo experiments and multiphysics simulations of microwave hyperthermia of biological tissues

---

Defended on September 28th, 2015

Evaluation committee:

Mrs. VIGNERAS Valérie	Professor at ENSCBP	Referee
Mr. SOBOT Robert	Professor at ENSEA, Université de Cergy-Pontoise	Referee
Mr. MOLINA Julien	Medical Doctor (MD), Ph.D.	Examiner
Mr. HOLE Stéphane	Professor at UPMC	Examiner
M. KOKABI Hamid	Professor at UPMC	Director
M. BELHADJ-TAHAR Nour-eddine	Associate Professor at UPMC	Co–Director

THÈSE de DOCTORAT

de

L'Université Pierre & Marie Curie

École Doctorale de Sciences Mécanique, Acoustique, Électronique et Robotique de Paris (SMAER)

Laboratoire d'Electronique et Electromagnétisme (L2E)

présentée par

CHEN Guoyan

Pour l'obtention du grade de

DOCTEUR EN ELECTRONIQUE

Caractérisations diélectriques, expérimentations ex vivo et simulations multiphysiques de l'hyperthermie micro-ondes des tissus biologiques

---

Soutenu le 28 Septembre 2015 devant le jury composé de :

Mme. VIGNERAS Valérie	Professeur à ENSCBP	Rapporteur
M. SOBOT Robert	Professeur à l'ENSEA, Université de Cergy-Pontoise	Rapporteur
M. MOLINA Julien	Praticien Hospitalier (PH), Ph.D.	Examinateur
M. HOLE Stéphane	Professeur à l'UPMC	Examinateur
M. KOKABI Hamid	Professeur à l'UPMC	Directeur
M. BELHADJ-TAHAR Nour-eddine	MCF (HDR) à l'UPMC	Co–Directeur

Acknowledgments

Many people helped and supported me during the realization of my PhD project.
I want to express my deepest gratitude to all of them.

To my supervisors professors Hamid KOKABI and Nour Eddine BELHADJ TAHAR
They taught me not only find the beauty of the scientific research, but also become a courage person in front of the difficulties. They inspire me the endless possibilities in the life.

To professor Georges Alquié and Madame Frédérique DESHOURS
Their suggestions and helps on my PhD project are very useful.

To all the colleagues in the laboratory L2E of UPMC
Sincerely thanks to them who ever give me their helps during these years.

To all the master internship students
Particularly to Alexendre LO, Isaak MOUNSI and Trong Phuoc HO
They ever work with me together and give me great helps.

To Mrs. Zhongxia QI and Mr. Shujia LI
Without their helps I cannot achieve my PhD.

My best thoughts and deepest thanks to my parents.
Without them I would certainly not be here and go further.

My last thought to the beautiful Paris, to the great France and to the beautiful China.

Abstract

Research and development of medical devices with various diagnostic and therapeutic applications have been driven and carried out because of the advances in electronic and electromagnetic domains. At present, no exiting microwave hyperthermia system can achieve using one single antenna or applicator for both diagnosis and therapeutic treatment at the same time. All of existing commercial microwave hyperthermia systems can just offer microwave hyperthermia treatment by using high microwave power.

In our project, a new microwave hyperemia system is designed and researched which could have both diagnostic and therapeutic functions. It means that using one applicator with a very low harmless microwave power level to do the diagnosis first. Measuring the dielectric properties of tissue allows examining if it is pathological or not. If the tissue has been found with pathological changes, then the thermal therapeutic treatment will be carried out on the pathological part by using the same applicator with higher microwave power.

In our research, microwave characterization of biological tissues on different temperatures with virtual line model of the open–ended coaxial probe method has been carried out. Ex vivo experiments on five different biological tissues with small microwave energy of 2.45GHz for microwave hyperthermia evaluation are carried out. Electromagnetic and thermal simulations by using COMSOL Multiphysics software with 2D axisymmetrical finite–element method for ex vivo microwave hyperthermia experiment are also designed, modeled and carried out. Trough the research, it seems certainly that there should be a flexible, feasible and suitable coaxial cable for both diagnosis and treatment of the minimally invasive therapy.

Table of contents

Introduction

Research and development of medical devices with various diagnostic and therapeutic applications have been driven and carried out because of the advances in electronic and electromagnetic domains. At present, microwave hyperthermia is considered as a minimally invasive therapy technique for the treatment of different disease, and it has been used and continuously researched in some medical fields: tumors, cardiac diseases, and women's endometrial diseases.

Microwave hyperthermia can be mainly operated by using several types of applicator: such as antenna, probe, or cable. According to the realistic requirements, the ideal model of microwave hyperthermia therapy should be operated in a very quick time with the proper power level to destroy pathological parts and not damage the surrounding normal tissues. The main advantages of microwave hyperthermia technique include: consistently higher treatment temperature, faster procedure, larger irradiated volume, improved convection profile, modified power level according to the real-time requirement, and possible uses for diagnosis.

The biological fundamental concepts for the cells and tissues are important for researches on microwave hyperthermia which is one type of thermal therapy. The major objective of thermal therapy based on transferring thermal energy into or out of human body is to efficiently treat pathological tissues without damaging normal tissues. For microwave hyperthermia therapy, the physical prosperities of treated biological tissues are very important such as dielectric permittivity and electrical conductivity. Dielectric characterizations of biological tissues (muscles and livers) in microwave frequencies as a function of temperature are being researched. Two methods of virtual line model: open–ended semi–rigid coaxial probe and flexible coaxial cable are used for the dielectric characterizations.

Microwave hyperthermia instrumentation system with a maximum output power level of 10 Watts at 2.45GHz allows doing the ex vivo tests and evaluating the microwave hyperthermia therapy. Five biological tissue samples: pork, beef, chicken (muscle), pork and calf's livers (liver) were tested. Two coaxial applicators: RG393 and Warrior cables are used for the ex vivo hyperthermia experiments. The aim temperature of microwave hyperthermia is minimum 40°C. Above 40°C on the tissue, it may have irreversible changes. After comparing the experimental results of different tissues and various experimental conditions, more detailed information can be obtained. Through the experiments, the existing inadequacies of current system can also be improved or studied for optimization.

Simulations for ex vivo microwave hyperthermia instrumentation which uses the open ended coaxial cable as the applicator for different biological tissues with a thickness of a few millimeters have been carried out by using COMSOL Multiphysics with microwave heating model. By comparing the experimental and simulated results, further researches can be carried out to satisfy the requirements of microwave hyperthermia therapy.

The final aim of our study is to show that the pathological biological tissue can be examined for diagnosis and heated or irradiated for hyperthermia by using a single microwave applicator. Microwave hyperthermia therapy as a minimally invasive technique, could make patients suffer less pain and reduce the risks of the surgical operation, and may become the better choice for the patients in the future.

Chapter 1
Biological fundamental concepts and electromagnetic hyperthermia

1.1 Biological fundamental concepts

1.1.1 Biological cells

All living organisms are made of cells. The smallest living unit of structure and function of all the organisms in the human body is the cell. Each human being contain about 100 trillion (10^{14}) cells. [1] These cells grouping together have certain characteristics which are important for the proper, essential, and basic functioning of tissues, organs, and human body systems. Cells, which are commonly several microns in diameter, are distinguished by their sizes and shapes which can be related to their specific functions. For example, the length of the muscle cells may be a few millimeters and that of the nerve cells (axons) may be over a meter.
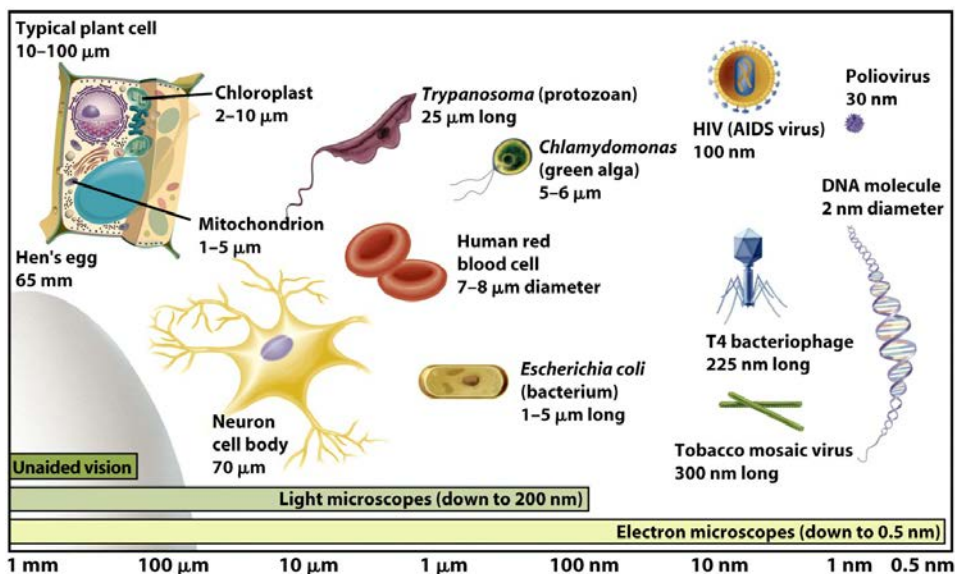
Figure 1.1: Typical planet cell [2]

The entire characteristics of a cell mainly include: a thin membrane or plasma which contains or holds the cell together called cytoplasm which is like a gel material within the membrane and usually a nucleus. In fact, not all cells have a nucleus, but some muscle cells have several nucleus and red blood cells have no nucleus. Within the cytoplasm, there are several types of specialized subunits called organelles which perform certain specific metabolic functions.
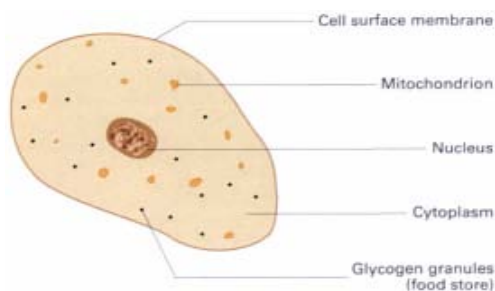
Figure 1.2: A typical animal cell [3]

The cell membrane separates biological cells into two parts: a highly specific intracellular chemical content and nonspecific extracellular solution. The membrane selectively controls the transport of chemical species into and out of the cell. [4]
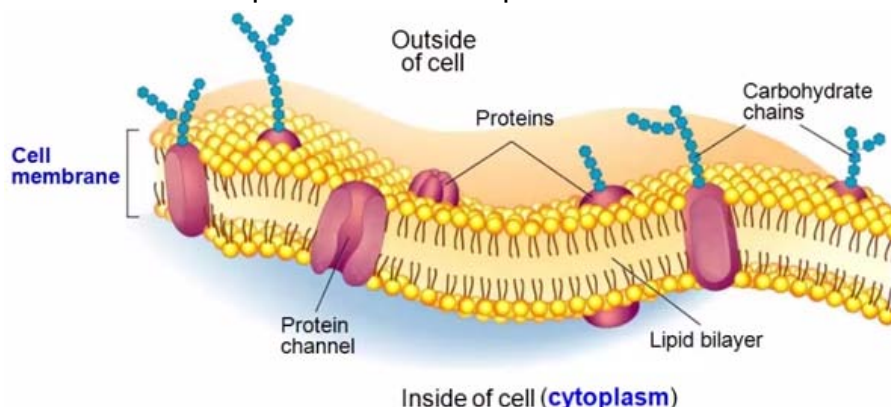
Figure 1.3: Cell membrane structure [5]

The human's cells have complex structures which are rich with complicated charged surfaces. When they are exposed to force, they can change their orientation and movement because of being stuffed with high charged atoms and molecules. The cell nucleus controls the cell activities and contains most of the human body's hereditary information in the chromosomes. Genetic materials are stored in strands along the chromosomes. Genes are usually composed of double stranded DNA (Deoxyribonucleic acid) which controls the most cellular activities in the form of twisted helix. A cell reproduces itself by using a blueprint stored in genetic materials in its nucleus.
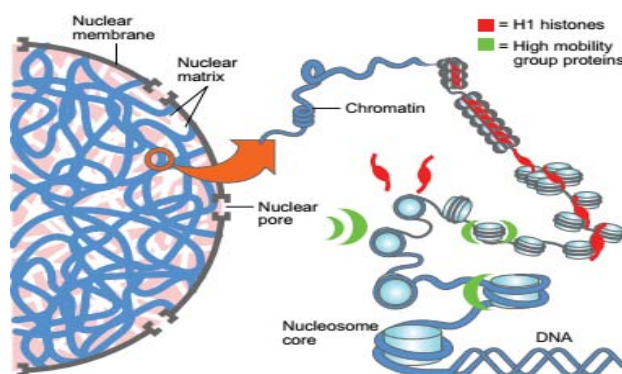
Figure 1.4: Organization of DNA [6]

Cells grow, change, and reproduce in a continuous cycle process which is referred to mitosis. Chromosomes in a cell nucleus are duplicated into two identical sets of chromosomes with its own nucleus. While the cells which do not have the nuclei like human red blood cells cannot divide.

1.1.2 Biological tissues
Similar cells from the same origin are grouped together and combined with their intercellular materials to form biological tissues. Organs are then formed by the functional grouping together of multiple tissues. There are four basic types of biological tissues: epithelial, connective, muscular, and nervous.

- Epithelial tissues such as the surface of the skin, the airways, and the reproductive tract are made up of cells in single or multilayered membranes. They serve as protective layers to perform function of protection and regulation of secretion and absorption of material in body organs and systems.

- Connective tissues consist of dispersed cells which typically lack intercellular contact and nonliving materials which are called an extracellular matrix such as fibers and gelatinous substances. It gives shape to human organs and holds them in place. Typical examples of connective tissue are blood and bone.

- Muscular tissues have several functions such as production of force and motion (either movement within internal organs); propulsion of blood through vessels, movement of food or body secretions through tracts and thermoregulation. Muscular tissue has three distinct categories: skeletal muscle (controlled voluntarily) found attached to skeletal elements and cartilage providing for important movement; visceral or smooth muscle (controlled involuntarily) found in the inner linings of organ; and cardiac muscle (controlled involuntarily) found in myocardium of the heart, allowing it to contract and pump blood throughout an organism. [7] [8]

- Nervous tissue is the main component of the two parts of the nervous system; the brain and spinal cord of the central nervous system (CNS), and the branching peripheral nerves of the peripheral nervous system (PNS). [9] Nervous tissues are composed of two main types of cells: nerve cells and glial cells which provide communication with other types of tissues in order to sense, control and govern human body activities. Nerve cells receive and transmit impulses. Glial cells surround neurons to support, protect, separate and nourish them.

1.1.3 Neoplasm, tumor and cancer

Neoplasm is an abnormal growth of tissue having four groups of: benign, in situ, malignant, and neoplasm of uncertain or unknown behavior.[10][11][12] When the abnormal growth of tissue forms a mass or appears enlarged in size, it is commonly referred to as a tumor (figure 1.5). Some neoplasms do not form a tumor. Cancer, also known as a malignant tumor or malignant neoplasm is a group of diseases involving uncontrolled abnormal cell growth with the potential to invade nearby parts of the body or spread to other parts of the body. [13][14] Not every change in the body's tissues will lead to a cancer except the pathological tissues which are not cured.
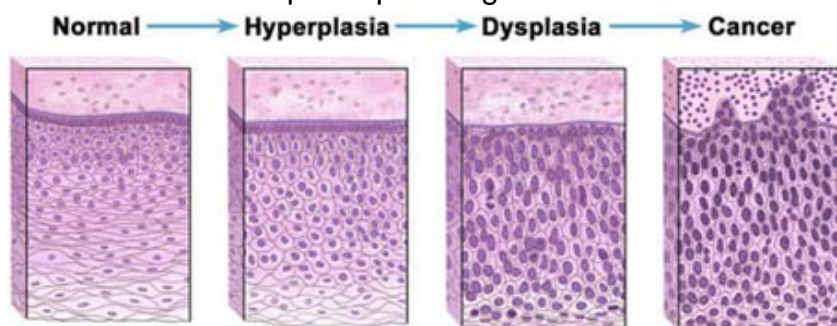

Figure 1.5: Multistep process of carcinogenesis [15]

The medical terms tumor and cancer are sometimes mentioned interchangeably which can make people misunderstand. In fact, a tumor is not necessarily a cancer. A cancer is a particularly threatening type of tumor. The tumor generally refers to a mass. The term cancer specifically refers to a new growth which is able to invade surrounding tissues, metastasize (spread to other organs) and which may eventually make unsuccessfully cured patient die. It is important to explain clearly the difference between tumor and cancer to the patients. Distinctions among the different neoplasms are listed in the table 1.1.

Neoplasm	It is an abnormal new growth of cells. Growth of *neoplastic* cells is more rapidly than it of normal cells. If it is not treated, *neoplastic* cells will continue to grow. Affect and damage on adjacent structures with uncontrolled cells growth. It can refer to benign (usually curable) or malignant (cancerous) growths.
Tumor	A tumor is a commonly used, but non-specific, term for a neoplasm. It generally refers to a mass with the increase in size. It can refer to benign (generally harmless) or malignant (cancerous) growths.
Benign tumor	Non-malignant / non-cancerous tumor. Tend to be slow growing tumors which are usually localized. Normally, it does not metastasize to other parts of the body or invade into the adjacent tissues. When they are removed, the patients are cured. If leave it untreated, some of them can grow larger in size and finally lead to serious disease.
Malignant tumor	Malignant tumors have cancerous growths. Fast growing tumors which infiltrate into the surrounding tissues. Often resistant to treatment, It can spread to other parts of the body with possible recurrence after cure and cause the patients' death.
Cancer	Considering as a malignant tumor (a malignant neoplasm). Primary cancer is concerns which start in a particular organ Metastasize cancer has spread from the organ which it arose to another organ.

Table 1.1: Distinctions among the different neoplasms [16]

There are more than 100 different known cancers which affect various parts of the body. Each type of cancer is unique with its own causes, symptoms, and methods of treatment. The most common 6 types of cancer which make human die are: lung, liver, stomach, colorectal, breast and oesophageal cancer. In 2012, World Health Organization (WHO) estimated that 14 million people were diagnosed with cancer across the world and 8.2 million people died from the disease. Annual cancer cases are expected to rise from 14 million in 2012 to 22 million within the next 2 decades. [13] Human cancer is the result of the accumulation of various genetic and epigenetic changes of normal cells almost anywhere in the human body. Normally, human cells

grow and divide to form new cells as the body needs them, but if the cells in a part of the body grow out of control, cancer will appear. Normal cells become cancer cells because of changes and damages to their DNA.

Normal cells constantly communicate with each other to keep human body healthy. Communications are carried on by using chemical signals produced in the body. The chemical signals are accepted by the receptors either on the surface or inside the cell. This triggers a flow of signals inside the cell sending messages to its nucleus. Finally, the messages get through to tell the cell properly switches certain genes on and off or to do something correct such as division and death.

For cancer cell, the signaling often goes wrong. For examples, the messages accepted by the nucleus might be sent too many times; the messages might not get through at all or be sent even though no chemical singling has not attached to receptors. Cancer cells might have extra receptors boosting the effects of the signals. Cancer cells grow much faster than the human body's own healthy cells. They can become detached from their neighbors (figure 1.6). That can explain why they are able to spread so quickly to other parts of the body once it has gained a foothold. Cancer cells grow out of control and become invasive. Different characteristics between normal cells and cancer cells are compared in the table 1.2 and what is especially mentioned is that the polarizations between cancerous and normal cells are opposite (figure 1.7).
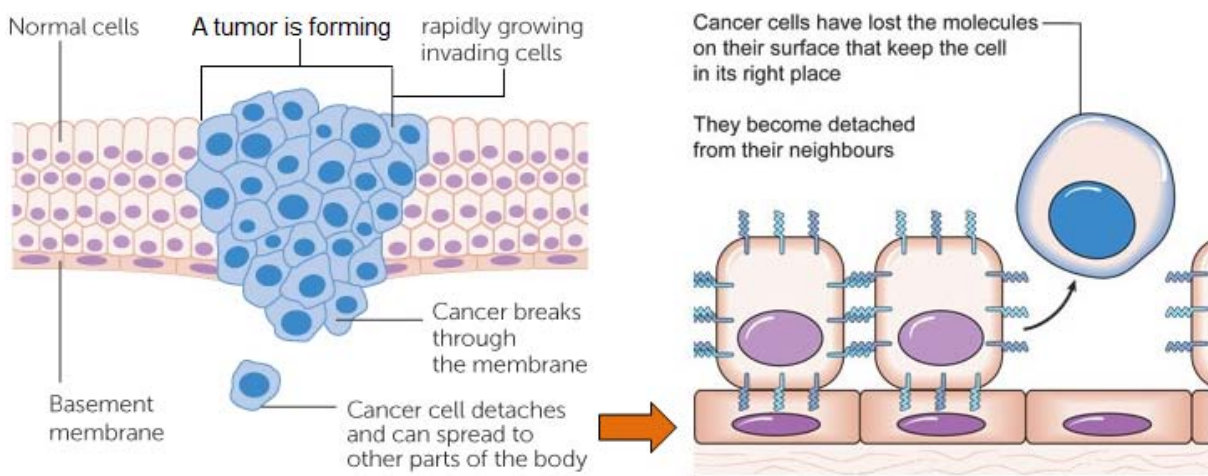
Figure 1.6: Characteristics of cancer cell [17]
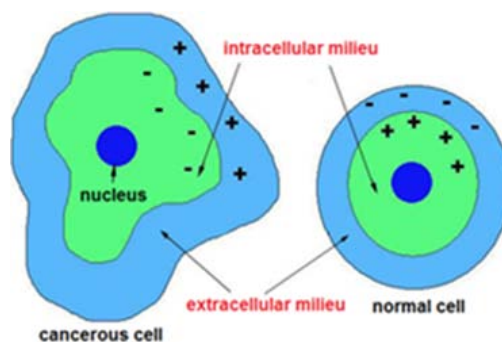
Figure 1.7: Difference of polarization between normal and cancerous cells [18]
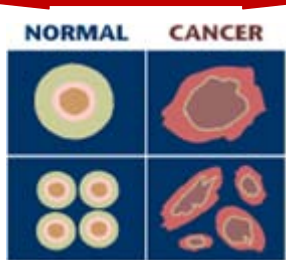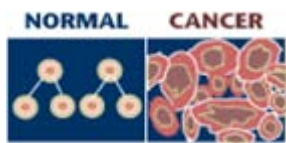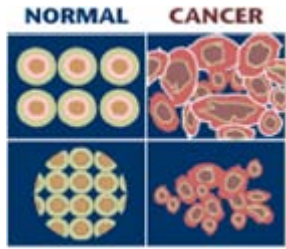
Normal cell ⬇	Difference	Cancer cell ⬇
Uniform and orderly	Cell size and shape ⬌ NORMAL CANCER	Large variations in cell size and shape. An irregularly large and variable shaped nucleus. Small cytoplasmic volume to nuclei.
Grow, divide and die in a controlled way with a predictable lifespan. Destroy themselves when damaged (apoptosis).	Cell division and death ⬌ NORMAL CANCER	Rapidly grow and divide. Outlive normal cell lifespan (immortal). Lost normal control mechanisms and don't stop growing. Probably prevent self-destruction when damaged.
Starting out as immature cells (stem cells). Acquiring and carrying on specific functions when they become mature or specialised.	Specialisation of cells ⬌ NORMAL CANCER	Do not carry on maturing. Can become less mature over time. Can lose specialised functions. Become more and more primitive.
Have a natural ability to stick together in the right place (cell adhesion). Molecules on the surface of the cell match those on its neighbours.	Cells sticking together ⬌ NORMAL CANCER	Lose the molecules on their surface which keep normal cells in the right place. Become detached from their neighbours.
Orderly and precisely grow and heal. Send chemical signals to each other all the time. Constantly communicate with each other. Obey signals and stop reproducing when reach their limit.	Obeying signals ⬌	Don't interact with other cells as normal cells do. Signaling goes wrong. Ignore signals from other cells. Genes in cells may be switched on and off wrongly.

Table1.2: Differences between normal and cancer cells [19] [20]

1.2 Electromagnetic hyperthermia

1.2.1 Electromagnetic therapy

In recent years, medical applications based on various sources of electromagnetic energy have been more and more widely investigated. Research and development of medical devices with various diagnostic and therapeutic applications have been also driven and carried out because of the advances in electronic and electromagnetic domains. Therapies using electromagnetic sources at radio frequencies and microwave frequencies can be classified in thermal therapy methods. Thermal therapy includes all therapeutic treatments based on transferring thermal energy into or out of human body. The major objective of thermal therapy is to efficiently treat pathological tissues without damaging normal tissues. It is considered as a minimally invasive alternative technique comparing with traditional surgery in the treatment of tumor and cancer. Figure 1.8 shows the schematic view of thermal therapy methods.
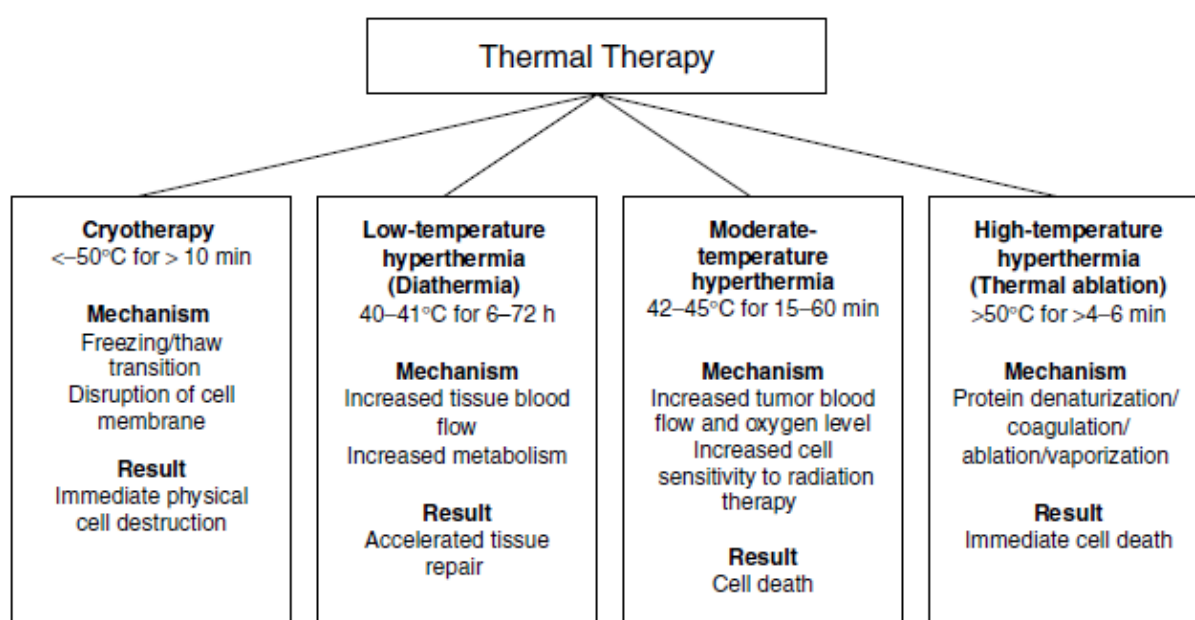
Figure 1.8: Schematic view of thermal therapy methods [21]

The cryotherapy is a treatment mainly with liquid nitrogen to reduce the tissue temperature below –50°C for more than 10 minutes. This allows the freezing and the disruption of the cell membrane leading to the physical cell destruction. For other heating methods above 40°C, according to the attained temperature level and treatment time duration, thermal therapy is generally categorized into three different modalities:

- **Diathermia** is to produce local heat in body tissues by electric currents for therapeutic purposes. Heating up to 41°C with applications in physiotherapy for the treatment of rheumatic diseases.
- **Hyperthermia** makes temperature of a part of the body or of the whole body be raised to a higher than normal level (41–45°C), which may allow other types of cancer treatments such as radiation therapy or chemotherapy to work better.

- **Thermal ablation** produces very high temperature (above 45°C) and can be used to destroy cells within a localized section of a tumor. This is commonly used in oncology for cancer treatment, in urology for benign prostatic hyperplasia (BPH) treatment, and in cardiology for heart stimulations and other areas. [21]

1.2.2 Effect of heat injury on biological tissues

Injury of the tissue by thermal energy has two distinct phases. The initial phase is direct heat injury which predominantly depends on the total energy applied to the tissue. Some studies demonstrate that tumor or cancer cells can be destroyed at lower temperatures than normal cells. The second phase is indirect injury after focal hyperthermia application which produces a progression of damage in the tissue.

The effects of heat injury are determined by the applied total thermal energy, attained temperature, rate of heat removal, and specific thermal sensitivity of tissue. The temperature elevation in a biological tissue generates multiple complex influences on cellular, sub–cellular and molecular levels. The main mechanism for cell death is probably protein denaturation, beyond 40°C, which leads to alterations in multi–molecular structures (e.g., membranes) and synthesis and repair of DNA. One of the most important influences is an increase in blood perfusion. It means that the physiological process guarantees the oxygen and chemical components of cells. An increase of blood flow is responsible for removing the heat excess via the blood vessels through the body.

Temperature Range (°C)	Time Require-ments	Physical Effects	Biological Effects
< −50	> 10 min	Freezing	Complete cellular destruction
0–25		Decreased permeability	Decreased blood perfusion, decreased cellular metabolism, hypothermic killing
30–39	No time limit	No change	Growth
40–46	30–60 min	Changes in the optical properties of tissue	Increased perfusion, thermotolerance induction, hyperthermic killing
47–50	> 10 min	Necrosis, coagulation	Protein denaturation, not subtle effects
> 50	After ~ 2 min	Necrosis, coagulation	Cell death
60–140	Seconds	Coagulation, ablation	Protein denaturation, membrane rupture, cell shrinkage
100–300	Seconds	Vaporization	Cell shrinkage and extracellular steam vacuole
> 300	Fraction of a second	Carbonization, smoke generation	Carbonization

Table 1.3: Effect of temperature on biological tissues [22]

Changes of physical and biological properties of tissue at different temperature levels with associated expose time are shown in the table 1.3. Classical hyperthermia cause irreversible cellular damage with temperature 42-45°C. Beyond 50°C,

apoptosis, the phenomenon of protein denaturation can cause immediate death of tumor cell. Beyond 100°C, vaporization phenomenon happens, because of the amount of water in the tissue decrease sharply. Beyond 300°C carbonization, charring and generation of smoke will happen.

1.2.3 Hyperthermia

Hyperthermia is a type of tumor or cancer treatment where body tissue is exposed to high temperatures (45°C). Research has shown that high temperatures can damage proteins and structures within tumor or cancer cells and kill them, usually with minimal injury to normal tissues. [23] It might be defined more precisely as raising the temperature above normal for a decided period of time in a part of or the whole human body. Hyperthermia is always implemented as part of a multimodal, oncological treatment strategy, i.e., in combination with radiotherapy or chemotherapy. The effectiveness of hyperthermia treatment is related to the temperature achieved during the treatment, the length of treatment, and cell and tissue characteristics. [24] To ensure that the desired temperature is reached, but not exceeded, the temperature of the tumor and surrounding tissues is monitored throughout the procedure. There are several types of hyperthermia such as: local hyperthermia, regional hyperthermia, external hyperthermia, whole–body hyperthermia and extracellular hyperthermia depending on the type of pathological tissue and its position.

- **Local hyperthermia** is to be used for increasing mainly the tumor temperature while sparing surrounding normal tissue with either external or interstitial techniques. Energy is delivered to a small area to heat the tumor. Local hyperthermia treatment is a well–established cancer treatment method. If a rise in temperature to 42°C can be obtained for one hour within a cancer tumor, the cancer cells will be destroyed. [25] Primary malignant tumors have poor blood circulation, which makes them more sensitive to changes in temperature. Local hyperthermia is used to heat a small area. It involves creating very high temperatures that destroy the heated cells. The heat may be applied using three different methods: external approaches; intraluminal or endocavitary methods and interstitial techniques.

- **Regional hyperthermia** is indicated for patients with locally advanced deep-seated tumors such as those in the pelvis or abdomen. The application of regional hyperthermia is, however, more complex than local heating, particularly because of the wide variation in physical and physiological properties of body tissues. It requires more sophisticated planning, thermometry, and quality assurance. Since regional heating techniques apply energy to the adjacent deep-seated tumors in a focused manner, energy will be delivered to the adjacent normal tissues. [26] Under such conditions, selective heating of tumors is only

possible when heat dissipation by blood flow in normal tissue is greater than that in tumor tissue.

- **Whole–body hyperthermia** is used to treat metastatic cancer that has spread throughout the body. To ensure that the desired temperature is reached, but not exceeded, the temperature of the tumor and surrounding tissue is monitored throughout hyperthermia treatment. Whole-body hyperthermia (to a limit of 42°C) is a distinctive and complex pathophysiological condition which has tremendous impact on tissue metabolism, blood flow, organ function, and tissue repair. [25]

- **Extracellular hyperthermia** is to heat up the targeted tissue by means of electric field, keeping the energy absorption within the extracellular liquid. It is based on a capacitively coupled energy transfer applied at a frequency that is primarily absorbed in the extracellular matrix due to its inability to penetrate the cell membrane. [27] Since the energy absorption for these effects is more significant than the temperature, it is also important to characterize the hyperthermia by thermal dose but not only by temperature.

1.2.4 Hyperthermia techniques

There are three main significantly developed hyperthermia techniques: ultrasound hyperthermia, radiofrequency hyperthermia, and microwave hyperthermia.

- **Ultrasound hyperthermia**: Ultrasound waves propagate at a frequency of 2–20 MHz through soft tissues. Absorption of ultrasound energy results in heating of the biological tissues. Theoretically, ultrasound has the best combination of small wavelengths and corresponding attenuation coefficient allowing penetration to deep sites with the ability to focus power into small size regions. The primary limitation of such systems is their inability to penetrate air and the difficulty in penetrating bone. Over the years, ultrasound devices capable of improved heating uniformity and controlled depth of penetration, mostly by using multiple applicators with phasing and power steering, have been designed. [28-34]

- **Radiofrequency hyperthermia (RF)**: the initial investigation of the use of radiofrequency waves in the body is in 1891 [35], which showed that RF waves which pass through living tissue cause a temperature increase in the tissue without causing neuromuscular excitation. For heating large tumors at depth, RF waves in the range of 10–120 MHz are generally used with wavelengths that are long compared to body dimensions. [36] A closed-loop circuit is created by placing a generator, a large dispersive electrode (ground pad), a patient acting as a resistor, and a needle electrode in series. An alternating electric field is created within the tissue of the patient. Ionic agitation in the tumor tissue creates frictional heating within the body, which can be tightly controlled through depositing the amount of RF energy. Studies have shown that RF hyperthermia induced lesions increase rapidly in size at the beginning of RF power application, and then the rate of increase diminishes rapidly as the resistance rises at the interface between electrode and tissue.

- **Microwave hyperthermia**: Microwave hyperthermia energy is used to destroy cancerous tumors. Microwave hyperthermia was evaluated in the 80s for the treatment of cancer and has been used for the medical treatment of prostate or breast cancer. Microwave hyperthermia has generally utilized antennas working at 915 MHz and 2450 MHz. Microwave hyperthermia is also frequently used in conjunction with other cancer therapies, such as radiation therapy where it can increase tumor blood flow helping to oxygenate poorly oxygenated malignant cells. Table 1.4 shows the types of hyperthermia for different pathological tissues. Table 1.5 shows a comparison among the different hyperthermia approaches.

For thermal radiation in the body caused by hyperthermia therapy, two important equations are involved: [37]

Specific absorption rate (SAR)

$$SAR = \frac{\sigma * E^2}{\rho} \qquad [2.1]$$

Modified Penn Bioheat equation

$$\rho C \frac{\delta T}{\delta t} = h_b (T_b - T) + \nabla(k \nabla T) + \rho * SAR \qquad [2.2]$$

with the definition of the parameters as follow :

σ: conductivity of tissue (S/m),

E: electric field (V/m),

ρ: density of tissue (kg/m^3),

C: specific heat tissue (J/mK),

k: thermal conductivity of tissue (W/mK),

T: temperature of tissue (°C)

T_b: blood temperature (°C)

h_b: convective heat transfer coefficient (kg/m^3).

SAR: parameter of heat characterization of tissue.

Penne Bioheat equations shows the heat transfer in human biological system. Two equations (2.1 and 2.2) are important in thermal hyperthermia study and used in research for experimentation, computational simulation or combination of both methods in order to control temperature required for hyperthermia treatment.

Hyperthermia type	Tumor size	Tumor character
Local hyperthermia	Deep-seated tumor (10 cm)	Small and local
	Superficial tumor (3cm)	(<3 or 4 cm)
Regional hyperthermia	Body limb or large organ	Area of 30 cm–40 cm
Whole–body hyperthermia	The whole human body	Metastases

Table 1.4: Summary of major hyperthermia methods related to the tumor properties [25]

	Hyperthermia approach		
	Ultrasound	**Radiofrequency**	**Microwaves**
Frequency	0,3 à 6 MHz	10 à 200 MHz	200 à 2450 MHZ
Applicator	• Piezoelectric conductor	• Electrodes • Coils • Waveguides, • Dipoles	• Waveguides • Antennas • Microstrip patches
Advantages	• Good focus performance in tissue. • No hot spots in fatty tissues. • Heating possible to 5–10cm depth with single transducer and up to 20cm depth with multiple transducers. • Temperature is easy to measure and control.	• Simple instrumentation. • Proven effective and worldwide availability. • No shield required. • Electrodes are not limited in size • Insulation can be accomplished. • Ability to treat different tumor types with large area.	• High temperature is available. • Heating large volumes is possible. • Specialized antennas for heating from body cavities have been developed. • Multiple applicators, coherent or incoherent, can be used. • Can avoid hot spots in the fatty tissues.
Disadvantages	• Heating area is small. No penetration of tissue-air interfaces. • Difficult in penetrating bone	• Difficult to control electric fields. • Only areas where fat is thin can be treated by capacitive systems. • RF tumor destruction is incomplete near blood vessels. • Device needs to be grounded.	• Heating is not localized at depth. • Limited penetration at high frequencies. • Temperature measurement is difficult. • Thermometry requires noninteracting probes. • Possible health effects on personnel.
Applications	• Treatment of superficial and deep regional tumors. Examples include surface lesions, head and neck, and lesions in extremities.	• Treatment for large and superficial tumors in neck, limb, chest, brain, abdomen, etc.	• For treatment of superficial tumors in breast, limb, prostate, and brain.

Table 1.5: Summary of major hyperthermia methods [25][21]

1.2.5 Thermal ablation

Ablation may be performed by surgery, hormones, drugs, radiofrequency, heat, or other methods. There are mainly two available ablation methods: thermal ablation and chemical ablation. In medicine, high temperature hyperthermia is considered as thermal ablation, which means the removal or destruction of a body part or tissue or its function. Thermal ablation methods include radiofrequency ablation, microwave ablation, laser ablation, and high density focus ultrasound (HIFU) by creating the thermal injury, and cryoablation which achieve cellular death through freezing. Chemical ablation methods include ethanol ablation, which cause diseased cellular death through direct toxicity, and acetic acid ablation. The applicators for thermal ablation techniques are different: electrodes for radio frequency ablation, antennas for microwave ablation, and fiber for laser ablation.

Based on realistic limitations of each thermal approach, any form of thermal therapy is unlikely to replace the others. Thermal ablation can be used to treat a tumor with a defined volume where surgery is difficult to be carried out (e.g., liver) or where organ function is needed to be preserved (e.g., prostate or uterus). However, thermal ablation for treatments of large bulky tumors such as bone, colorectal cancer primaries, soft tissue sarcomas, head and neck nodules and superficial disease (e.g., skin) is not quite helpful. In order to preserve surrounding critical normal tissue structures, more subtle moderate temperature hyperthermia is preferred.

All the mentioned thermal therapies above belong to the minimally invasive therapy techniques for the treatment of different diseases, which are being researched and developed continuously. Minimally invasive techniques could make patients suffer less pain and reduce the risks of the surgical operation. With the developing minimally invasive technologies, they will become better choices for the patients in the future.

1.2.6 Physical characteristics of microwave hyperthermia

With microwave hyperthermia medical therapy, an electromagnetic source (antenna) is directly positioned in the target biological tissue and a proper microwave power is injected to destroy the pathological tissue. The concept of using microwave hyperthermia might come from the microwave oven. The microwave hyperthermia and microwave oven have the similar basic principle.
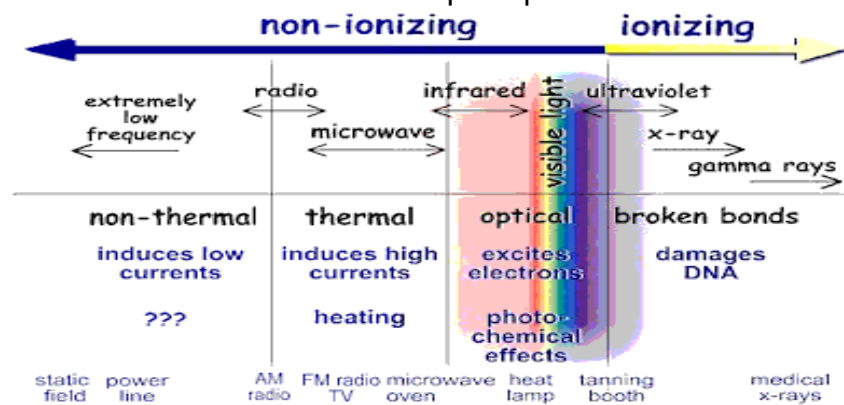
Figure 1.9: Different types of electromagnetic radiation [38]

Microwave hyperthermia refers to the region of the electromagnetic spectrum with frequencies from 0.9GHz to 2.450 GHz, which is between common infrared and radio frequencies (figure 1.9). Microwave hyperthermia works in the form of non-ionizing microwave radiation at the frequency of 2.45GHz, which heats a dielectric biological tissue. Water of the tissue absorbs energy from the microwave in a process of dielectric heating which is caused by water dipole rotation. The generated power density per volume by dielectric heating could be calculated by the formula:

$$p = \omega \cdot \varepsilon_r'' \cdot \varepsilon_0 \cdot E^2 \quad [2.3]$$

where ω is the angular frequency, ε_r'' is the imaginary part of the complex relative permittivity, ε_0 is the permittivity of free space and *E* the electric field strength.

Water molecules (H_2O) are polar. The electric charges on the water molecules are not symmetric. The alignment and the charges on the atoms of the water are that: the hydrogen side of the molecule has a positive charge, and the oxygen side has a negative charge. Microwave radiation has electric charges too. The representation of the microwave can be considered as the electric charges on the wave flipping between positive and negative. When the oscillating electric charges from microwave radiation interact maximally with water molecules, it causes them flip (figure 1.10). Because of the microwave radiations of different frequencies, the electrical charges on the water molecules could flip forth and back 2 to 5 billion times per second.

Figure 1.10: Interaction between water molecules and microwaves

The vigorous movement of water molecules raises the temperature which is a measurement of how fast the water molecules move in a substance. Electromagnetic microwaves heat matter by agitating its water molecules in the surrounding tissue, producing friction and therefore heating.

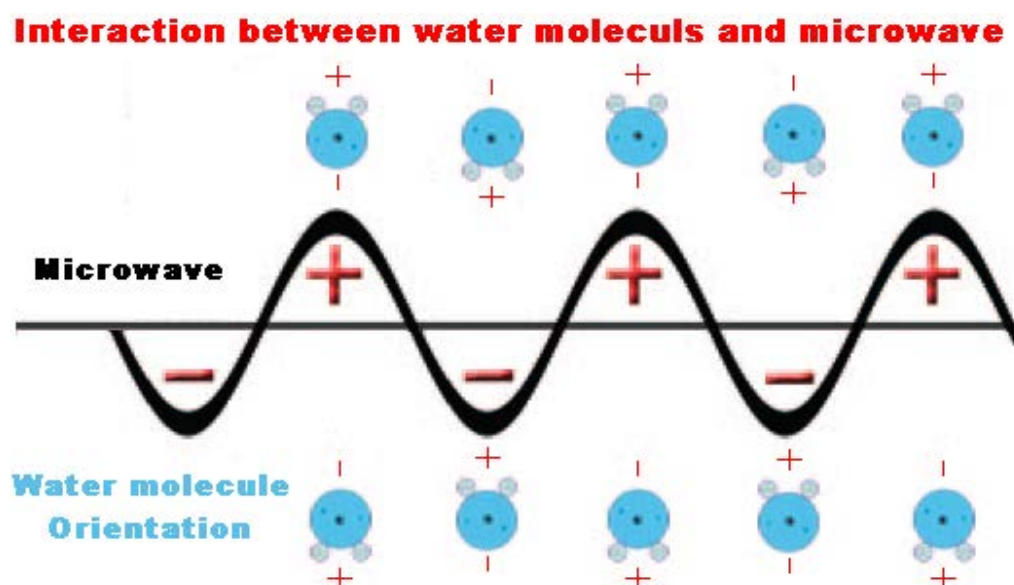**1.2.7 Current development of microwave hyperthermia**

Microwave hyperthermia systems have been researched and developed by academic or industrial laboratories over the last decade. Many microwave hyperthermia researches for benign and cancerous tumor treatment are still in the experimental, preclinical, or early–stage clinical phase and some of them have been commercialized and available for different clinical treatments:

- **Angiodynamics–Acculis Microwave Tissue Ablation (MTA) System** with a single applicator at 2.45 GHz operating frequency can generate microwave powers from 60W to 140W. It has a liquid cooled applicator with three available lengths of 14 cm, 19 cm and 29 cm. For applying maximum microwave power of 140W, it can achieve 4.5cm (diameter) x 5.5cm (length) cylindrical ablation in 6 minutes. [39]

- **ABLATECH–AMICA** (**A**pparatus for **MIC**rowave **A**blation) **system** works at frequency of 2.45GHz and can deliver an adjustable microwave power from 0 to 140W and a net available power of 90W at the applicator extremity. The main advantage of this microwave ablation system is that it can manage "backward heating" –energy that is not absorbed by the tissues. The AMICA-Probes antennas are equipped with a mini-choke at λ/4 combining with liquid cooling system to confine the electromagnetic field on the distal portion of the antenna. [40]

- **BSD Medical Corporation–MicroThermX–Microwave Ablation System** consists of a single generator working at 915 MHz and an amplifier. It sends continuous wave microwave energy with 180W maximum (60W maximum per antenna) by one single antenna or up to three simultaneous antennas to soft tissue for uses of coagulation or ablation. SynchroWave antennas of Synchronous Wave Alignment™ technology with cooling circuit can be used for open surgical as well as percutaneous ablation procedures. One antenna can have 3.1cm x 2.0cm ablation zone and 7.0cm x 6.5cm ablation zone for three antennas. [41]

- **Covidien–Evident™ MW Ablation System** generates the microwave energy of 45W at 915MHz operating frequency to create contiguous ablation zones. Maximum to three antennas can be activated at the same time to produce three lesions or one large lesion (spacing of 1.5–2cm) in ten minutes. [42]

One important thing that should be mentioned about the existing commercial microwave hyperthermia systems is that: no exiting system can achieve using one single antenna or applicator for both diagnosis and therapeutic treatment at the same time. All of them can just offer microwave hyperthermia treatment by using high microwave power. In our project, a new microwave hyperthermia system is designed and researched which could have both diagnostic and therapeutic functions. It means that using one applicator with a very low harmless microwave power level to do the diagnosis first to check if the tissue is normal or not. If the tissue has been found with pathological changes, then the therapeutic treatment will be carried out on the pathological part by using the same applicator with higher microwave power.

Chapter 2
Dielectric characterizations of biological tissues in microwave frequencies

2.1 Introduction

Dielectric properties are very important for studying of the microwave hyperthermia heating process in the biological tissues. The objective of this chapter is to use an already existing open ended coaxial cable technique to measure the complex dielectric permittivity for the characterization of biological tissues in the radiofrequency and microwave field. These temperature–dependent dielectric property characterizations can also help to improve the results of multiphyscial simulations in the microwave hyperthermia of biological tissues.

In fact, dielectric properties of biological tissues are the key factors for the dissipation of electromagnetic energy in the human body. For microwave hyperthermia treatment, measurements of the basic parameters are very important. The determination of the dielectric parameters of biological tissues is also a promising method in the medical diagnosis and imaging.

2.2 Permittivity

Permittivity is one of basic physical parameters of a material. It is the parameter describing dielectric properties which influence reflection of electromagnetic waves at interfaces and the attenuation of wave energy within the material. The complex relative permittivity ε^* of a material to that of free space can be expressed in the following form:

$$\varepsilon^* = \varepsilon' - j\varepsilon''$$

ε': Dielectric constant $\quad\quad$ ε'': Dielectric loss factor

The real part of permittivity ε' is a measure of how much energy from an external electric field is stored in the material. The imaginary part of permittivity ε'' is called loss factor which is a measure of the dissipation or loss of a material due to an external electric field. The imaginary part of permittivity ε'' is always greater than zero and is usually much smaller than ε'. The loss factor ε'' includes the effects of both dielectric loss and conductivity. The complex permittivity is drawn as a simple vector diagram in figure 2.1, ε' and ε'' are 90° out of phase. The relative "lossiness" of a material is the ratio of the energy lost to the energy stored.
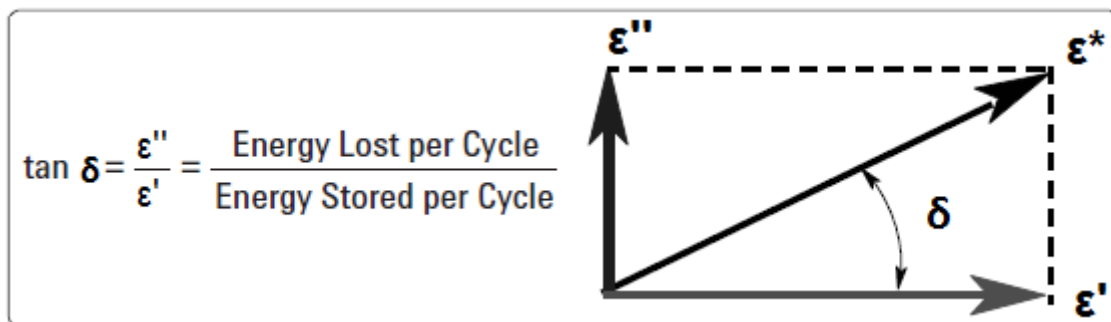

Figure 2.1: Loss tangent vector diagram

The loss tangent or tan δ is defined as the ratio of the imaginary part of the dielectric constant to the real part (figure 2.1). It is called tangent loss (tan δ) or dissipation factor. For very low loss materials, since tan δ ≈ δ, the loss tangent can be expressed in angle units, milliradians or microradians.

2.3 Dielectric mechanisms

There are essentially four basic kinds of polarization mechanisms (figure 2.2):

- **Interfacial or space charge polarization**: surfaces, grain boundaries, interphase boundaries (including the surface of precipitates) may be charged, i.e. they contain dipoles which may become oriented to some degree in an external field and thus contribute to the polarization of the material.

- **Orientation (Dipolar) polarization**: the materials (usually liquid or gaseous) must have natural dipoles which can rotate freely. In thermal equilibrium, the dipoles will be randomly oriented and thus carry no net polarization. The external field aligns these dipoles to some extent and thus induces a polarization of the material. The friction accompanying the orientation of the dipole will contribute to the dielectric losses. The dipole rotation causes a variation in both ε' and ε'' at the relaxation frequency which usually occurs in the microwave region. The paradigmatic water exhibits a strong orientation polarization.

- **Ionic polarization**: in this case a (solid) material must have some ionic character. It then automatically has internal dipoles, but these built-in dipoles exactly cancel each other and are unable to rotate. The external field then induces net dipoles by slightly displacing the ions from their rest position. The paradigmatic materials are all simple ionic crystals like NaCl.

- **Electronic polarization**: also called atom or atomic polarization. An electrical field will always displace the center of charge of the electrons with respect to the nucleus and thus induce a dipole moment as discussed before. The paradigmatic materials for the simple case of atoms with a spherical symmetry are the noble gases in all aggregate forms.

The material has its corresponding dielectric mechanisms or polarization effects at different frequencies (Figure 2.2). Dipole orientation and ionic conduction interact strongly at microwave frequencies. Water molecules which are important for microwave hyperthermia are permanent dipoles. They rotate to follow an alternating electric field. Atomic and electronic mechanisms are relatively weak and usually constant over the microwave region. Each dielectric mechanism has a characteristic "cutoff frequency." As frequency increases, the slow mechanisms drop out in turn, leaving the faster ones to contribute to ε'. The loss factor (ε'') shows a corresponding peak at each critical frequency. The magnitude and "cutoff frequency" of each mechanism is unique for different materials. For example, water has a strong dipolar effect at low frequencies, but its dielectric constant decrease dramatically around 22GHz and Teflon has no dipolar mechanisms and its permittivity is remarkably constant well into the millimeter–wave region.
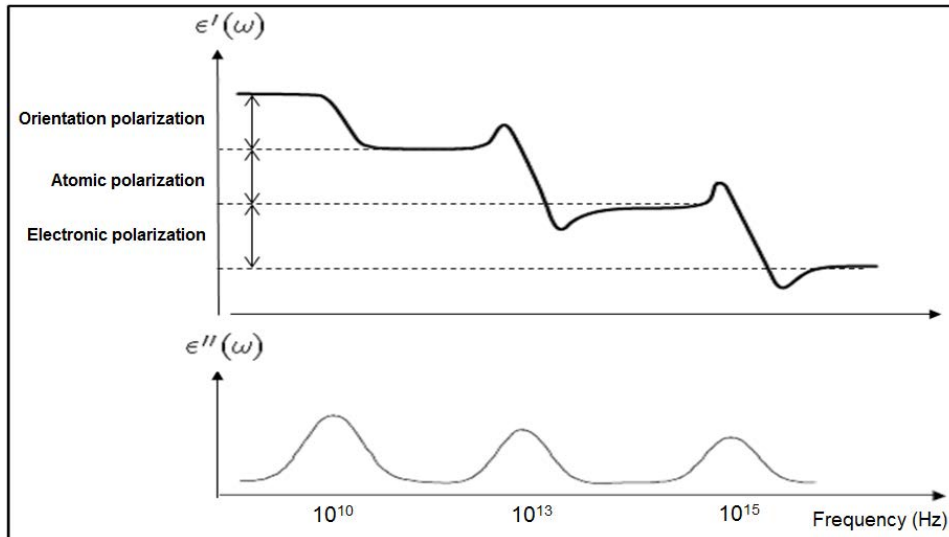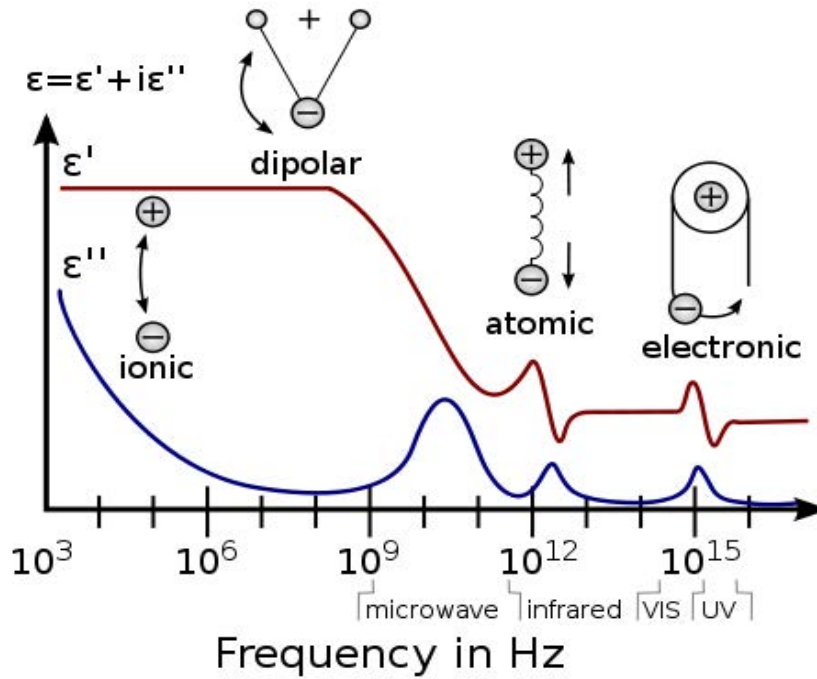
Figure 2.2: Frequency response of different dielectric mechanisms [43] [44]

2.4 Relaxation time

Relaxation time, τ is a measure of the mobility of the molecules or dipoles which exist in the material. It is the time required for a displaced system aligned in an electric field to return to 1/e of its random equilibrium value (or the time required for dipoles to become oriented in an electric field). When an electric field is applied, liquid and solid materials have molecules are in a condensed state with limited freedom to move. Constant collisions cause internal friction so that the molecules turn slowly and exponentially approach the final state of orientation polarization with relaxation time constant τ. When the field is switched off, the sequence is reversed and random distribution is restored with the same time constant. In the following equation, f_c is relaxation frequency related to τ.

$$\tau = \frac{1}{\omega_c} = \frac{1}{2\pi f_c}$$

At frequencies below relaxation, the alternating electric field is slow enough so the dipoles can keep pace with the field variations. Polarization could develop fully, so the loss (ε'') is directly proportional to the frequency. With the increase of frequency, ε'' continues to increase but the storage ε' begins to decrease due to the phase lag between the dipole alignment and the electric field. Above the relaxation frequency both ε'' and ε' drop off as the electric field is too fast to influence the dipole rotation and the dipolar polarization disappears (figure 2.3).

2.5 Debye relation

Materials that exhibit a single relaxation time constant can be modeled by the Debye relation as a characteristic response in permittivity as a function of frequency (figure 2.3). ε' is constant above and below the relaxation with the transition occurring near the relaxation frequency f_c. ε'' is small above and below relaxation with peaks in the transition region at the relaxation frequency f_c.

Debye equation:

$$\mathcal{E}(\omega) = \mathcal{E}_\infty + \frac{\mathcal{E}_s - \mathcal{E}_\infty}{1 + j\omega\tau^{(1-\alpha)}}$$

For $\omega = 0$, $\mathcal{E}(0) = \mathcal{E}_s$

For $\omega = \infty$, $\mathcal{E}(\infty) = \mathcal{E}_\infty$

$\mathcal{E}_s$: static value for $\lambda = \infty$, λ: wavelength in vacuum (or air)
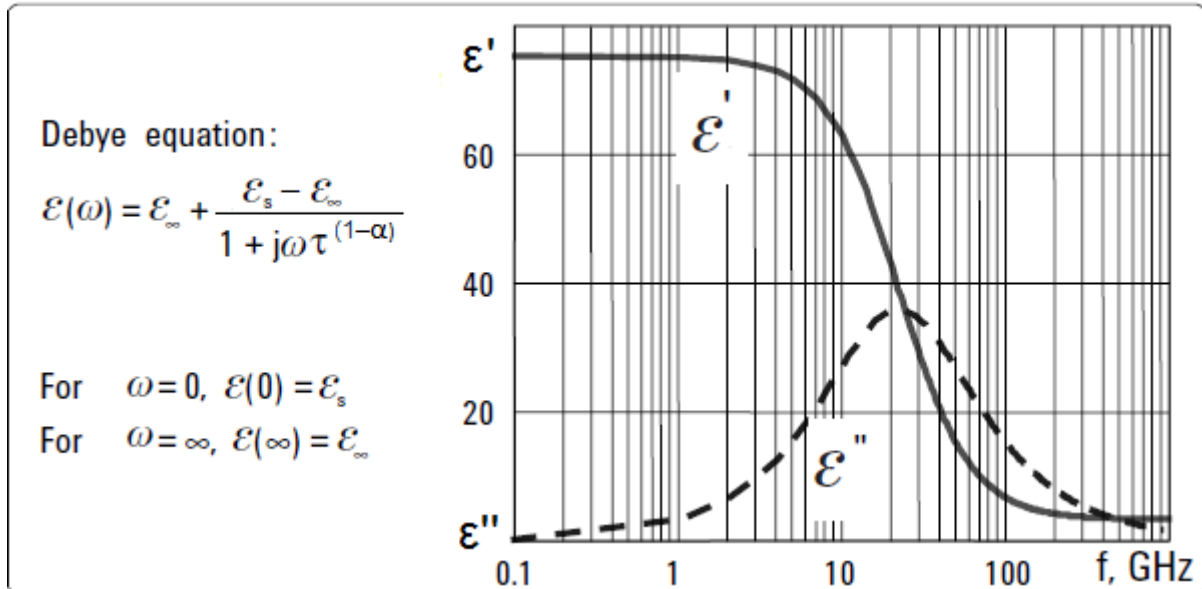
$\mathcal{E}_\infty$: optical value (infinite frequency) for $\lambda = 0$, τ: characteristic relaxation time

ω: $2\pi c/\lambda$ (c: velocity of light in vacuum) α: distribution parameter $(0<\alpha<1)$(for water $\alpha=0$)

$$\varepsilon' = \frac{\varepsilon_s - \varepsilon_\infty}{1+(\omega\tau)^2} \quad \& \quad \varepsilon'' = \frac{(\varepsilon_s - \varepsilon_\infty)\omega\tau}{1+(\omega\tau)^2}$$

Figure 2.3: An example of Debye relaxation of water at 30°C [44]

2.6 Cole–Cole diagram

The complex permittivity could be shown on a Cole-Cole diagram by plotting the ε'' on the vertical axis and ε' on the horizontal axis with frequency as the independent parameter (Figure 2.4). A material which has a single relaxation frequency (Debye relation) will appear as a semicircle with its center lying on the horizontal $\varepsilon'' = 0$ axis and the peak of the loss factor occurring at relaxation frequency f_c. A material with multiple relaxation frequencies will be a semicircle (symmetric distribution) or an arc

(nonsymmetrical distribution) with its center lying below the horizontal $\varepsilon'' = 0$ axis. The frequency moves counter clockwise on the curve.
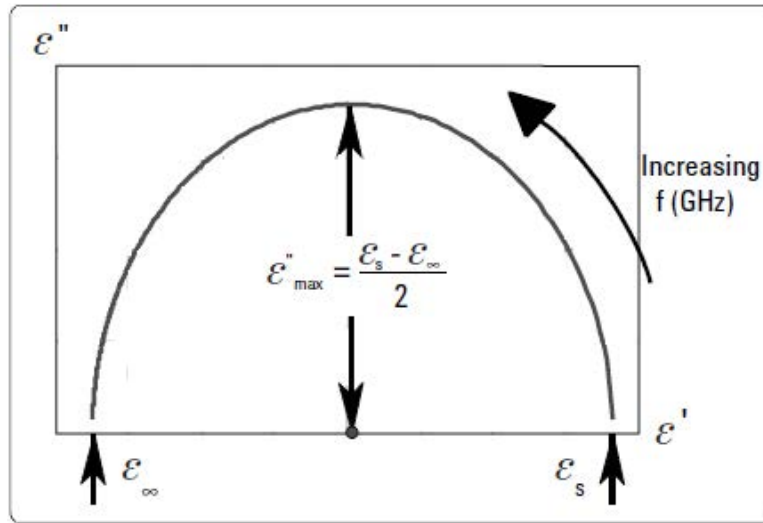
Figure 2.4: Cole–Cole diagram [44]

2.7 Measurement techniques of dielectric characterizations

Choice of techniques for measuring dielectric properties of materials under test depends on practical requirements such as: the frequency of interest, the required measurement accuracy, the expected value of complex permittivity, material own properties (i.e., homogeneous and isotropic), the material structure (i.e., liquid, powder, solid, or sheet), sample size or volume restrictions, destructive or non–destructive, contacting or non-contacting and temperature. Summary of techniques of dielectric characterizations for materials under test are presented in figure 2.5 and compared in table 2.1.

Figure 2.5: Summary of measurement techniques of dielectric characterizations [45]

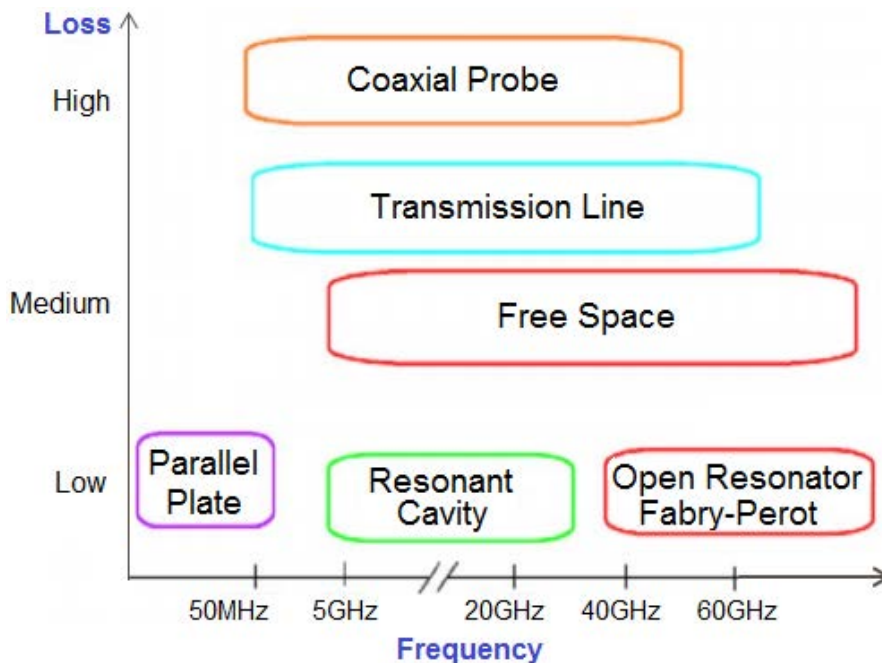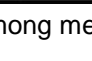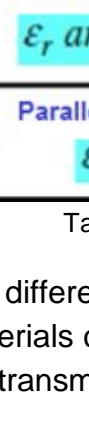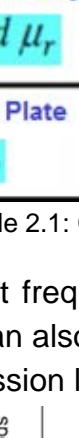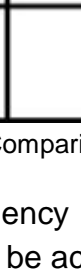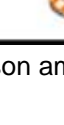|		
Coaxial Probe ε_r		Broadband, convenient, non-destructive Suitable for lossy liquid, semi-solid material
Transmission Line ε_r and μ_r		Broadband Suitable for lossy to low loss samples machineable solids Requirement of large size of samples
Free Space ε_r and μ_r		Non-contacting, non-destructive Suitable for high temperatures Requirement of large, flat samples Limited by practical sample size
Resonant Cavity ε_r and μ_r		Accurate Suitable for low loss, small samples substrates, thin films
Parallel Plate ε_r		Suitable for low frequency Thin sample, flat sheet

Table 2.1: Comparison among measurement techniques of dielectric properties [45]

For different frequency range, dielectric characterizations of complex permittivity of materials can also be achieved with several methods such as the resonance method, the transmission line method, quasi-optical method, and reflection method (figure 2.6).
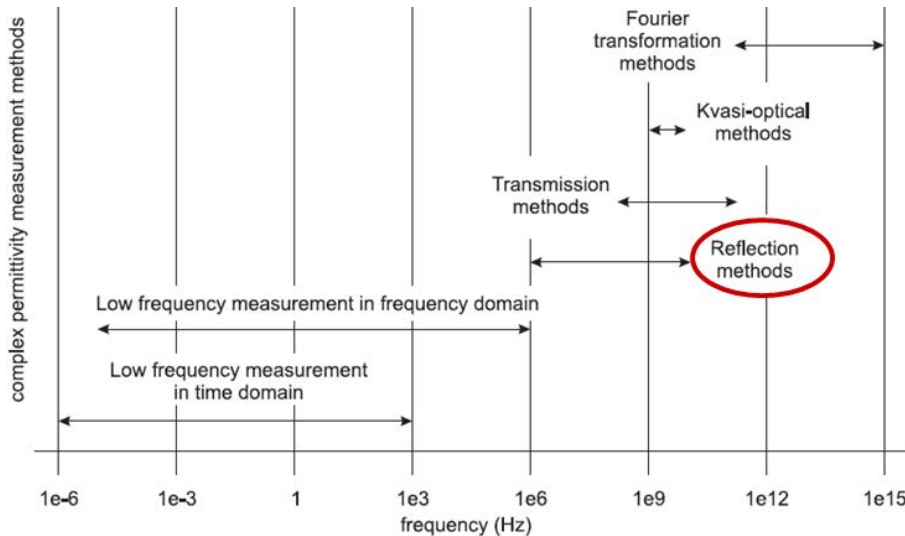
Figure 2.6: Measurement techniques for dielectric characterizations in different frequency ranges

The adopted open–ended coaxial probe method for the measurement of dielectric properties of materials has several characteristics:

- Simple and convenient (non destructive)
- Broadband (from 0.2 to up to 20 GHz)
- Suitable for liquids or semi-solids
- For both medium–loss and high–loss media
- Not suitable for materials with low dielectric (plastics, oils, etc.)
- No air gaps between probe and material
- Accurate and fast

The open–ended coaxial probe technique is useful in measuring the permittivity of nonmagnetic materials. The open–ended coaxial probe is a cut off planar section of a transmission line. The semi–solid material is measured by touching with the flat planar section of the probe. The liquid material is measured by immersing the probe into it. The vector network analyzer is used for the acquisition of the measured reflected signal S_{11} in a selected frequency range. Matlab program is used for the calculations to convert measured S_{11} to the corresponding complex permittivity ε* and the electrical conductivity (figure 2.7). [46]
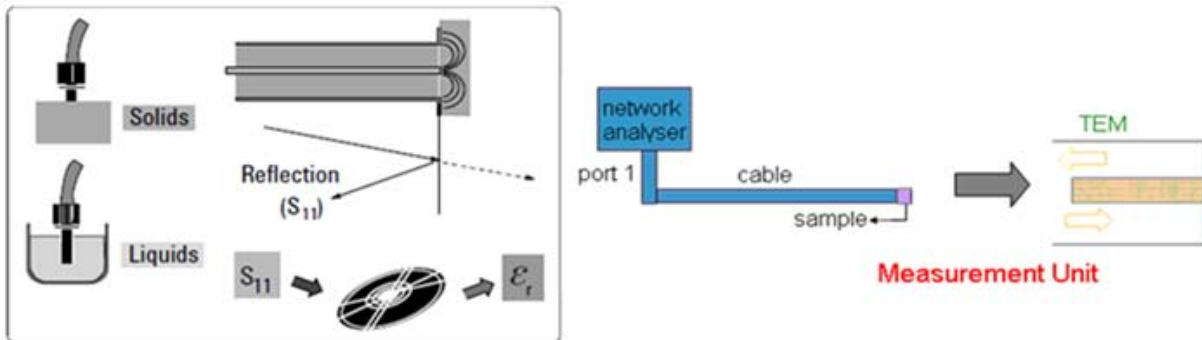
Figure 2.7: The open–ended coaxial probe method

2.8 Open–ended coaxial probe model analysis

Due to the extensive uses of open-ended coaxial probes in the measurement of biological substances, a number of models for open-ended coaxial probes have been studied and developed. [47-53] There are four typical models to describe the open–ended coaxial probes terminated by semi–infinite homogenous materials: capacitive model, radiation model or antenna model, virtual line model, and rational function model. Virtual line model is used for the experiments of dielectric characterization. For open–ended probe method, the material under test, where the probe is terminated, can be modeled as a virtual part of the transmission line. The transmission line consists of a part of physical line with length D and a part of virtual line with length L.
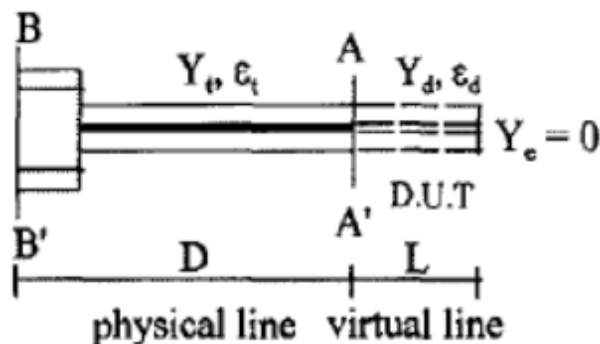
Figure 2.8: Equivalent circuit model of the virtual line [54]

This virtual line is terminated by an open circuit (figure 2.8). The complex admittance at probe end (plane A–A ') is given by:

$$Y_L = Y_d \frac{Y_E + jY_d \tan(\beta_d L)}{Y_d + jY_E \tan(\beta_d L)} \qquad \text{equation [2.1]}$$

- Y_L: Admittance at the input of the virtual line
- Y_d: Characteristic admittance of the virtual line
- Y_E: Admittance at the extremity of the virtual line (terminated with an open circuit, $Y_E = 0$)
- β_d: Propagation constant in the virtual line. (dielectric medium)
- L: Length of the virtual line

It means that:

$$Y_L = jY_d \tan(\beta_d L) \qquad \text{equation [2.2]}$$

Y_d can be expressed as a function of physical parameters of the transmission line as follows:

$$Y_d = \frac{\sqrt{\varepsilon_d}}{60\ln\left(\frac{b}{a}\right)} \qquad \text{equation [2.3]}$$

- a and b: inner and outer diameters of coaxial probe
- ε_d: complex permittivity of measured material

The admittance Y_L can be related to the characteristic admittance of probe Y_t, and the measured reflection coefficient at plane AA' as follows:

$$Y_L = \frac{1 - \Gamma_m e^{2j\beta_t D}}{1 + \Gamma_m e^{2j\beta_t D}} Y_t \qquad \text{equation [2.4]}$$

Where

$$Y_t = \frac{\sqrt{\varepsilon_t}}{60\ln\left(\frac{b}{a}\right)} \qquad \text{equation [2.5]}$$

- Y_t: Characteristic admittance of the probe.
- β_t: Propagation constant in the probe.
- D: Physical length of the probe,
- Γ_m: Complex reflection coefficient measured at plane BB'
- ε_t: Dielectric constant of dielectric material inside the coaxial line

Combining equations (2.2), (2.3), and (2.4), equation (2.5) is obtained

$$\varepsilon_d = \frac{-jC\sqrt{\varepsilon_t}}{2\pi f L} \frac{1 - \Gamma_m e^{2j\beta_t D}}{1 + \Gamma_m e^{2j\beta_t D}} \cot\left(\frac{2\pi f L \sqrt{\varepsilon_d}}{C}\right) \qquad \text{equation [2.6]}$$

- C: Wave velocity in free space
- f: Measuring frequency

The probe parameters *D* and *L* at each measuring frequency are needed to be known to evaluate the relative dielectric constant and loss factor of the test medium. These two variables are not directly measurable, since their existence is hypothetical. The determination of *D* and *L* is based on measuring reflection coefficient of two media standards (air and known liquid). Finally, the dielectric parameters of tested material can be obtained through a recursive flow chart (figure 2.9) by using these two standards with known dielectric values.
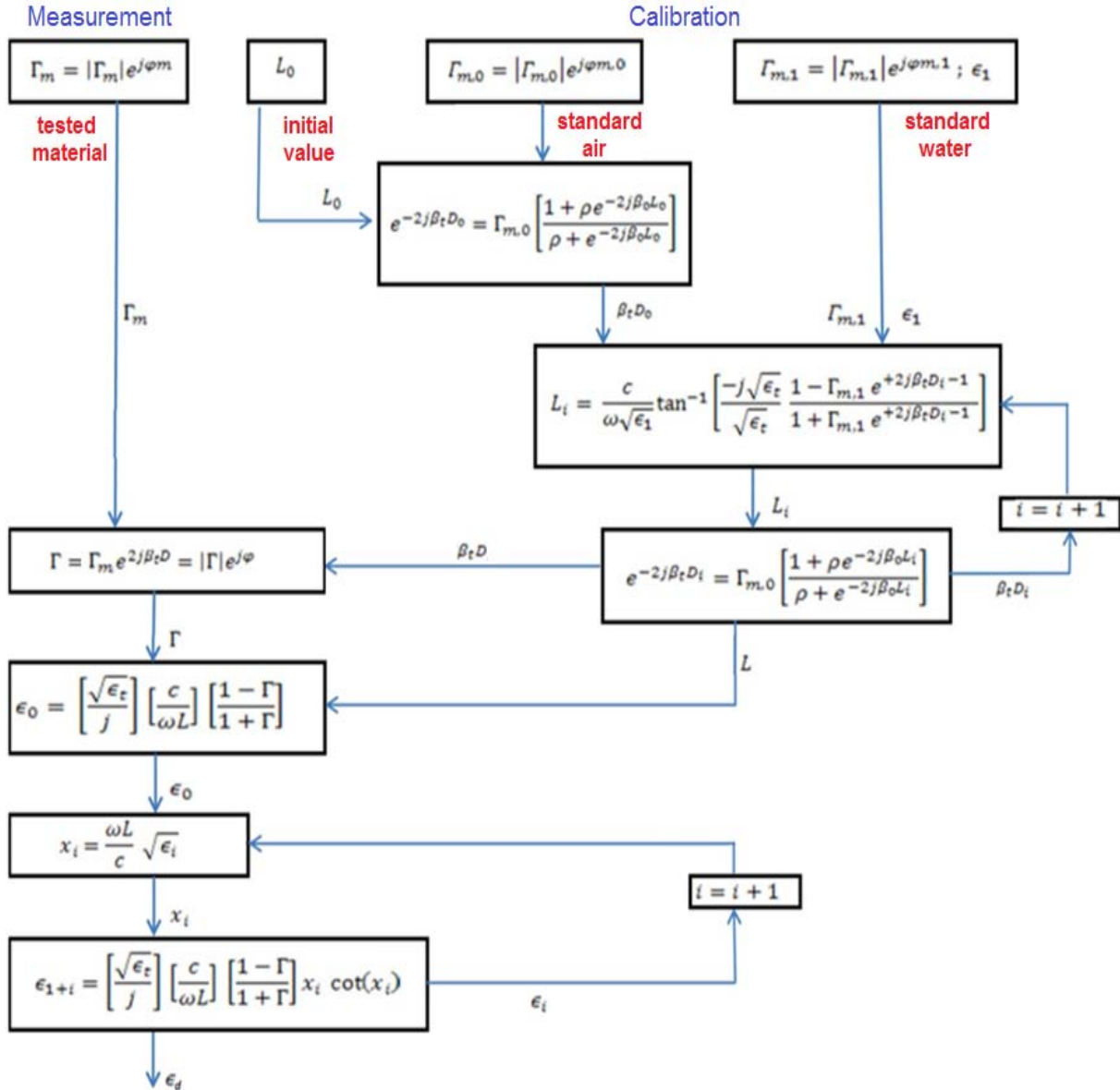
Figure 2.9: Flow chart of determination of dielectric parameters with virtual line model [55]

2.9 Dielectric characterization measurement system
The dielectric characterization measurement system is composed of four main parts:
- Vector network analyzer (VNA)–Anritsu MS2034A (50MHz–4GHz),
- Open–ended coaxial probe (1st method) or coaxial cable (2nd method),
- Heating tool–PROXXON MICRO Heat gun MH550,
- Digital multimeter with measuring temperature system–Meterman 33XR.
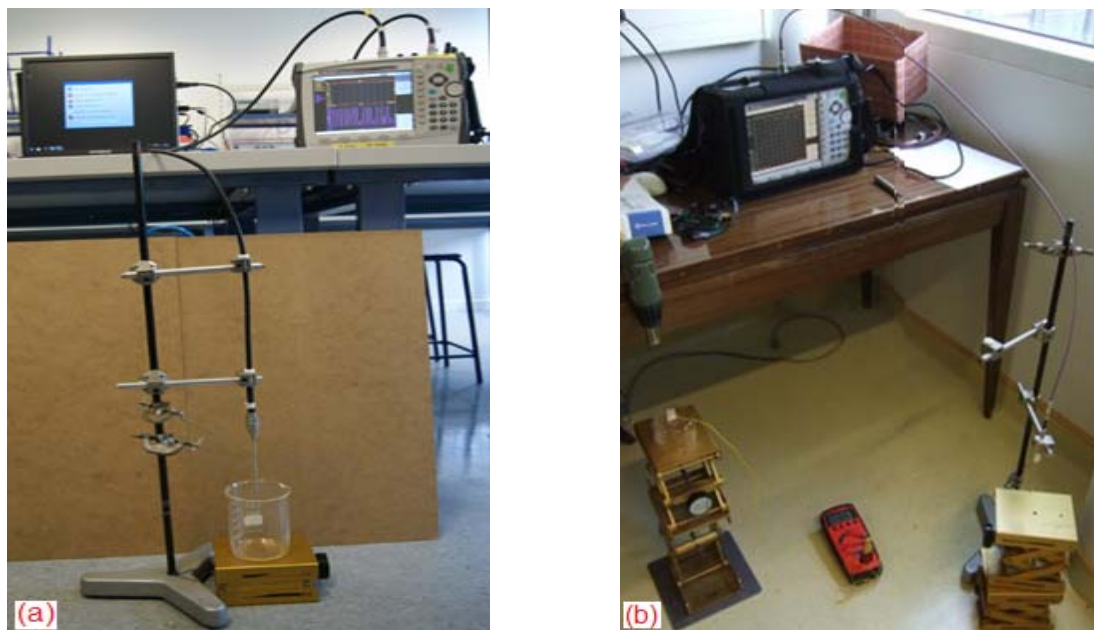
Figure 2.10: Dielectric characterization system for (a) liquid and (b) biological tissue measurements

The measured reflection coefficient S_{11} parameter of the sample is obtained by VNA. Some fundamental experimental rules should be respected for dielectric characterizations:

- It's better to start network analyzer a few hours before measurements to make sure the stablity of temperature in the frequency response,

- Calibration of the network analyzer should be carried out before measurement. The VNA Master offers FlexCal calibration mode of 1–Port and OSL (open/short/load) calibration method which reduces source match, directivity, and frequency response errors.

- Cleaning coaxial probe's or cable's extremity which is in contact with the sample with a volatile liquid (eg. isopropanol) after each measurement.

- For measurement of liquid, coaxial probe or cable should be immersed into the liquid in order to keep homogeneous condition (Figure 2.11).

- For measurement of semi-solids like biological tissue, coaxial probe's or cable's extremity should be in contact tightly with the measured material, and there should be no gap between them (Figure 2.11).

Figure 2.11: Coaxial probe's extremity should contact well with the measured materials

For measurement of S_{11} parameter in liquids, the coaxial probe or coaxial cable is immersed to a depth coressponding to 150ml of the total 300ml liquid (Figure 2.11). For measurement of S_{11} parameter of biological tissue samples, the extremity of coaxial probe or coaxial cable is in contact directly with the surface of tissue (Figure 2.11) and there should be no air gap between them. In order to obatin the accurate experimental results, all biological tissues are cut into the pieces with a diameter of about 4.5cm and thickness of 3~5mm (measured by a Mitutoya absolute digital caliper with two digits after the decimal point) for normalization.

The S_{11} parameter has been measured in the frequency range 50MHz–4GHz with 551 points and stored by VNA. All measured 551 values of S_{11} are processed by Matlab to obtain the physical parameters of tested materials. The parameters of dielectric dispersion (ε_∞, ε_s, τ, and α) of two standards and three known liquid materials vary with temperatures (Table 2.2). In order to compare the measued results and the literature values of known liquids, the corresponding literature values of them should be checked and used for each measurement. If the experimental and literature values are in correspondence with each other, then standard materials can be used to obtain the accurate results for tested materials.

Distilled water							Ethanol					
T (°C)	18	20	22	23	24	25	T (°C)	18	20	22	23	24	25
ε_s	81,12	80,40	79,62	79,23	78,84	78,45	ε_s	25,39	25,07	24,77	24,62	24,47	24,32
ε_∞	5,16	5,2	5,2	5,2	5,2	5,2	ε_∞	4,28	4,26	4,25	4,24	4,23	4,23
α	0	0	0	0	0	0	α	0	0	0	0	0	0
λ (cm)	1,91	1,78	1,69	1,65	1,61	1,57	λ (cm)	28,6	9,6	25,84	25,26	24,68	24,1

Methanol							Isopropanol					
T (°C)	18	20	22	23	24	25	T (°C)	18	20	22	23	24	25
ε_s	34,06	33,64	33,26	33,04	32,84	32,65	ε_s	19,54	19	19	19	19	19
ε_∞	5,74	5,70	5,66	5,64	5,62	5,6	ε_∞	3,55	3,2	3,20	3,2	3,2	3,2
α	0	0	0	0	0	0	α	0	0	0	0	0	0
λ (cm)	10,52	10	9,6	9,4	9,2	9	λ (cm)	72,5	55	55	55	55	55

Table 2.2: Parameters of dielectric dispersion (ε_∞, ε_s, α and λ) of standard and known liquids at different temperatures [56]

The ultimate aim of our study is to use only one microwave applicator to synchronously achieve two functions: diagnostics and hyperthermia. Each material has its own physical parameters such as complex permittivity and conductivity. By measuring these parameters, healthy and pathological human tissues can be distinguished, and then microwave hyperthermia can be carried out according to real therapeutic requirement. The characteristics of human tissue are also dependent of temperature variation. It is important to determine the changing characteristics with temperature. Besides the previous thin semi–rigid coaxial probe (figure 2.12), we have also considered and used the microwave hyperthermia applicator–a flexible coaxial cable of one meter (figure 2.13)–the Warrior cable of MegaPhase F520 with GrooveTube® Technology, for dielectric characterization experiments.

Two **methods** have been defined and used with two applicators for dielectric characterization measurements: **coaxial probe** (figure 2.12) and **coaxial cable** (figure 2.13).
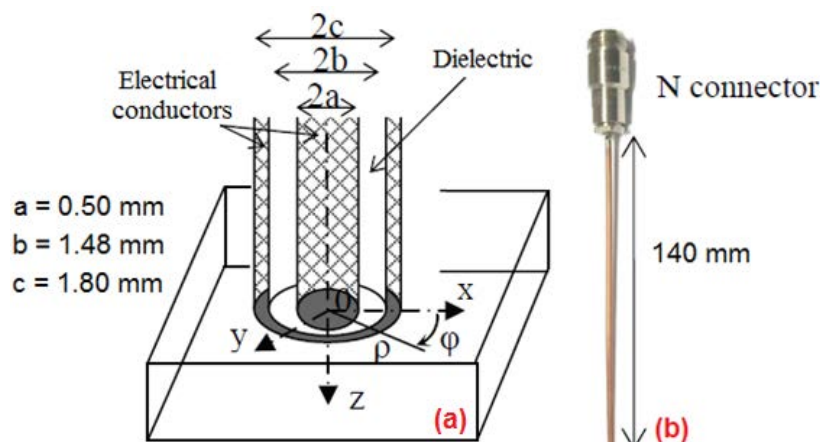
Figure 2.12: (a) Open-ended coaxial probe geometry, and (b) dielectric coaxial semi–rigid probe
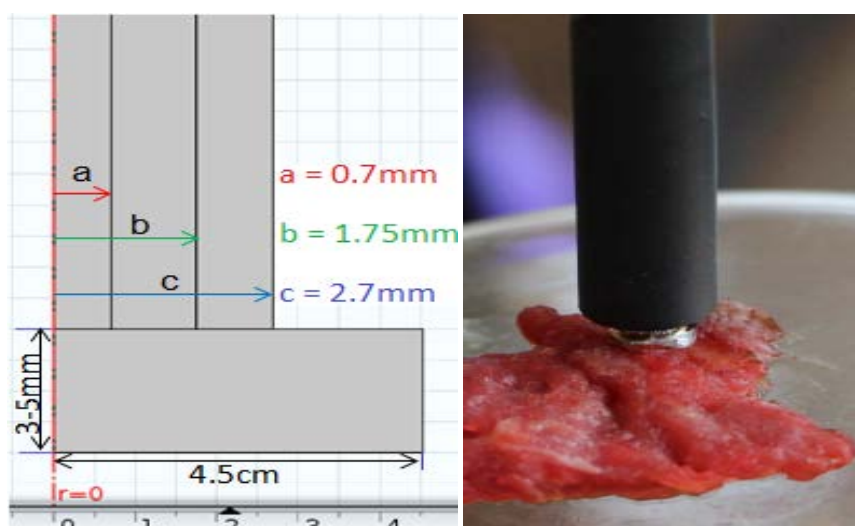
Figure 2.13: Flexible Warrior cable of Megaphase F520 with GrooveTube® Technology

There are **two protocols** for dielectric characterization measurements:
1st: all the experimental measurements of fresh raw biological tissue samples were carried out at ambient temperature after the testing experiments of known liquids.
- two standards: air and distilled water (24°C),
- three tested liquids: ethanol, methanol, and isopropanol with known literature dielectric values (24°C),

2nd: for all biological tissues:(pork muscle, beef muscle, chicken, pork liver, and calf's liver), the physical parameters were measured as a function of temperature from 20°C to 50°C with a step change of 5°C. All the fresh raw biological tissue samples are placed on an adjustable height metal bench under the fixed electric heat gun and heated by it. The temperatures are supervised by the Digital multimeter. The frequency band of VNA varied from 50 MHz to 4 GHz (measuring 551 data points of reflection parameter S_{11}).

2.10 Dielectric characterization by the semi–rigid coaxial probe

It's important to use a good quality cable between the VNA and the semi–rigid coaxial probe and avoid any movement during the measurements. For each set of experimental results, $\varepsilon'(f)$ and $\varepsilon''(f)$ of the complex permittivity, the electrical conductivity $\sigma(f)$ and the loss angle (tanδ), all as a function of frequency are presented and compared with the literature data. Besides the experimental Cole–Cole diagram has been shown and compared with literature values. All obatined experimental results are kept with two digits after the decimal point.

2.10.1 Experimental results for standard materials and known liquids:

a) Experimental results of standard – **air** (ambient T=24°C)

At ambient temperature (24°C), the blue experimental curves of $\varepsilon'(f)$, $\varepsilon''(f)$, $\sigma(f)$, tanδ and Cole–Cole diagram for air are shown in figure 2.14. For comparison, the red curves show the literature values ε'_{air} = 1 and ε''_{air} = 0 for all frequencies, so the Cole–Cole diagram for air is theoretically a point. Experimentally, there is a resonance at the high frequency band because of the open–ended extremity of the coaxial probe.

Figure 2.14: Dielectric characterization of air at ambient temperature (24°C)

b) Experimental results of standard – **distilled water** (ambient T=24°C)
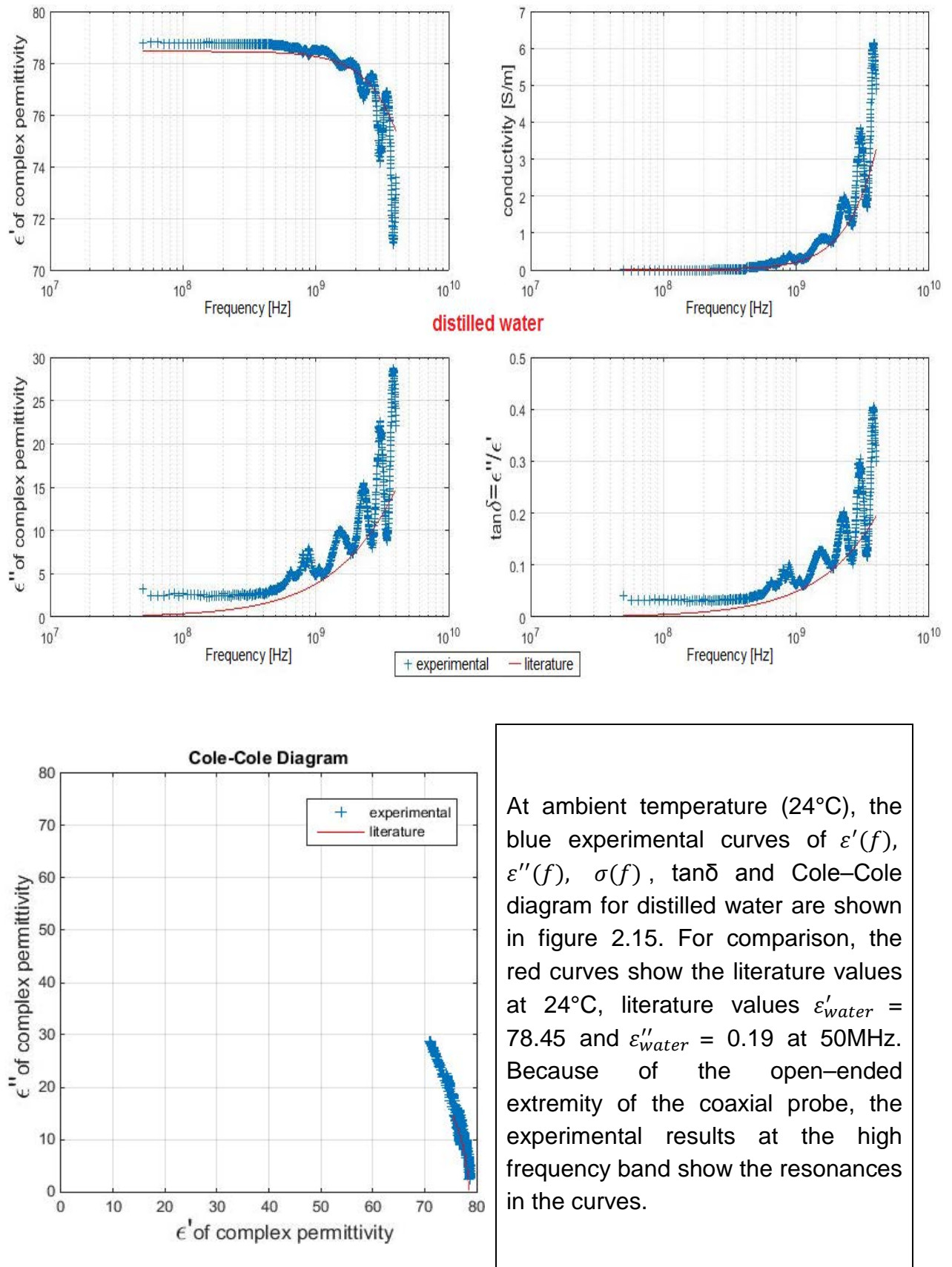
distilled water

+ experimental   — literature

At ambient temperature (24°C), the blue experimental curves of $\varepsilon'(f)$, $\varepsilon''(f)$, $\sigma(f)$, tanδ and Cole–Cole diagram for distilled water are shown in figure 2.15. For comparison, the red curves show the literature values at 24°C, literature values ε'_{water} = 78.45 and ε''_{water} = 0.19 at 50MHz. Because of the open–ended extremity of the coaxial probe, the experimental results at the high frequency band show the resonances in the curves.

Figure 2.15: Dielectric characterization of distilled water at ambient temperature (24°C)

c) Experimental results of known liquid – **ethanol** (ambient T=24°C)
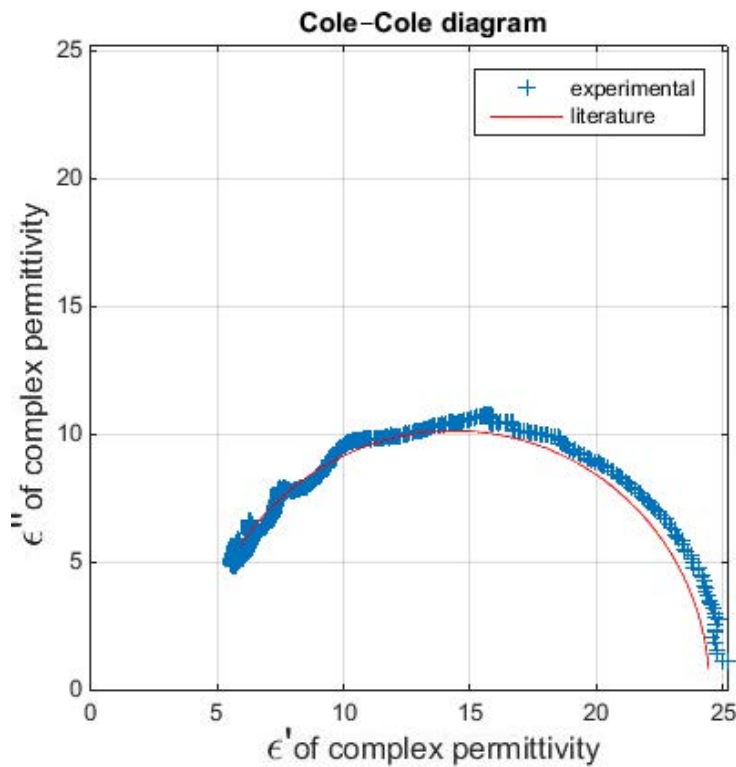
ethanol

+ experimental — literature

Cole–Cole diagram

At ambient temperature (24°C), the blue experimental curves of $\varepsilon'(f)$, $\varepsilon''(f)$, $\sigma(f)$, tanδ and Cole–Cole diagram for ethanol are shown in figure 2.16.

For comparison, the red curves show the literature values of ethanol at 24°C, $\varepsilon'_{ethanol}$ = 24.43 and $\varepsilon''_{ethanol}$ = 0.83 at 50MHz. $\varepsilon''(f)$ increases first and decreases from its critical frequency (f_c). There is a little difference between literature f_c and experimental f_c, because λ_c (f) for literature values varies from 27cm at 20°C to 12.2cm at 30°C. Its exact value for 24°C is N/A.
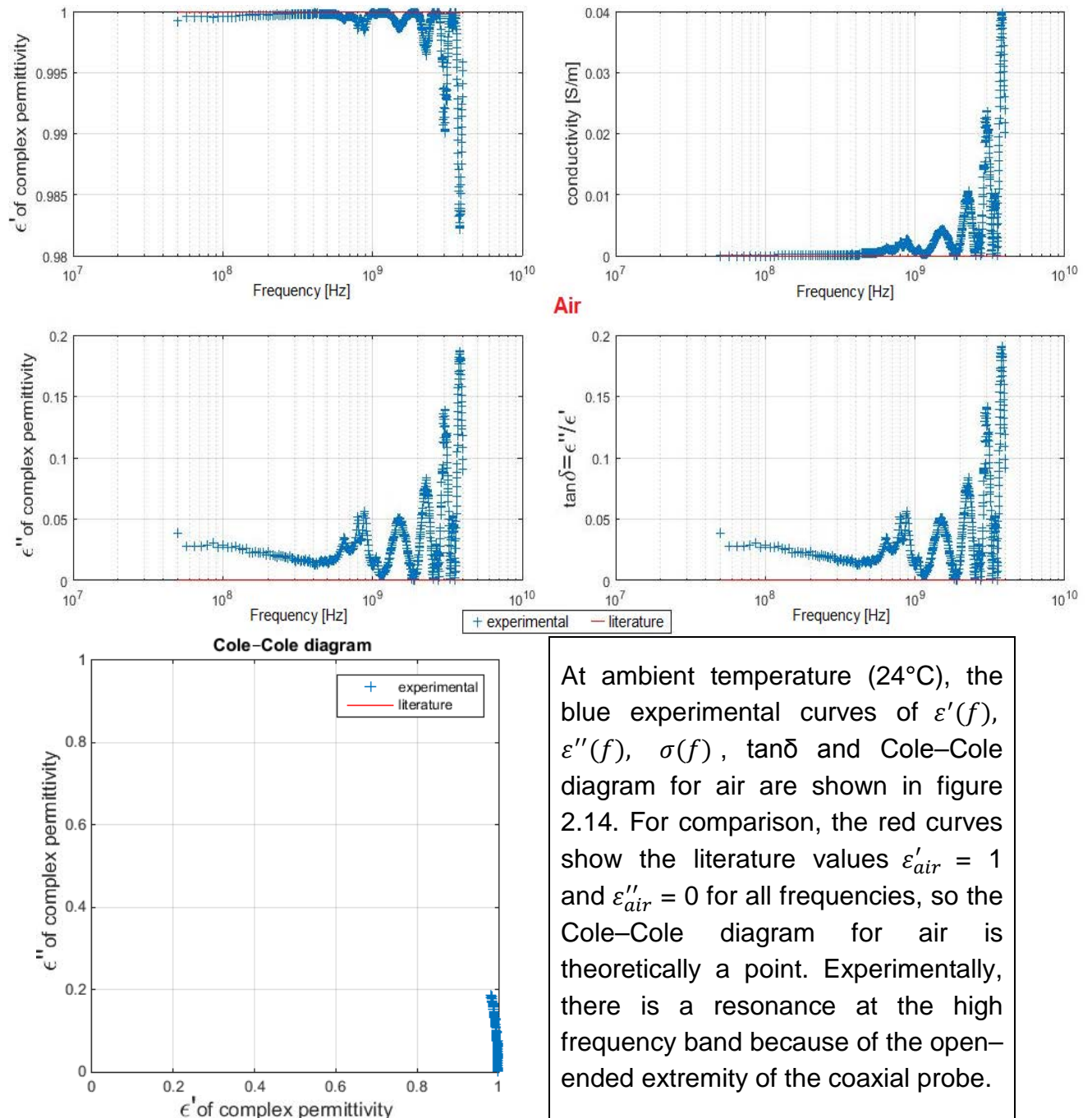
Figure 2.16: Dielectric characterization of ethanol at ambient temperature (24°C)

d) Experimental results of known liquid – **methanol** (ambient T=24°C)

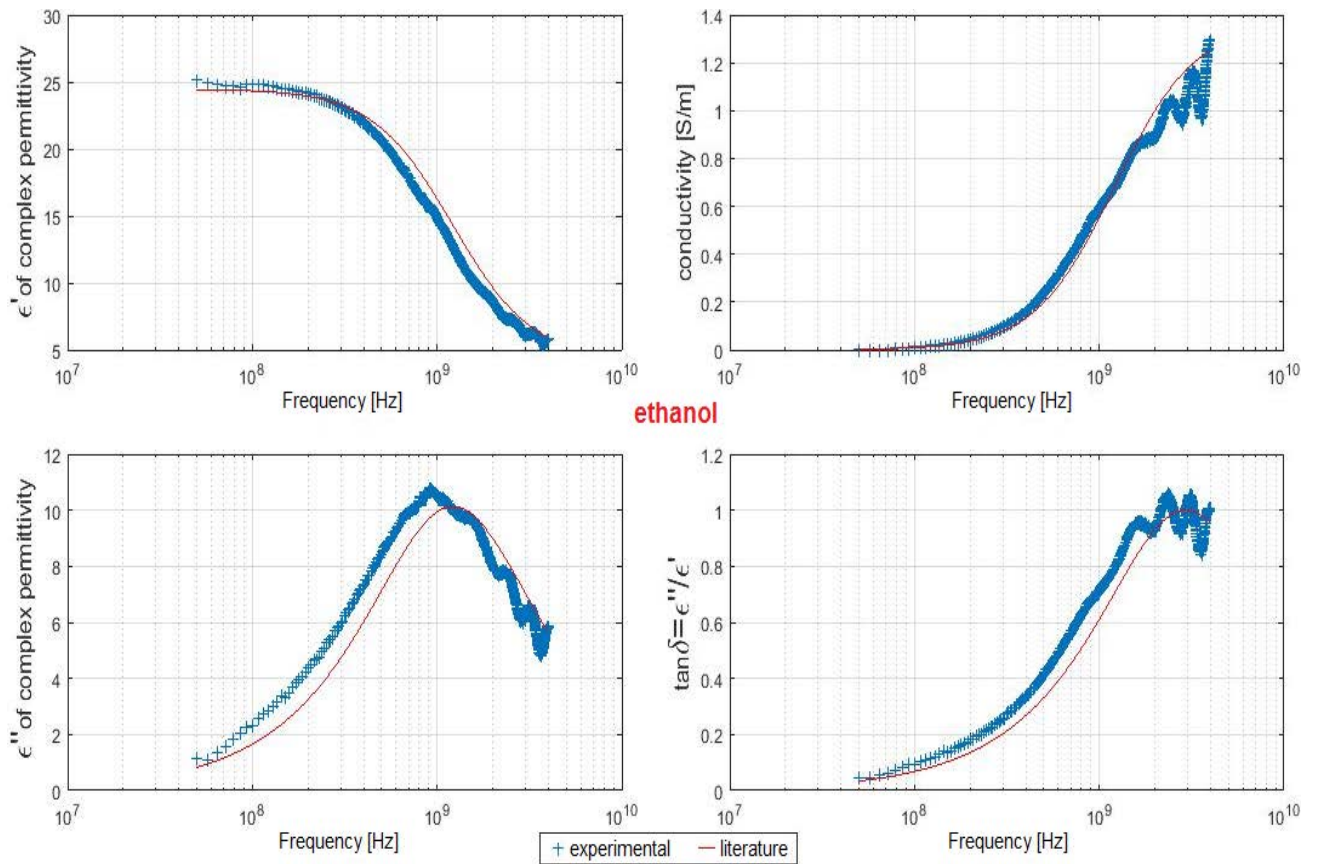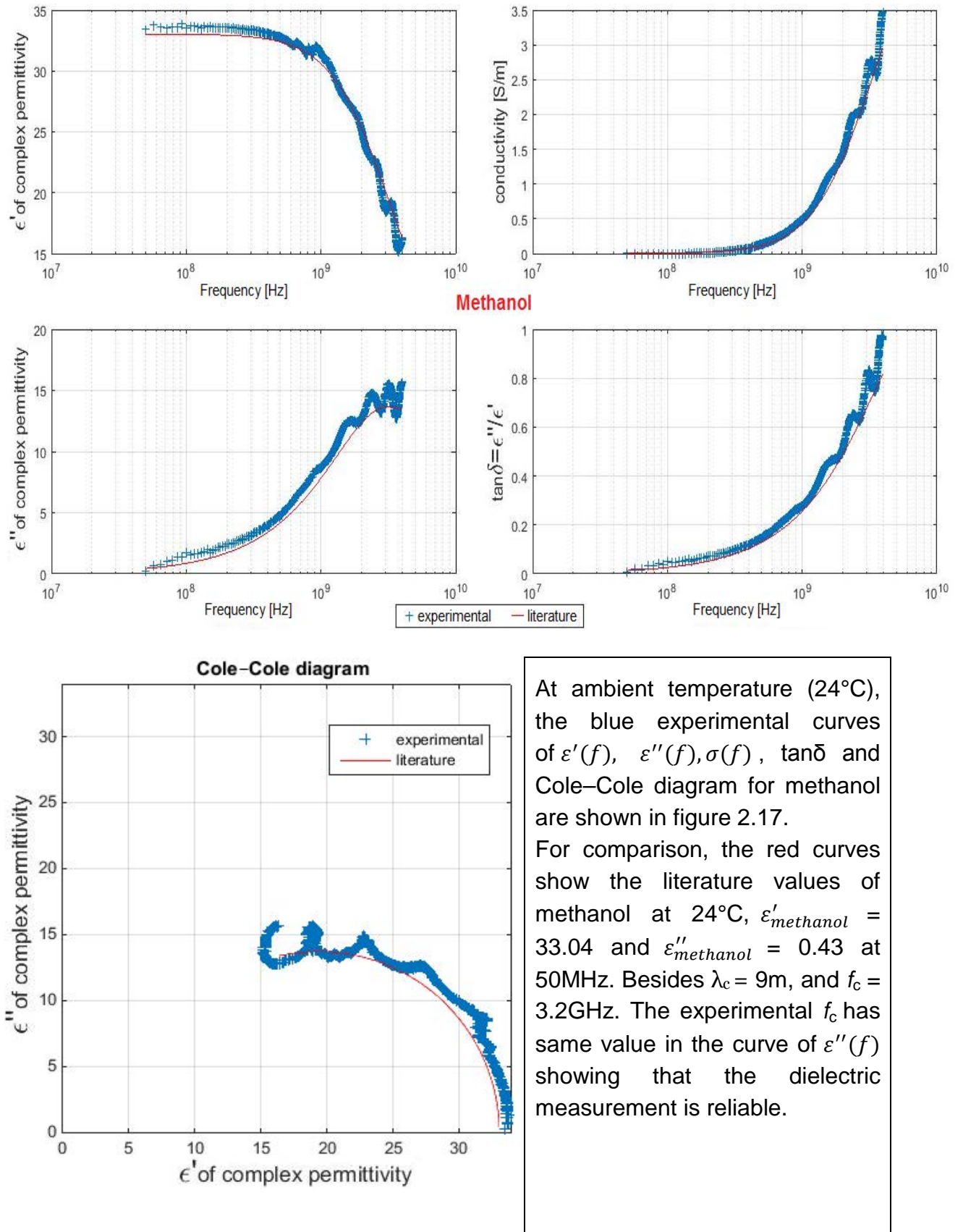Figure 2.17: Dielectric characterization of methanol at ambient temperature (24°C)

At ambient temperature (24°C), the blue experimental curves of $\varepsilon'(f)$, $\varepsilon''(f), \sigma(f)$, tanδ and Cole−Cole diagram for methanol are shown in figure 2.17.

For comparison, the red curves show the literature values of methanol at 24°C, $\varepsilon'_{methanol}$ = 33.04 and $\varepsilon''_{methanol}$ = 0.43 at 50MHz. Besides λ_c = 9m, and f_c = 3.2GHz. The experimental f_c has same value in the curve of $\varepsilon''(f)$ showing that the dielectric measurement is reliable.

e) Experimental results of known liquid – **isopropanol** (ambient T=24°C)

For isopropanol of 24°C, the blue experimental curves of $\varepsilon'(f)$, $\varepsilon''(f)$, $\sigma(f)$, tanδ, and Cole–Cole diagram correspond well with the red curves of literature values (figure 2.18). Literature values at 24°C: $\varepsilon'_{isopropanol}$ = 18.87, $\varepsilon''_{isopropanol}$ = 1.44 at 50MHz. λ_c = 55m, and f_c = 0.54GHz. The experimental f_c =0.46GHz has a little difference with the theoretical one in the curve of $\varepsilon''(f)$ because of a phase shift, but the dielectric measurement is still reliable. Therefore measurement for biological tissues can be carried out.
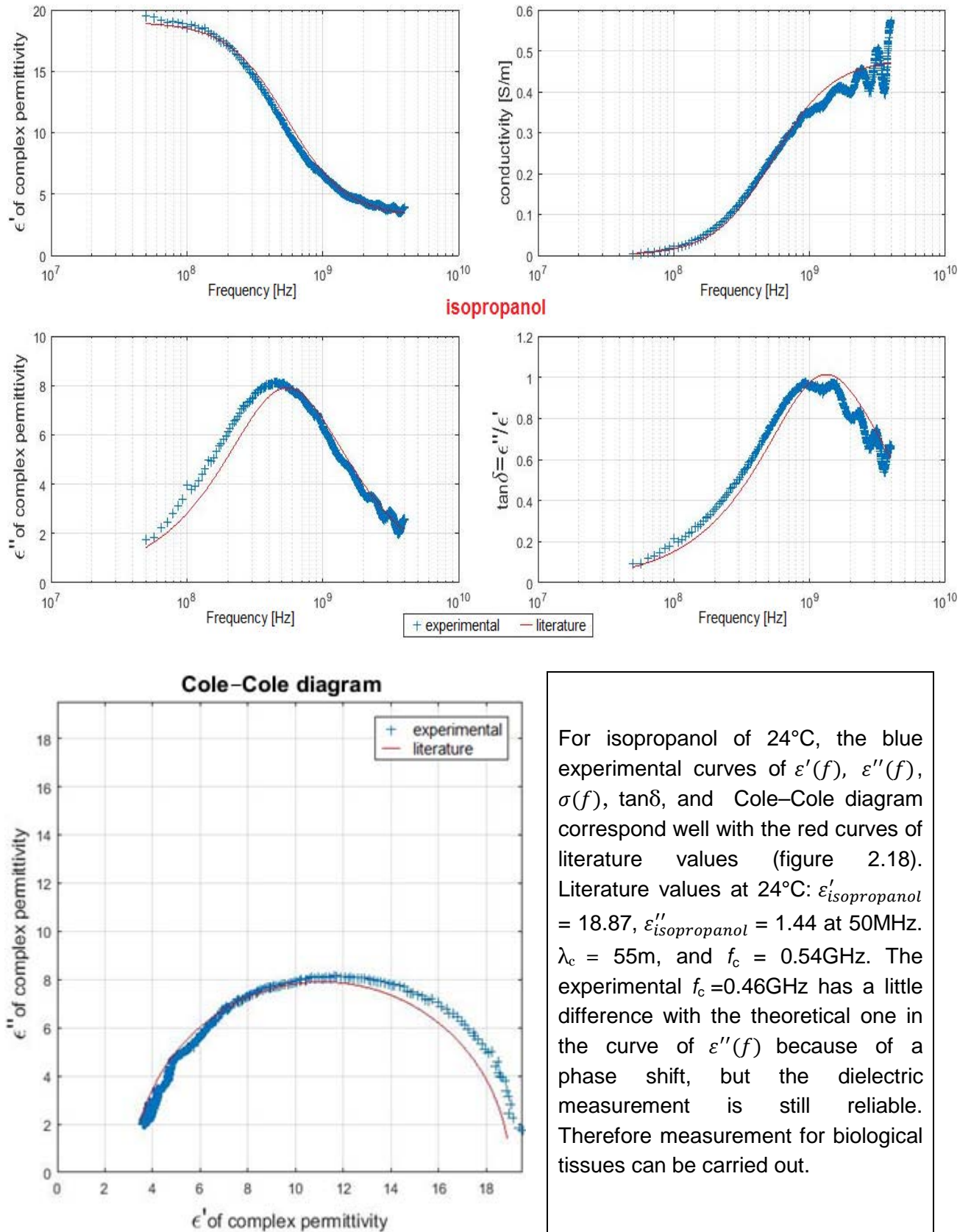
Figure 2.18: Dielectric characterization of isopropanol at ambient temperature (24°C)

2.10.2 Experimental results for tested biological tissues:

For each set of experimental results, $\varepsilon'(f)$ and $\varepsilon''(f)$ of the complex permittivity, the electrical conductivity $\sigma(f)$, the loss angle tanδ, $\varepsilon'(f)$ and $\sigma(f)$ all as a function of frequency are presented. The thicknesses of all samples are measured by a Mitutoya absolute digital caliper with two digits after the decimal point.

1st protocol: natural biological tissues (20°C)

Muscle

a) Experimental results of **pork** (thickness: 3.22mm)

Pork muscle

For natural pork muscle of 20°C, both $\varepsilon'(f)$ and $\varepsilon''(f)$ decrease. $\sigma(f)$ increases (figure 2.19).

At 2.45GHz,

ε'_{pork} = 49.53,
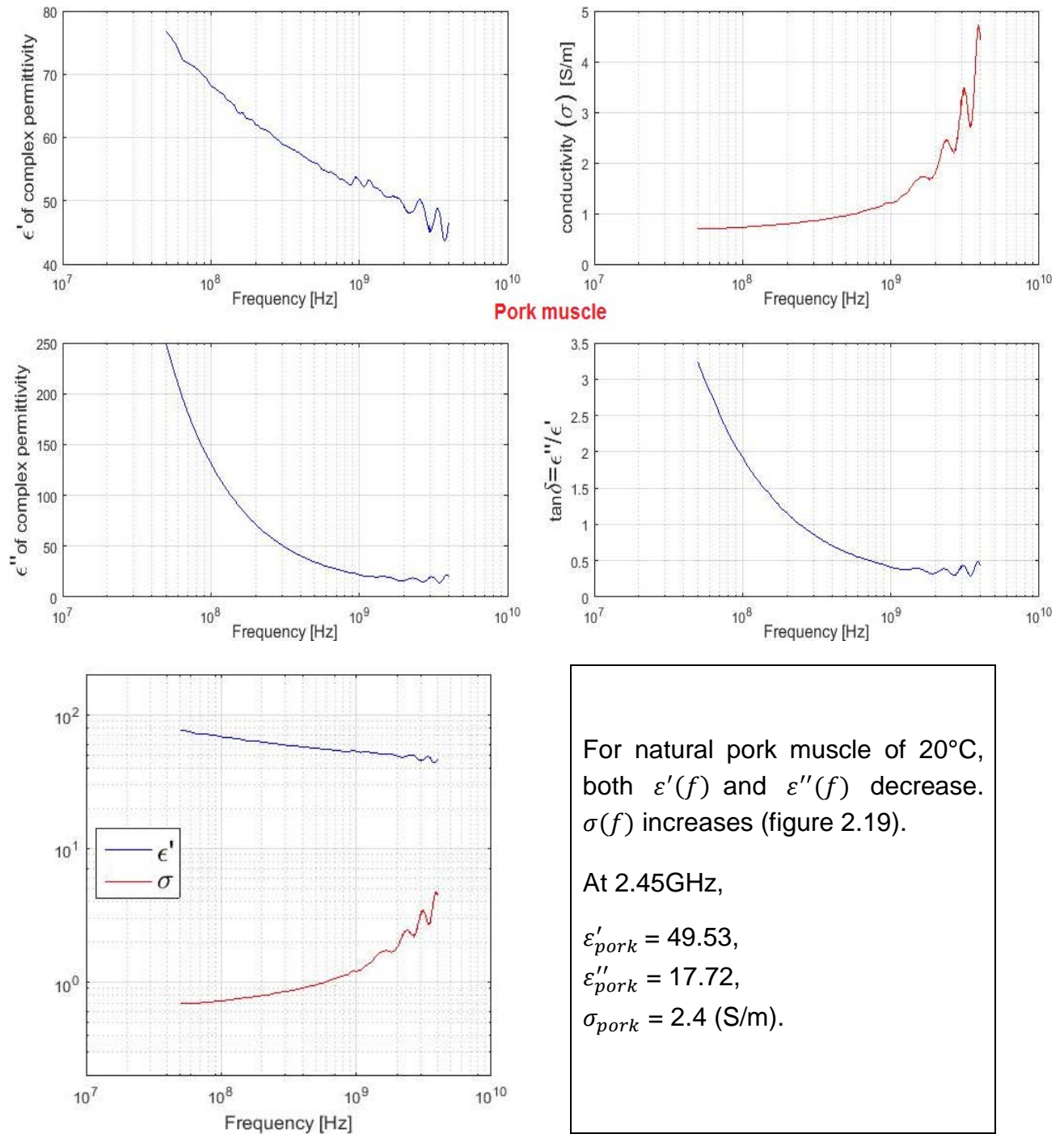ε''_{pork} = 17.72,
σ_{pork} = 2.4 (S/m).

Figure 2.19: Dielectric characterization of pork (thickness: 3.22mm) of 20°C

b) Experimental results of **beef** (thickness: 3.53mm)

beef muscle

For natural beef muscle of 20°C, both $\varepsilon'(f)$ and $\varepsilon''(f)$ decreas. $\sigma(f)$ increases (figure 2.20).

At 2.45GHz,

ε'_{beef} = 49.99,
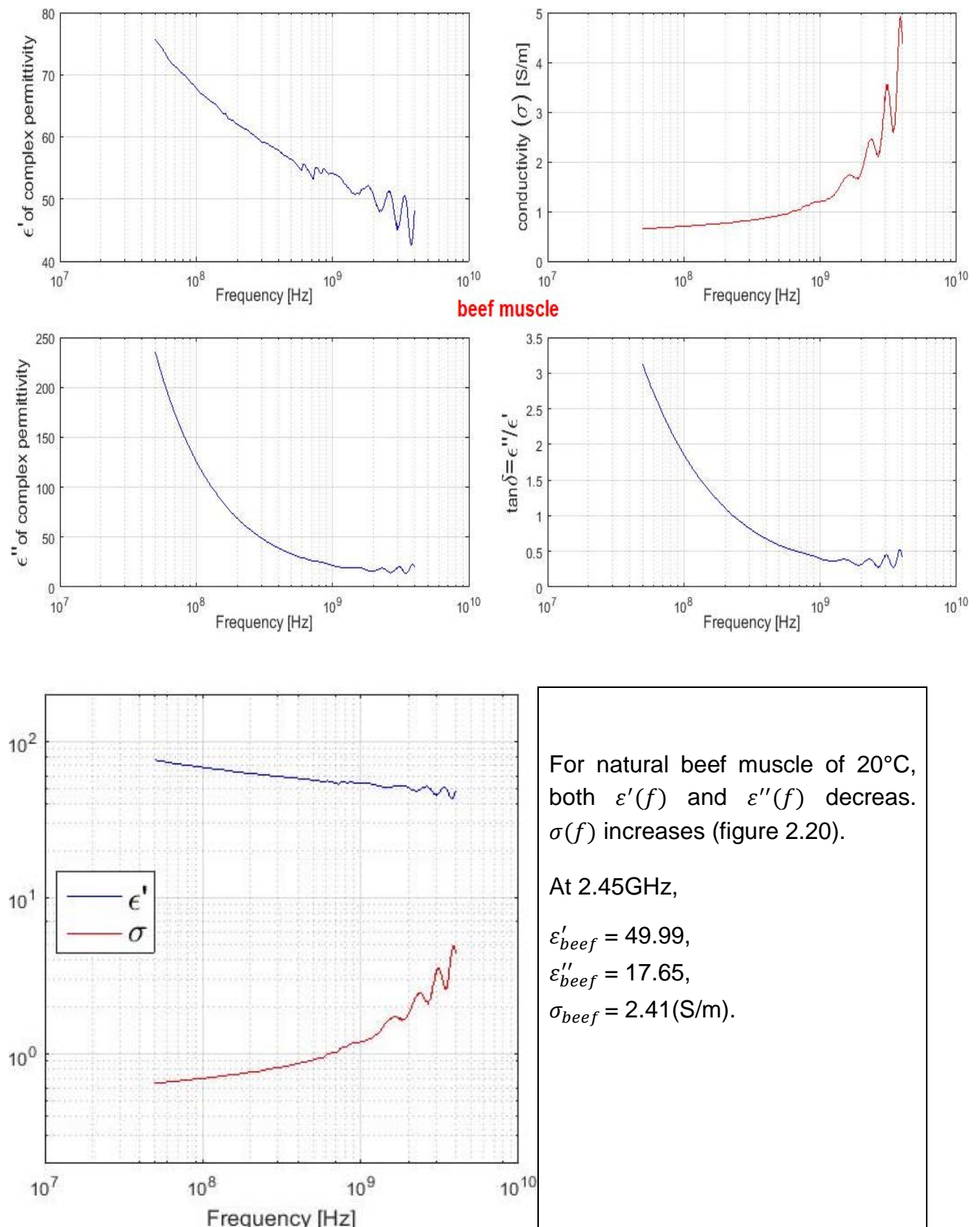ε''_{beef} = 17.65,
σ_{beef} = 2.41(S/m).

Figure 2.20: Dielectric characterization of beef (thickness: 3.53mm) of 20°C

c) Experimental results of **chicken** (thickness: 3.52mm)

For natural chicken muscle of 20°C, both $\varepsilon'(f)$ and $\varepsilon''(f)$ decrease. $\sigma(f)$ increases (figure 2.21).

At 2.45GHz,

$\varepsilon'_{chicken}$ = 49.97,
$\varepsilon''_{chicken}$ = 18.27,
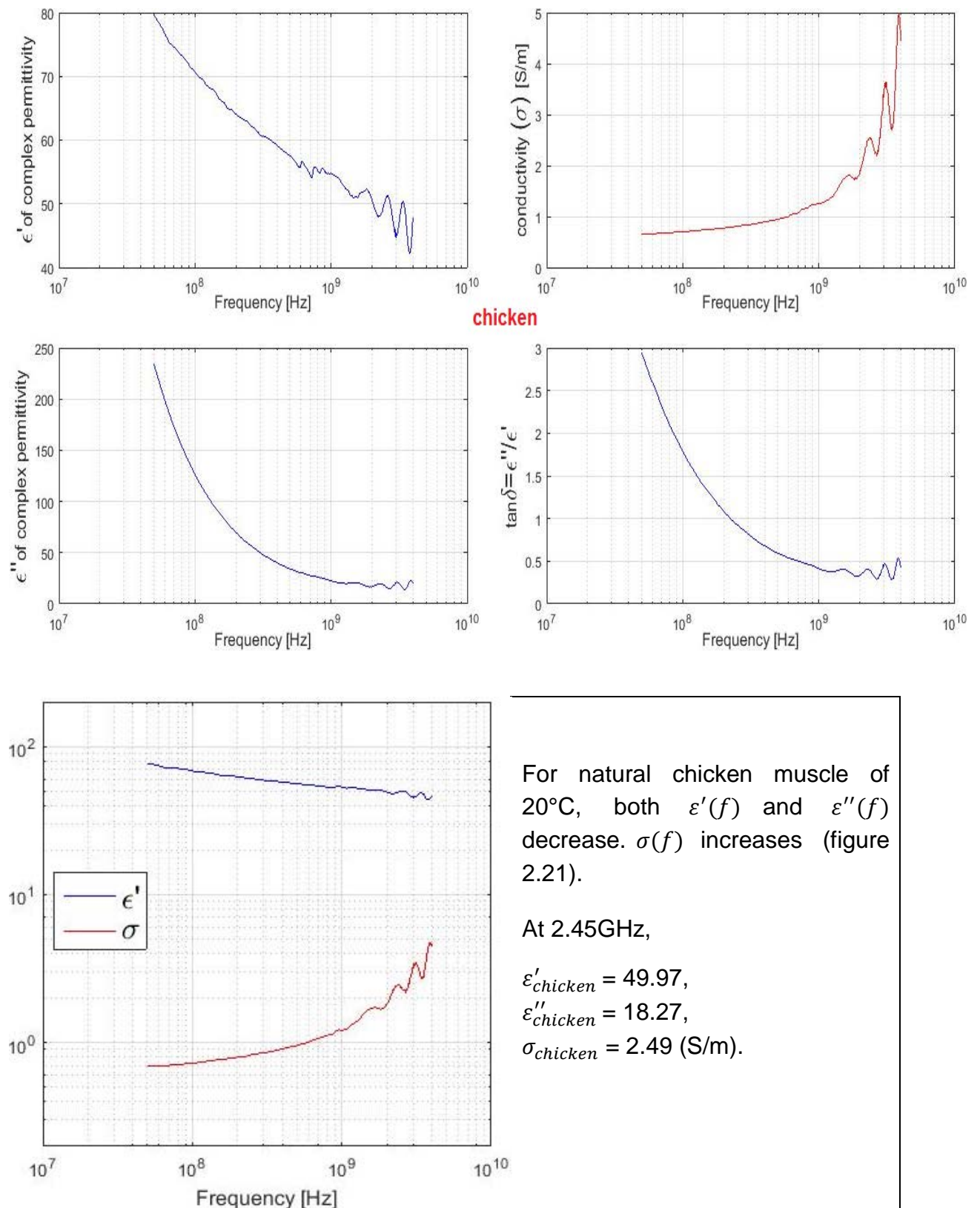$\sigma_{chicken}$ = 2.49 (S/m).

Figure 2.21: Dielectric characterization of chicken (thickness: 3.52mm) of 20°C

Liver

d) Experimental results of **pork liver** (thickness: 4.48mm)

For pork liver of 20°C, both $\varepsilon'(f)$ and $\varepsilon''(f)$ decrease and $\sigma(f)$ increases (figure 2.22).

At 2.45GHz,

$\varepsilon'_{pork\ liver}$ = 44.68,
$\varepsilon''_{pork\ liver}$ = 13.83,
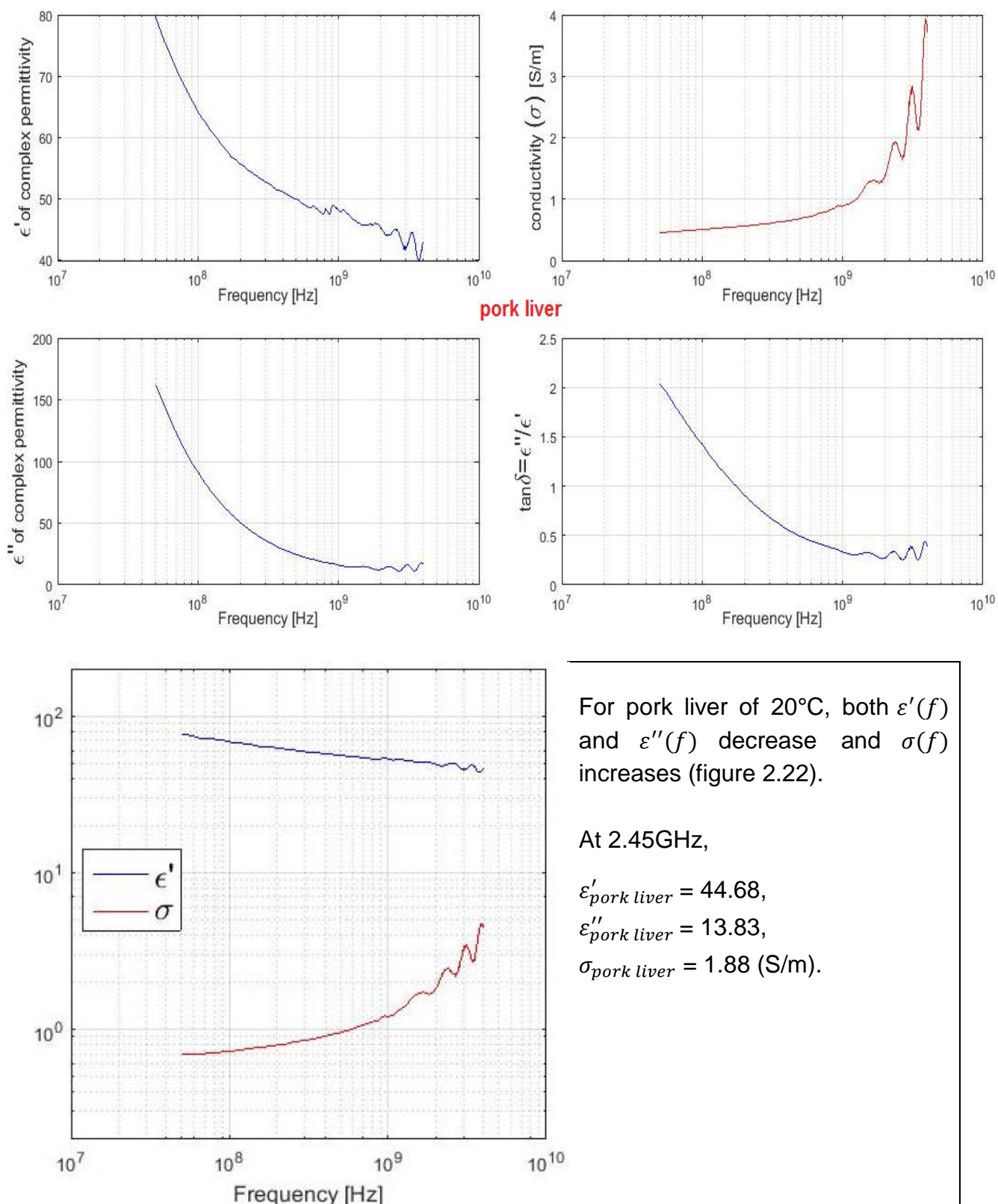$\sigma_{pork\ liver}$ = 1.88 (S/m).

Figure 2.22: Dielectric characterization of pork liver (thickness: 4.48mm) of 20°C

e) Experimental results of **calf's liver** (thickness: 4.52mm)

For natural calf's liver of 20°C, both $\varepsilon'(f)$ and $\varepsilon''(f)$ decrease. $\sigma(f)$ increases (figure 2.22).

At 2.45GHz,

$\varepsilon'_{calf's\ liver}$ = 47.24,

$\varepsilon'_{calf's\ liver}$ = 16.12,

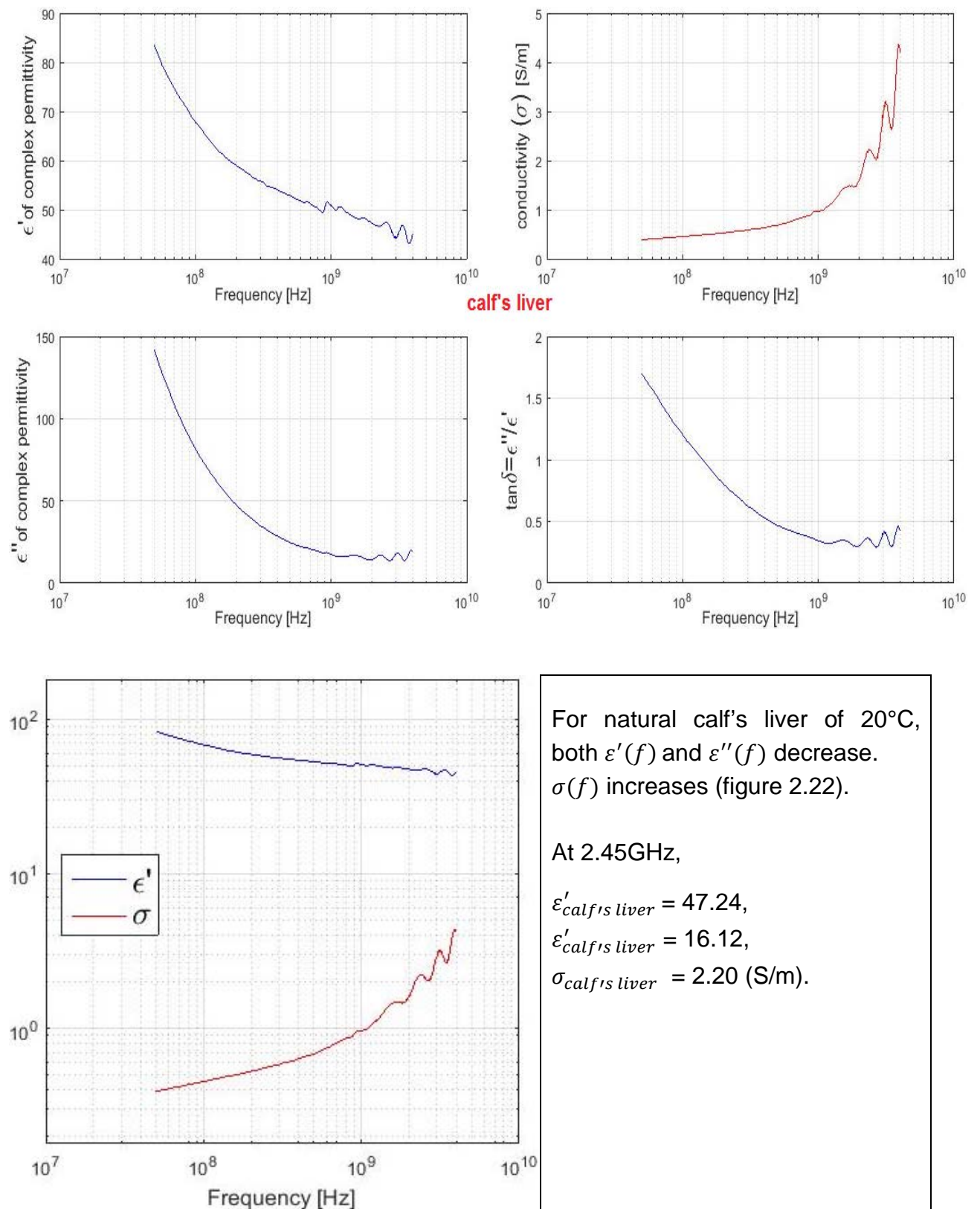$\sigma_{calf's\ liver}$ = 2.20 (S/m).

Figure 2.23: Dielectric characterization of calf's liver (thickness: 4.52mm) of 20°C

Comparisons among **five different raw biological tissues** (thicknesses: 3~5mm):
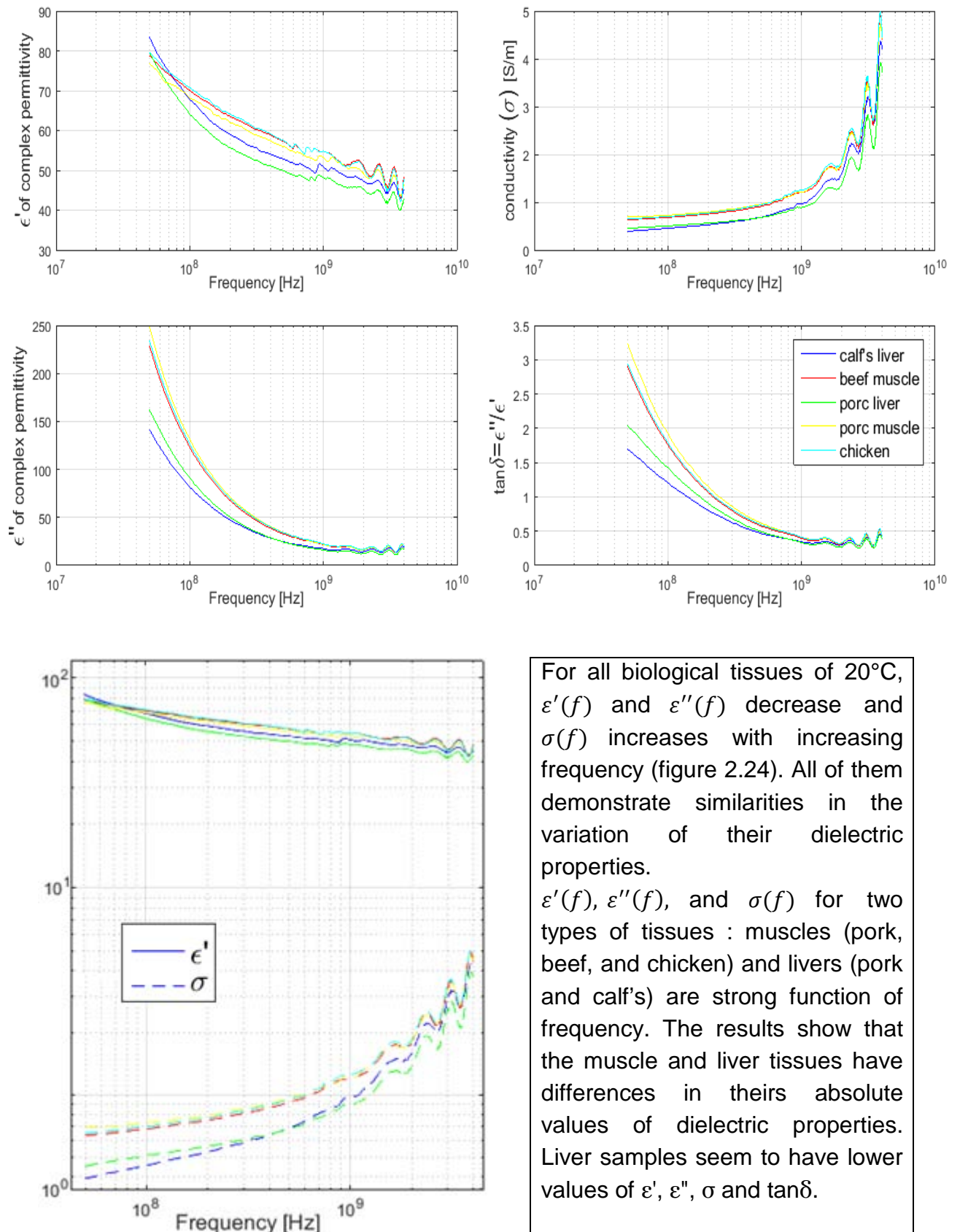

For all biological tissues of 20°C, $\varepsilon'(f)$ and $\varepsilon''(f)$ decrease and $\sigma(f)$ increases with increasing frequency (figure 2.24). All of them demonstrate similarities in the variation of their dielectric properties.

$\varepsilon'(f)$, $\varepsilon''(f)$, and $\sigma(f)$ for two types of tissues : muscles (pork, beef, and chicken) and livers (pork and calf's) are strong function of frequency. The results show that the muscle and liver tissues have differences in theirs absolute values of dielectric properties. Liver samples seem to have lower values of ε', ε", σ and tanδ.

Figure 2.24: Comparisons of dielectric properties among five raw natural biological tissues of 20°C
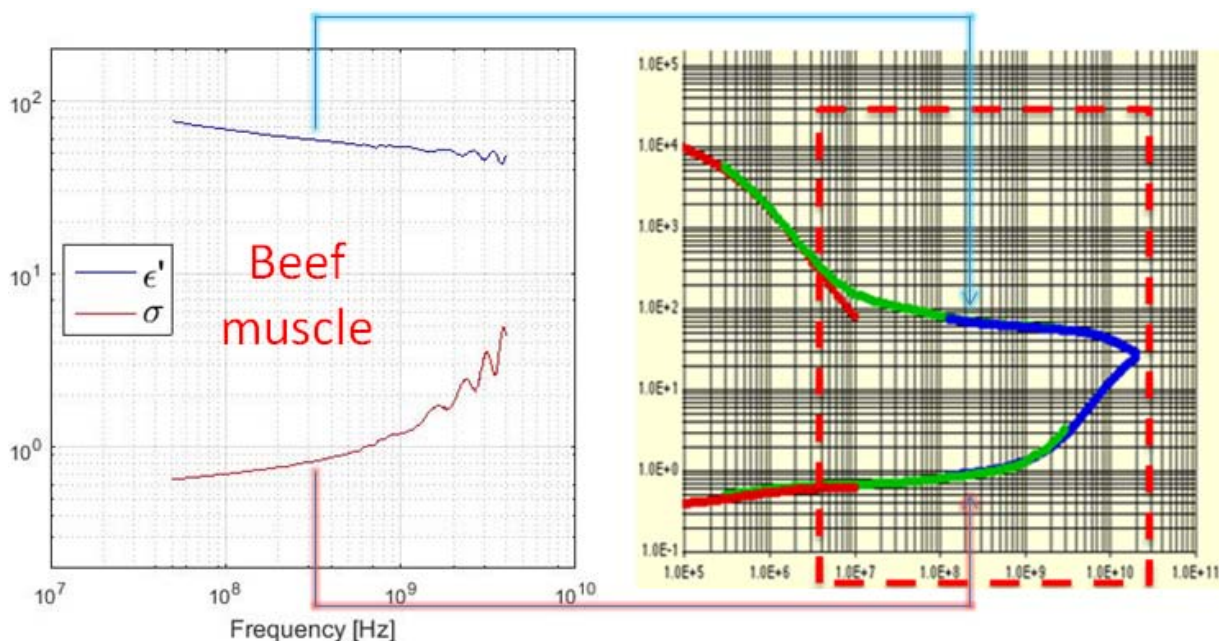
Figure 2.25: Comparisons for ε' (*f*) and σ (*f*) of beef muscle between experimental results (left) and those of literature (right) [57]
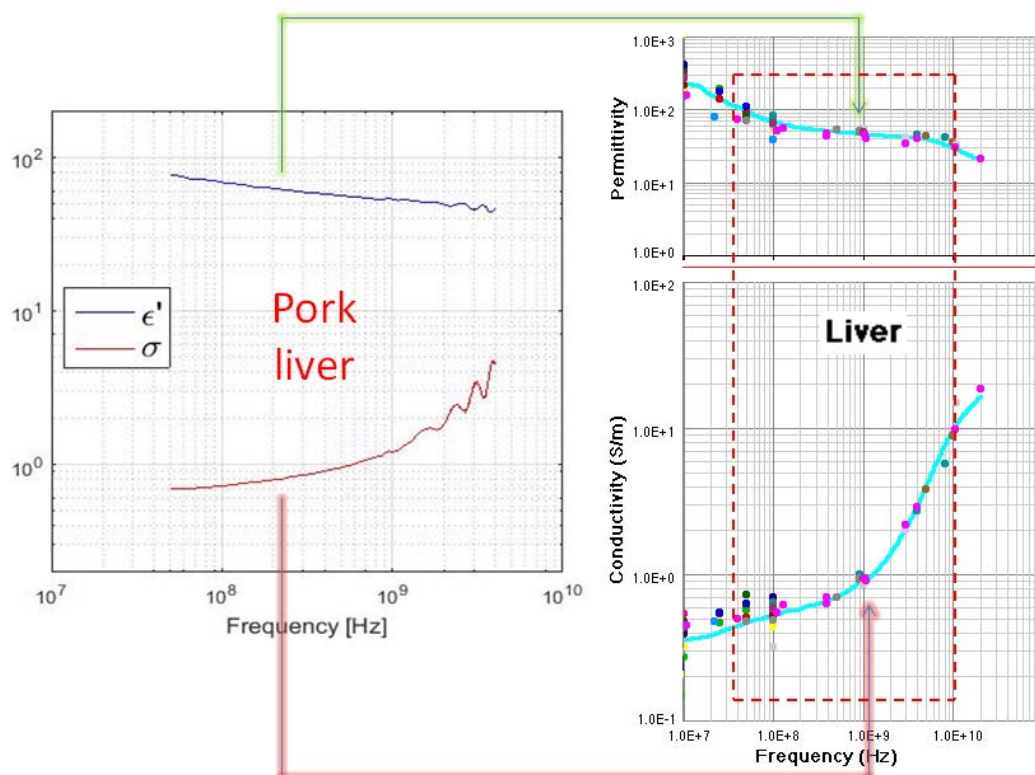

Figure 2.26: Comparisons for ε' (*f*) and σ (*f*) of pork liver between experimental results (left) and those of literature (right) [57]

Experimental results obtained by coaxial probe (e.g. beef muscle and pork liver) of raw natural biological tissues (20°C) correlate well with other literature values (figures 2.25 and 2.26).

2nd protocol: Dielectric characterization as a function of temperature (20°C to 50°C)

In order to study the dielectric properties as a function of temperature, all the biological tissues of two types (muscle and liver) have been heated by the heat gun from 20°C to 50°C with a step change of 5°C. Dielectric properties of these two different categories of animal biological tissues with different thickness have been characterized at each temperature. The results of ε' of complex permittivity (T), ε'' of complex permittivity (T), conductivity–σ (T) for muscle samples (pork, beef and chicken) and liver samples (pork and calf's) are presented and compared below.

Muscle samples

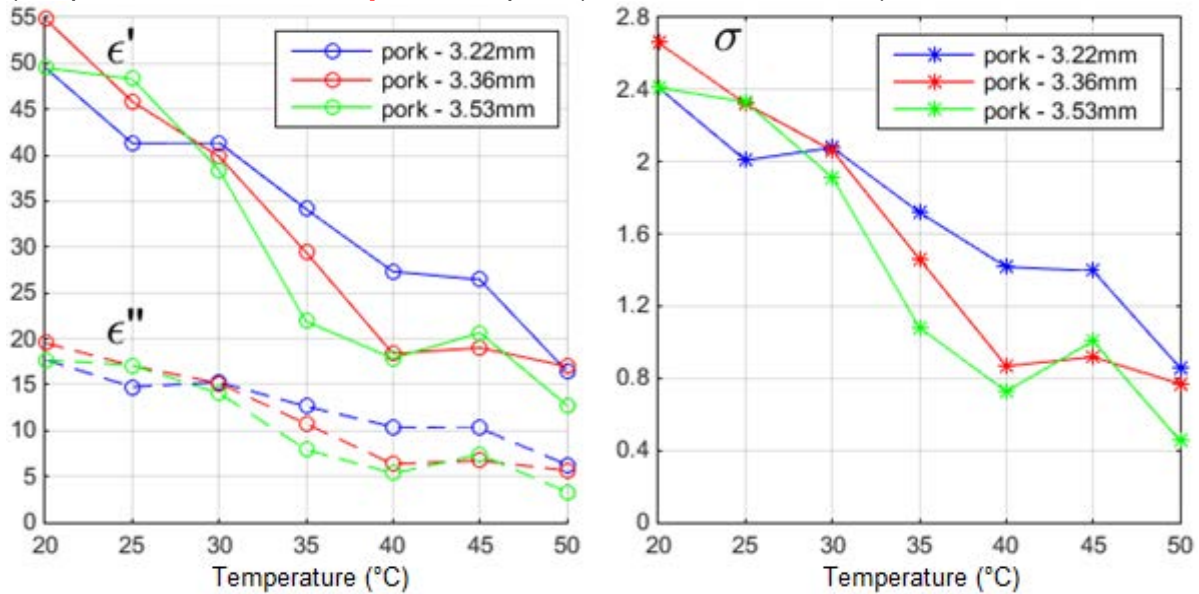a) Experimental results of **pork** samples (thicknesses: 3~4mm):

Figure 2.27: Comparisons among three pork samples with different thickness characterized as a function of temperature between 20 and 50 °C

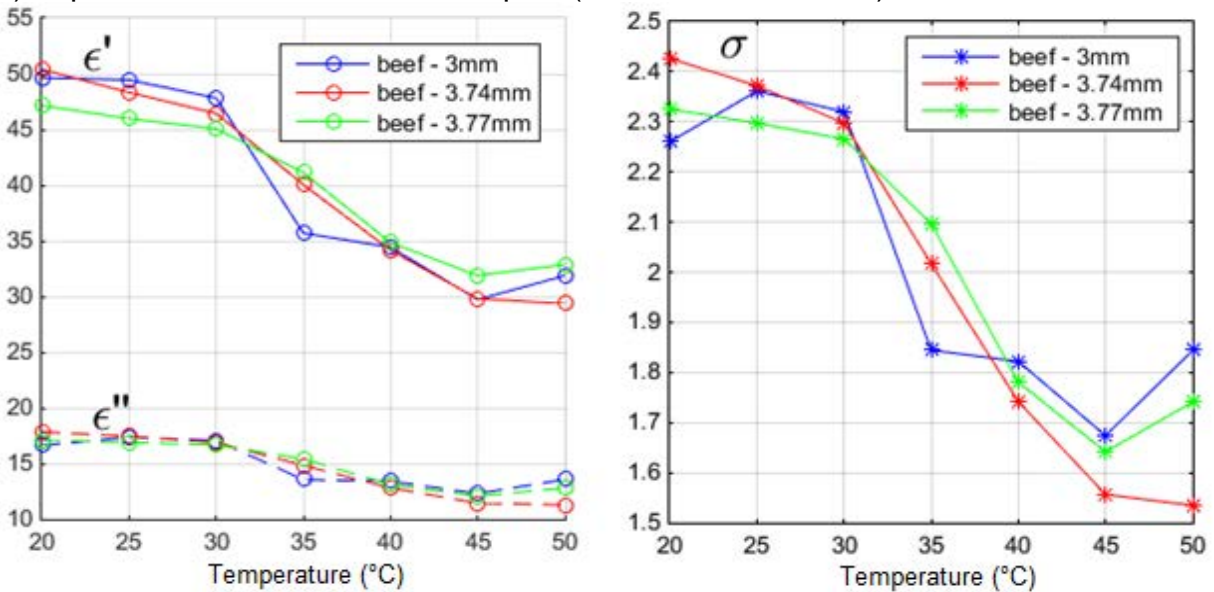b) Experimental results of **beef** samples (thicknesses: 3~4mm):

Figure 2.28: Comparisons among three beef samples with different thickness characterized as a function of temperature between 20 and 50 °C

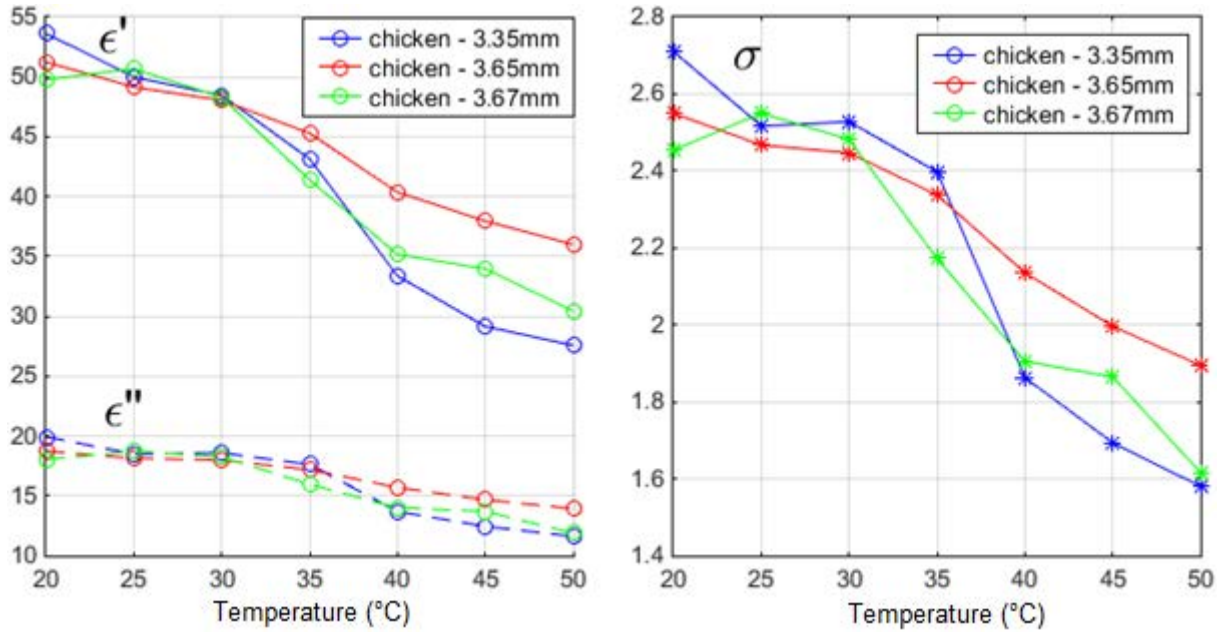c) Experimental results of **chicken** samples (thicknesses: 3~4mm):

Figure 2.29: Comparisons among three chicken samples with different thickness characterized as a function of temperature between 20 and 50 °C

Liver samples

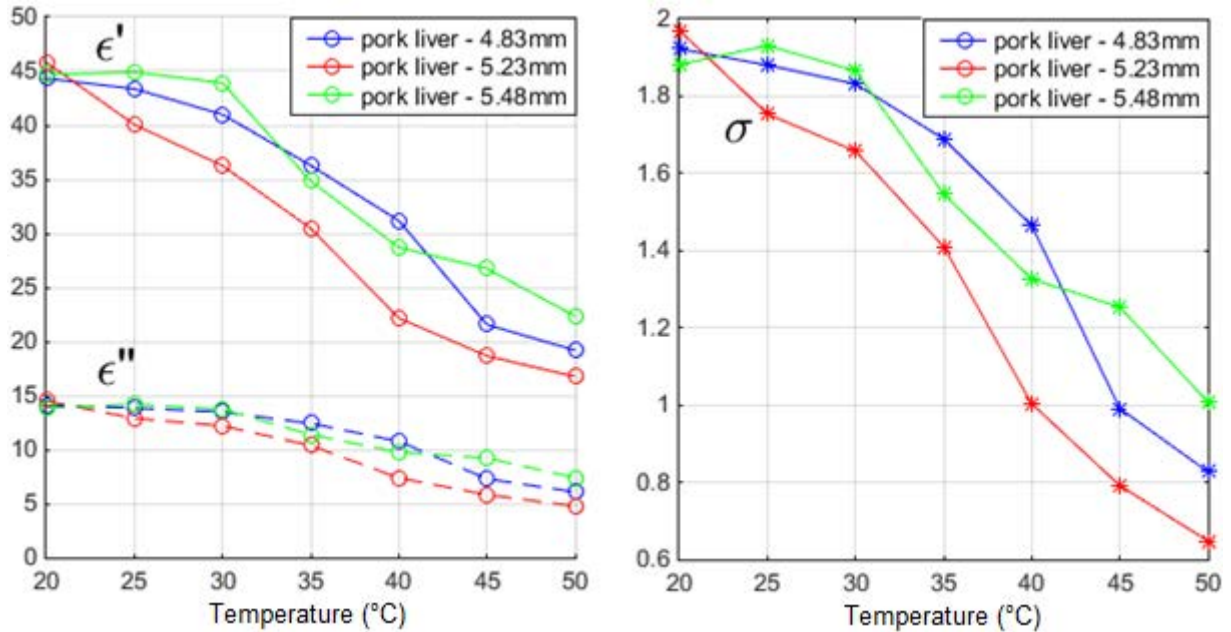d) Experimental results of **pork liver** samples (thicknesses: 4~6mm):

Figure 2.30: Comparisons among three pork liver samples with different thickness characterized as a function of temperature between 20 and 50 °C

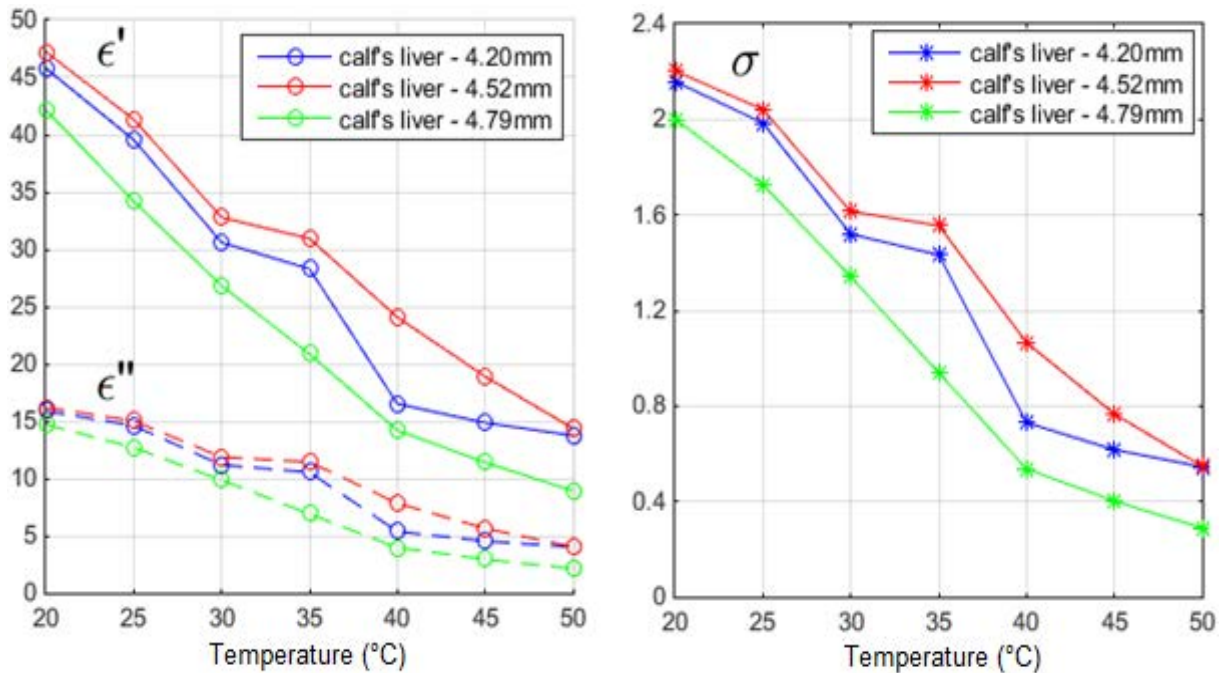e) Experimental results of **calf's liver** samples (thicknesses: 4~5mm):

Figure 2.31: Comparisons among three calf's liver samples with different thickness characterized as a function of temperature between 20 and 50 °C

Dielectric properties of all considered biological tissues vary with temperature. In general, for all types of biological tissues, $\varepsilon'(\mathrm{T})$, $\varepsilon''(\mathrm{T})$ and $\sigma(T)$ decrease with temperature between 20°C and 50°C despite experimental errors. More than 5 pieces of each type of sample have been measured and characterized.

At 20°C, before heating, all measured samples of each muscle (pork, beef, and chicken) and each liver sample (pork and calf) have similar values of ε', ε'' and σ; but after heating till 50°C, because of experimental tolerances (e.g. state of freshness and dimensions of the samples), there have been slight variation of ε', ε'' and σ among the same type samples.

2.11 Dielectric characterization measurement by the flexible coaxial cable

In order to verify if the flexible coaxial cable which will be used also for hyperthermia experiments can be used for dielectric characterization, all dielectric characterizations done with the semi-rigid coaxial probe have been achieved again by using the coaxial flexible cable. The results are presented in the following sections.

For each set of experimental results, $\varepsilon'(f)$ and $\varepsilon''(f)$ of the complex permittivity, the electrical conductivity $\sigma(f)$, and the loss angle (tanδ), all as a function of frequency are presented and compared with the literature data. Besides the experimental Cole–Cole diagram has been shown and compared with literature values.

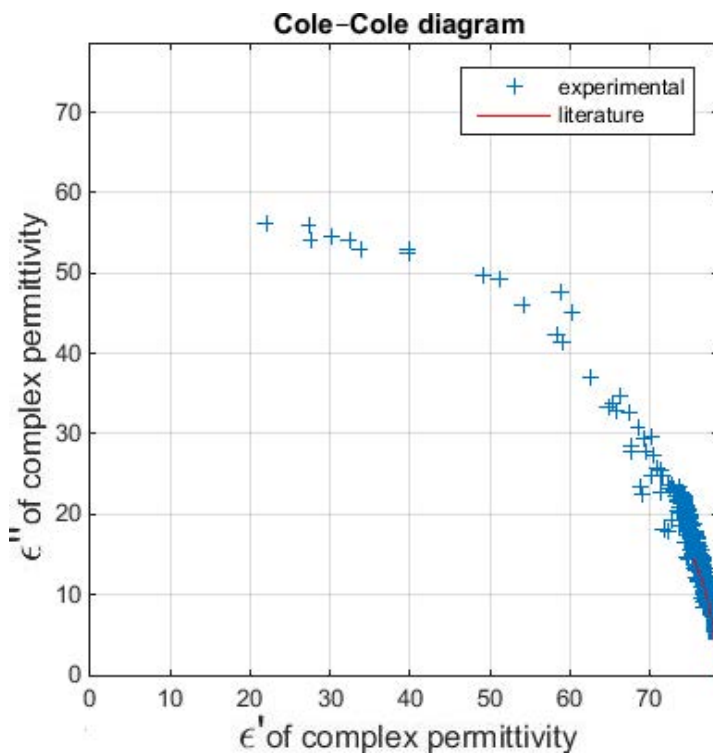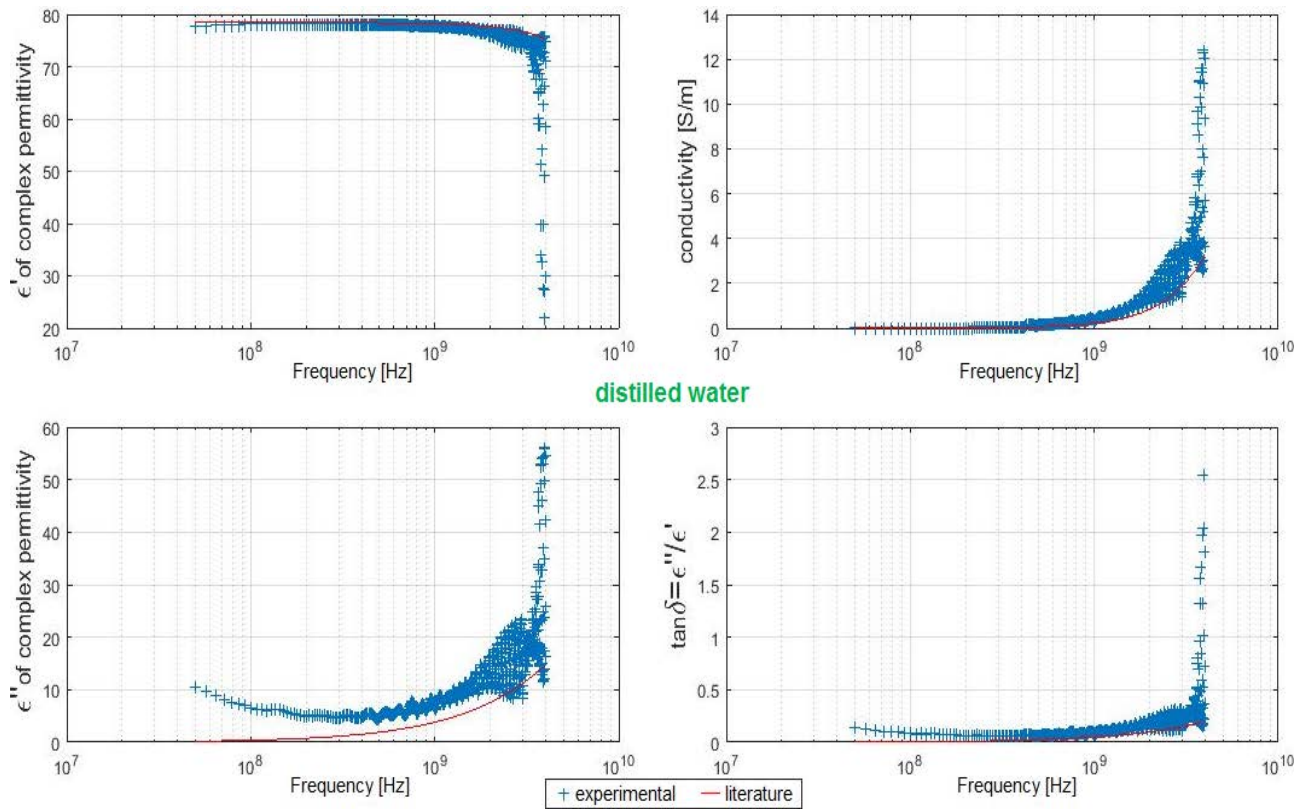## 2.11.1 Experimental results for standard materials and known liquids:

a) Experimental results of standard – **air** (ambient T=24°C)

Air
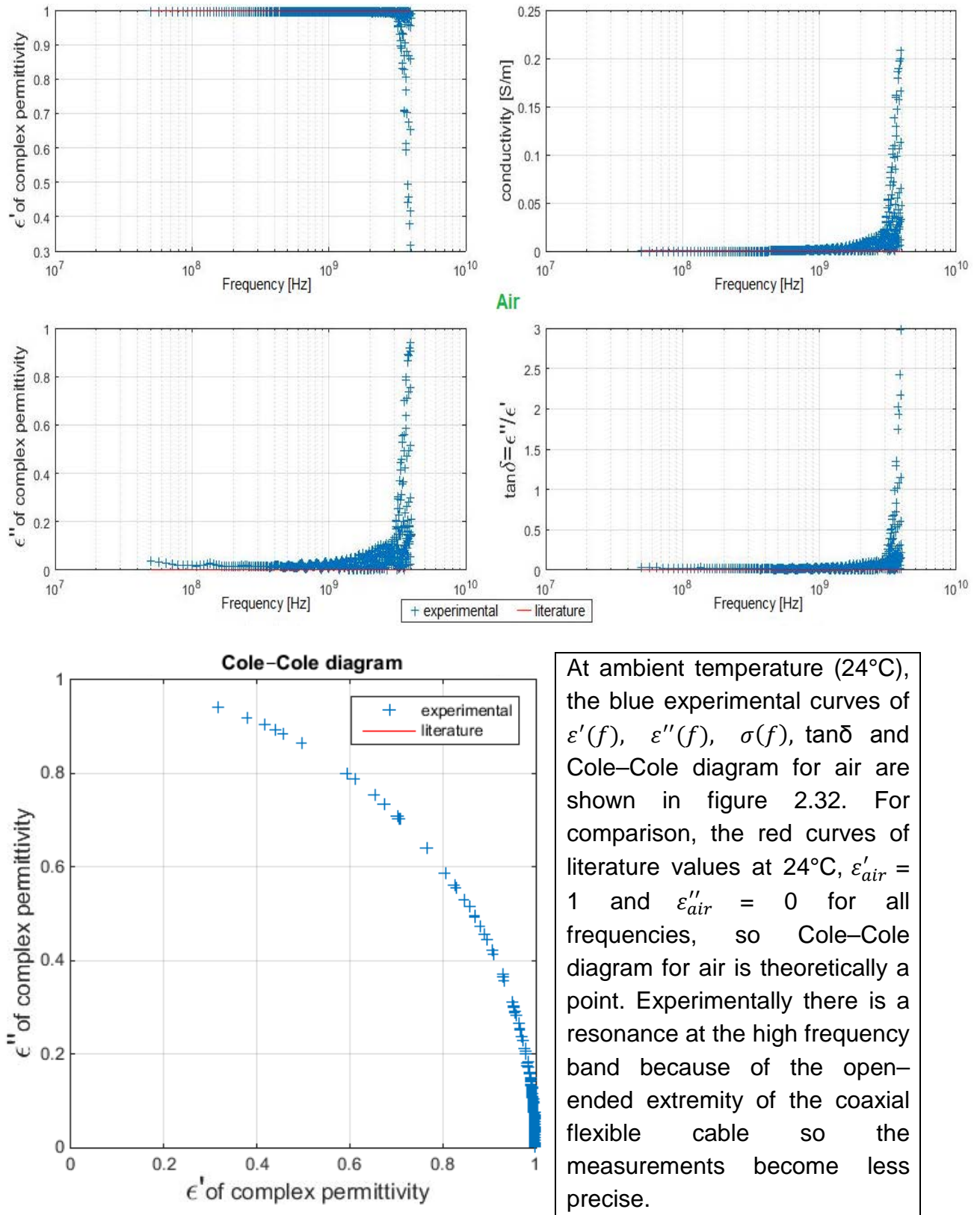
At ambient temperature (24°C), the blue experimental curves of $\varepsilon'(f)$, $\varepsilon''(f)$, $\sigma(f)$, tanδ and Cole–Cole diagram for air are shown in figure 2.32. For comparison, the red curves of literature values at 24°C, ε'_{air} = 1 and ε''_{air} = 0 for all frequencies, so Cole–Cole diagram for air is theoretically a point. Experimentally there is a resonance at the high frequency band because of the open–ended extremity of the coaxial flexible cable so the measurements become less precise.

Figure 2.32: Dielectric characterization of air at ambient temperature (24°C)
using the flexible coaxial cable.

b) Experimental results of standard – **distilled water** (ambient T=24°C)

Figure 2.33: Dielectric characterization of distilled water at ambient temperature (24°C)
using the flexible coaxial cable

At ambient temperature (24°C), the blue experimental curves of $\varepsilon'(f)$, $\varepsilon''(f)$, $\sigma(f)$, tanδ and Cole–Cole diagram for distilled water are shown in figure 2.33. For comparison, the red curves of literature values at 24°C, ε'_{water} = 78.45 and ε''_{water} = 0.19 at 50MHz. Experimentally there is a resonance at the high frequency band because of the open–ended extremity of the coaxial flexible cable so the measurements become less precise.

c) Experimental results of known liquid – **ethanol** (ambient T=24°C)

ethanol

+ experimental   — literature

Cole−Cole diagram

+ experimental
— literature

At ambient temperature (24°C), the blue experimental curves of $\varepsilon'(f)$, $\varepsilon''(f)$, $\sigma(f)$, tanδ and Cole–Cole diagram for ethanol are shown in figure 2.34.

For comparison, the red curves of literature values at 24°C, $\varepsilon'_{ethanol}=$ 24.43 and $\varepsilon''_{ethanol} = 0.83$ at 50MHz. $\varepsilon''(f)$ increases first and decreases from its critical frequency (f_c). There is a little difference between literature and experimental values of f_c, because λ$_c$ (*f*) for literature values varies from 27cm at 20°C to 12.2cm at 30°C. Its exact value for 24°C is N/A.
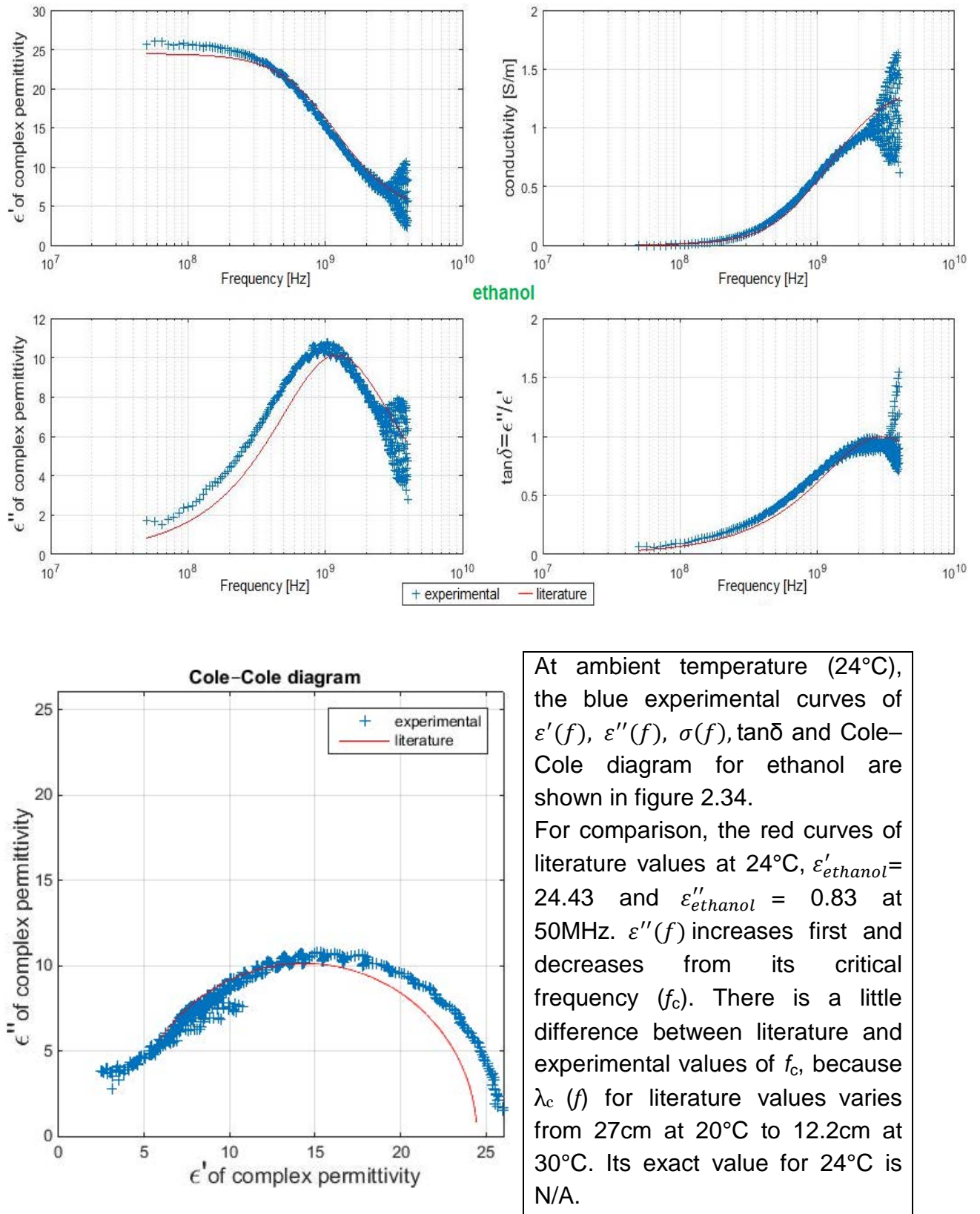
Figure 2.34: Dielectric characterization of ethanol at ambient temperature (24°C) using the flexible coaxial cable

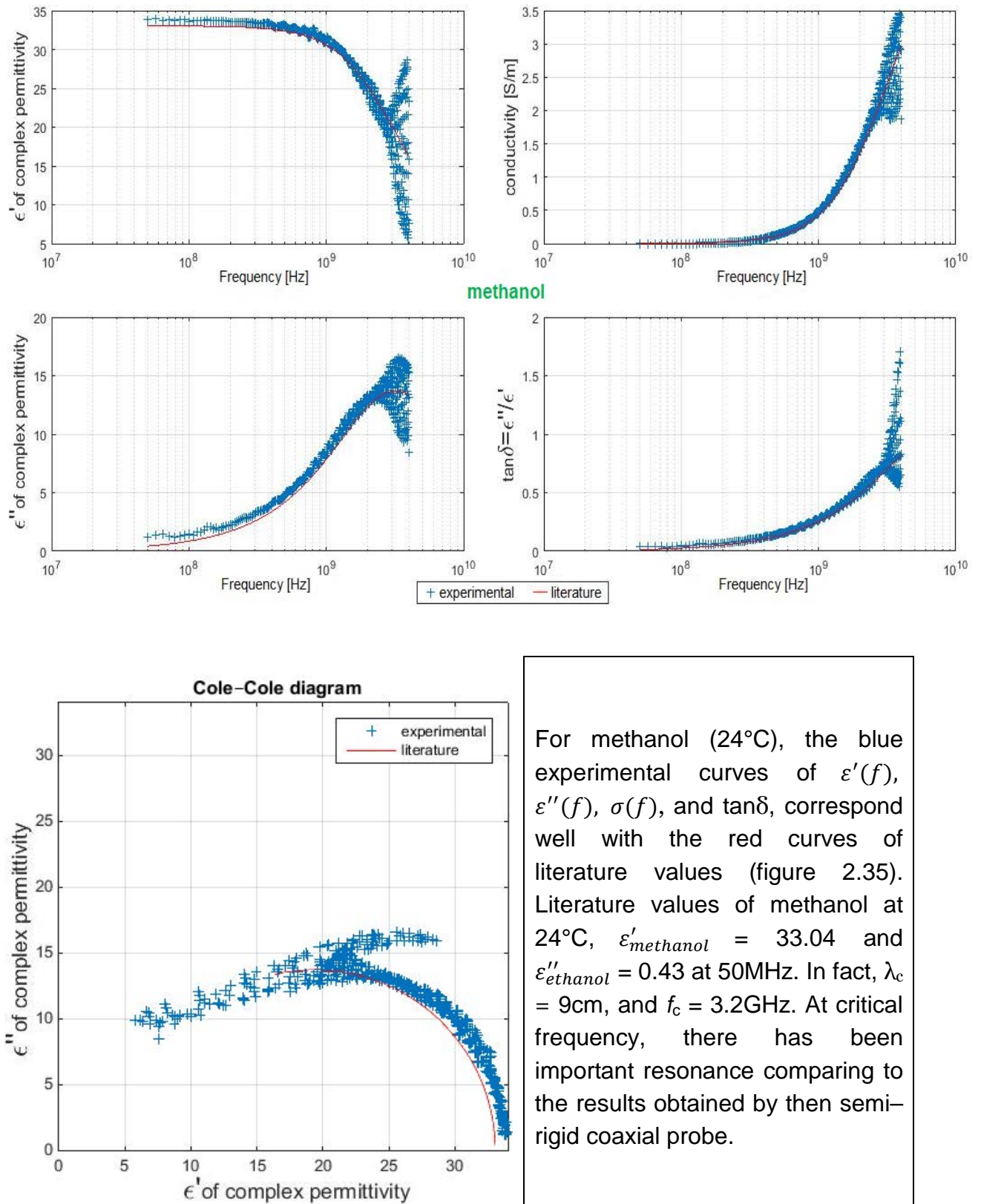d) Experimental results of known liquid – **methanol** (ambient T=24°C)

methanol

+ experimental — literature

Cole−Cole diagram

+ experimental
— literature

For methanol (24°C), the blue experimental curves of $\varepsilon'(f)$, $\varepsilon''(f)$, $\sigma(f)$, and tanδ, correspond well with the red curves of literature values (figure 2.35). Literature values of methanol at 24°C, $\varepsilon'_{methanol}$ = 33.04 and $\varepsilon''_{ethanol}$ = 0.43 at 50MHz. In fact, λ_c = 9cm, and f_c = 3.2GHz. At critical frequency, there has been important resonance comparing to the results obtained by then semi–rigid coaxial probe.
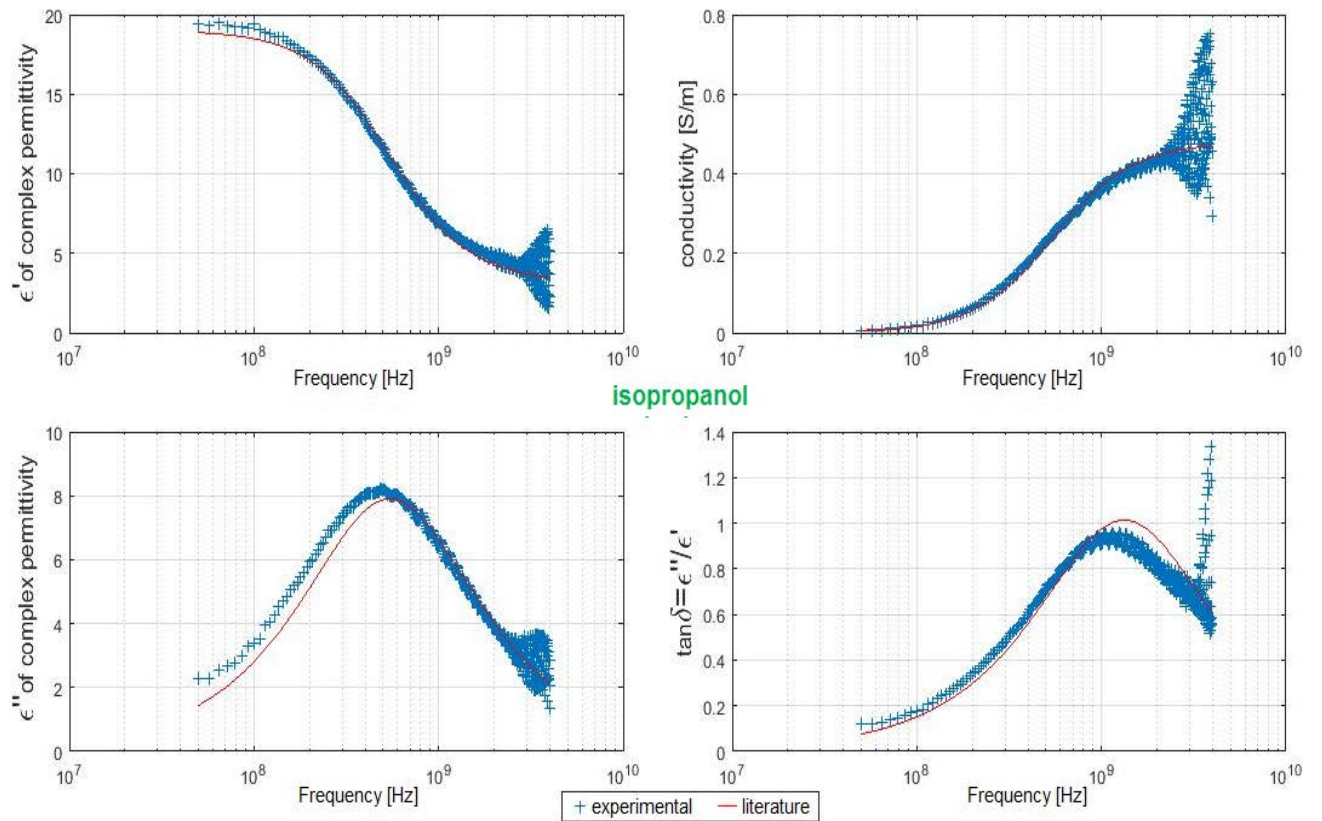
Figure 2.35: Dielectric characterization of methanol at ambient temperature (24°C)
using the flexible coaxial cable

e) Experimental results of known liquid – **isopropanol** (ambient T=24°C)
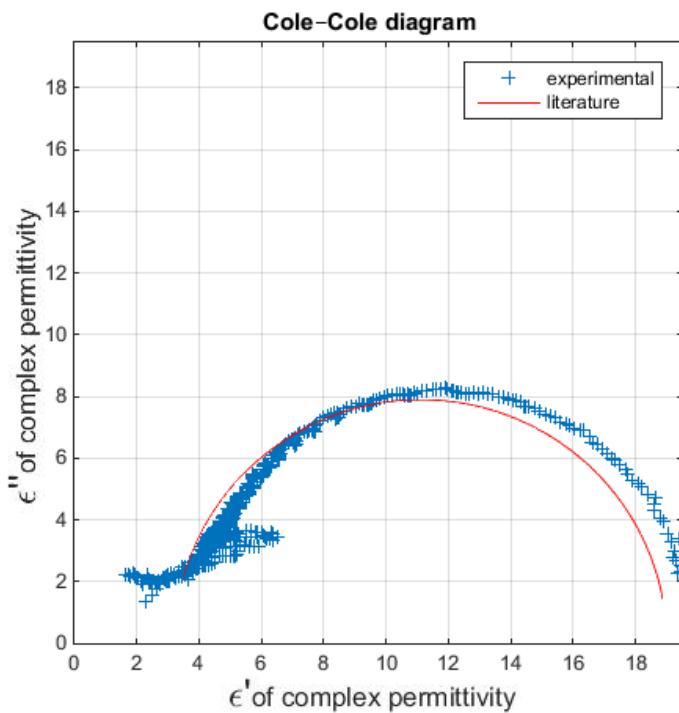
isopropanol

At ambient temperature (24°C), the blue experimental curves of $\varepsilon'(f)$, $\varepsilon''(f)$, $\sigma(f)$, tanδ and Cole–Cole diagram of liquid isopropanol, correspond with the red curves of literature values (figure 2.36). Literature values at 24°C, ε'_{water} = 24.43, ε''_{water} = 0.83 at 50MHz. λ_c = 55cm, and f_c = 0.54GHz. The experimental f_c = 0.48GHz is closer to the literature value comparing to f_c = 0.46GHz obtained by the semi–rigid coaxial cable. Although there is more resonance for the flexible coaxial cable at high frequency, the flexible coaxial cable can still be considered for use in dielectric measurements.

Figure 2.36: Dielectric characterization of isopropanol at ambient temperature (24°C)
using the flexible coaxial cable

2.11.2 Experimental results for natural biological tissues:

For each set of experimental results, $\varepsilon'(f)$ and $\varepsilon''(f)$ of the complex permittivity, the electrical conductivity $\sigma(f)$, the loss angle tanδ, $\varepsilon'(f)$ and $\sigma(f)$ all as a function of frequency are presented.

1st protocol: natural biological tissues (20°C)

Muscle samples

a) Experimental results of **pork** (thickness: 3.84mm)

For pork muscle of 20°C, both $\varepsilon'(f)$ and $\varepsilon''(f)$ decrease. $\sigma(f)$ increases (figure 2.37). As the flexible coaxial cable is longer (100cm) than the semi–rigid coaxial probe (14cm), that's why there is more resonance at high frequency.

At 2.45GHz,
ε'_{pork} = 54.85,
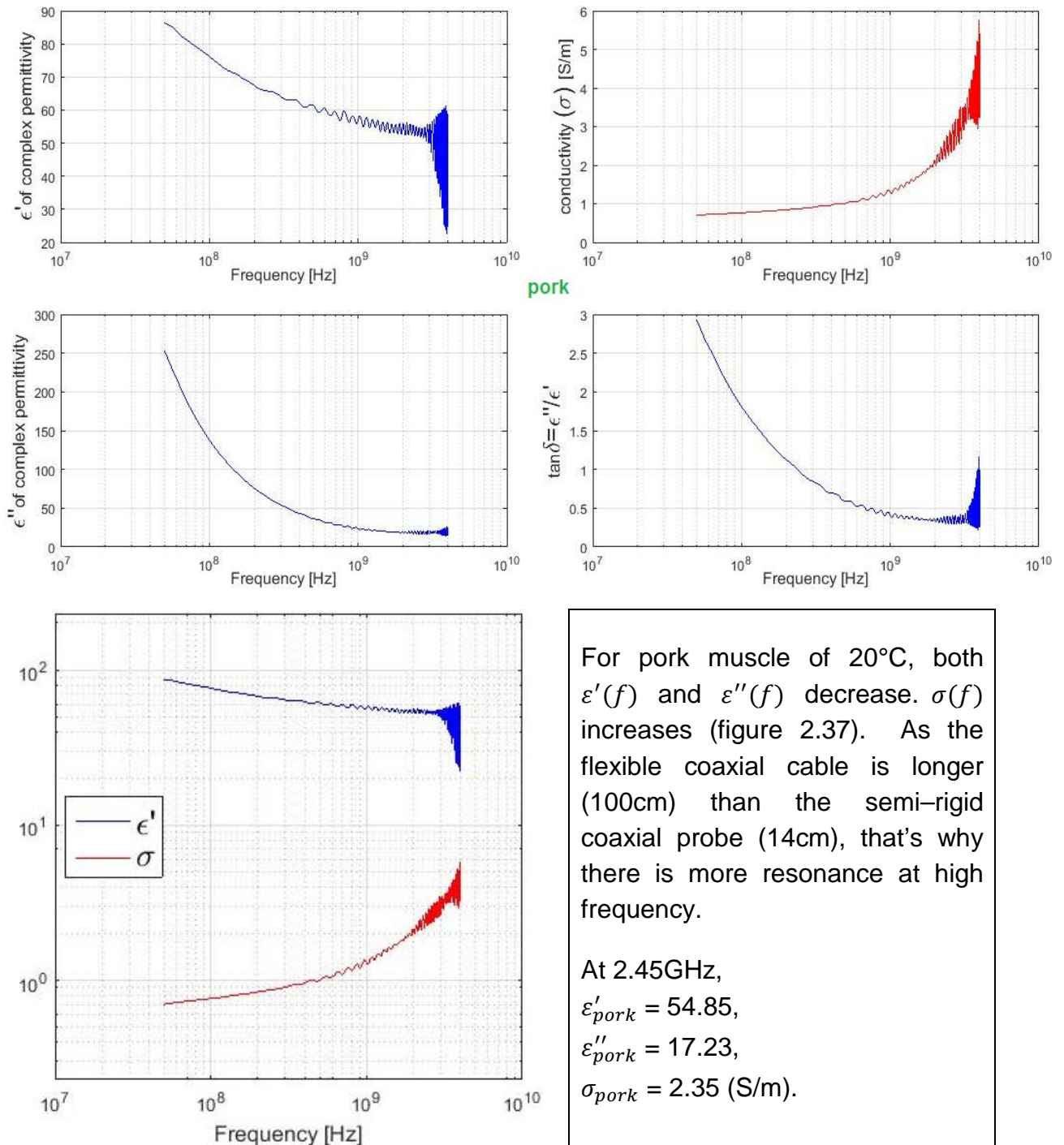ε''_{pork} = 17.23,
σ_{pork} = 2.35 (S/m).

Figure 2.37: Dielectric characterization of pork (thickness: 3.84mm) of 20°C
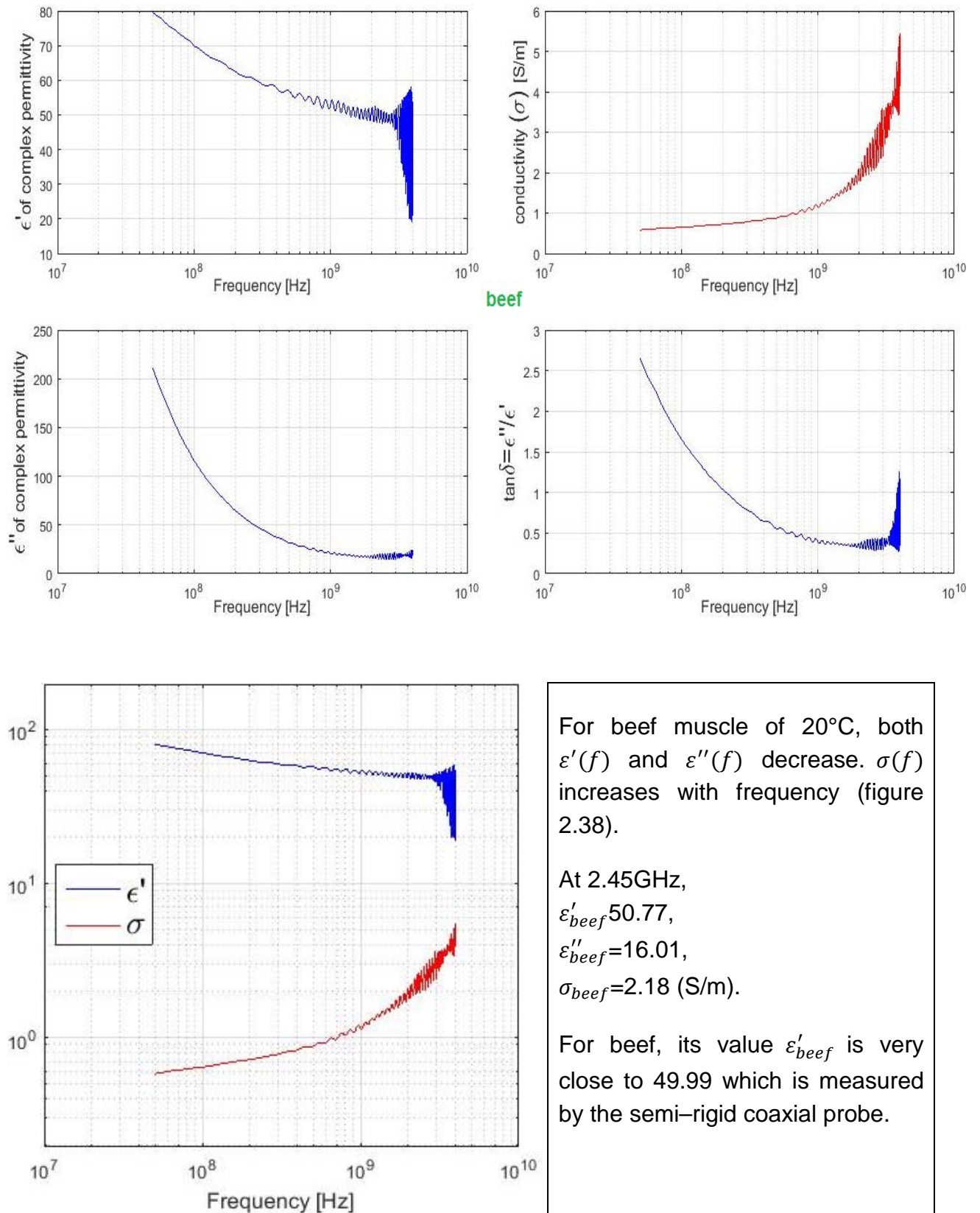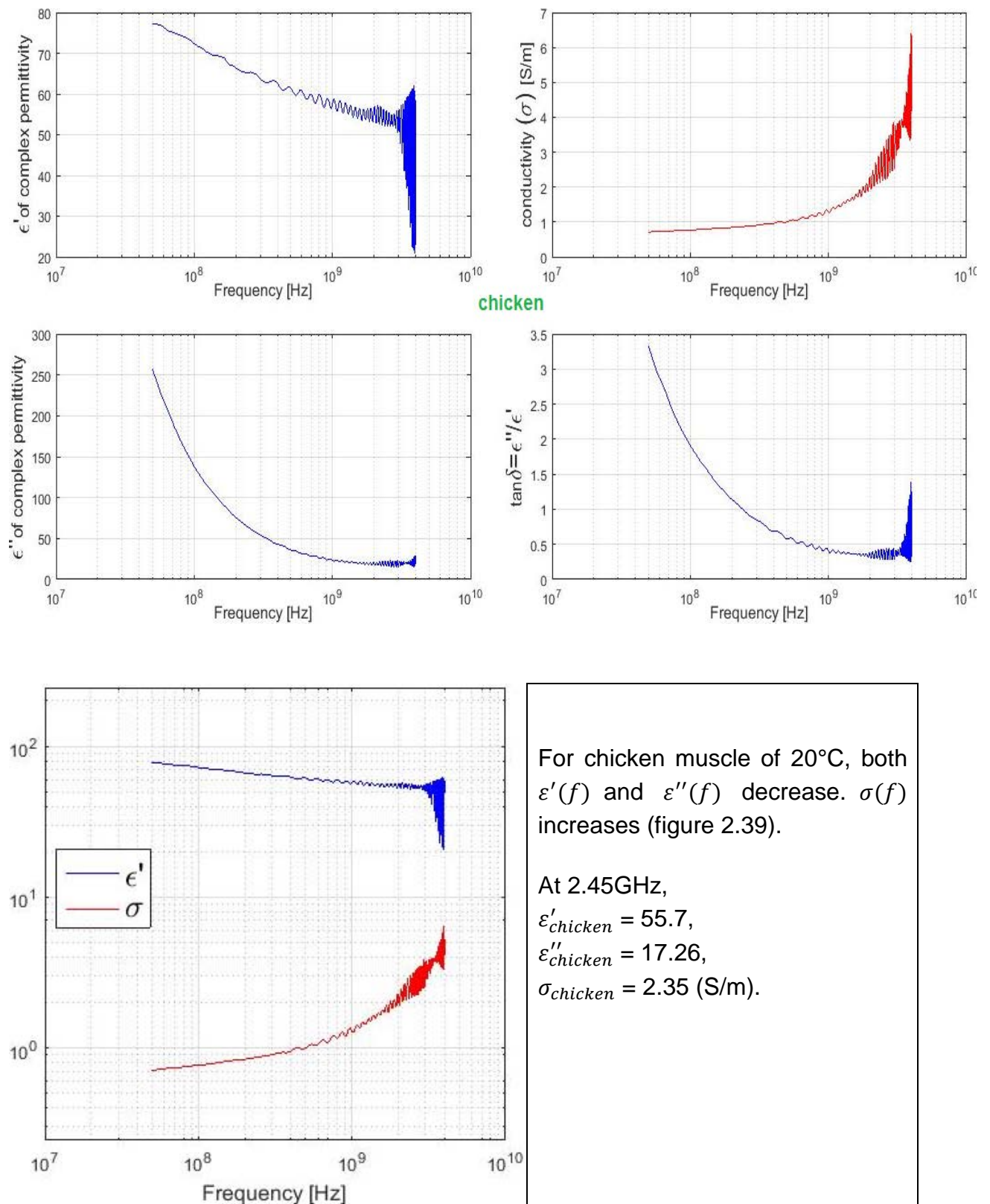
b) Experimental results of **beef** (thickness: 3.33mm)

For beef muscle of 20°C, both $\varepsilon'(f)$ and $\varepsilon''(f)$ decrease. $\sigma(f)$ increases with frequency (figure 2.38).

At 2.45GHz,
ε'_{beef}50.77,
ε''_{beef}=16.01,
σ_{beef}=2.18 (S/m).

For beef, its value ε'_{beef} is very close to 49.99 which is measured by the semi–rigid coaxial probe.

Figure 2.38: Dielectric characterization of beef (thickness: 3.33mm) of 20°C

c) Experimental results of **chicken** (thickness: 3.30mm)

For chicken muscle of 20°C, both $\varepsilon'(f)$ and $\varepsilon''(f)$ decrease. $\sigma(f)$ increases (figure 2.39).

At 2.45GHz,
$\varepsilon'_{chicken}$ = 55.7,
$\varepsilon''_{chicken}$ = 17.26,
$\sigma_{chicken}$ = 2.35 (S/m).

Figure 2.39: Dielectric characterization of chicken (thickness: 3.30mm) of 20°C

Liver samples
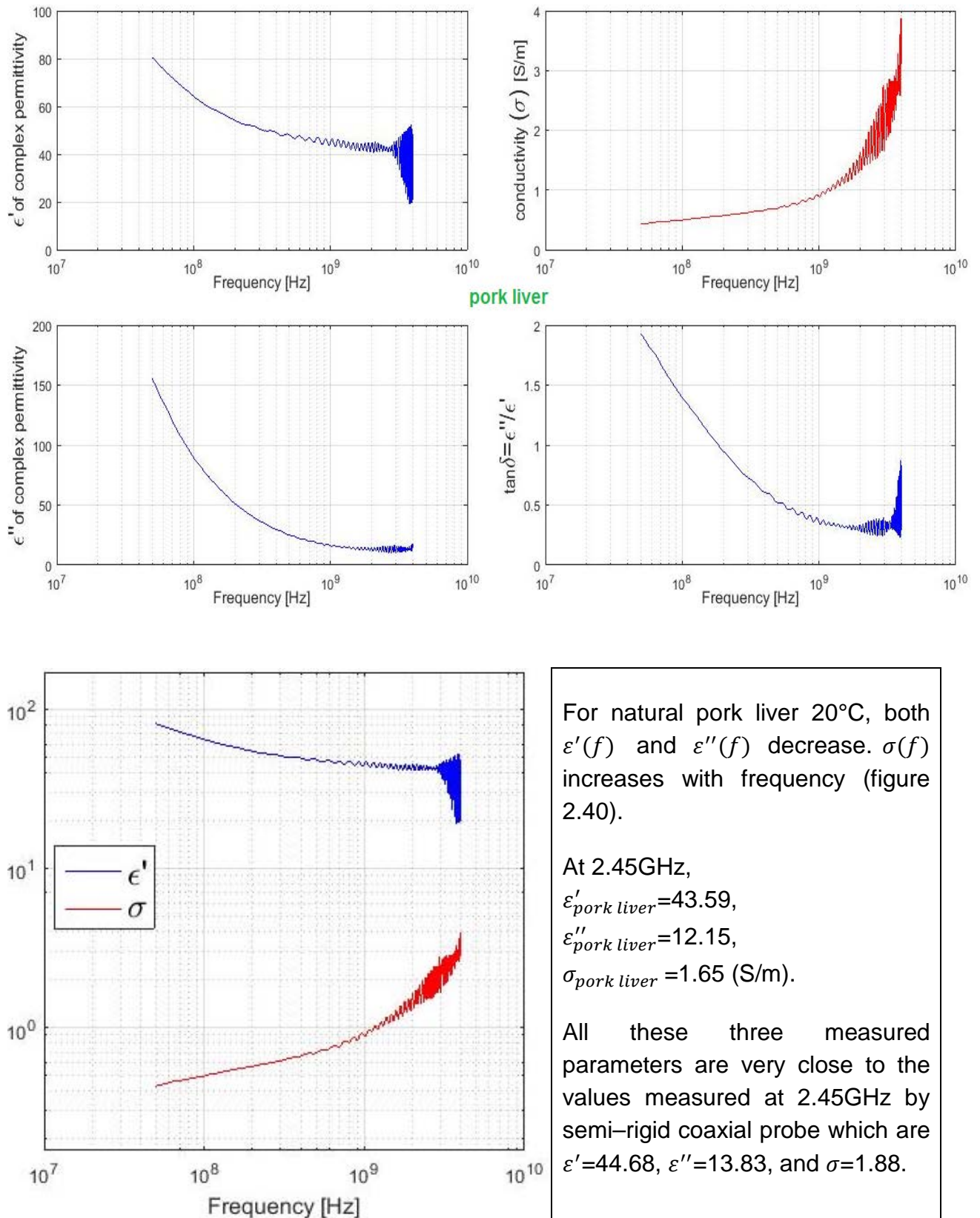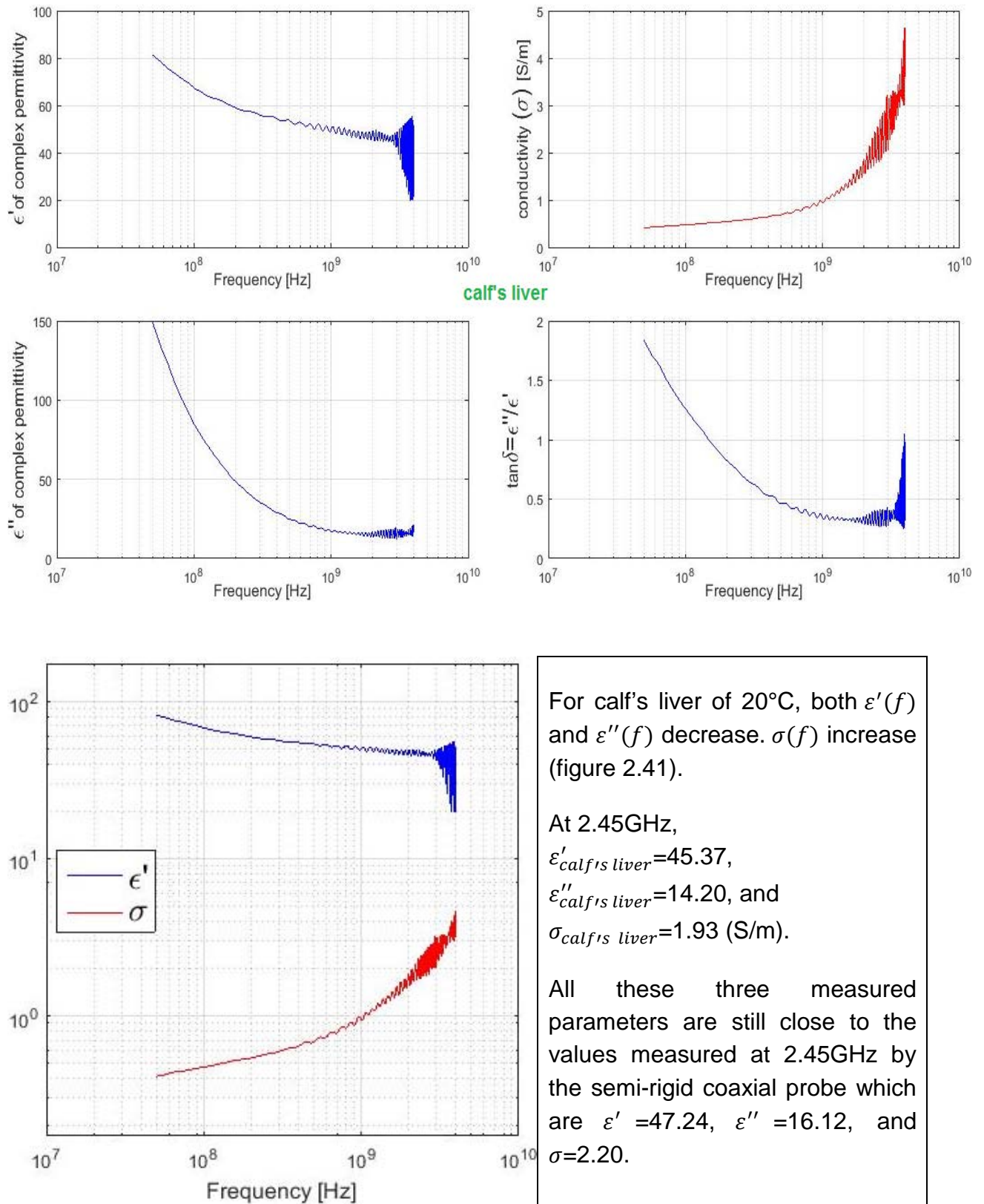
d) Experimental results of **pork liver** (thickness: 3.44mm)

pork liver

For natural pork liver 20°C, both $\varepsilon'(f)$ and $\varepsilon''(f)$ decrease. $\sigma(f)$ increases with frequency (figure 2.40).

At 2.45GHz,
$\varepsilon'_{pork\ liver}$=43.59,
$\varepsilon''_{pork\ liver}$=12.15,
$\sigma_{pork\ liver}$ =1.65 (S/m).

All these three measured parameters are very close to the values measured at 2.45GHz by semi–rigid coaxial probe which are ε'=44.68, ε''=13.83, and σ=1.88.

Figure 2.40: Dielectric characterization of pork liver (thickness: 3.44mm) of 20°C

e) Experimental results of **calf's liver** (thickness: 3.62mm)

For calf's liver of 20°C, both $\varepsilon'(f)$ and $\varepsilon''(f)$ decrease. $\sigma(f)$ increase (figure 2.41).

At 2.45GHz,
$\varepsilon'_{calf's\ liver}$=45.37,
$\varepsilon''_{calf's\ liver}$=14.20, and
$\sigma_{calf's\ liver}$=1.93 (S/m).

All these three measured parameters are still close to the values measured at 2.45GHz by the semi-rigid coaxial probe which are ε' =47.24, ε'' =16.12, and σ=2.20.

Figure 2.41: Dielectric characterization of calf's liver (3.62mm) of 20°C

2nd protocol: Dielectric characterization as a function of temperature (20°C to 50°C) using the flexible coaxial cable

Muscle

a) Experimental results of **pork** samples (thicknesses: 3~4mm):

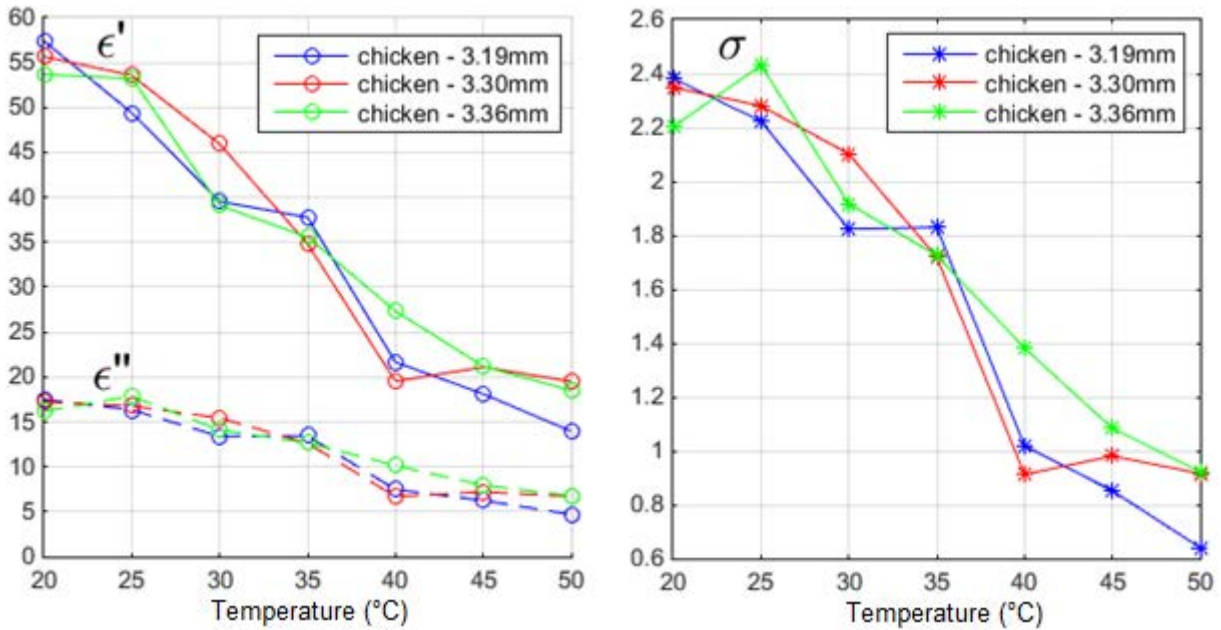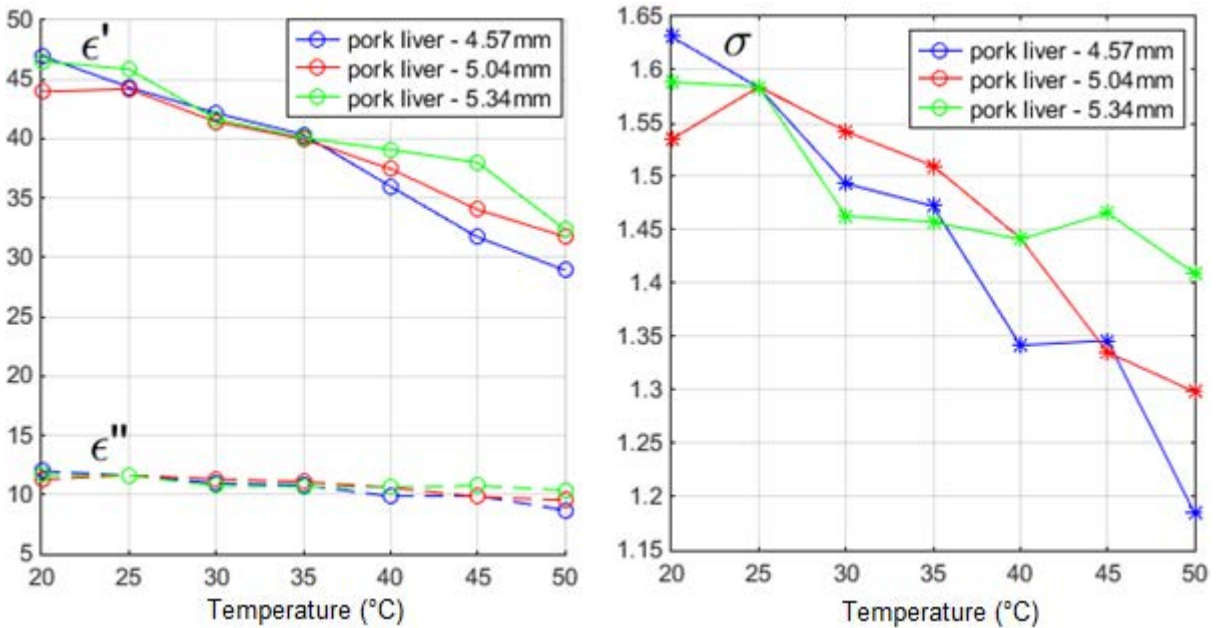ε' of complex permittivity (T), ε'' of complex permittivity (T),   conductivity–σ (T)

Figure 2.42: Comparisons among three pork samples with different thickness characterized as a function of temperature between 20 and 50 °C

b) Experimental results of **beef** samples (thicknesses: 3~4mm):

ε' of complex permittivity (T), ε'' of complex permittivity (T),   conductivity–σ (T)

Figure 2.43: Comparisons among three beef samples with different thickness characterized as a function of temperature between 20 and 50 °C

c) Experimental results of **chicken** samples (thicknesses: 3~4mm):

$\varepsilon'$of complex permittivity (T), $\varepsilon''$of complex permittivity (T),   conductivity–σ (T)

Figure 2.44: Comparisons among three chicken samples with different thickness characterized as a function of temperature between 20 and 50 °C

Liver samples

d) Experimental results of **pork liver** samples (thicknesses: 4~6mm):

$\varepsilon'$of complex permittivity (T), $\varepsilon''$of complex permittivity (T),   conductivity–σ (T)

Figure 2.45: Comparisons among three pork liver samples with different thickness characterized as a function of temperature between 20 and 50 °C

e) Experimental results of **calf's liver** samples (thicknesses: 3~4mm):

ε' of complex permittivity (T), ε'' of complex permittivity (T),   conductivity–σ (T)

Figure 2.46: Comparisons among three calf's liver samples

Dielectric properties of all biological tissues vary with temperature. ε'(T), ε''(T) and $\sigma(T)$ are measured for more than 5 pieces of each type of sample. For all types of biological tissue, when the temperature increases, all dielectric parameters decrease. In fact, before heating, all measured samples of muscles (pork, beef, and chicken) and livers (pork and calf's) have similar values of ε', ε'' and σ; but after heating at 50°C, because of experimental errors (e.g. freshness and dimensions of samples), there have been slight variations of ε', ε'' and σ among the same type samples.

2.12 Comparisons

Firstly, we compare the experimental results measured by two different applicators (semi–rigid coaxial probe and flexible coaxial cable) of 24°C known liquids with their literature values at 2.45GHz (table 2.3 and 2.4). Secondly, we compare the average values of ε', ε'' and σ of three samples of each biological tissue (20°C) measured by coaxial probe and coaxial cable at 2.45GHz (table 2.5). Values of dielectric properties ($\varepsilon'(f)$, $\varepsilon''(f)$ and $\sigma(f)$) for raw natural biological tissues measured by coaxial probe and coaxial cable are well corresponding. Thirdly, we compare $\varepsilon'(f)$, and $\sigma(f)$ of raw natural biological tissues (T=20°C) measured by semi–rigid coaxial probe and flexible coaxial cable. The coaxial probe can be considered having more precise because of its smaller radius and length. At last, we compare the average measured value with the corresponding error bars of ε' and ε'' of three samples of each type biological tissue as a function of temperature (20°C to 50°C) measured by semi–rigid coaxial probe and flexible coaxial cable (table 2.6).

For all biological types of tissue, the general tendency is a decrease of dielectric parameters ε' and ε'' with increasing temperature. For pork and calf's liver, the measured values correspond better with each other than the other three tissues. The

dielectric properties of tissues change with temperature. Below about 40°C, these changes are still generally reversible. At higher temperature level, thermal damage will result in irreversible changes in the dielectric and electrical properties of biological tissue (see chapter 1). The extent of change level depends on the biological tissue type, dimensions, and duration of heating.

Known liquids	ε'			ε''		
	Experimental	Literature	Relative error (%)	Experimental	Literature	Relative error (%)
Distill water	77,151	77,267	0,150	12,296	9,235	33,143
Ethanol	8,891	8,207	8,340	7,679	8,071	4,860
Methanol	22,760	22,889	0,564	14,759	13,234	11,520
Isopropanol	4,176	3,947	5,815	3,341	3,353	0,370

Table 2.3: Comparisons between experimental and literature values of ε' and ε'' of known liquids (24°C) measured by semi-rigid coaxial probe at 2.45GHz

Known liquids	ε'			ε''		
	Experimental	Literature	Relative error (%)	Experimental	Literature	Relative error (%)
Distill water	77,27	77,27	0,00	8,18	9,24	11,45
Ethanol	7,84	8,21	4,51	6,96	8,07	13,78
Methanol	22,58	22,89	1,35	13,02	13,23	1,59
Isopropanol	4,46	3,95	13,07	3,19	3,35	4,80

Table 2.4: Comparisons between experimental and literature values of ε' and ε'' of known liquids (24°C) measured by flexible coaxial cable at 2.45GHz

complex permittivity	fresh biological samples	coaxial probe ε'_p	coaxial cable ε'_c	difference
	pork	51.31	53.03	3.24%
	beef	49.07	50.95	3.68%
ε'	chicken	54.29	55.60	2.35%
	pork liver	44.95	45.85	1.94%
	calf's liver	45.06	47.65	5.34%
	fresh biological samples	coaxial probe ε''_p	coaxial cable ε''_c	difference
	pork	18.33	16.70	8.83%
	beef	17.19	15.90	7.26%
ε''	chicken	18.91	16.99	14.7%
	pork liver	14.15	11.65	17.62%
	calf's liver	15.60	14.61	8.60%
conductivity	fresh biological samples	coaxial probe σ_p	coaxial cable σ_c	difference
	pork	2.49	2.27	8.83%
$\sigma = \varepsilon'' \varepsilon_0 \omega$	beef	2.34	2.17	7.26%
	chicken	2.71	2.31	14.7%
$\varepsilon_0 = 8.85 \times 10^{-12}$ $[\text{F} \cdot m^{-1}]$	pork liver	1.93	1.59	17.62%
	calf's liver	2.12	1.93	8.60%

Table 2.5: Comparisons of average values of ε', ε'' and σ of three samples of each biological tissue (20°C) measured by semi-rigid coaxial probe and flexible coaxial cable at 2.45GHz

pork

beef

chicken

Table 2.6: comparisons of $\varepsilon'(f)$, and $\sigma(f)$ of raw natural biological tissues (T=20°C) measured by semi–rigid coaxial probe and flexible coaxial cable. The coaxial probe can be considered having more precise because of its smaller radius and length.

pork liver

calf's liver

Table 2.7: comparisons of average measured value with the corresponding error bars of ε' and ε'' of three samples of each type biological tissue as a function of temperature (20°C to 50°C) measured by semi–rigid coaxial probe and flexible coaxial cable

2.13 Experimental errors

Experimental errors may arise from the following sources:

- Noise from VNA,
- Calibration accuracy,
- Tolerance on measured sample thickness,
- Dimensional normalization of the samples,
- Freshness of the samples,
- Surface roughness of the samples,
- Repeatability of sample's thickness during the sample preparation,
- Repeatability of sample placement,
- Sample orientation with respect to plane of polarization,
- Alignment error heating between sample and heat gun,
- Distance between MICRO heat gun and biological sample,
- Duration of heating of biological samples by the MICRO heat gun,
- Temperature measurement.

2.14 Conclusion

Two methods of virtual line model, open–ended coaxial probe and flexible coaxial warrior cable with two protocols, at room temperature or with variable temperature (20°C to 50°C) have been used for dielectric characterization measurement. Obtained values of dielectric parameters ($\varepsilon'(f)$, $\varepsilon''(f)$ and $\sigma(f)$) of known liquids and raw natural biological tissues measured by semi–rigid coaxial probe and flexible cable correspond well with their literature values. The curves of dielectric measurements of methanol and isopropanol have the best correspondence between the experimental and literature values among all the liquid samples. Therefore, the dielectric characterization method with the virtual line model has been approved as a feasible method.

Because of the open ended extremity of coaxial cable, there are resonances at high frequencies. In fact, the calibration can only be carried out for the connection part of N connector, but not for the extremity of the coaxial probe or cable. The flexible coaxial cable (100cm) is much longer than the coaxial probe (14cm), that's why it shows more resonance. For these reasons, a program of post treatment of measured data should be written to obtain better experimental results. For the future, APC7 could be also considered to replace the coaxial line in order to get better calibration and reduce the resonance for the high frequency range, so that more precise experimental values could be obtained.

For dielectric characterization of biological tissue as a function of temperature, all the measured dielectric parameters $\varepsilon'(\mathrm{T})$, $\varepsilon''(\mathrm{T})$ and $\sigma(T)$ showed a decrease with increasing temperature. Dielectric properties of all biological tissues vary with temperature. The obtained values of dielectric properties at different temperatures now can be used for the simulations of ex–vivo microwave hyperthermia experiments.

Chapter 3
Microwave hyperthermia instrumentation and ex vivo experiments on the biological tissues

3.1 Introduction

Microwave hyperthermia is being used for cancer treatment since the early 1980s in many countries around the world. Biologically, cancerous tissues cannot survive above ~41°C, while healthy tissue can survive up to ~45°C. Selective killing of cancerous cells can be carried out. [58] Ex vivo experiments of microwave hyperthermia on biological tissues were carried out using an adapted instrumentation at the laboratory L2E of UPMC. The final purpose of all the experiments is to show that pathological biological tissues can be examined for diagnosis and heated or irradiated for hyperthermia by using a single microwave applicator. According to the realistic requirements, the ideal model of microwave hyperthermia should be operated in a very quick time with the proper power level to destroy pathological parts and not harm the surrounding normal tissues. For minimally invasive treatment, shorten the treatment time allows to reduce the risks of the surgeries, and decrease the pains of the patients as much as possible are important. During the ex vivo experiments, different biological animal tissue samples were tested like: pork, beef, chicken, pork liver and calf's liver. Current microwave hyperthermia instrumentation system allows doing the ex vivo tests by two different applicators: open–ended coaxial cable RG393 and Warrior cable with two experimental protocols: constant microwave power and step changing microwave power to evaluate the microwave hyperthermia effects on the biological tissues.

3.2 Microwave hyperthermia ex vivo instrumentation system
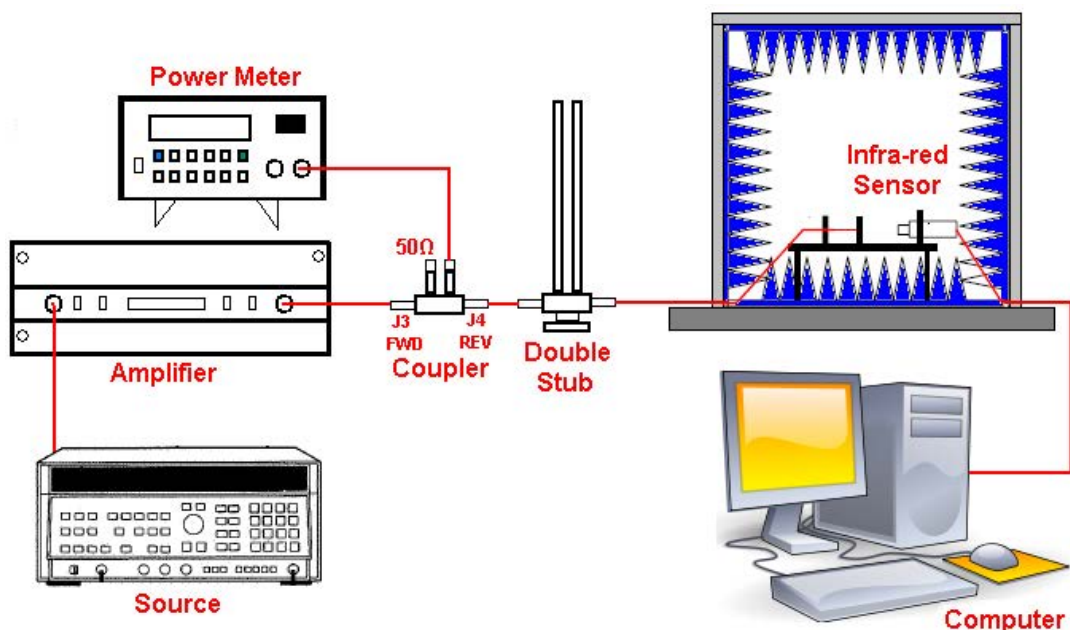
Figure 3.1: Schematic view of the microwave hyperthermia ex-vivo instrumentation

Microwave hyperthermia instrumentation which is used for the irradiation experiments consists of several main parts (figure 3.1):

- **Source**–HP 8340A Synthesized Sweeper, whose frequency range is between 10MHz and 26.5GHz, offers the output power between –110dBm and +10dBm (annex 4).

- **Amplifier** (25S1G4A) amplifies the power from the source and it can be controlled to deliver a maximum value of 10 watts with 10 gains for experimental requirement of microwave hyperthermia. Its Frequency Response range is from 0.8 to 4.2 GHz (annex 5).

- **Power meter**–HP 437B, a low-cost, high performance, programmable single-channel average power meter. Using with HP 8481A sensor, it can measure power in the range of –70 to +44dBm over the frequency range of 100KHz to 50GHz. Power meter is connected to a coupler and shows the real–time reflected power from the load (biological tissue). The double stubs are adjusted synchronously corresponding to the reflecting power shown on the power meter panel. The smaller number of power level (dBm) is read, the better impedance matching is obtained (annex 6).

- **Double stub tuner** (DS–109L) Impedance Matching Device produced by Weinschel Associates Ltd is used for ensuring optimum power transmission from the source to the load. Its frequency range is from 0.4GHz to 4 GHz. The length of stubs can get to 38cm (annex 7).

- **Infra–red sensor** is used to measure the temperature of samples irradiated by the microwave. In the effective measuring distance, it can measure the temperatures of samples without contacting with them. Thermocouples are not used for this experiment because they will disturb the distribution of the electric field. The measurement temperature range of IR sensor is from -20°C to 500°C (annex 9). The schema of the infra–red sensor specification (figure 3.2) shows that the distance between sensor and object should be smaller than 360mm and the testing spot diameter will be less than 12mm (D:S 30:1), because, in this range, the measuring sensibility is high and infra–red sensor guarantees that 90% of energy can be detected. It can get two aspect advantages: smooth surface of measuring sample and higher detecting sensibility.
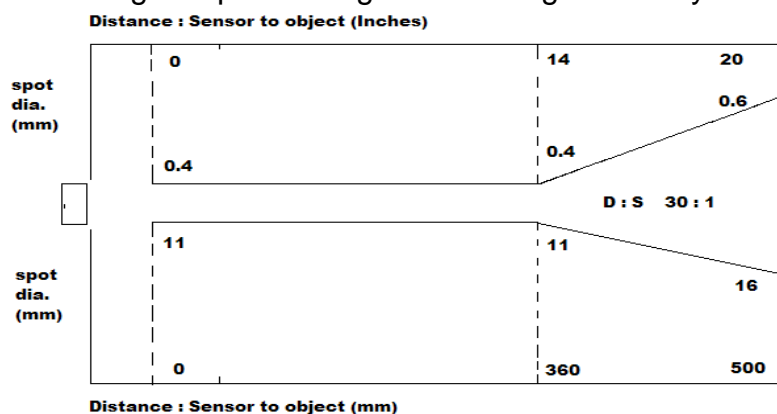
Figure 3.2: Geometrical specifications of the infra–red sensor

- **Absorbing foam Wall** (APM12), it is made of carbon black powder and polyurethane foam. It is used to provide a shielded environment for microwave hyperthermia instrumentation. The absorbing foam wall has arrays of pyramid shaped pieces and offers an effective protection. The five absorbing foam wall constitute the small anechoic chamber. According to the electrical filed characterization of the chamber that we accomplished, when the chamber is completely covered, the leakage of microwave energy out of anechoic chamber is even smaller than the signal of mobile phone which is emitted by the nearest base station. The microwave hyperthermia instrumentation is very safe and harmless for the operator (annex 10).
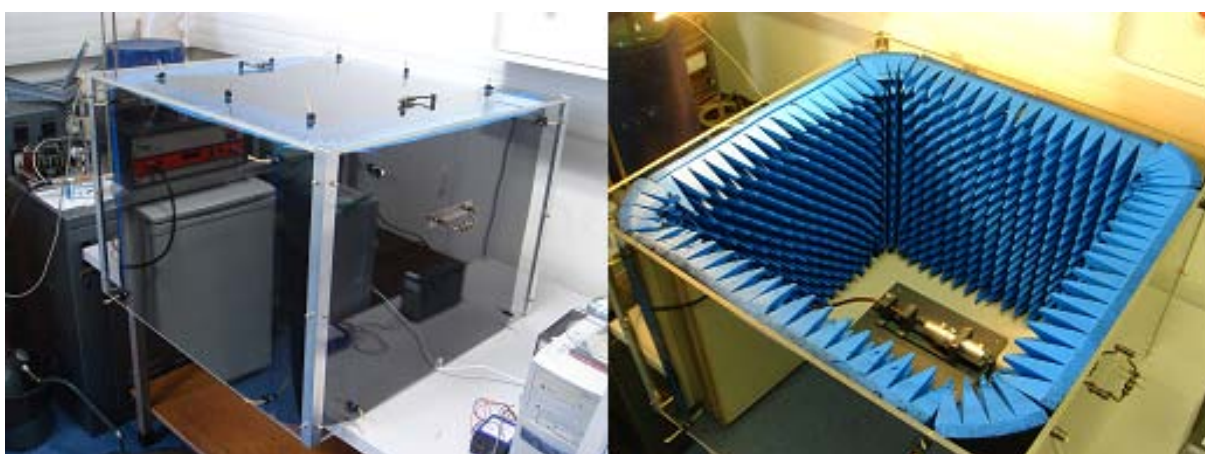
Figure 3.3: Exterior and interior of the small anechoic chamber
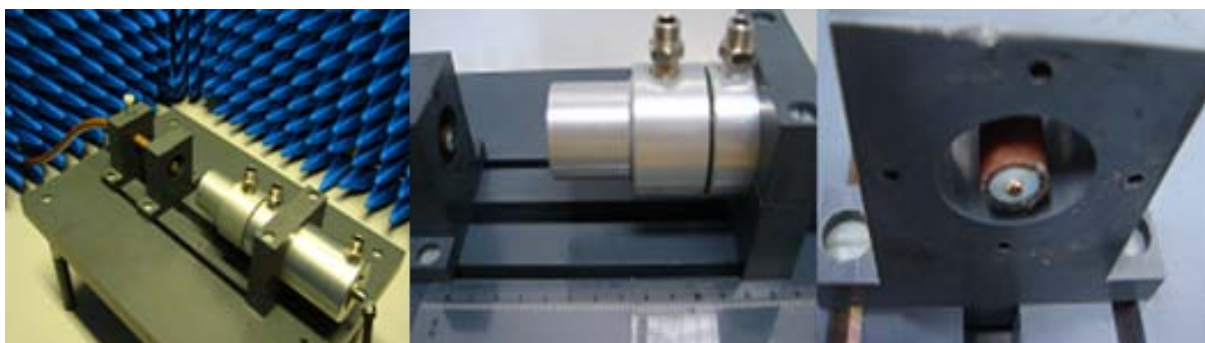
Figure 3.4: Experimental bench of microwave hyperthermia instrumentation with infra–red sensor and the open–ended coaxial applicator–coaxial cable RG393

- **Circular plastic sample holders**–there are two types: white sample holder and gray sampler holder. Both of them have the same outer diameter of 4cm (figure 3.5). Comparing with their inter diameters, white sample holder of 1.0cm is smaller than gray holder of 1.5cm, so the gray sampler holder is put in front of the infra–red sensor in order to ensure the accuracy of temperature measurement on sample's surface (figure 3.6). The thickness of the gray holder is 2.85mm and it of white holder is 1.85mm. For two sample holders which sandwich the biological tissue between them, they are needed to be fixed on the experimental bench with white plastic Teflon screws. The length of white screw is 9mm, so it means that, maximally, the thickness of the biological sample for microwave hyperthermia experiments is 4.3mm (figure 3.6).
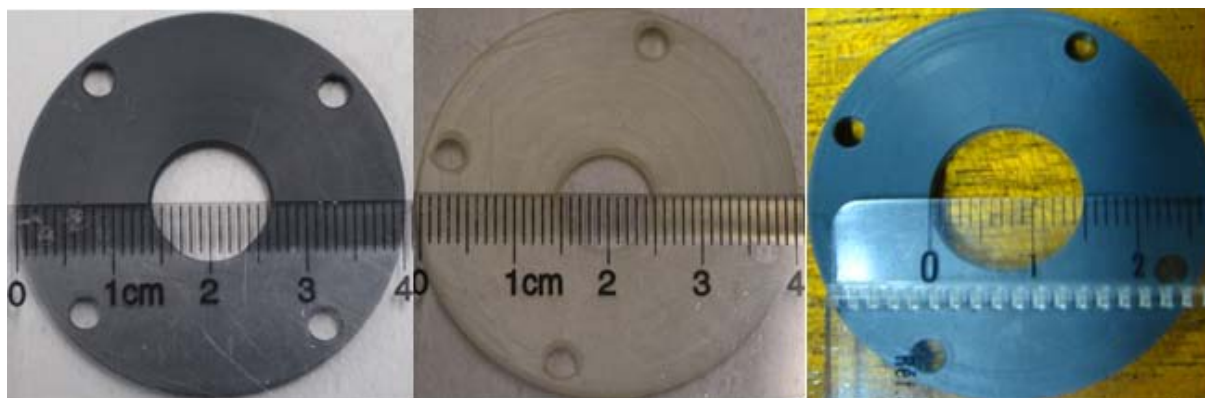
Figure 3.5: Dimensions of outer and inner diameters of gray and white sample holders

Figure 3.6: Maximum thickness of biological sample can be 4.3mm
corresponding to the length of the sample holders fixture screws

- **Microwave hyperthermia applicator**–cable RG393 is used in wireless communication, broadcast and military equipments for transmission of radio frequency signals. It has four parts: inner conductor–silver plated copper covered steel, dielectric–solid PTFE, outer conductor (braid wire)–silver plated copper and double shield and jacket–FEP (annex 8).
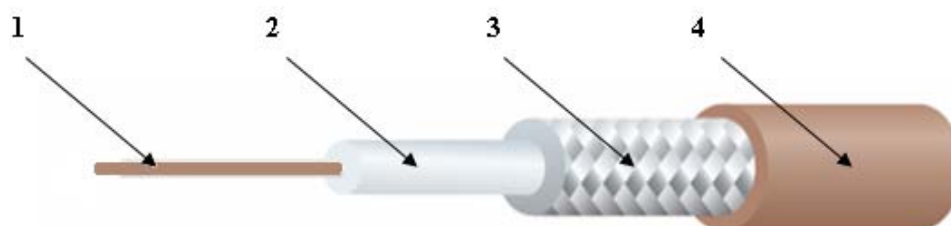
Figure 3.7: Structure of the coaxial cable RG393:
1: inner conductor–Ag plated Cu, 2: dielectric–PTFE, 3: outer conductor–Ag plated Cu, 4: jacket–FEP

- **Microwave hyperthermia applicator**–Warrior cable of Megaphase F520 which is used for measurement of dielectric properties of biological tissue is an alternative applicator. Its maximum operating frequency is up to 50GHz. It has excellent shielding effectiveness (minimum–110dBm) and super stable stability under flexure. It is more flexible than the cable RG393. For actual requirement, it could replace rigid cable RG393 (annex 3).

Figure 3.8: Structure of coaxial cable:
inner conductor–solid Ag-plated Cu, dielectric–PTFE, and outer conductor–GrooveTube® Cu

3.3 Microwave hyperthermia experiment procedure

With the adjustment of the power level of the microwave source and the considering losses measured in the connecting cables, microwave power at the operating frequency of 2.45GHz with a maximum output of 10W at the extremity of coaxial cable is available for biological tissue irradiation. Five different types of biological tissues were used for microwave hyperthermia experiments: pork, beef and chicken (muscle type); pork and calf's livers (liver type). The thicknesses of all the samples are approximately between 2 and 4.3mm and their diameters are about 4.5cm.

Microwave applicator contacts tightly with the irradiated surface–applicator side of biological tissue sample. Superficial temperature of the sample on the infra–red sensor side is measured and stored every second. The experimental temperatures about 40°C–50°C are considered, because the pathological tissue will be destroyed in this temperature range.
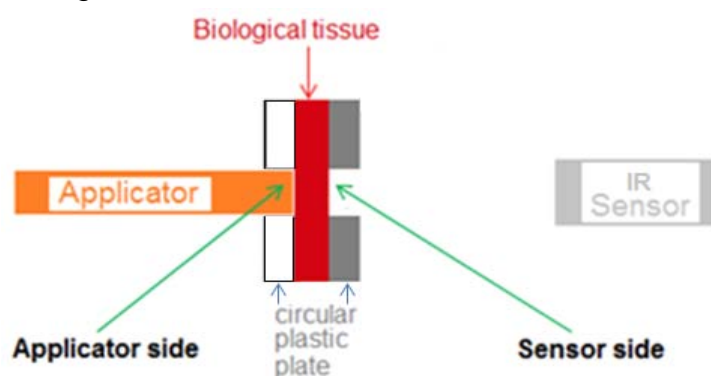
Figure 3.9: Schema of irradiated and measured temperature sides of the biological tissue fixed by the circular plastic sample holders

Two different applicators are used for microwave hyperthermia experiments: **coaxial cable RG393** (figure 3.7) and **Warrior cable** which has been tested for dielectric characterization measurement (figure 3.8).

Two protocols have been defined for the microwave hyperthermia experiments:

1st: Applying a constant microwave power for a period of 210 seconds: the emitted microwave hyperthermia power keeps a constant value during the whole heating period. It means that the microwave power level rises directly from 0W to a certain power level (for example: 1, 2, or 3W) and kept at this level for 210 seconds. At the following 210 seconds, the microwave was cut off, so there is no delivered microwave power to the biological tissue (figure 3.10).
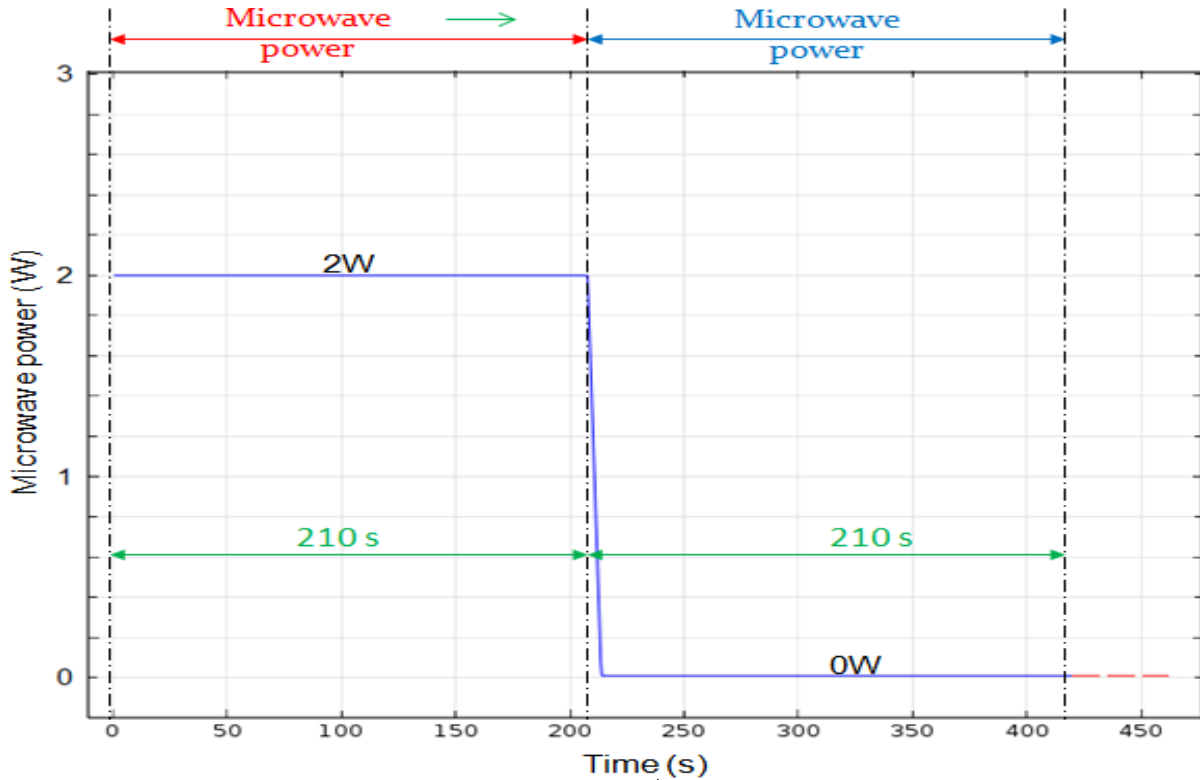
Figure 3.10: Schematic of the 1st experimental protocol:
application of a constant microwave power during 210s

2nd: Applying a step microwave power: the emitted incident microwave power increases progressively from 1W to 3W every 120 seconds, and decrease from 3W to 0W every 60 seconds (figure 3.11).
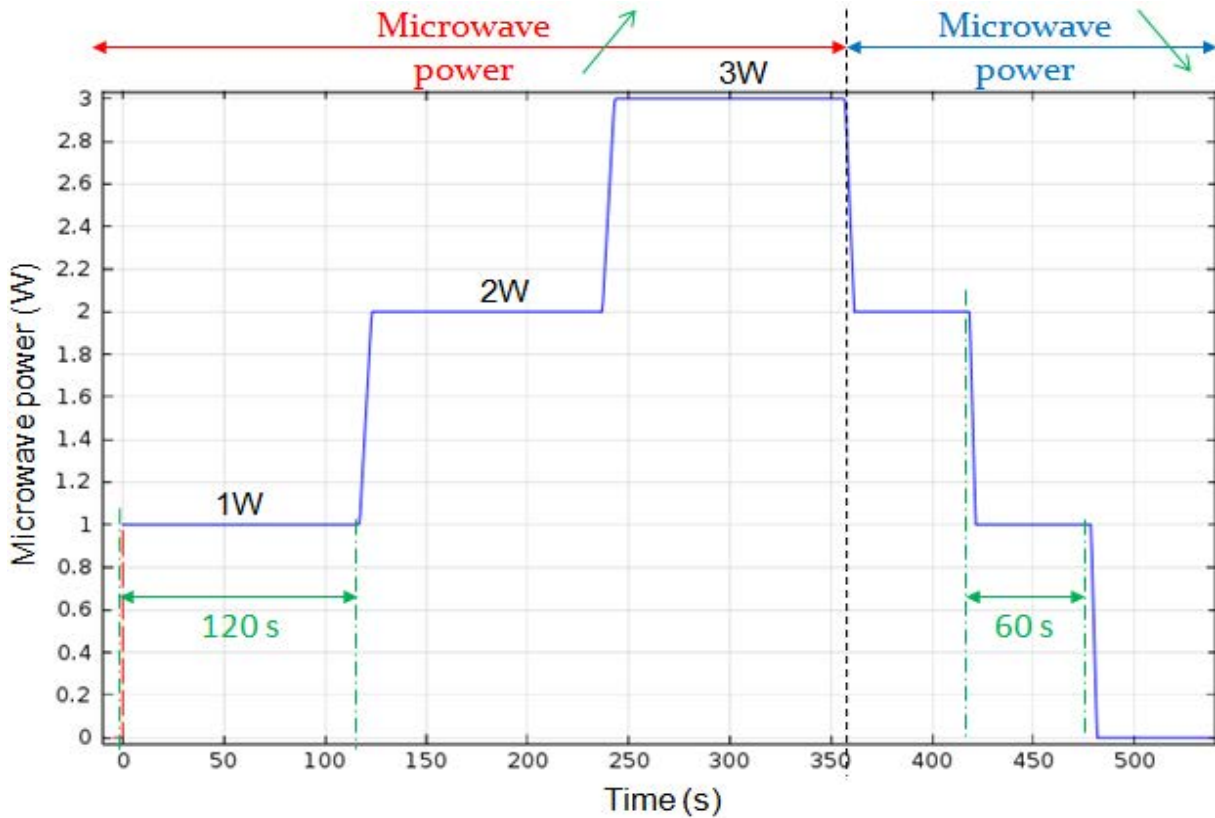

Figure 3.11: Schematic of the 2nd experimental protocol:
application of a progressively changing microwave power

3.4 Experimental results of coaxial cable RG393

Measured reflection power levels (-dBm) by power meter are noted at different time in each figure.

a) Experimental results of pork samples of different thicknesses.

1st protocol: constant microwave power
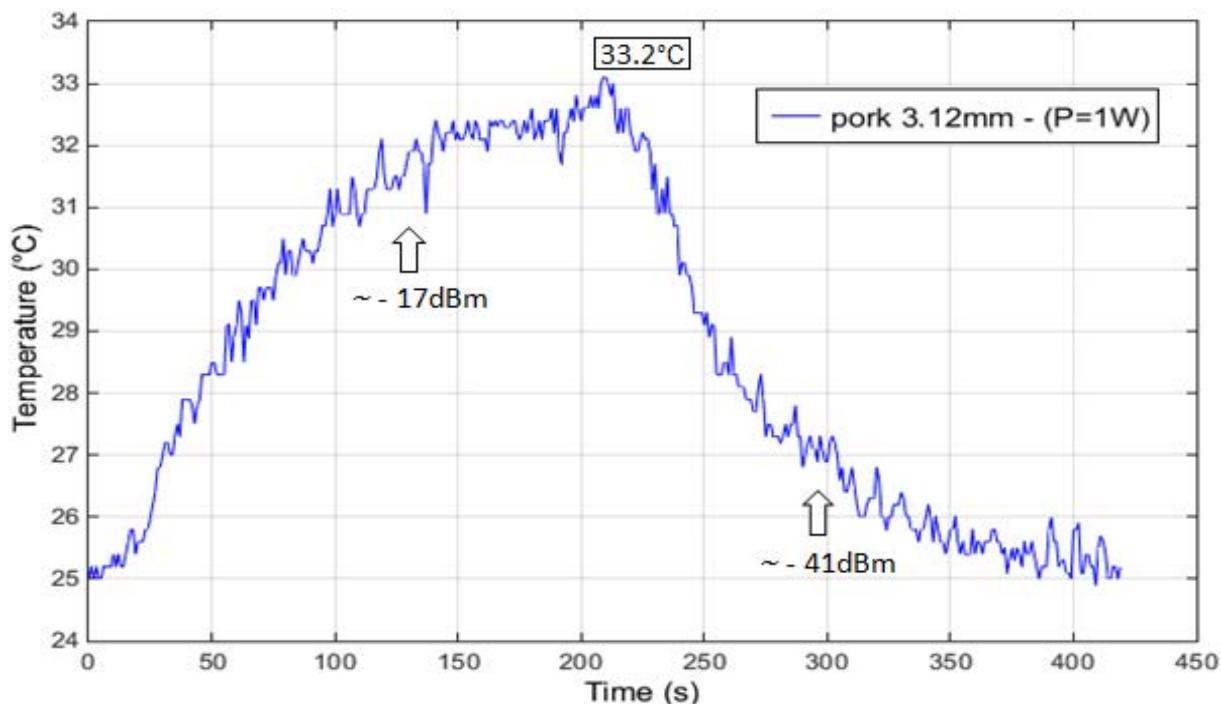
Figure 3.12: Temperature variation of the irradiated pork (thickness: 3.12 mm)
with constant microwave power P=1W
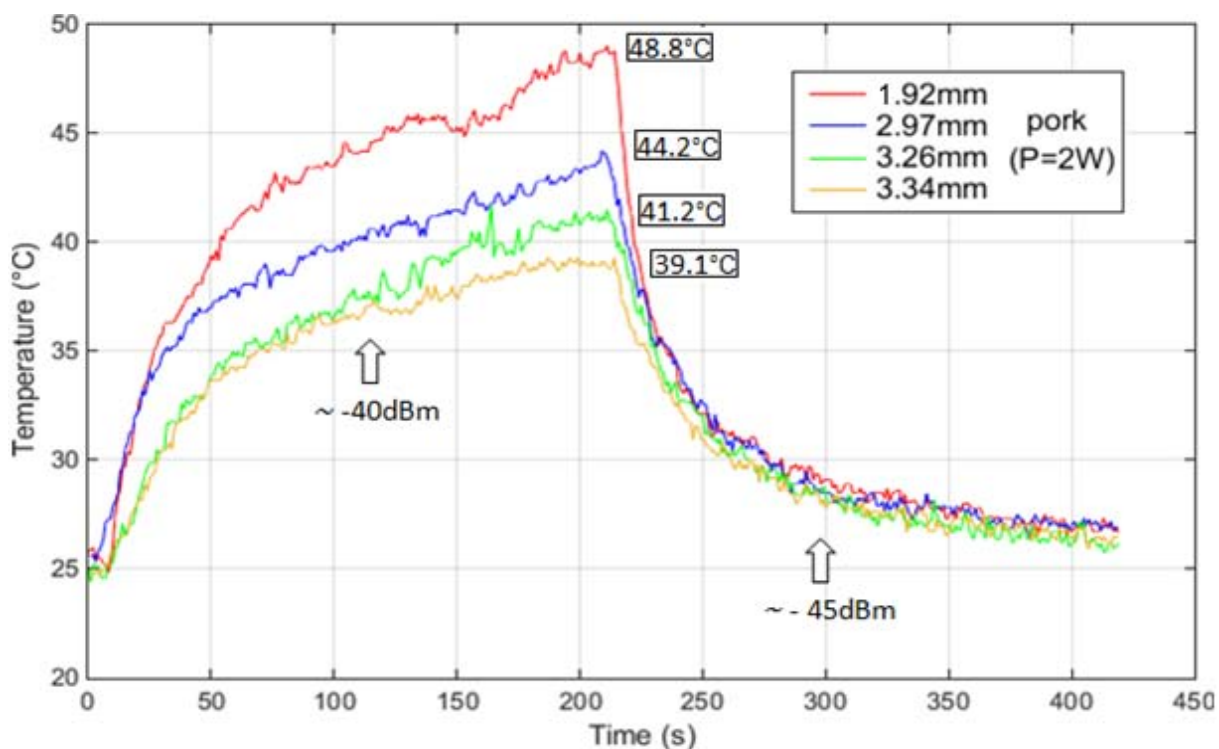
Figure 3.13: Comparison of temperature variations of the irradiated pork samples of different thickness
with a constant microwave power P=2W
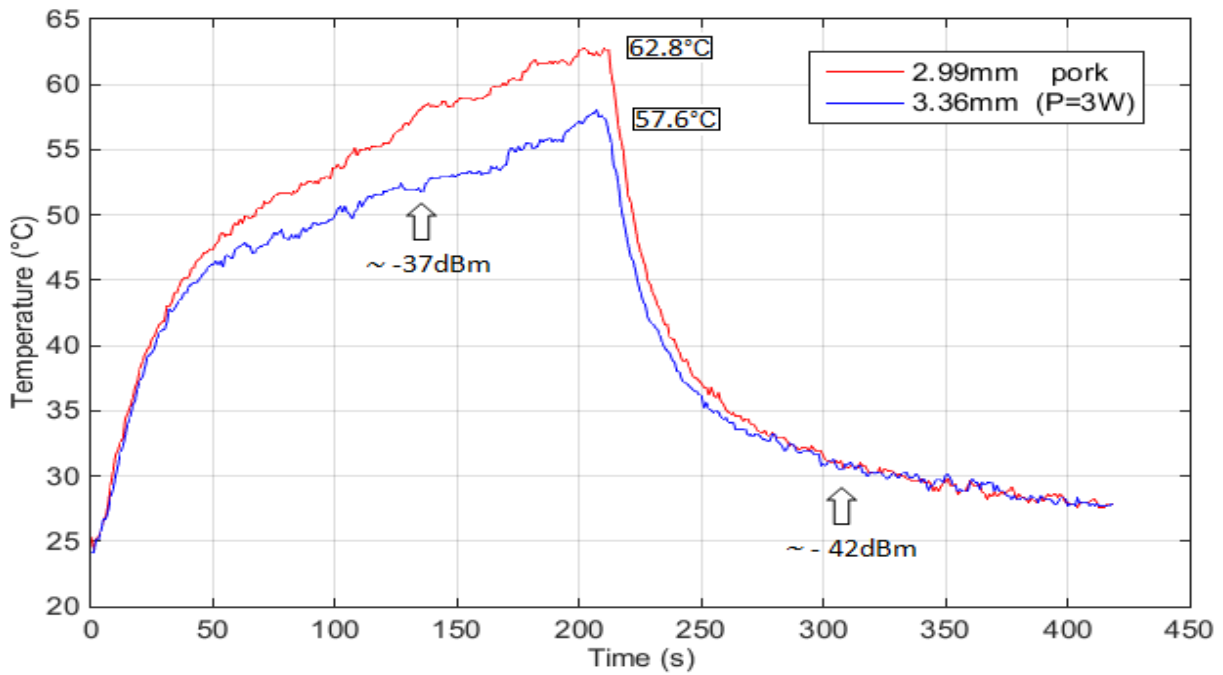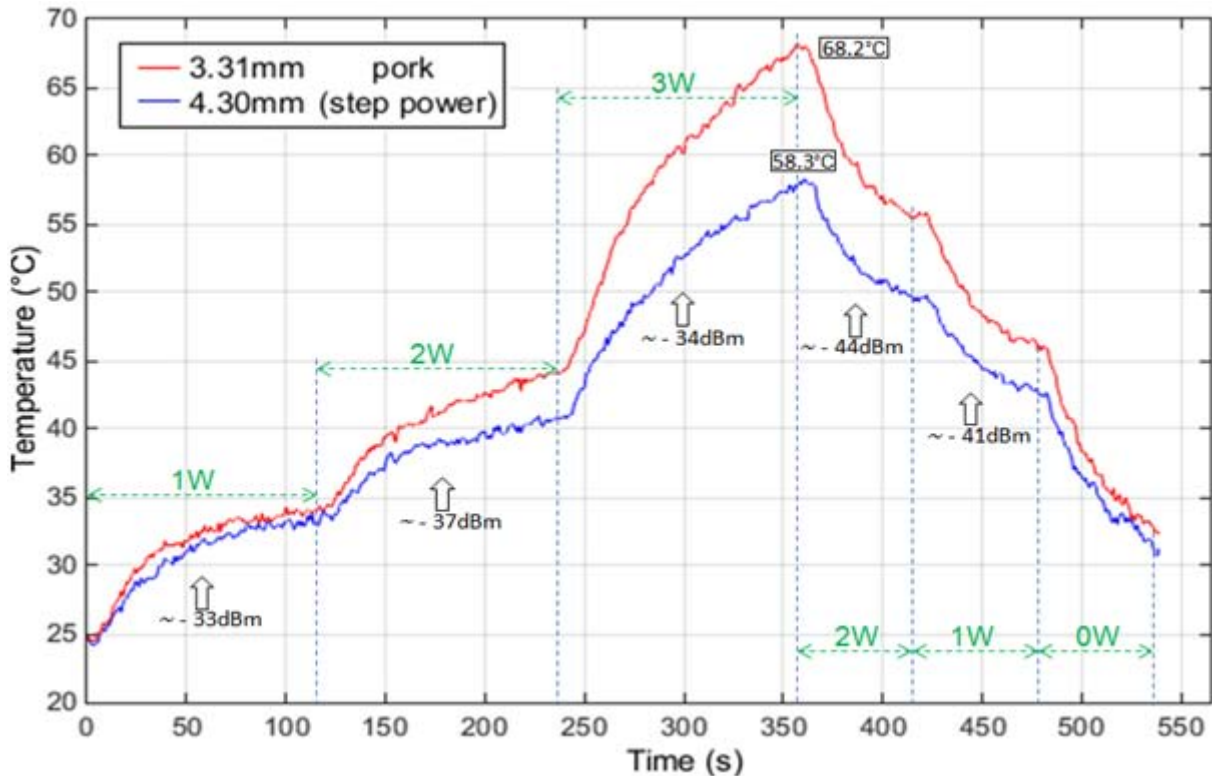
Figure 3.14: Comparison of temperature variations of the irradiated pork samples of different thicknesses with a constant microwave power P=3W

When the same level power is applied to each sample with different thicknesses, thinner sample which is heated can get higher temperature. For P=3W, at the 210th second, thinner 2.99mm pork sample attaints T_{max} = 62.8°C, but 3.36mm sample attains only T_{max} = 57.6°C. The difference of thickness is about 0.35mm between these two samples and the difference of maximum attainted temperature is $T_{difference}$ = ~5.2°C (figure 3.14). For pork muscle samples with similar thicknesses of about 3.2mm, higher constant power level applied to the sample allows obtaining higher temperature (figure 3.15).
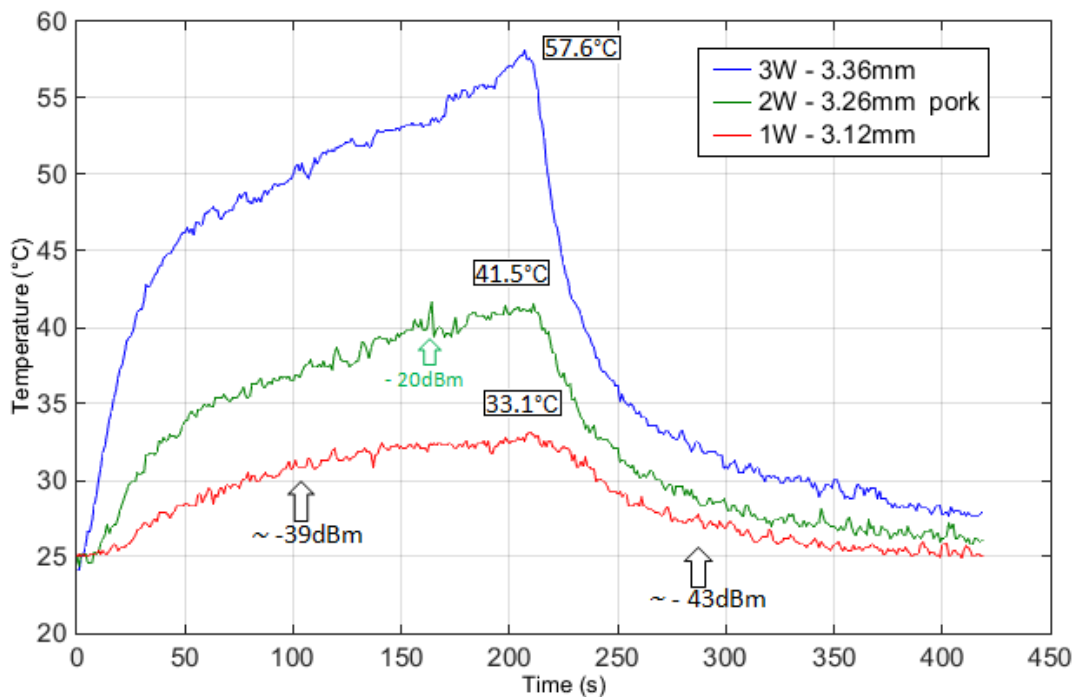
Figure 3.15: Comparison of temperature variations on pork samples of similar thicknesses with different applied constant microwave power levels (P=1, 2 and 3W)

2nd protocol: step microwave power

When progressively changing step power is applied to the samples, thinner sample attains higher temperature. At the 360th second, 3.31mm pork sample attains T_{max} = 68.2°C; while another 4.30mm sample attains T_{max} = 58.3°C. The thickness difference between them is about 0.6mm and $T_{difference}$ ≈ 10°C (figure 3.16). Besides the morphology study of these samples shows that in the center of surface–cable side of irradiated 3.31mm pork, it has been burned, but on other surface–infra red sensor side, the color of tissue is not red any more, but is still white. The properties of tissue are changed (figure 3.17).

Figure 3.16: Comparison of temperature variations of the irradiated pork samples
of two different thicknesses with progressively changing step microwave power
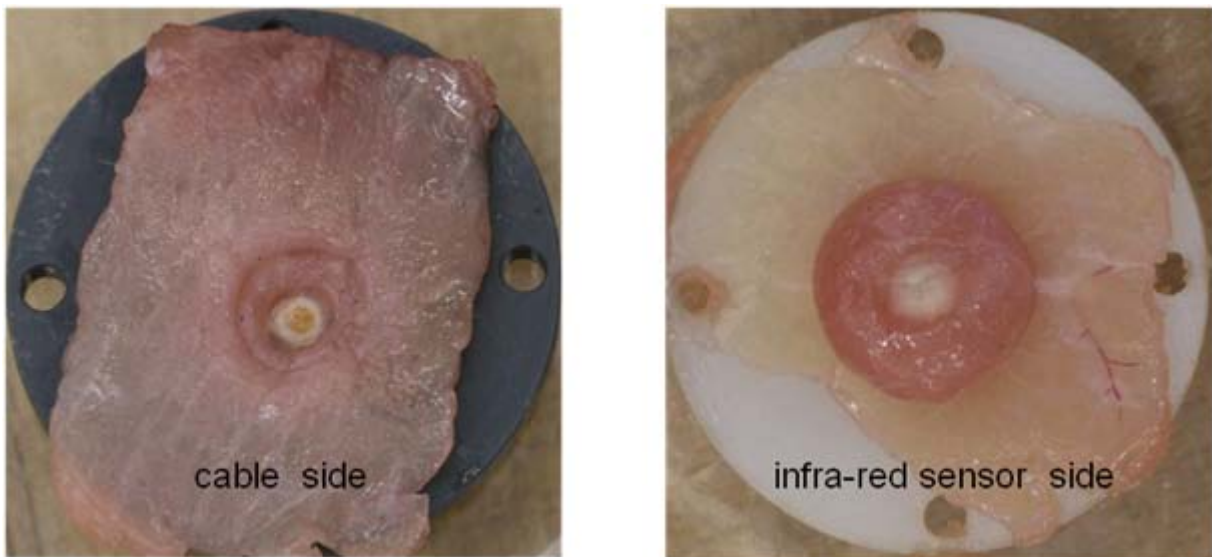
Figure 3.17: Comparison of morphology images of cable side and infra–red sensor side
of the irradiated 3.38mm pork sample with step microwave power protocol

b) Experimental results of beef samples of different thicknesses.

1st protocol: constant microwave power
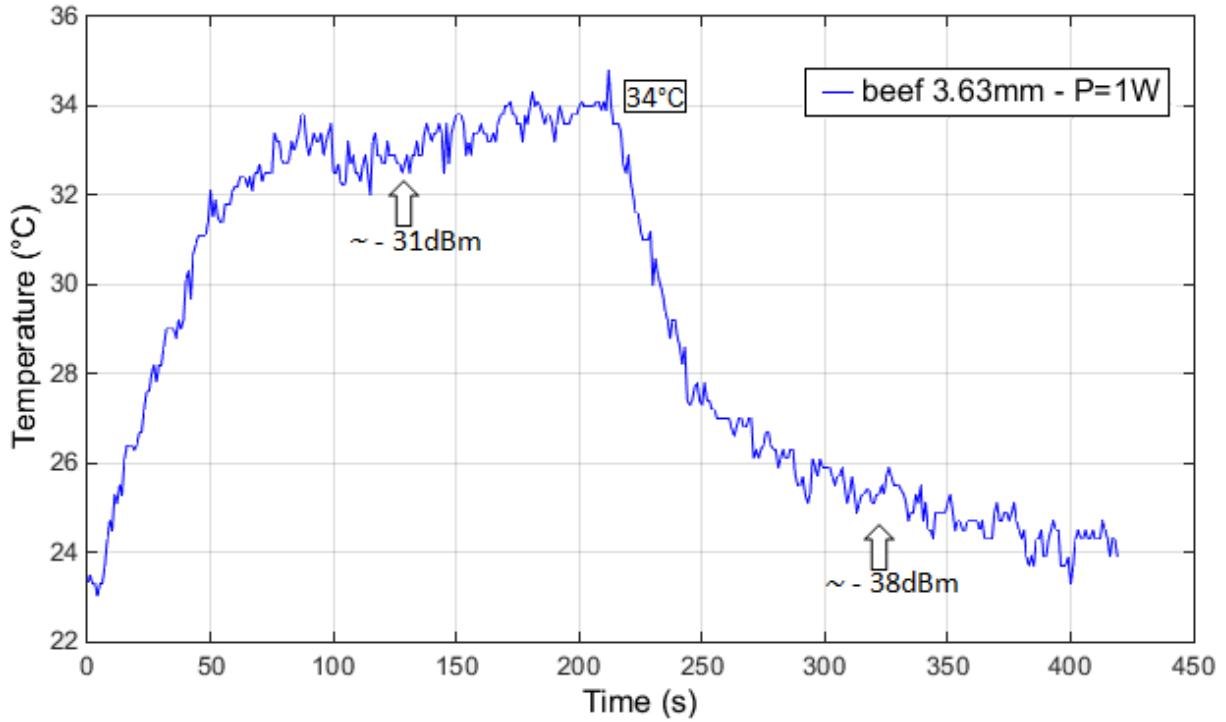
Figure 3.18: Temperature variation of the irradiated beef (thickness: 3.63 mm)
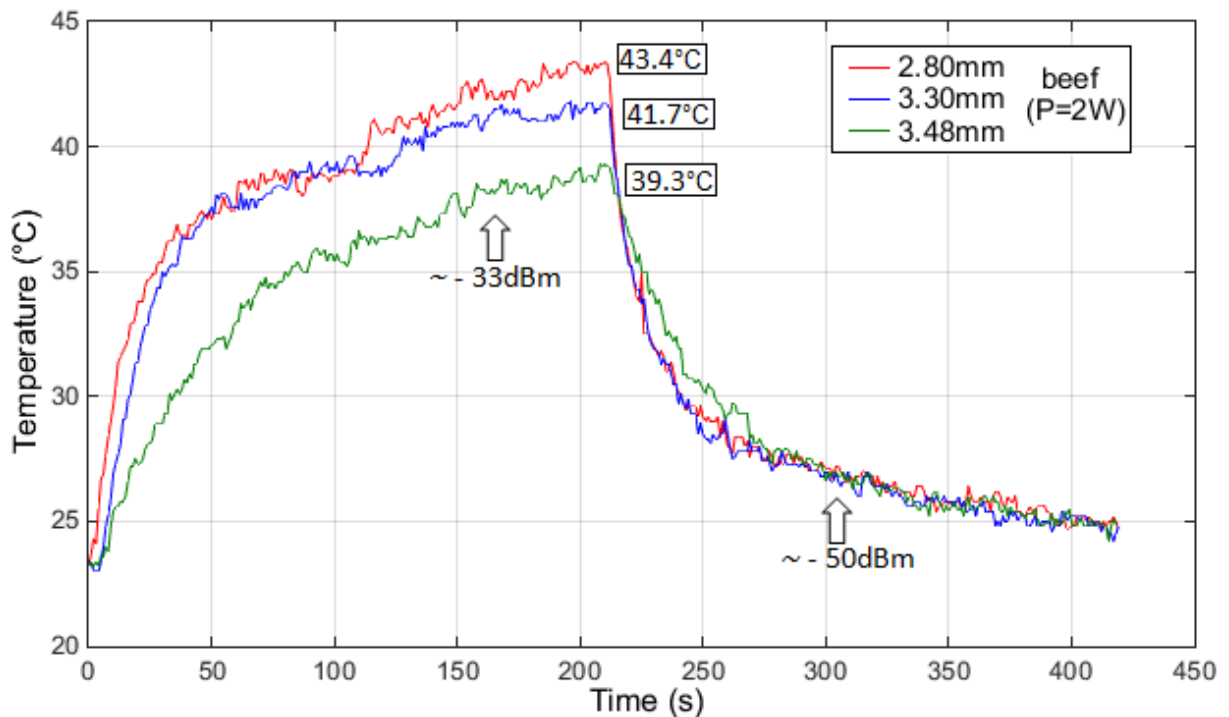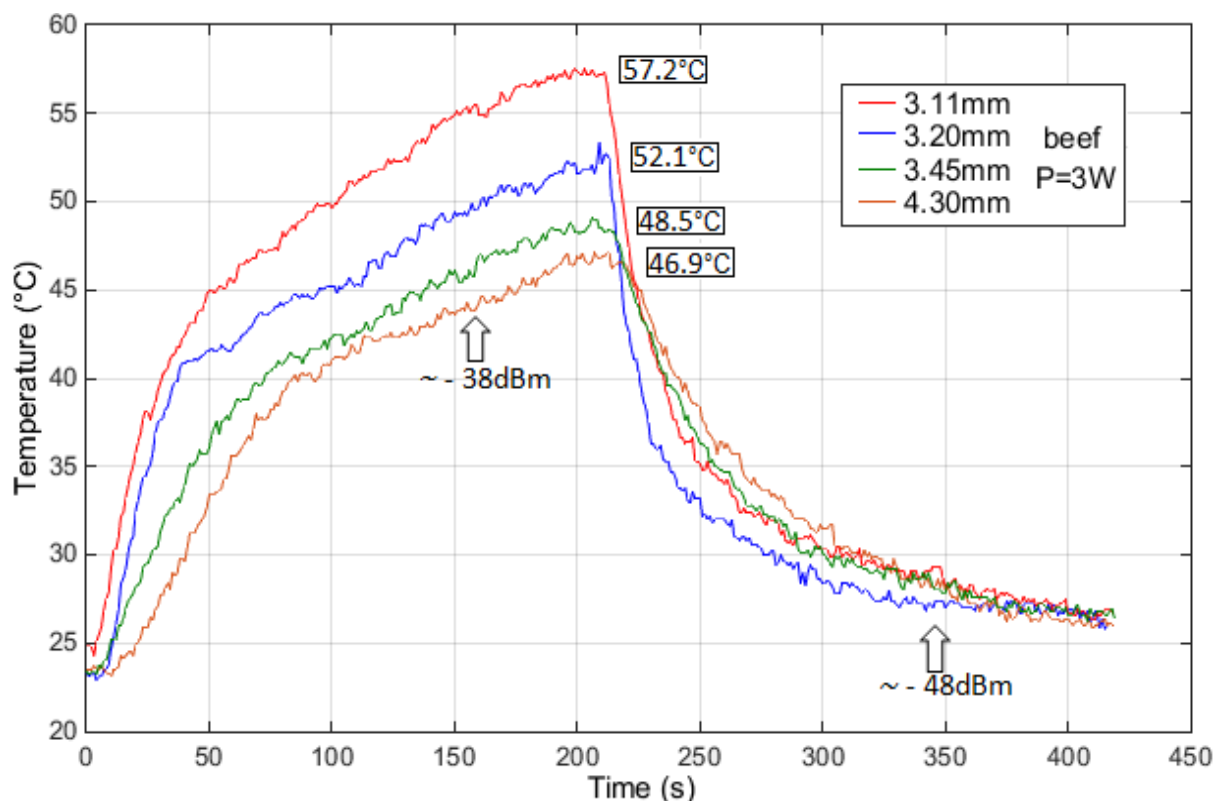with constant microwave power P=1W.

Figure 3.19: Comparison of temperature variations of the irradiated beef samples of different thickness
with a constant microwave power P=2W.

As for the pork samples, when constant power of same level is applied to beef samples of different thicknesses, thinner thickness leads to higher temperatures in the sample and measured on the infra–red sensor side (figures 3.18 and 3.19).

Figure 3.20: Comparison of temperature variations of the irradiated beef samples of different thickness with a constant microwave power P=3W.
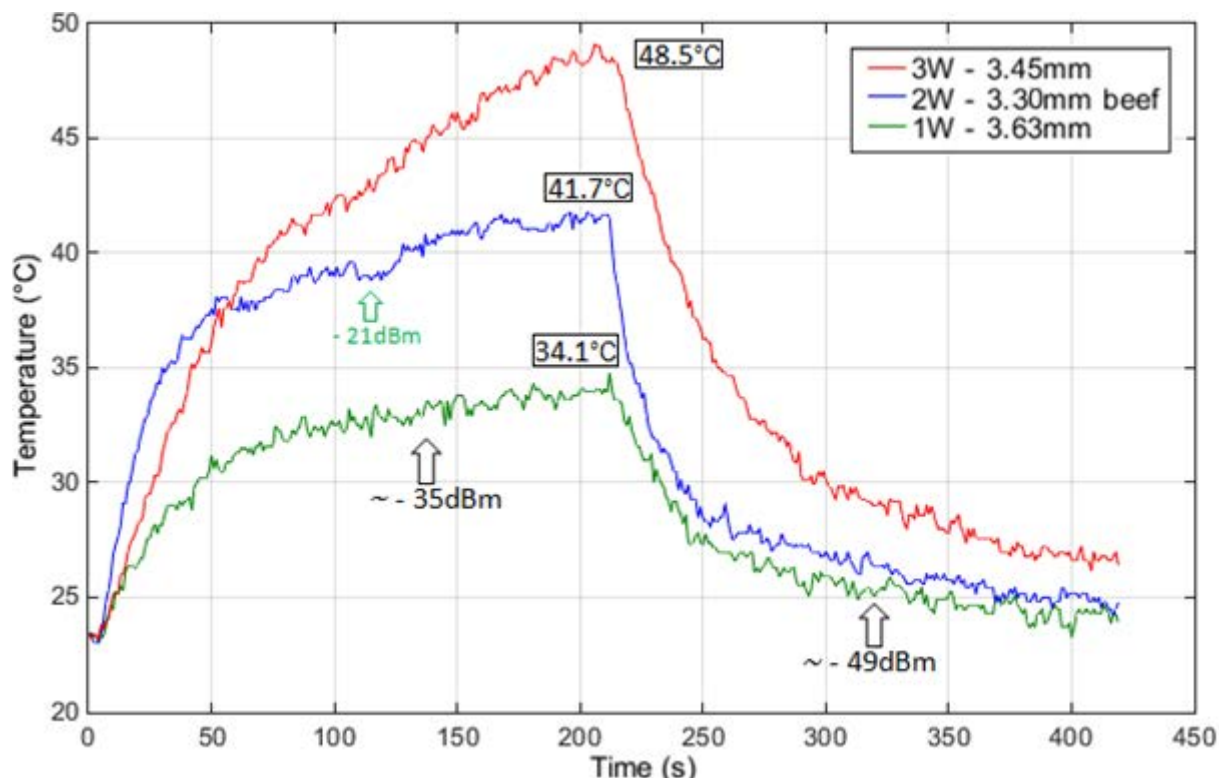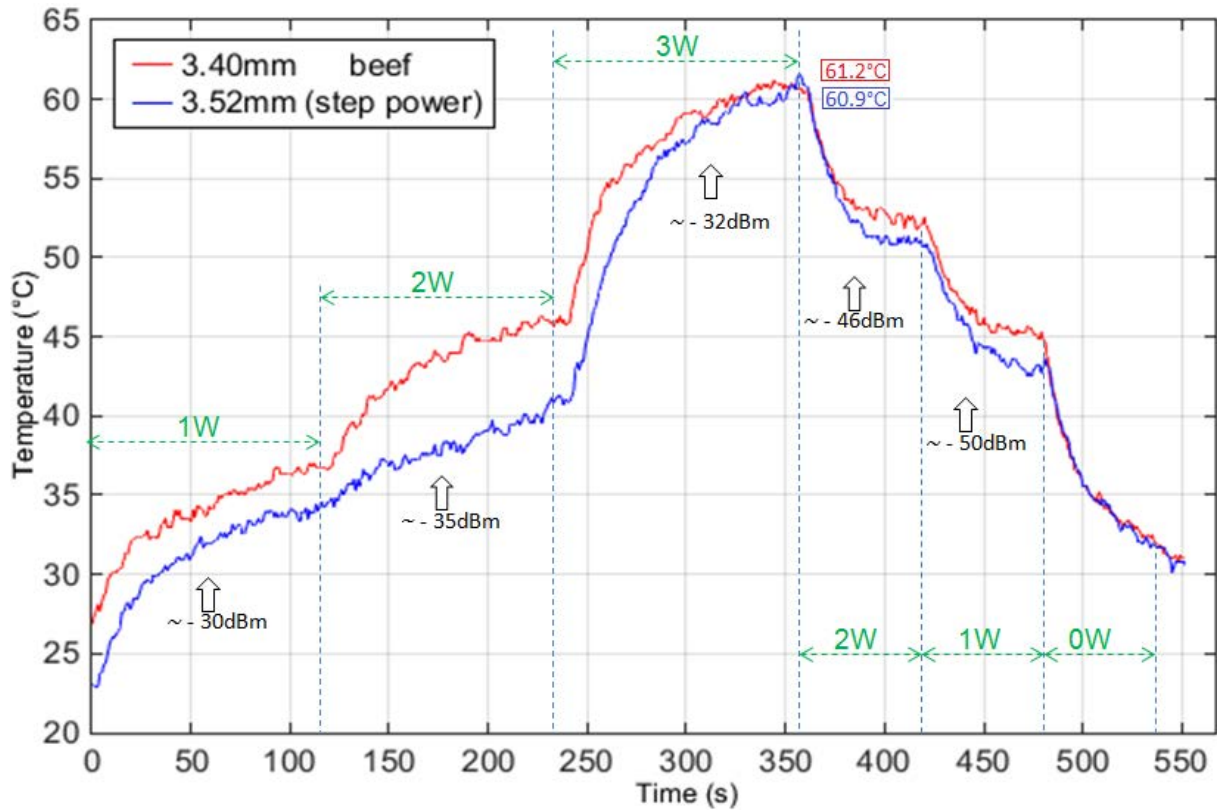

Figure 3.21: Comparison of temperatures on the beef samples of similar thicknesses with different constant microwave power levels (P=1, 2 and 3W)

For beef muscle samples with similar thicknesses about 3~4mm, higher constant power applied to the sample allows to obtain higher temperature (figure 3.21).

2nd protocol: step microwave power

Figure 3.22: Comparison of temperature variations of the irradiated beef samples
of two different thicknesses with progressively changing step microwave power
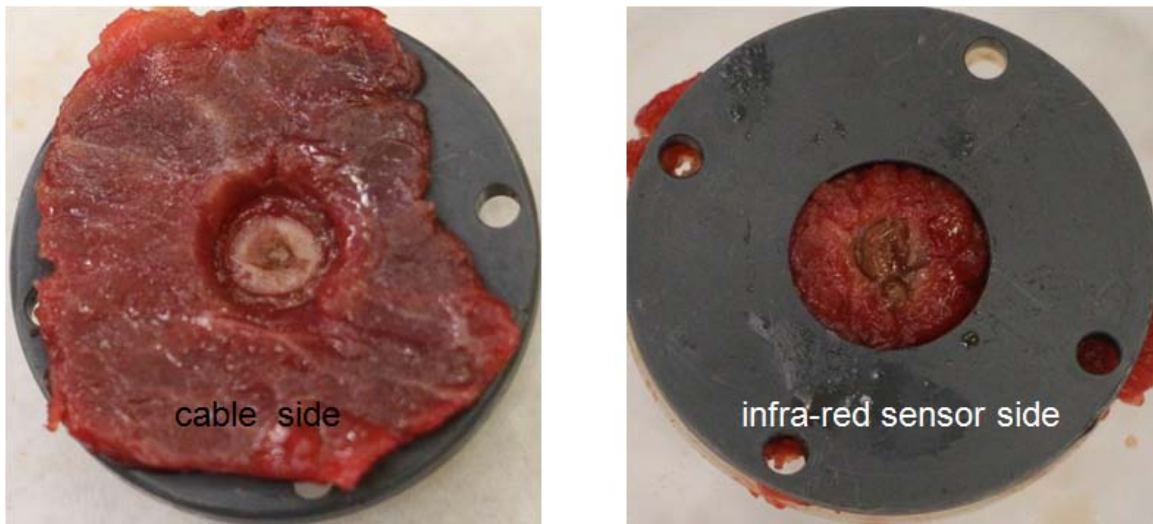

Figure 3.23: Comparison of morphology images of cable side and infrared sensor side
of the irradiated 3.40mm beef sample with step microwave power protocol.

When progressively changing step power is applied to the samples, thinner sample attains higher temperatures. At the 360th second, 3.40mm beef sample reaches T_{max} = 61.2°C and 3.52mm beef sample attains T_{max} = 60.9°C (figure 3.22). Their maximum temperatures are very close. In the center of irradiated surface–cable side of beef sample (thickness: 3.40mm), it has been burned, but on infrared sensor side surface, the color of tissue is not any more red but brown. The original properties of beef have changed because of being heated.

c) **Experimental results of chicken samples of different thicknesses.**
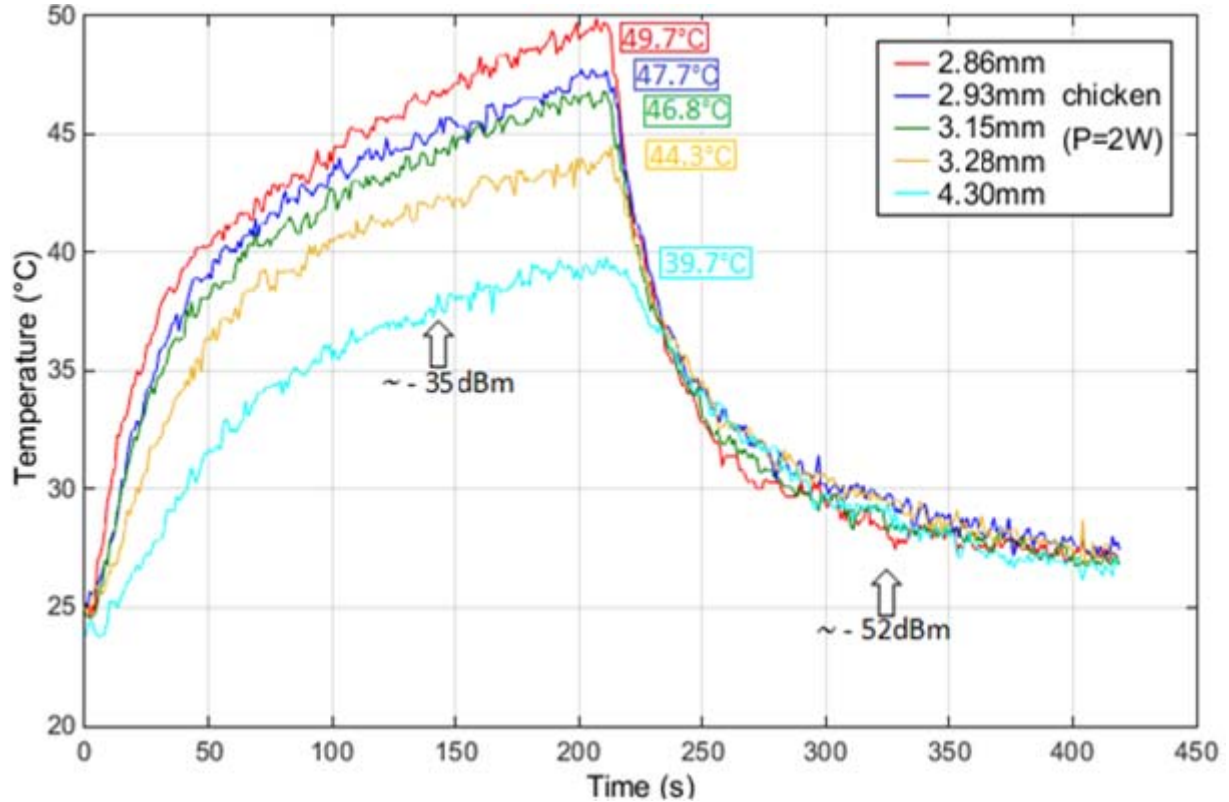
1st protocol: constant microwave power

Figure 3.24: Temperature variation of the irradiated chicken samples of different thickness
with a constant microwave power P=2W.
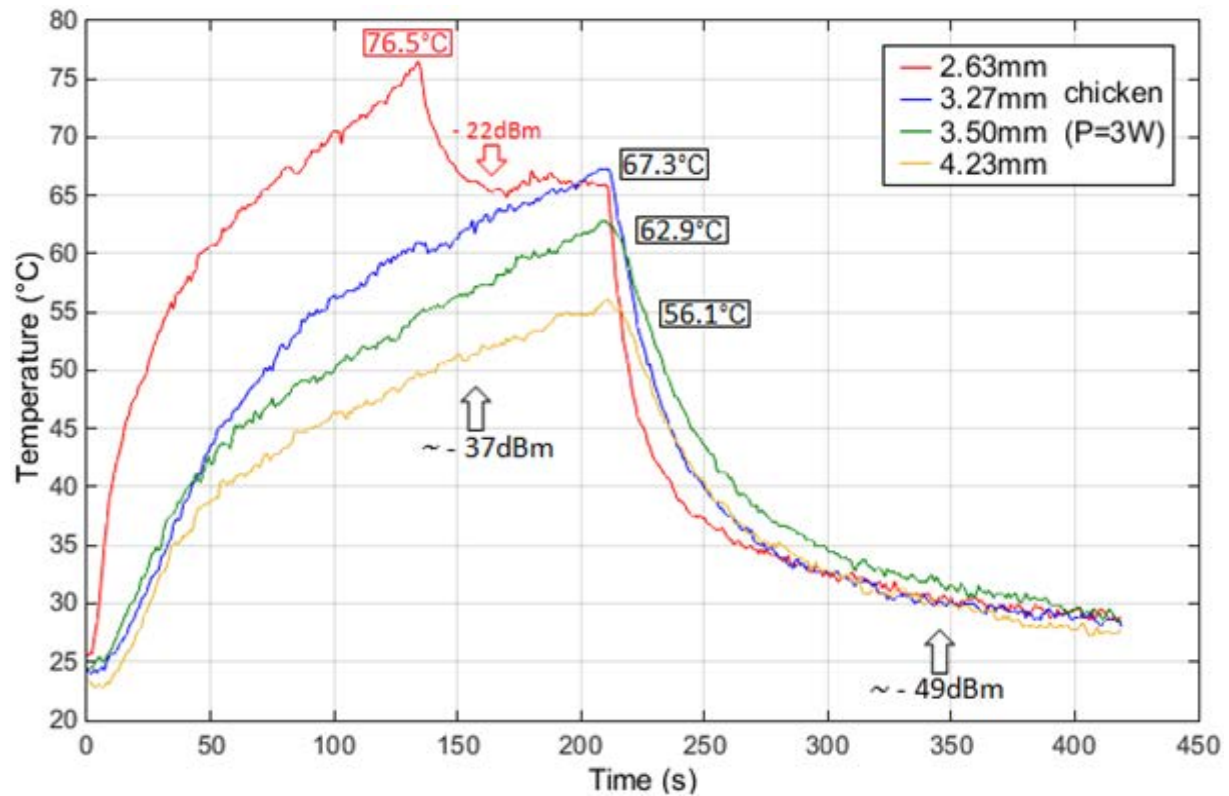

Figure 3.25: Temperature variation of the irradiated chicken samples of different thickness
with a constant microwave power P=3W
(For the sample with smallest thickness, a dielectric breakdown has been observed after 134s)

For the chicken samples of different thickness irradiated by P=3W, we have observed a dielectric breakdown for the thinnest sample (2.63mm). In fact, the average values of reflecting power were approximate –37dBm for applying power on period and –49dBm for no power period for other samples, but for 2.63mm thick sample, from the 134th second to the 210th second, power meter showed approximately –22dBm. At 134th second, the thinnest sample had been strongly burned on the cable side and a short creaking noise was heard. On the sensor side, the surface had become white comparing to other red parts. The original properties of the chicken have changed irreversibly. The double stubs immediately became difficult to control, so there was more reflecting power. That's why the temperature of infra–red sensor side decreased immediately and sharply.
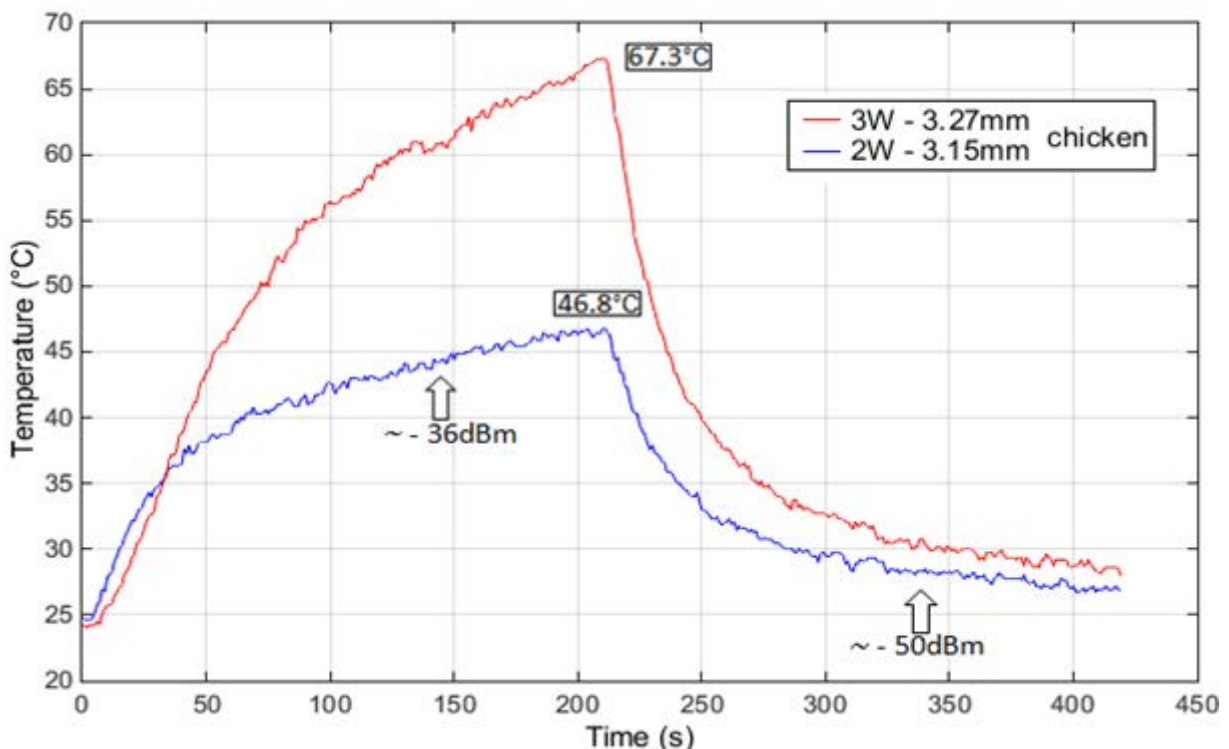

Figure 3.26: Comparison of temperature variations on chicken samples of almost same thickness with different applied constant microwave power levels (P=2 and 3W)
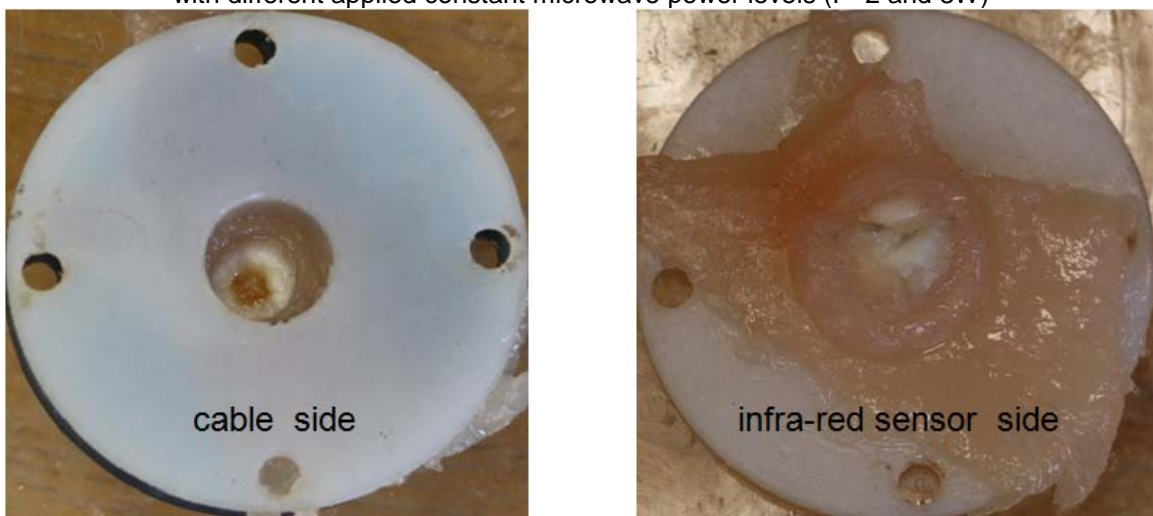

Figure 3.27: Comparison of morphology images of cable side and infraer–red sensor side of the irradiated 3.17mm thick chicken sample with P=3W
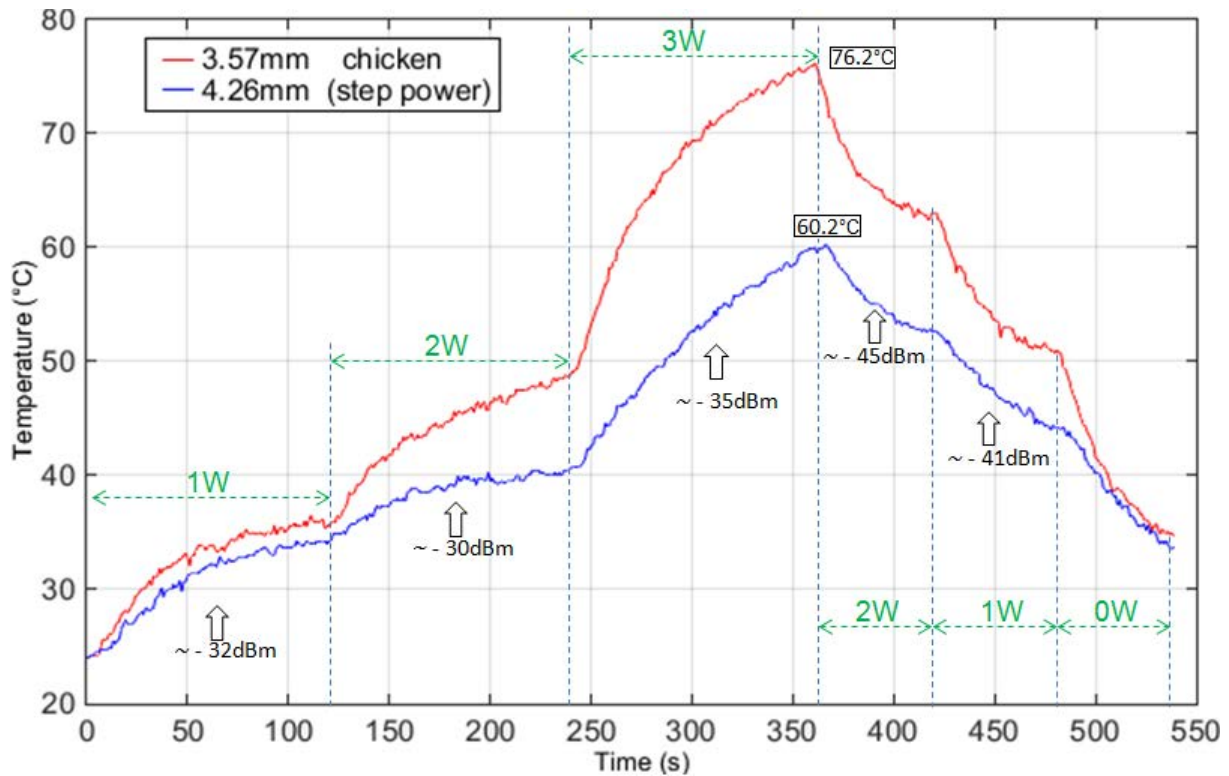
2nd protocol: step microwave power

Figure 3.28: Comparison of temperature variations of the irradiated chicken samples
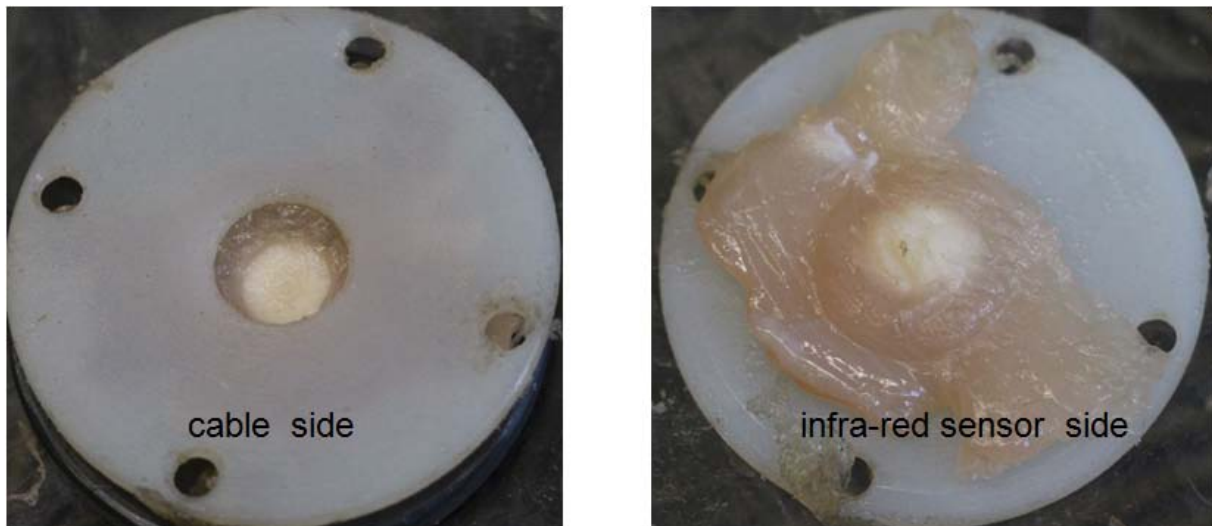of two different thicknesses with progressively changing step microwave power

Figure 3.29: Comparison of morphology images of cable side and infrared sensor side
of the irradiated 3.57mm thick chicken sample with step microwave power protocol

Applying progressively changing step power to the samples, thinner chicken sample (3.57mm) attained higher temperature T_{max} = 76.2°C at the 360th second. For chicken sample of 4.26mm thickness, T_{max} = 60.2°C (figure 3.28). The difference of temperature for both samples is $T_{difference}$ = 16°C. For 3.57mm thick chicken sample, the original properties of both sides had changed, and the color became white and had no more original color in the irradiated zone (figure 3.29).

d) Experimental results of pork liver samples of different thicknesses.

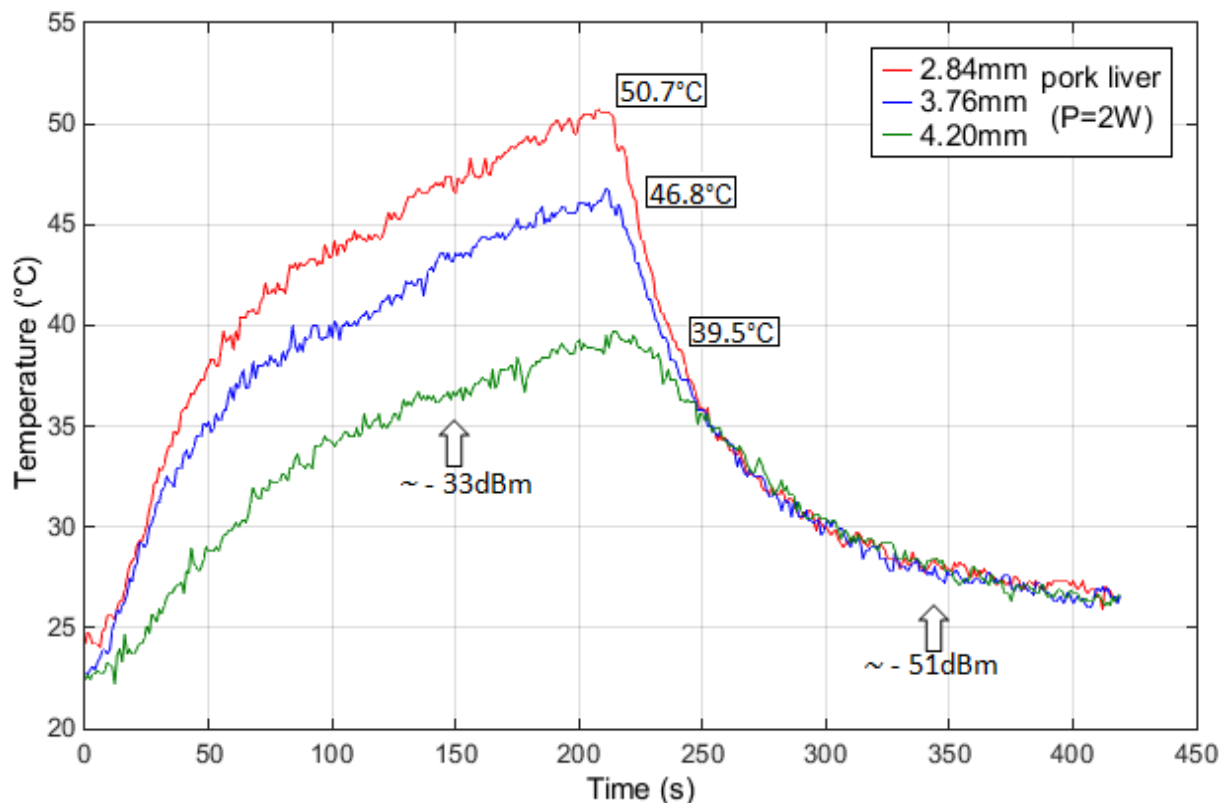1st protocol: constant microwave power

Figure 3.30: Comparison of temperature variations of the irradiated pork liver samples of different thicknesses with a constant microwave power P=2W
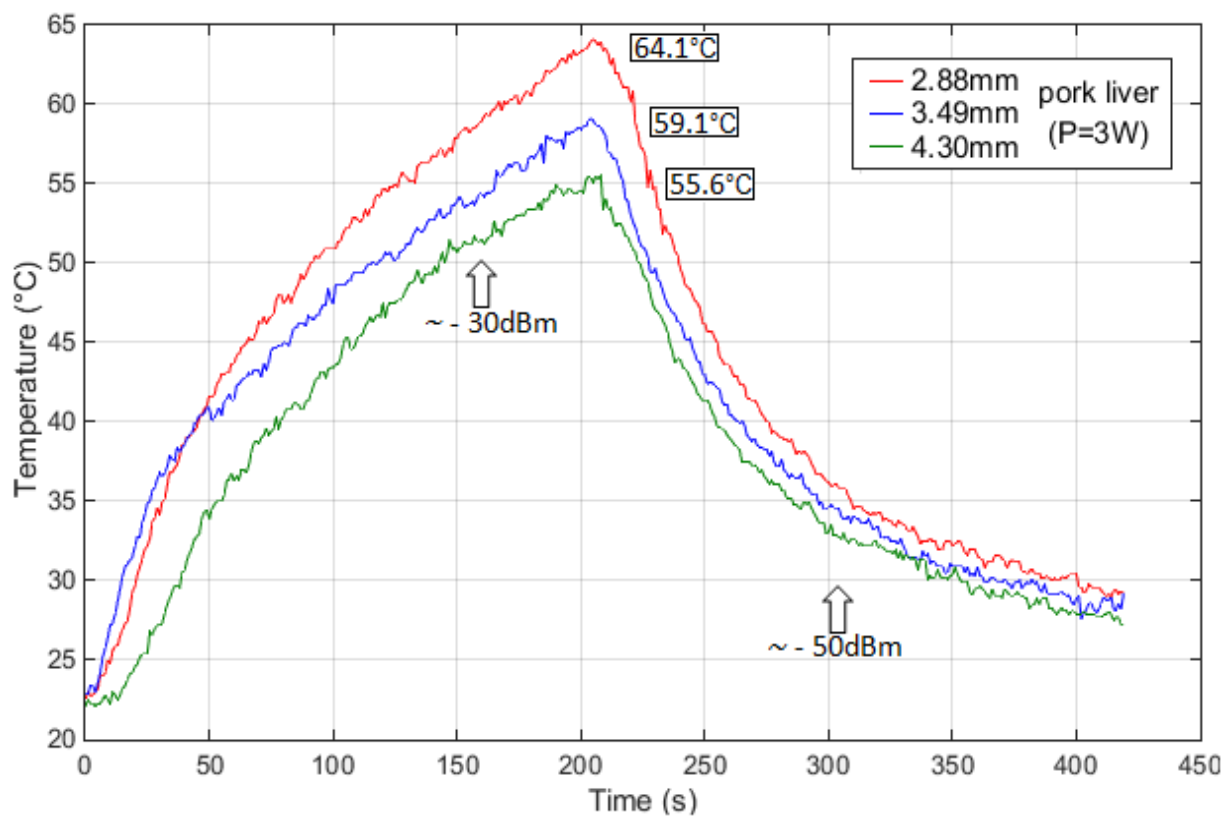

Figure 3.31: Comparison of temperature variations of the irradiated pork liver samples of different thicknesses with a constant microwave power P=3W
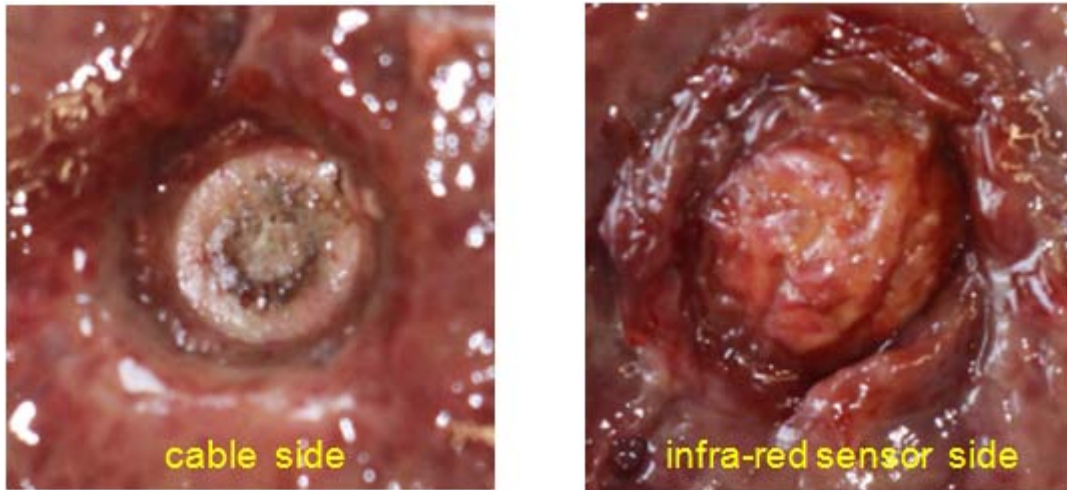
Figure 3.32: Comparison of morphology images of cable side and infrared sensor side
of the irradiated 4.30mm thick pork liver sample with P=3W.

Applying constant power on the pork liver samples, thinner sample obtained higher temperature. With constant power P=3W, 4.30mm thick pork liver attained T_{max} = 55.6°C. As shown in the figure3.32, for the cable side, in the central part, there has been a small circle of carbonization; for the sensor side, the sample morphology shows that the irradiated part has become harder and drier. Before and after irradiation, pork liver had completely two different morphologies. The properties have been completely changed because of the heat.
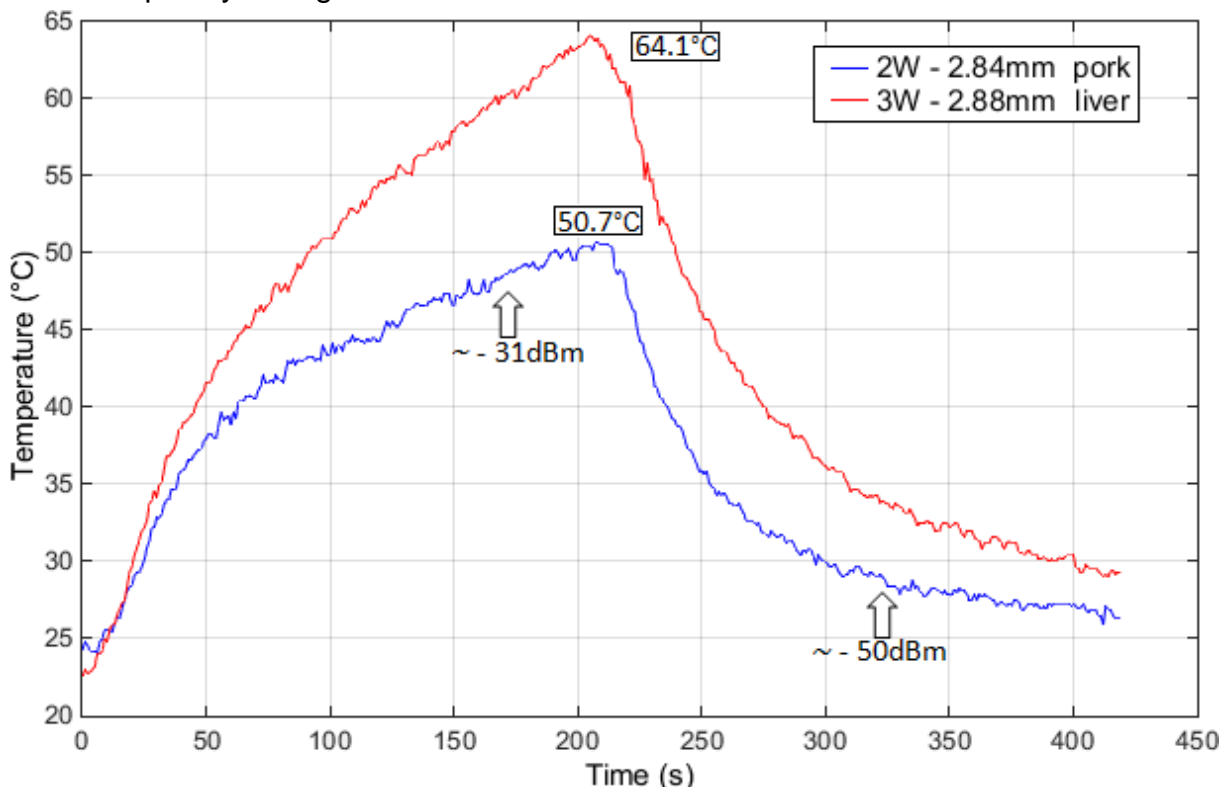

Figure 3.33: Comparison of temperature variations on pork liver samples of almost same thickness
with different applied constant microwave power levels (P=2 and 3W)

For samples of similar thickness, higher applied constant power leads to higher temperature (figure 3.33). For 2.88mm thick sample and P=3W, T_{max} = 64.1°C. For 2.84mm thick sample and P=2W, we observe T_{max} = 50.7°C.
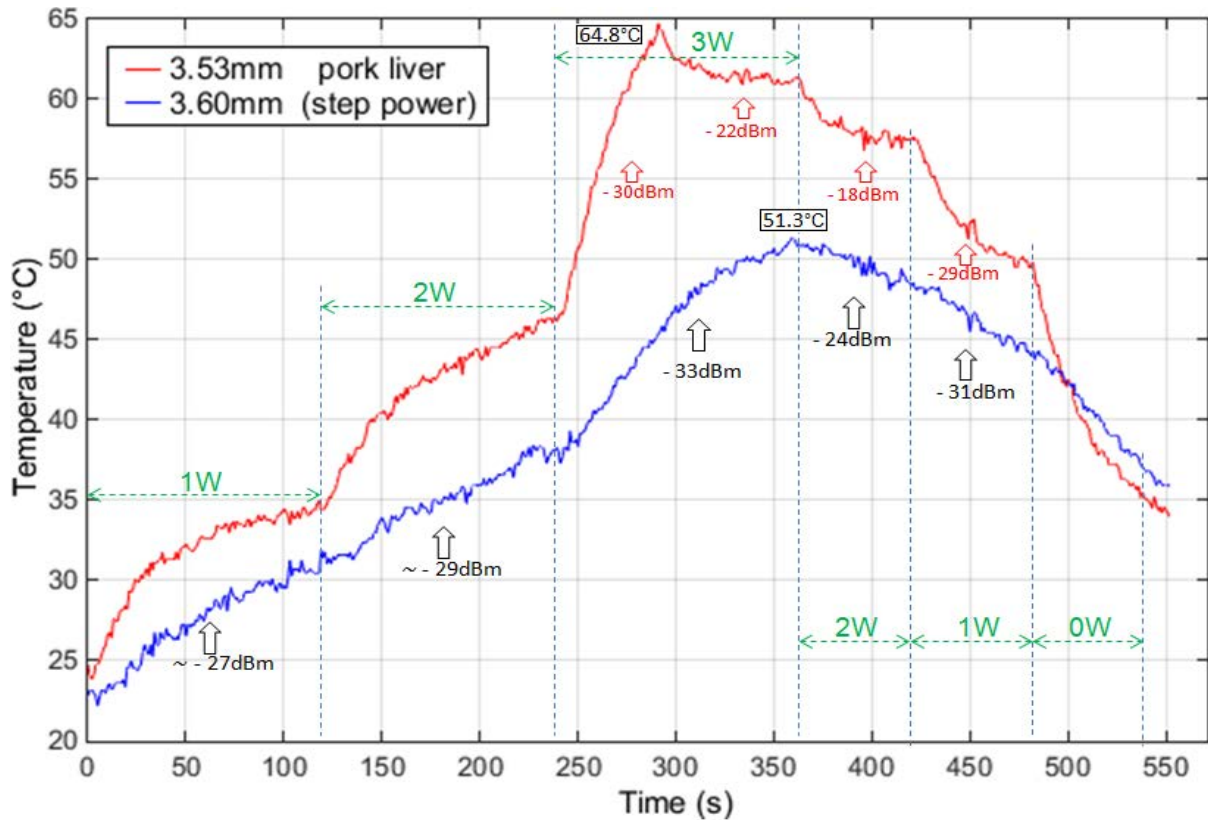
2nd protocol: step microwave power

Figure 3.34: Comparison of temperature variations of the irradiated pork liver samples of two different thicknesses with progressively changing step microwave power

Figure 3.35: Comparison of morphology images of cable side and infrared sensor side of the irradiated 3.53mm thick pork liver sample with step microwave power protocol

At the beginning of heating periods of P=1 and 2W, average values of reflecting power were approximately –27dBm and –29dBm, both samples have similar increasing tendency of temperature. But for P=3W period: thinner pork liver 3.53mm sample attained T_{max} = 68.1°C at 291s; then its temperature started to decrease; more reflecting power was observed on the power meter. The morphology of this sample (figure3.35) shows that a circle of carbonization on the surface of cable side which has been strongly burned and a short creaking noise was heard. On the sensor side, the surface had become dark, hard and dry comparing to other red

parts. The original properties of pork liver have been strongly changed. The double stubs became more difficult to control and that's why there was more reflecting power (−18dBm and −22dBm). For 3.60mm thick pork liver, the tendencies of temperature increasing and decreasing are more linear than the 3.53mm thick sample with T_{max} = 51.3°C; and its temperature started to decrease at the 360th second when the power decreased from 3 to 2 Watt

e) Experimental results of calf's liver samples of different thicknesses.

1st protocol: constant microwave power

Figure 3.36: Temperature variation of the irradiated calf's liver sample (thickness: 3.35 mm) with a constant microwave power P=1W

Figure 3.37: Comparison of temperature variations of the irradiated calf's liver samples of different thicknesses with a constant microwave power P=2W
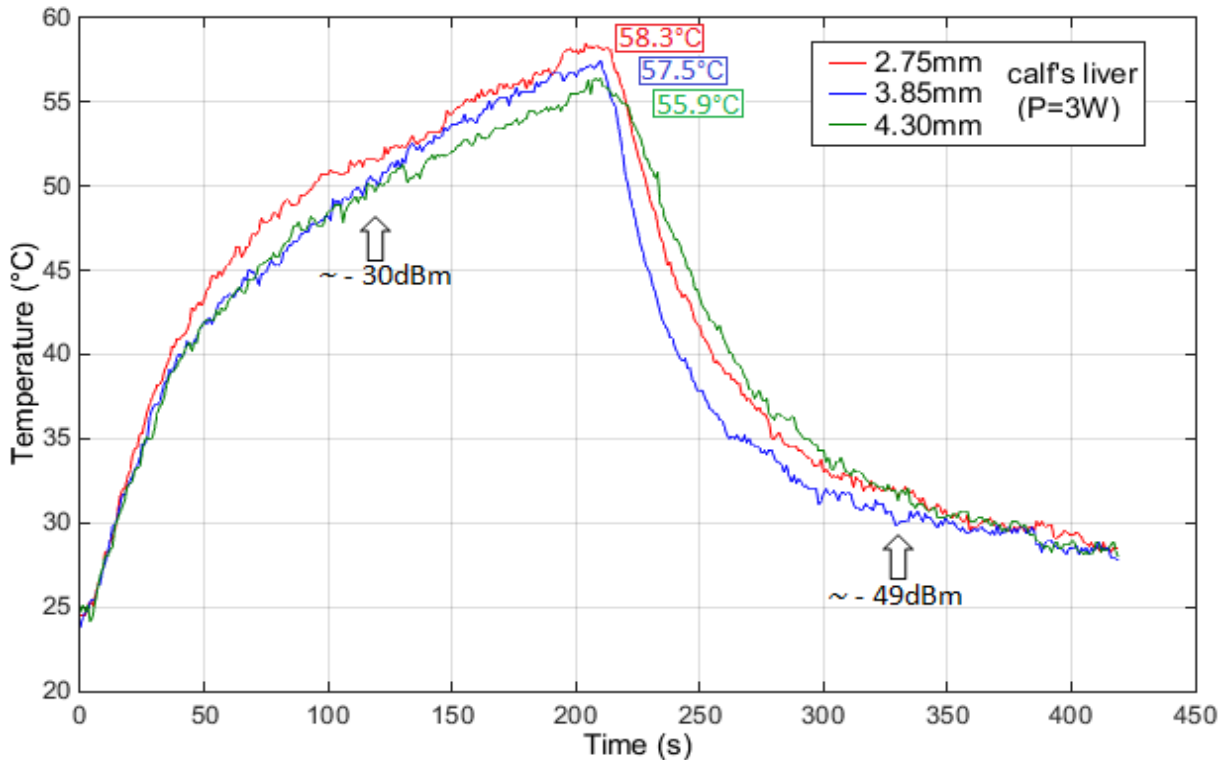
Figure 3.38: Temperature on the calf's liver samples with constant microwave power P=3W

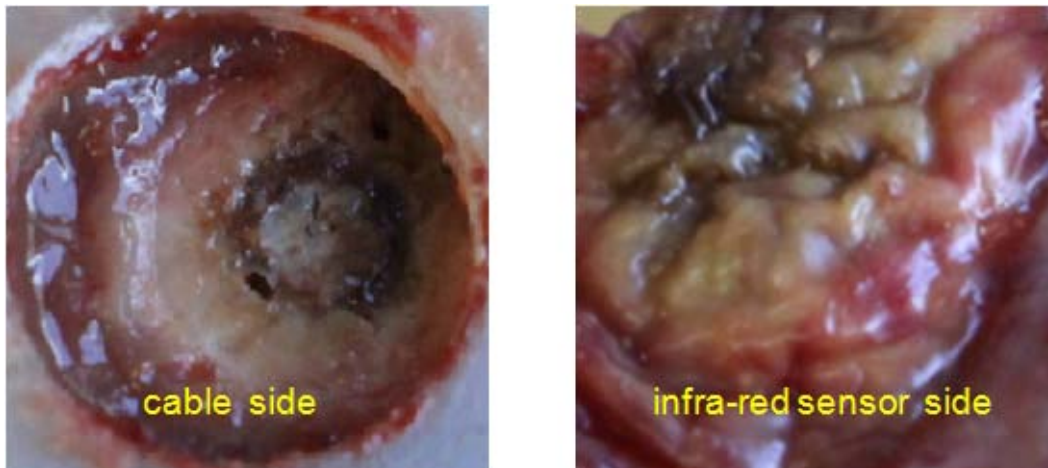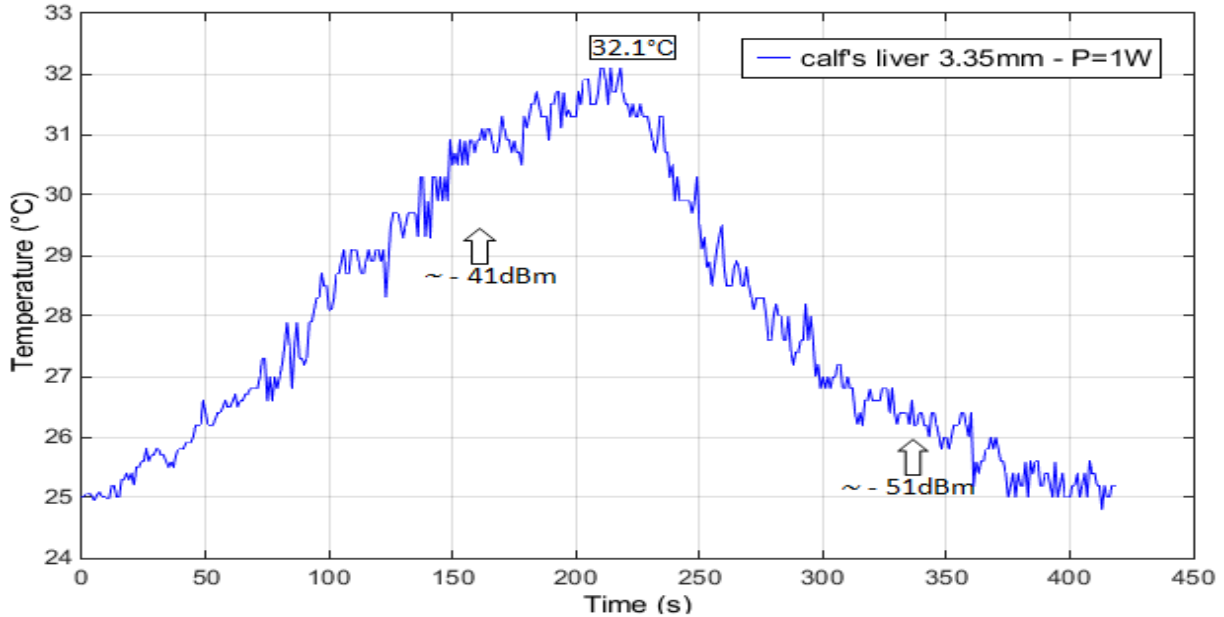Figure 3.39: Comparison of morphology images of cable side and infrared sensor side
of the irradiated 4.30mm thick calf's liver sample with P=3W

Applying higher power on the calf's liver samples has allowed obtaining higher temperature. For P=2W, there are two separate groups of temperature curves: one group with thickness about 3mm, T_{max} = ~47°C; and for the other group with thickness about 4mm, T_{max} = ~43°C (figure 3.37). For P=3W, 4.30mm thick calf's liver attained T_{max} = 55.9°C which is almost same as T_{max} = 55.6°C of pork liver with the same power level. For the cable side, in the central part, color of calf's liver changed into dark brown and it is not red any more for the sensor side. Before and after irradiation, the heated part of calf's liver had completely changed and became harder and drier. Therefore, the properties of calf's liver have been completely changed because of the heat (figure 3.39).
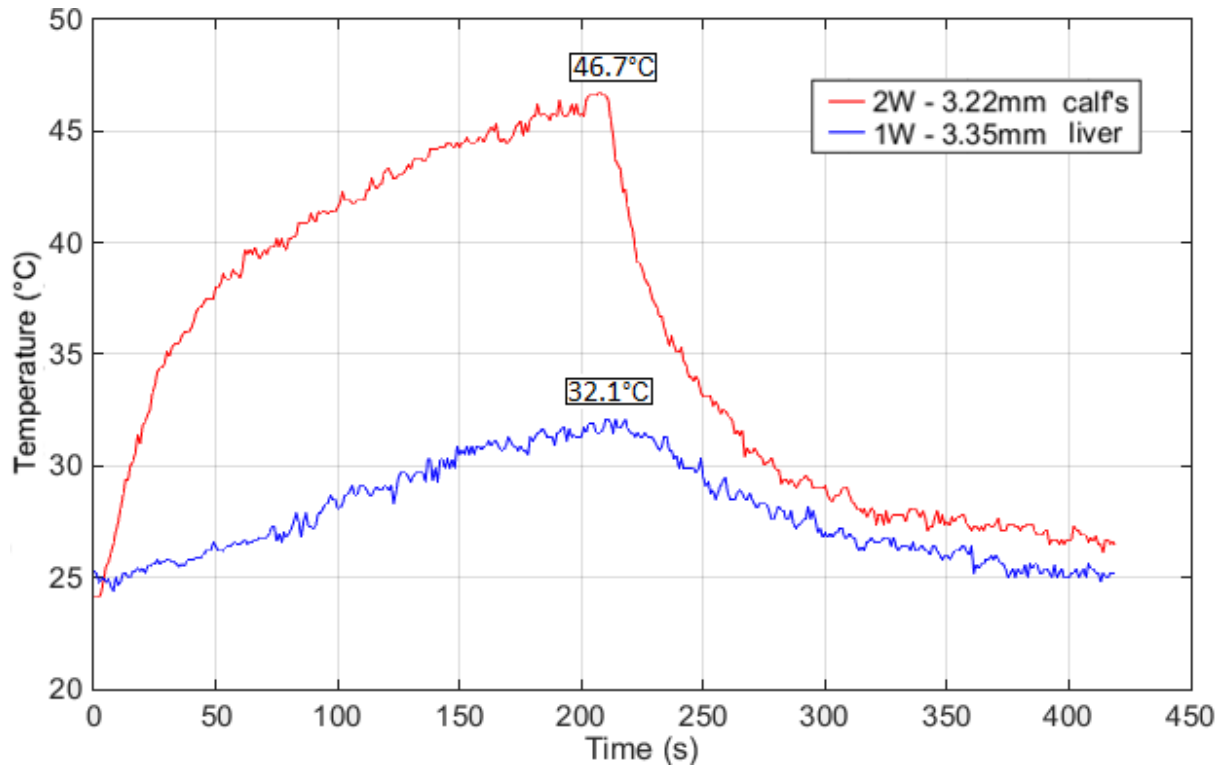
Figure 3.40: Comparison of temperature variations on calf's liver samples of different thicknesses with different applied constant microwave power levels (P=1 and 2W)

2nd protocol: step microwave power
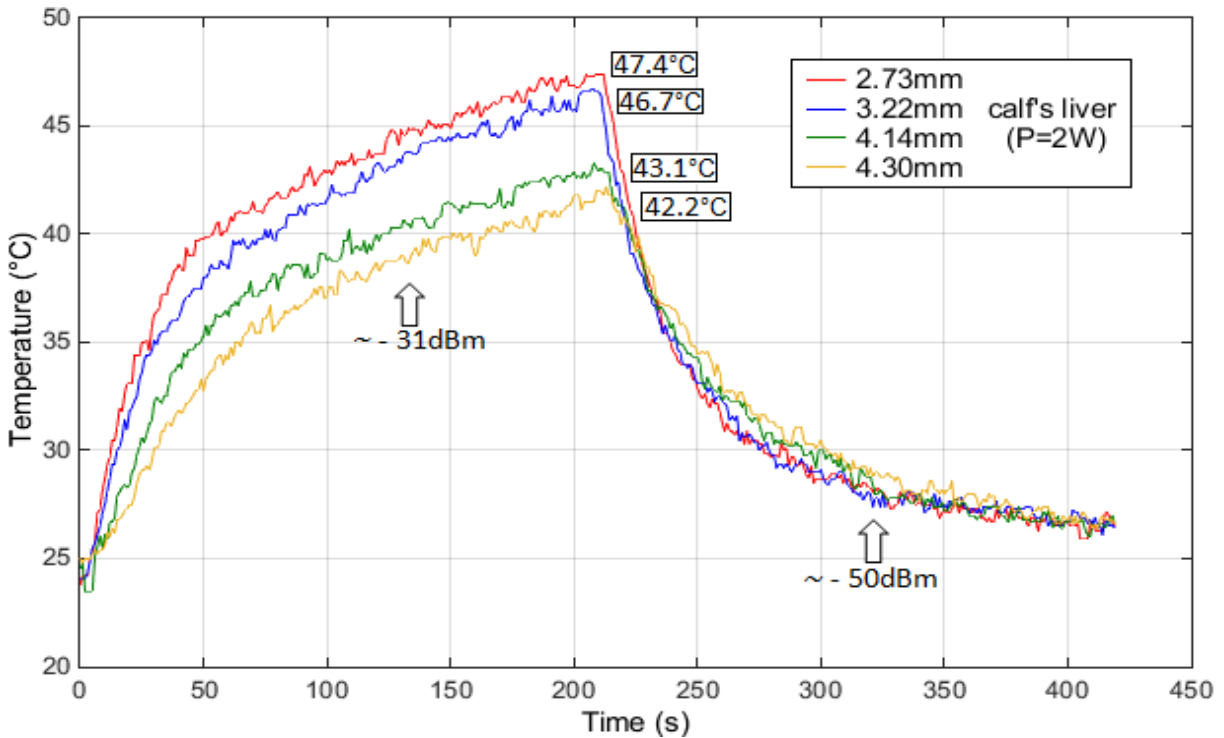

Figure 3.41: Comparison of temperature variations of the irradiated calf's liver samples of two different thicknesses with progressively changing step microwave power

Applying progressively changing step power on the samples has allowed thinner calf's liver sample (3.46mm) attaining higher temperature T_{max} = 59.6°C at the 360th second. For calf's liver sample of 3.94mm thickness, T_{max} = 41.3°C (figure 3.41). The difference of temperature for these samples has reached $T_{difference}$ = 18.3°C. For thinner 3.46mm sample, its step changing temperature tendency for each power level is clear, but for the thicker 3.94mm sample, its temperature variations are almost a straight line for both temperature increasing and decreasing parts.

3.5 Experimental results of Warrior cable

a) Experimental results of pork samples of different thicknesses.

1st protocol: constant microwave power

Measured reflection power levels are noted at different times.
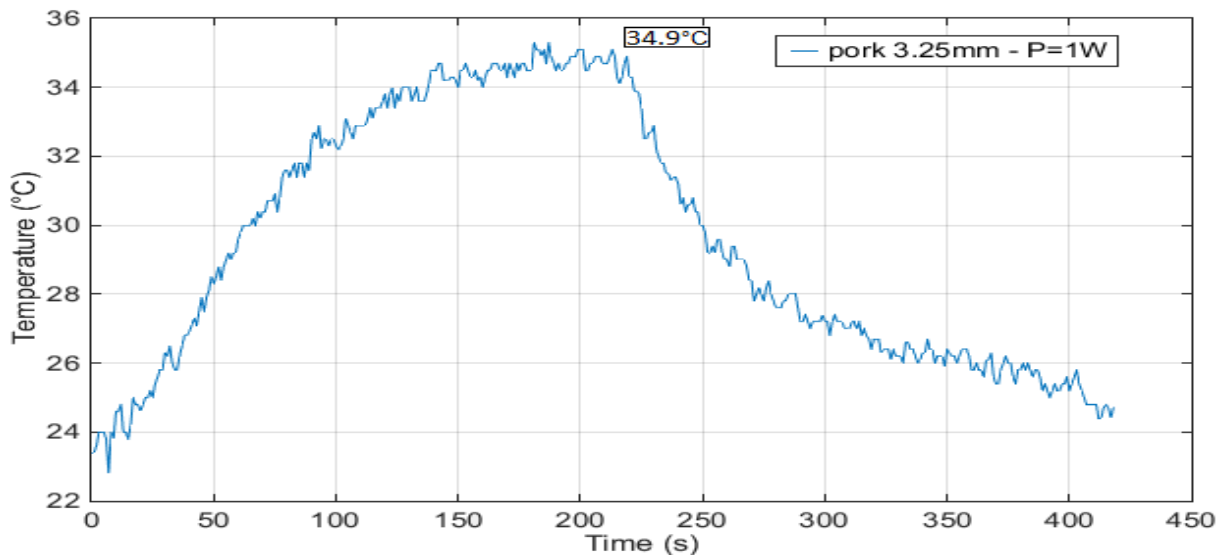
Figure 3.42: Temperature variation of the irradiated pork sample (thickness 3.25 mm)
with constant microwave power P=1W

Figure 3.43: Comparison of temperature variations of the irradiated pork samples
of two different thicknesses with a constant microwave power P=2W

Figure 3.44: Comparison of temperature variations of the irradiated pork samples
of two different thicknesses with a constant microwave power P=3W

Figure 3.45: Comparison of temperatures on the pork samples of similar thicknesses
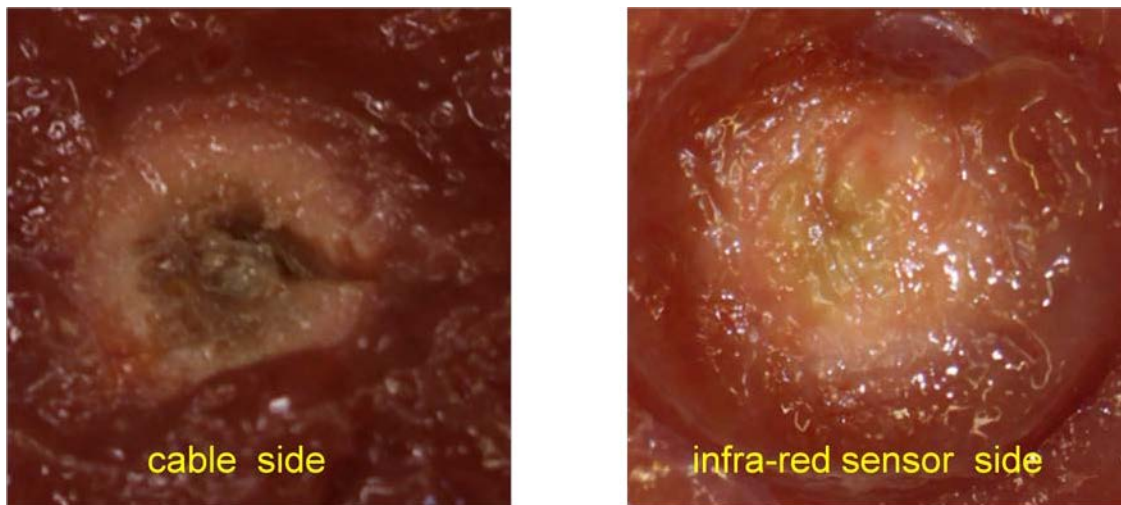with different constant microwave power levels (P=1, 2 and 3W)
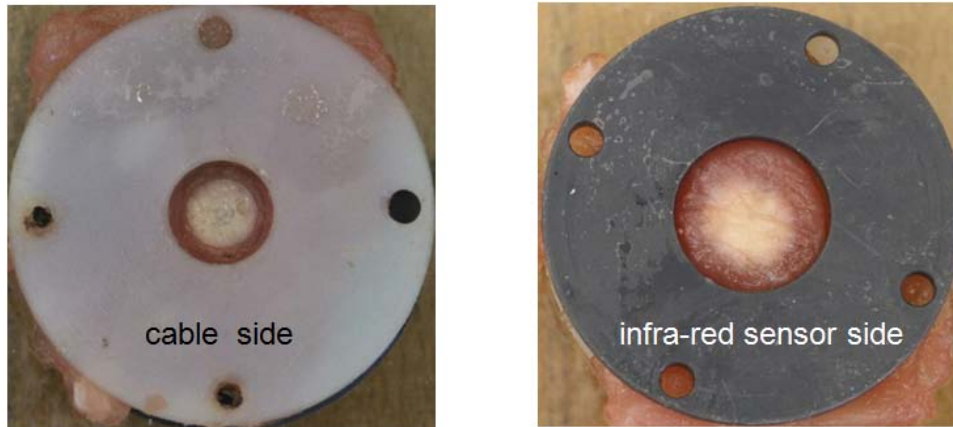
Figure 3.46: Comparison of morphology images of cable side and infrared sensor side of the irradiated 3.10mm thick pork sample with P=2W.

For P=2W, pork sample with thickness of 3.10mm, T_{max} = 51.4°C; sample of 2.18mm, T_{max} = 55.3°C (figure 3.43). Thinner sample has attained higher temperature. The irradiated central part of 3.10mm sample had become white and other parts were still red (figure 3.46). For P=3W, for the two samples of thicknesses of 3.14mm and 3.40mm, before the 25th second, their temperatures increased very quickly with sharp slopes in the curves. But from the 26th second, the increasing slops of temperature curves become smoother immediately. The double stubs became difficult to control (–18dBm for P=3W). The creaking noises were also heard for both samples. Their temperatures increased very slowly after 33.7°C (figure 3.44 & figure 3.45). This shows that a slight dielectric breakdown has happened for P=3W in these samples.

2nd protocol: step microwave power
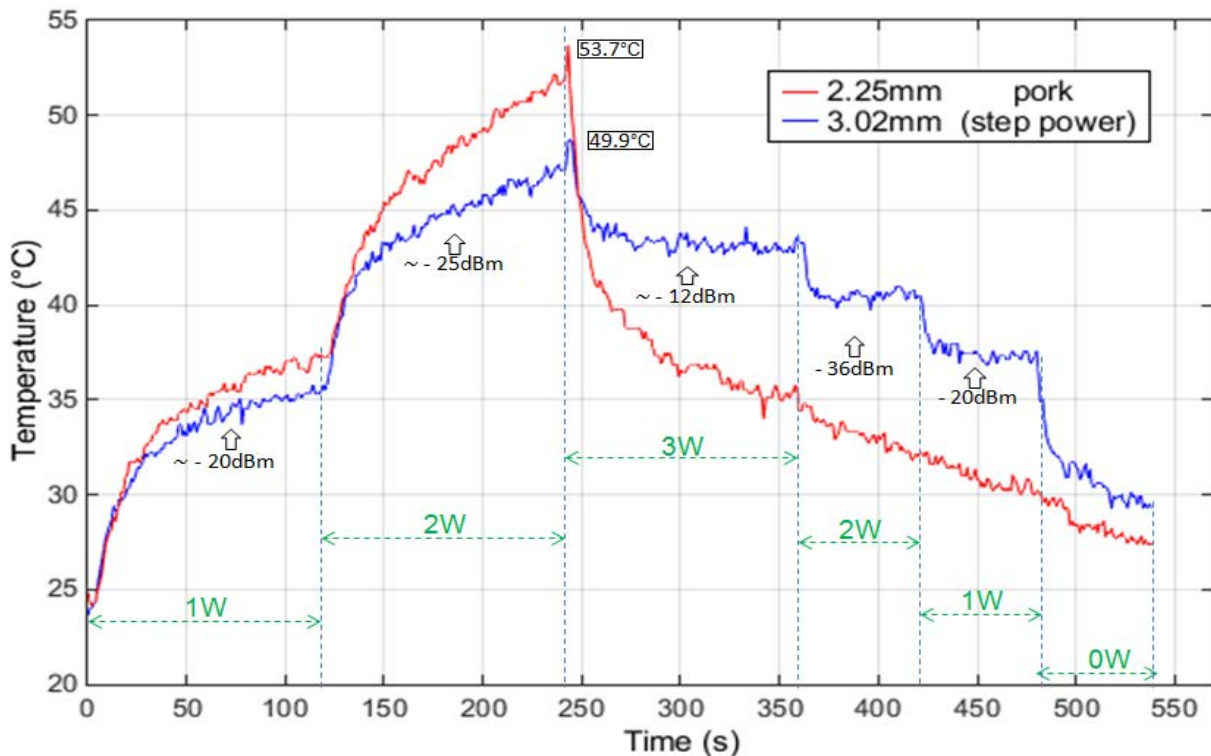
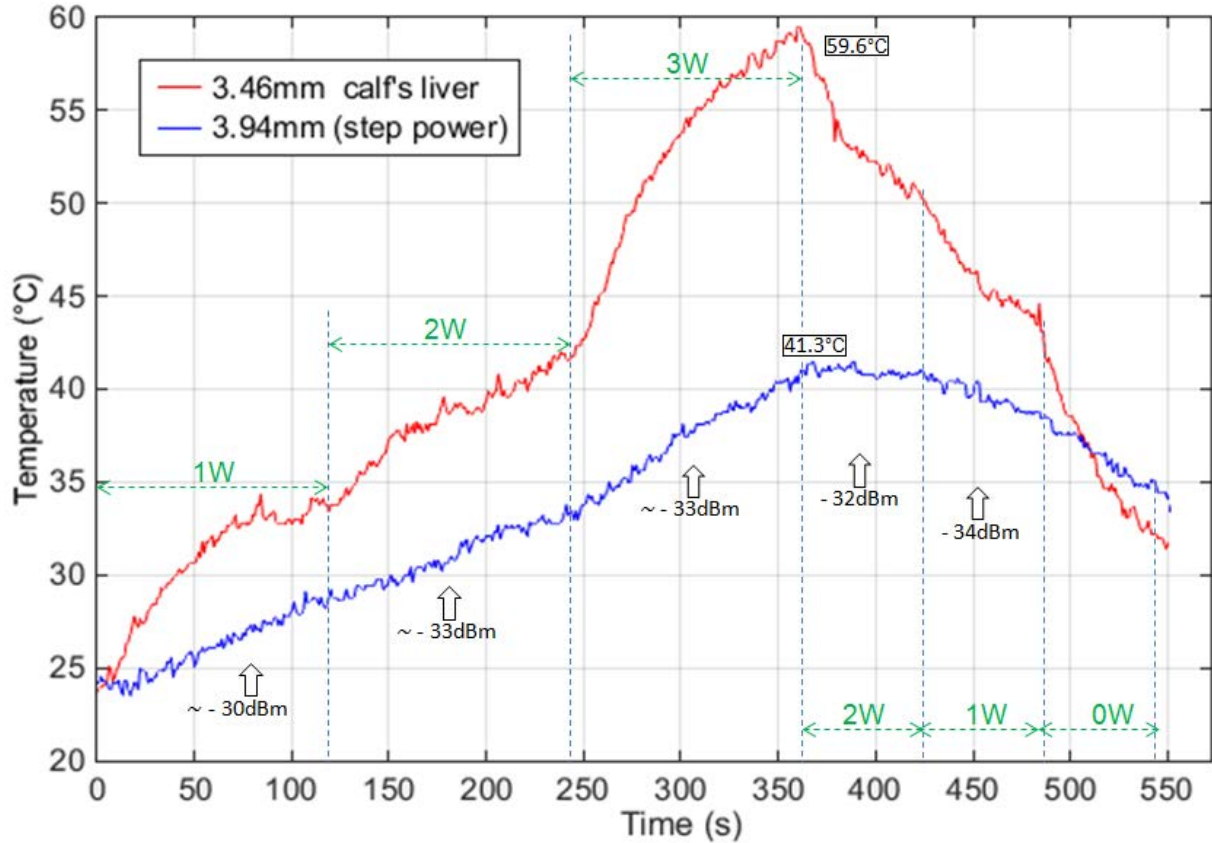Figure 3.47: Comparison of temperature variations of the irradiated pork samples of two different thicknesses with progressively changing step microwave power (For both samples, a dielectric breakdown seems to happen after 240s)

The temperatures of both samples of 2.25mm and 3.02mm thickness irradiated by the step microwave power increase for P=1W and P=2W. For thinner sample, higher temperature is obtained. Once P=3W was applied to both samples which had reached their T_{max} = 53.7°C and T_{max} = 49.9°C at the 240th second, they started to not follow the applied power tendency to continue increasing their temperatures. For 2.25mm pork, it has been carbonized and it did not respond at all to the applied power. It had an irreversible change. Its temperature decreased immediately with a tendency like without an applied power. For 3.02mm thick sample, its temperature decreased but still could respond or follow the change of applied step microwave power. After 240 seconds, temperature variation corresponding with step power were clear, but the temperature of 3.02mm thick sample kept a saturated status for each power level and kept a constant value. For both of these samples, a dielectric breakdown seems to happen after 240s but in a different degree depending on their thickness.

b) Experimental results of beef samples of different thicknesses.

1st protocol: constant microwave power

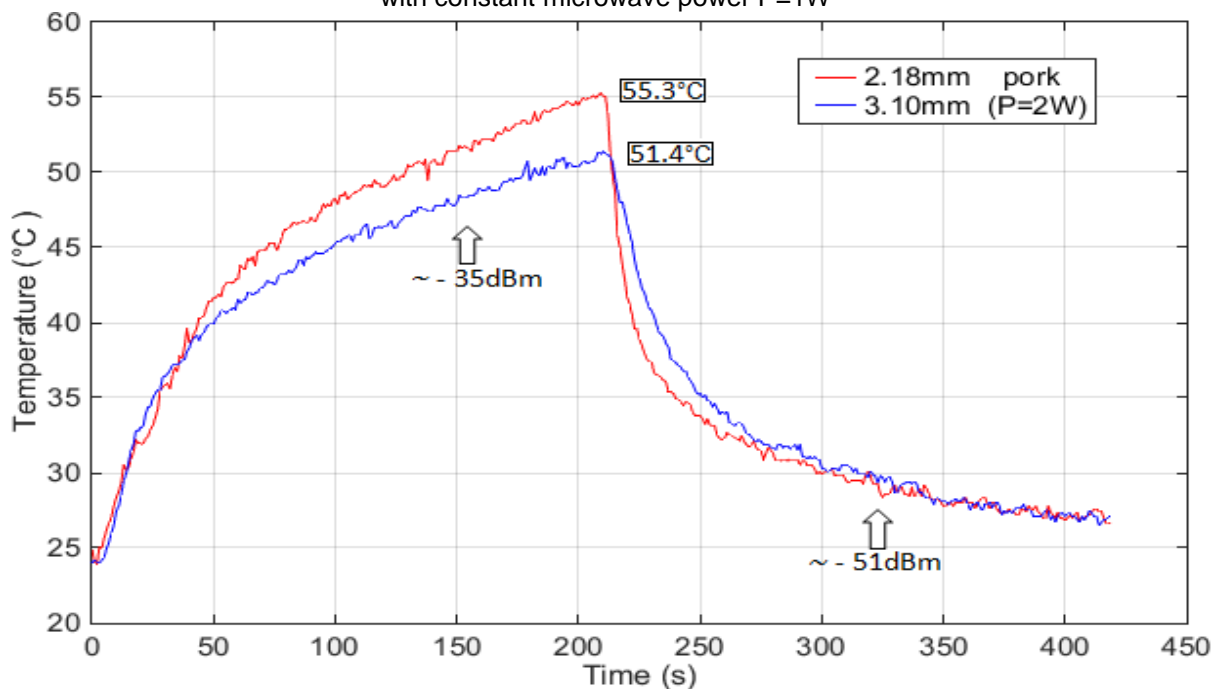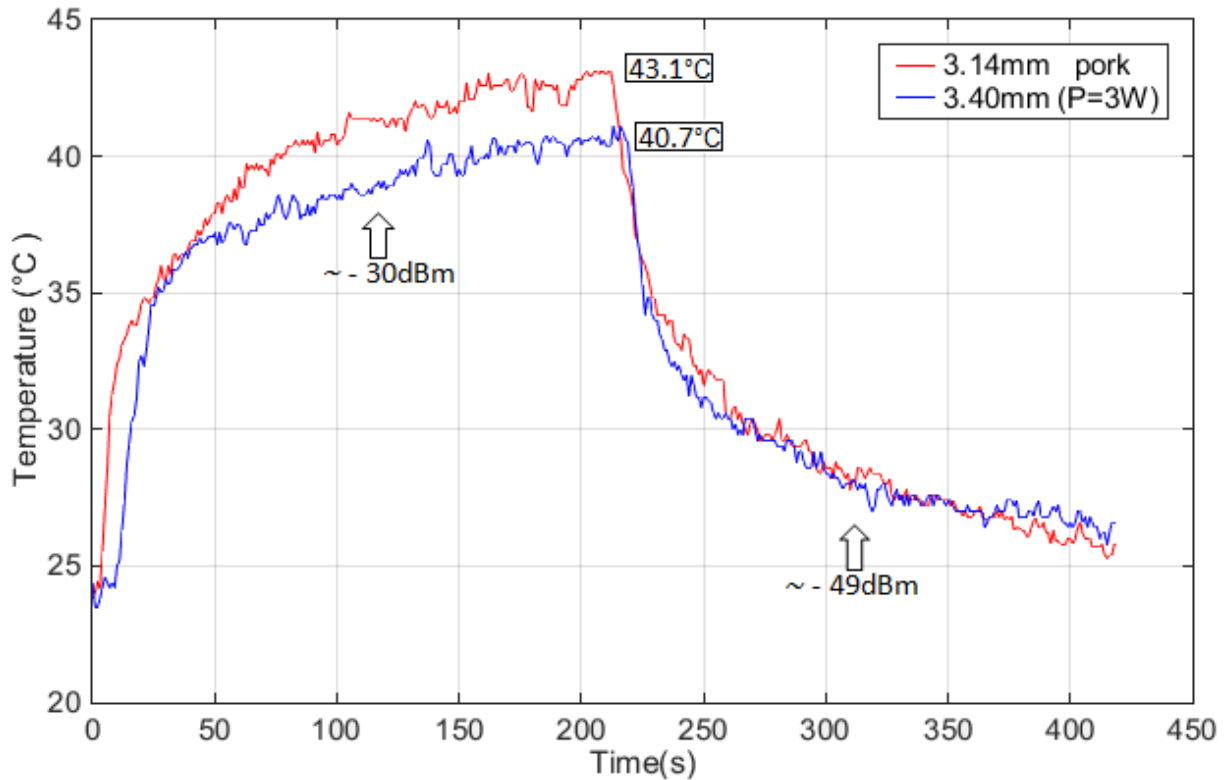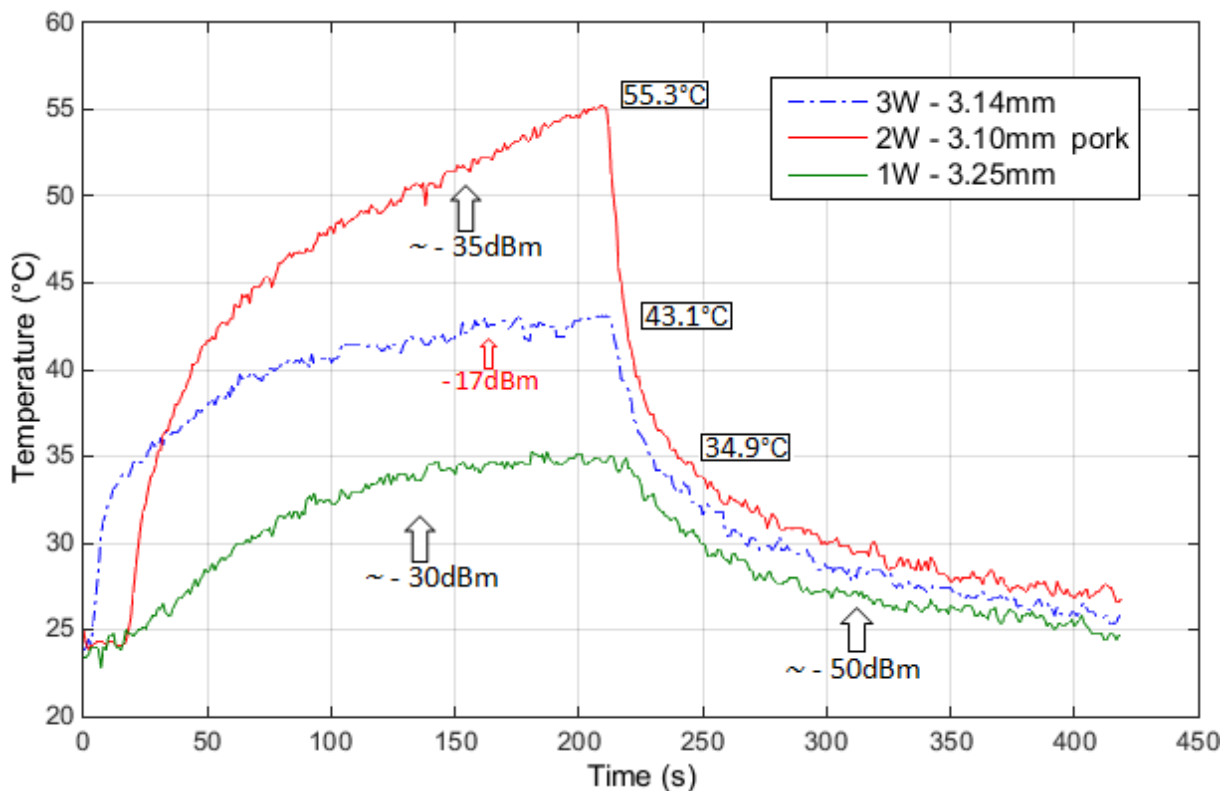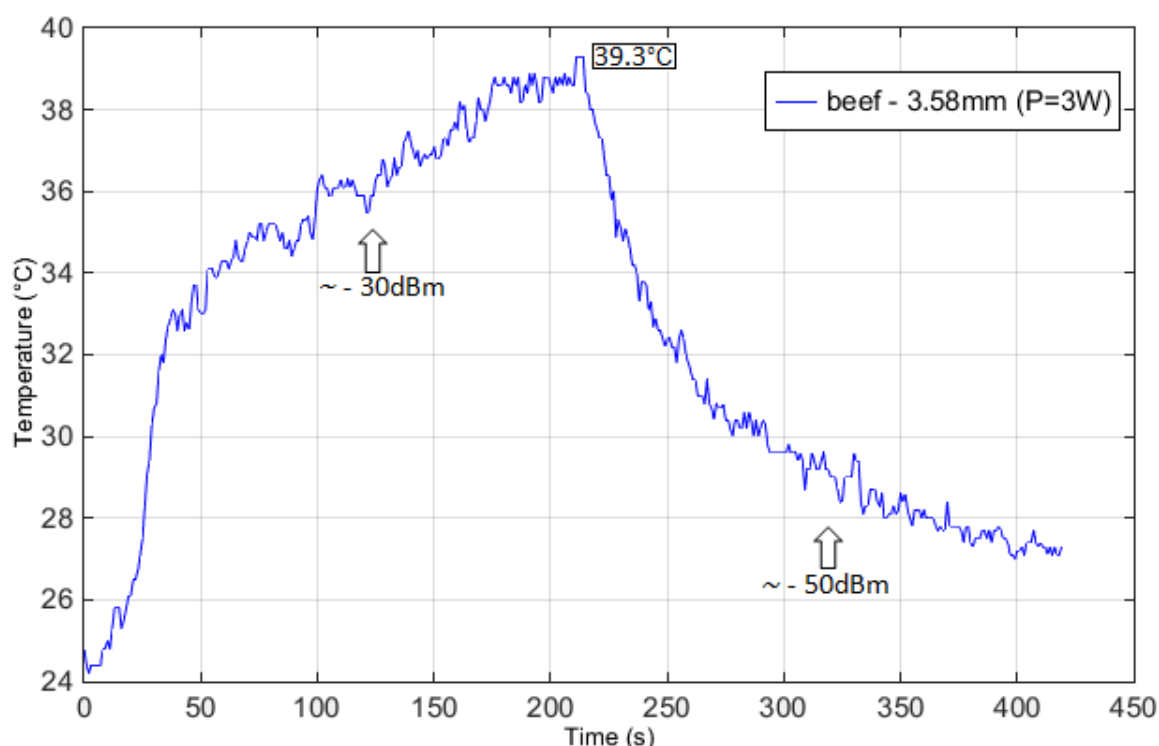

Figure 3.48: Temperature variation of the irradiated beef sample (thickness 3.58 mm) with constant microwave power P=3W

As pork samples irradiated with P=3W by Warrior cable, the beef also shows the similar temperature curve with P=3W. For beef of 3.58mm thickness, T_{max} = 39.3°C. At the beginning, the increasing temperature has a very sharp slope. The temperature increased 8.3°C very quickly during the first 38 seconds from 24.8°C to

33.1°C; but from the 39th to the 210th second, the temperature only increased 6.2°C during 171 seconds.

Warrior cable has less attenuations than the coaxial cable RG393 and can operate well with P=2W; but for P=3W, it cannot work well any more. Applying the constant power P=3W to all three samples, when their temperatures reached about 33°C, their slopes started to have a smooth trend, the temperatures increased slowly; In a case of applying a progressively changing step power, once the power was adjusted to 3W, the samples seemed to not follow or stop immediately responding to step power. The data of Warrior cable is not very complete. More researches about its characteristics should be carried out.

3.6 Comparisons among different irradiated biological samples

In the following curves, we have compiled the results obtained with the coaxial cable RG393 on different biological tissues in order to compare the heating abilities with different power levels.

a) Comparisons among samples heated by coaxial cable RG393

It seems easier to heat chicken comparing to pork and beef (figure3.49).

Figure 3.49: Comparison of temperature variations among different irradiated muscle samples (beef, pork and chicken) of similar thickness with a constant power P=2W by using the coaxial cable RG393

It seems much easier to heat chicken comparing to pork and beef with this power level (figure 3.50).
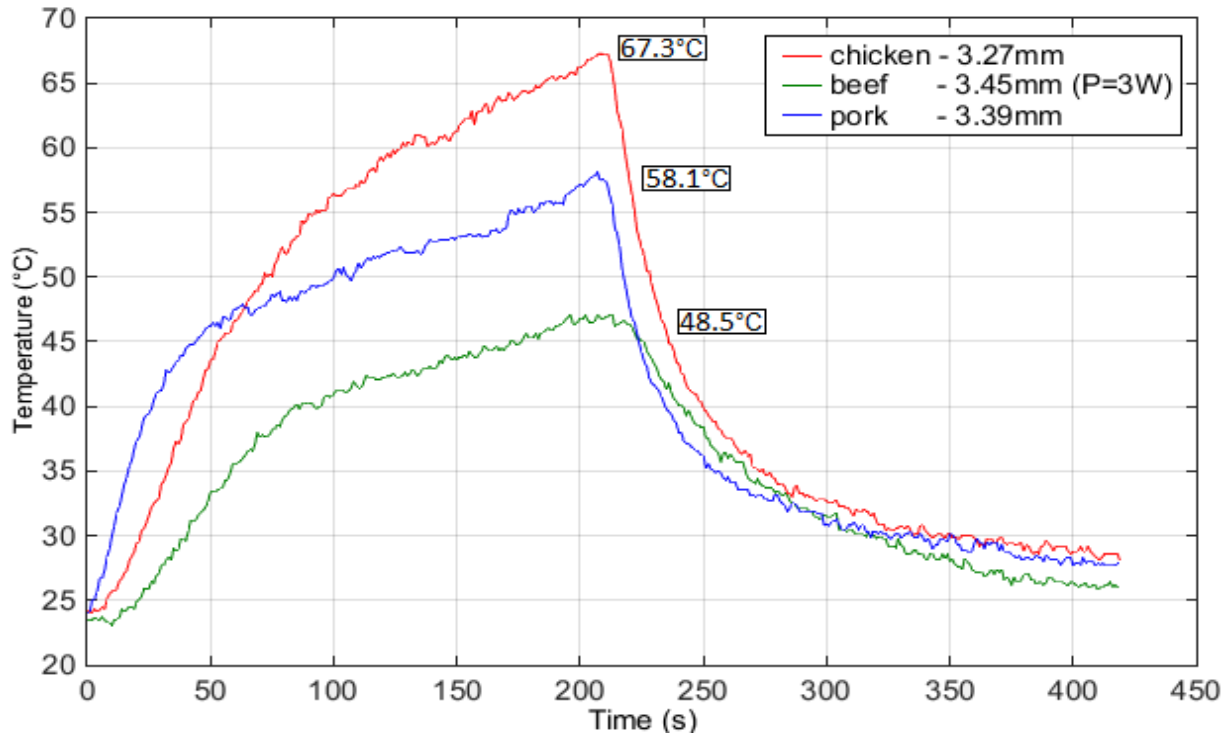
Figure 3.50: Comparison of temperature variations among different muscle irradiated samples (beef, pork and chicken) of similar thickness with a constant power P=3W by using the coaxial cable RG393
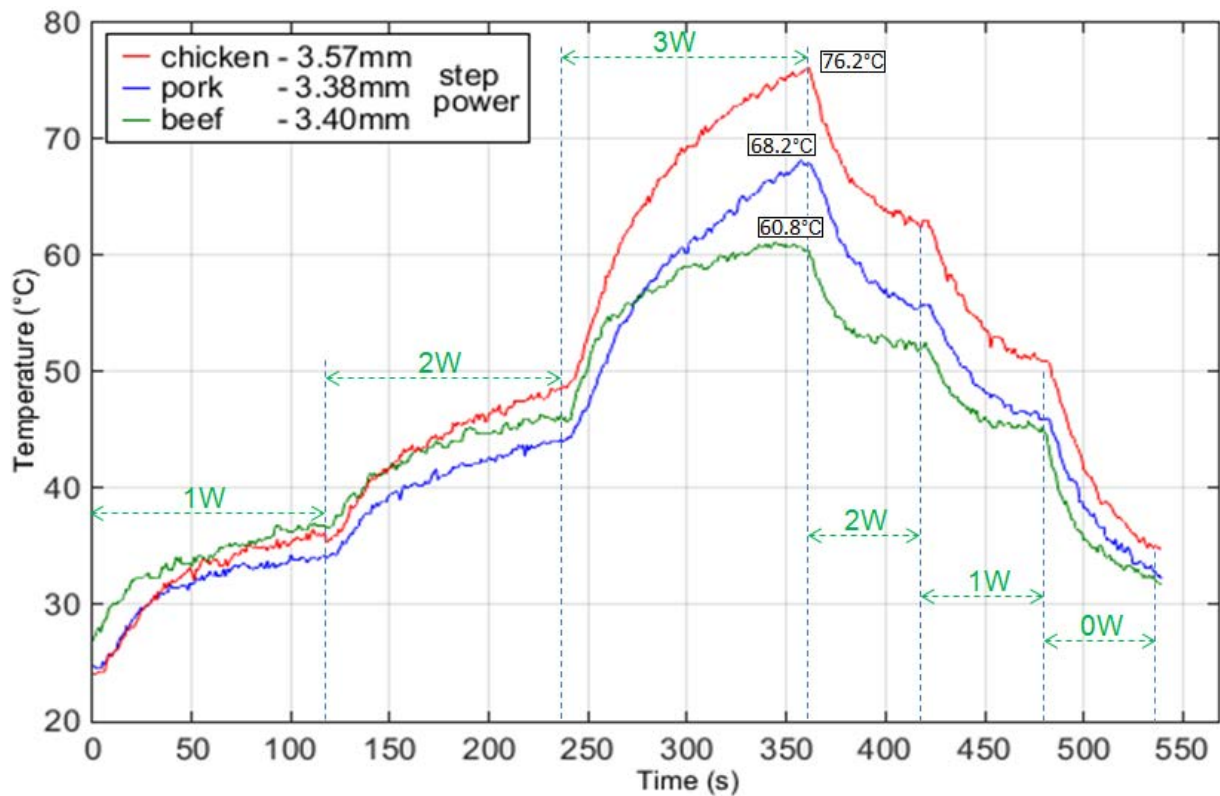
Figure 3.51: Comparison of temperature variations among different irradiated muscle samples (beef, pork and chicken) of similar thickness by applying a progressively changing step power

For all muscles, they have similar tendencies of temperature response. For muscle samples of similar thicknesses, chicken samples always attained the highest temperatures (T_{max} of chicken > T_{max} of pork > T_{max} of beef) with same type and same power level. Smaller constant powers applied to the samples allowed obtaining smaller differences of temperatures among them (table 3.1, figures 3.50 and 3.51).

Constant power level : P=2W		
sample	T_{max}	$T_{difference}$
chicken	46.8° C	
pork	44.2° C	2.6°C
beef	41.7° C	2.5°C

Constant power level : P=3W		
sample	T_{max}	$T_{difference}$
chicken	67.5° C	
pork	58.1° C	9.4°C
beef	48.5° C	9.6°C

Step power (P= 1W → 3W → 0W)		
sample	T_{max}	$T_{difference}$
chicken	76.2° C	
pork	68.2° C	8.0°C
beef	60.8° C	7.8°C

For each power level or type by using the coaxial cable RG393, the gradient of temperature seems to be a constant value between two neighboring samples. The higher power level leads to bigger gradient value.

Table 3.1: Comparisons among values of obtained T_{max} of muscle samples heated by the coaxial cable RG393
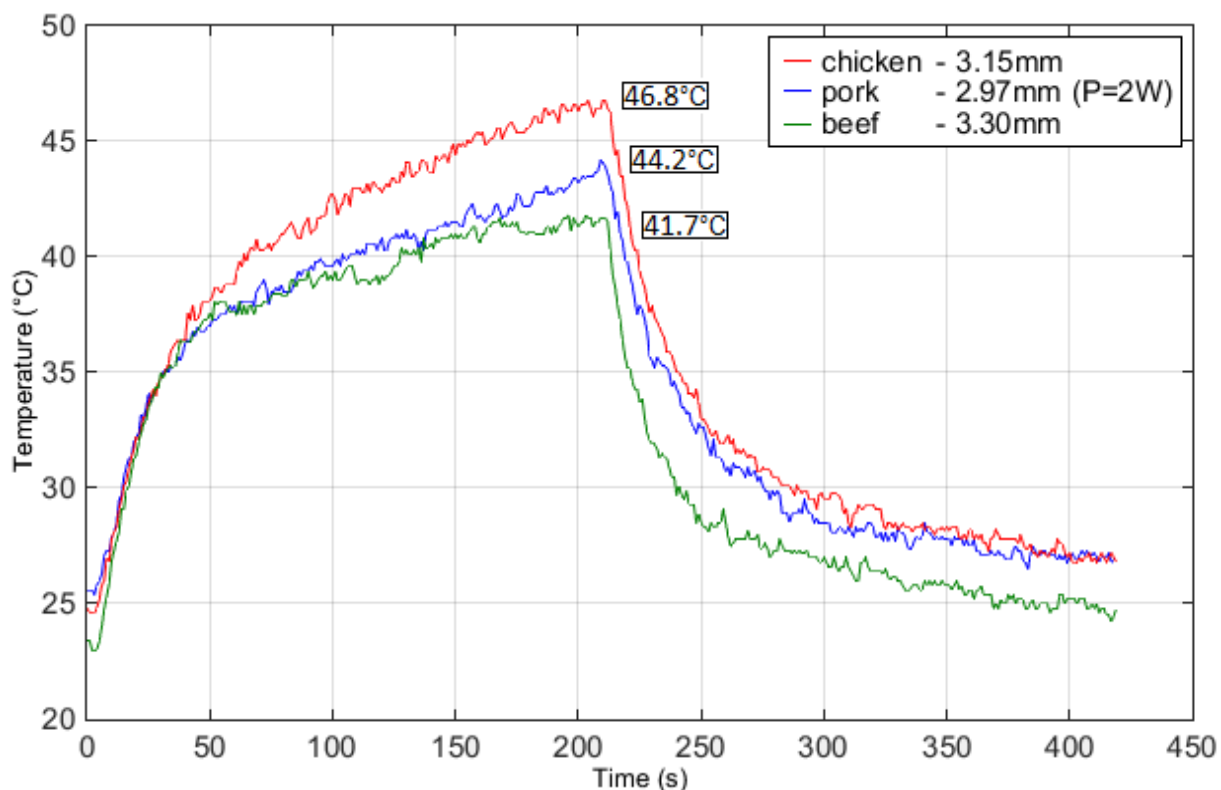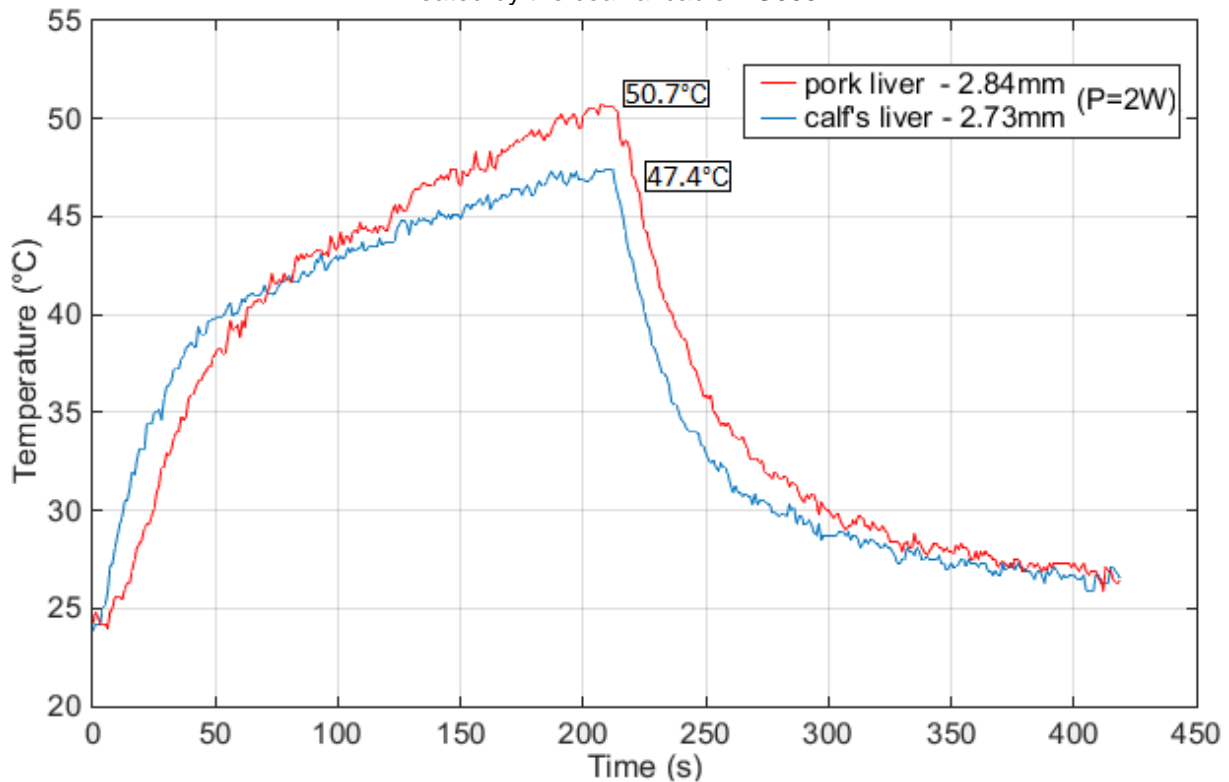

Figure 3.52: Comparison of temperature variations between different irradiated liver samples (pork and calf's) of similar thickness with constant power P=2W by using the coaxial cable RG393
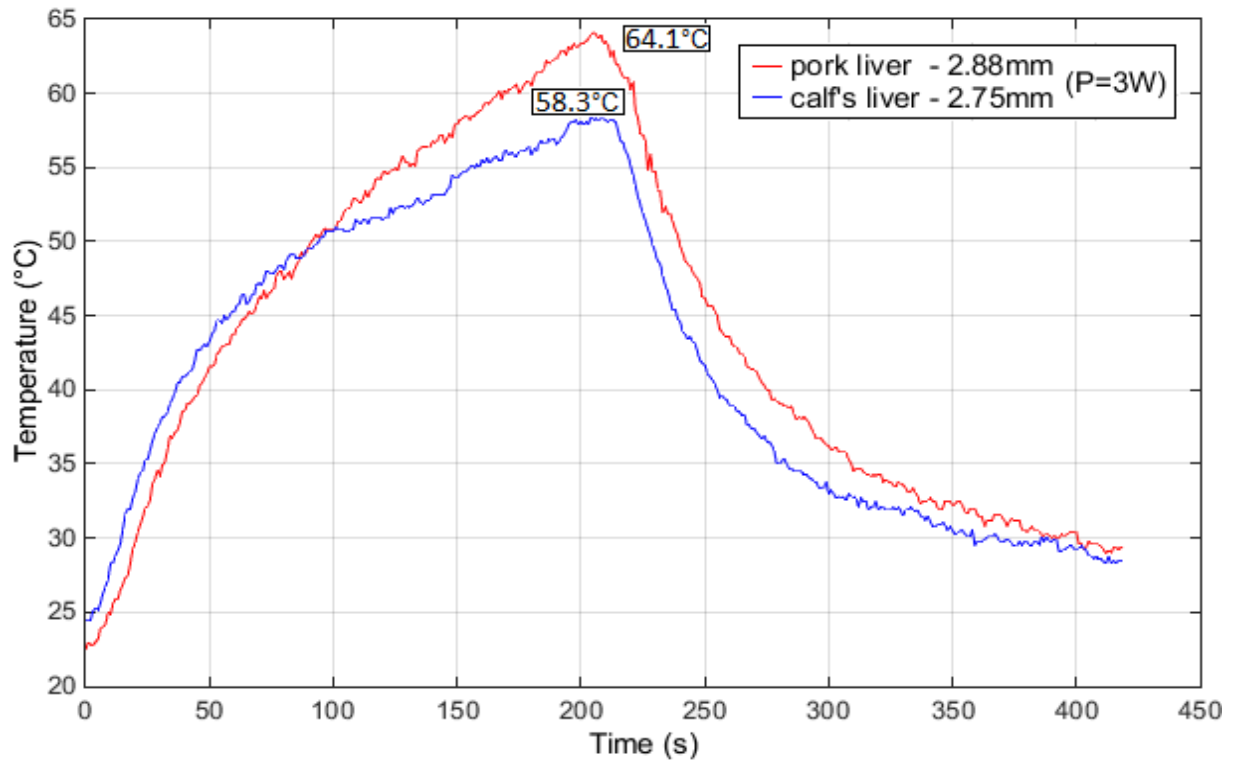
Figure 3.53: Comparison of temperature variations between different irradiated liver samples (pork and calf's) of similar thickness with constant power P=3W by using the coaxial cable RG393

For liver samples irradiated by a constant power level (figure 3.52 and 3.53), T_{max} of pork liver is higher than T_{max} of calf's liver. At the beginning, calf's liver responded to the power more quickly which means its temperature increased a little faster, but after certain seconds (e.g. t = 70s for P=2W and t = 90s for P=3W) its slope became smoother than that of pork liver. There is a crossing point for each power level curve.
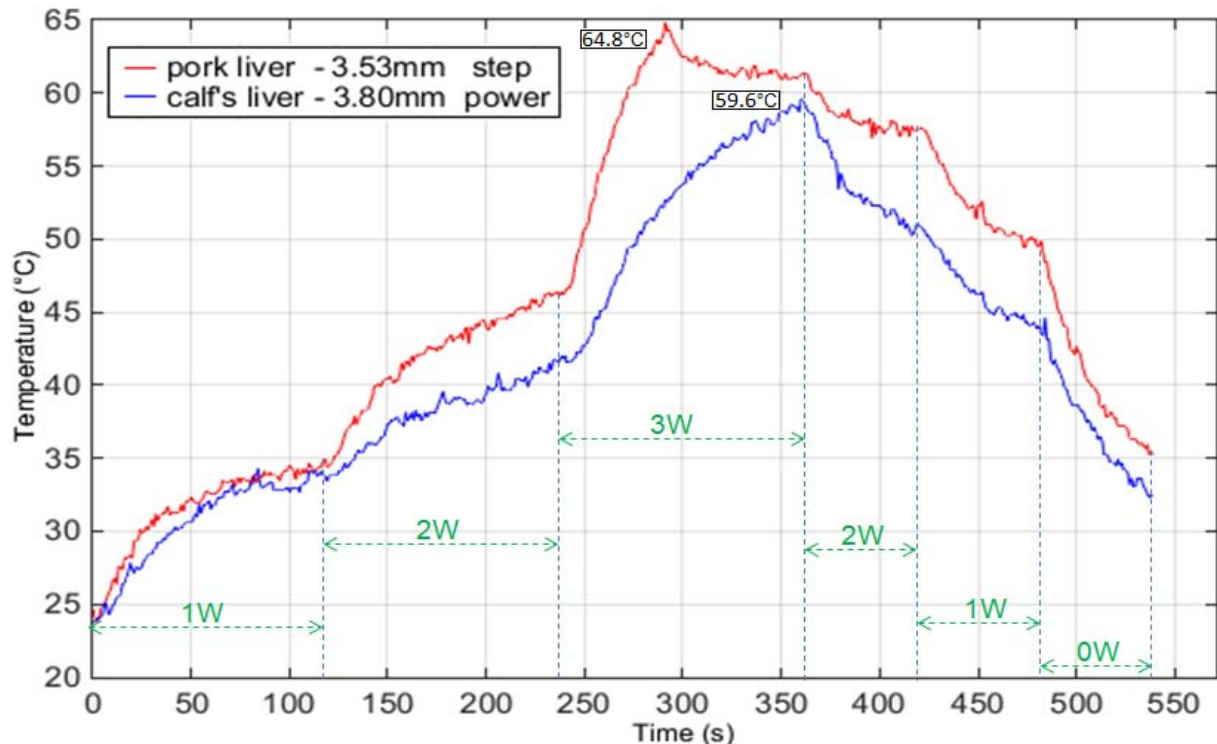
Figure 3.54: Comparison of temperature variations between different liver samples (pork and calf's) of similar thickness irradiated by a changing step power

For the samples of similar thickness with applying a step power, T_{max} of pork liver is still higher than T_{max} of calf's liver. But the properties of pork liver showed some kind of irreversible changes. In fact, from the 290th second, although a power of 3W is still applied, the temperature of pork liver started to decrease from T_{max} = 64.8°C to a saturation, but it restarted to correspond to the progressively decreasing microwave power from the 360th second. Response of temperature of calf's liver followed normally the progressively changing step power.

b) Comparisons among samples heated by Warrior cable
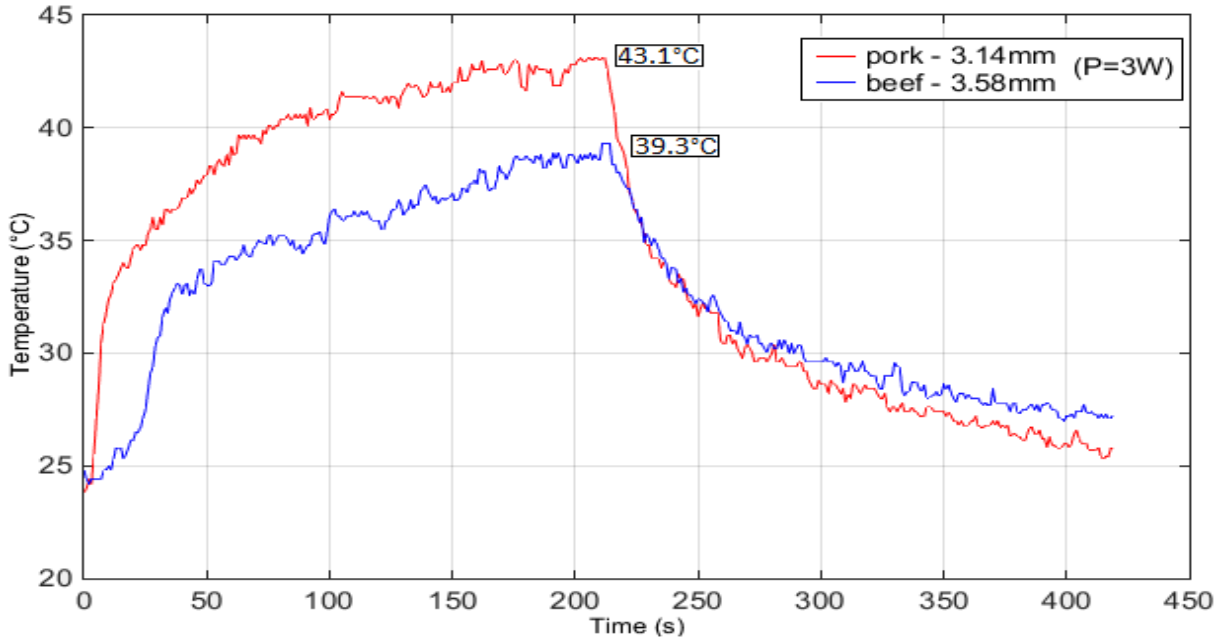
Figure 3.55: Comparison of temperature variations between pork and beef samples with constant power level P=3W by using Warrior cable.

c) Comparisons of experimental results of biological samples heated by coaxial cable RG393 and Warrior cable
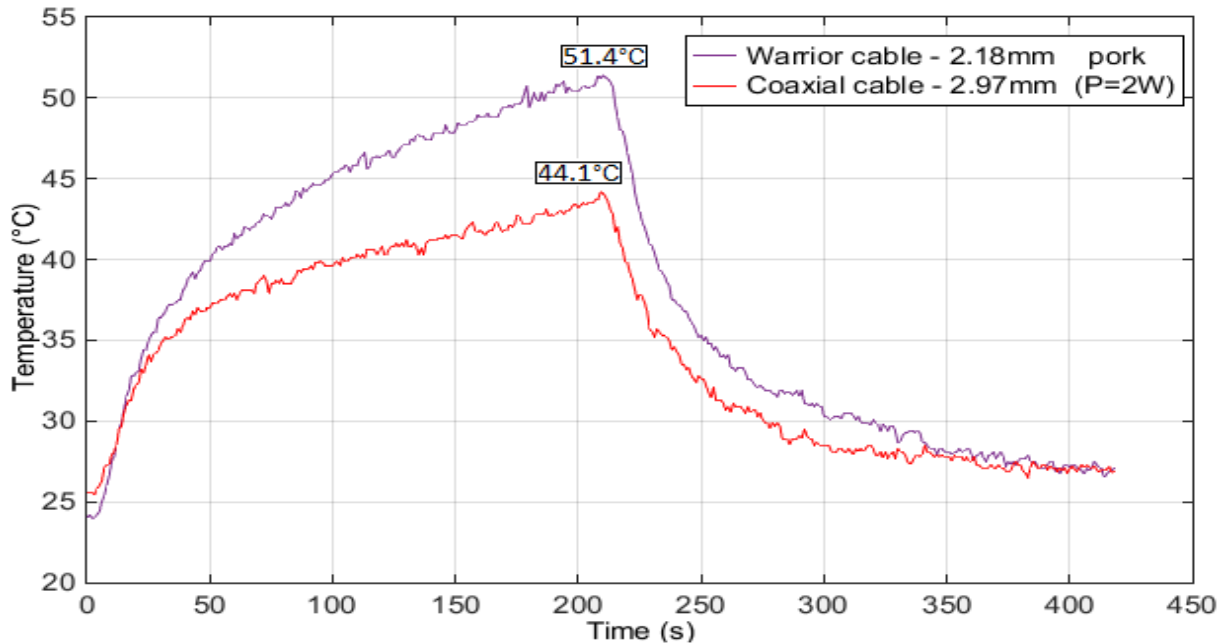
Figure 3.56: Comparison of temperature variations of pork samples heated by the coaxial cable RG393 and the Warrior cable with a constant power level P=2W
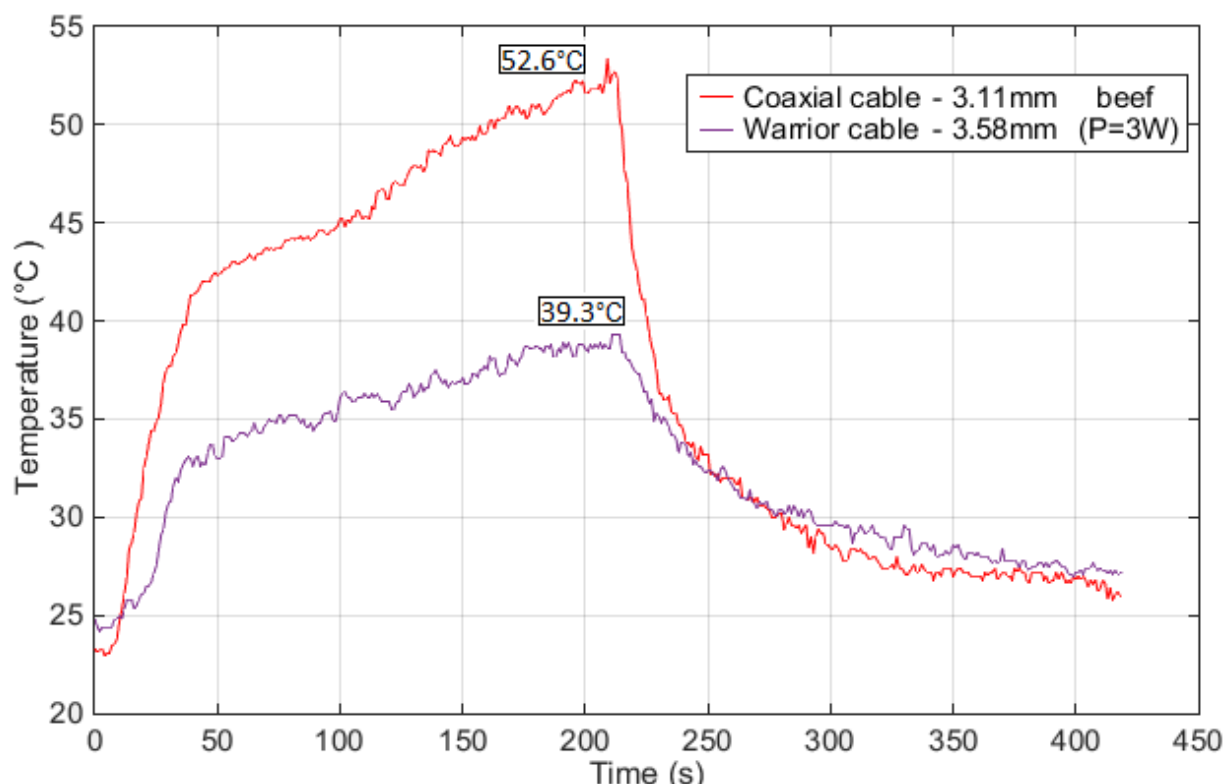
Figure 3.57: Comparison of temperature variations of beef samples heated by the coaxial cable RG393 and the Warrior cable with a constant power level P=3W

For P=3W, Warrior cable cannot work as well as P=2W. Comparing pork and beef with each other, both of them can reach 33°C in a very short time with a sharp slope, but after that, both of their slopes present a smoother trend, so the temperatures continue but more slowly. Obtained T_{max} of pork is higher than that of beef irradiated by Warrior cable like the same result of coaxial cable RG393 (figure 3.55).

When P=2W, both coaxial cable RG393 and Warrior cable can operate or heat biological tissues well. Because of less attenuation of Warrior cable, for pork samples, obtained T_{max} by Warrior cable is higher than that obtained by coaxial cable RG393 although the thicknesses of two pork samples are different. Highest temperature obtained by the coaxial cable RG393 is much higher than it obtained by Warrior cable (difference between 13.3°C)(figure 3.57).

3.7 Conclusion

Microwave hyperthermia ex vivo experiments have been achieved by using two different open–ended applicators of different dimensions and specifications: coaxial cable RG 393 and Warrior cable. Two experimental protocols have been also adopted: applied constant power and progressively changing step power. The temperature variations have been measured during microwave hyperthermia by an infra–red sensor which is in front of the sample. The temperature of applicator side of the sample which is in contact with the coaxial applicator cannot be measured directly.

Several samples of different thicknesses of five different biological tissues, muscle samples (pork, beef and chicken) and liver (pork and calf's), have been studied. Morphologies of the samples have been also examined by pictures taken before and after irradiation.

For all samples with constant applied power, higher temperature can be obtained with higher power level up to a certain limit. Besides thinner sample thickness can also lead higher attained temperature. For the experiments with variable microwave power (step power), temperature curves of different samples have similar changing tendency which are correspondent with or respond to the changes of applied microwave power.

The curves of temperature variations as a function of time have a sharp slope of increase at the beginning, and later they have smoother increase. The maximum temperatures present an expression T_{max} of chicken $>$ T_{max} of pork $>$ T_{max} of beef among all muscle samples of all types of experiments. T_{max} of pork liver is higher than that of calf's liver for all types of liver experiments. for all types of liver experiments.

Coaxial cable RG 393 can heat tissues up to the temperatures more than 60°C with P=3W. For destroying the pathological tissue, 50°C is enough. At present, the more flexible Warrior cable operates as well as the coaxial cable RG393 up to a power level of 2W to heat the biological tissues and attain about 50°C. But data of Warrior cable is not very complete. More researches about its characteristics should be carried out. For the ex vivo experiments, in order to be closer to the requirements of the real surgeries, the manual impedance matching procedure of the microwave hyperthermia instrumentation could be optimized by using an automatic impedance matching device. A more flexible thinner applicator and more precise temperature measurement device might be considered.

Different thicknesses of irradiated biological tissues may affect the measured temperature values. The thicknesses of biological samples cannot be measured very precisely as they are soft and deformable and it can also lead to the experimental errors. A method for precise thickness measurement should be considered for future studies. It seems certainly that there can be a flexible and suitable coaxial cable to be used for both diagnosis and hyperthermia treatment (therapy). For further researches, human healthy and pathological tissues should be used for experiments.

<div align="center">

Chapter 4
COMSOL Multiphysics simulation of ex vivo microwave
hyperthermia instrumentation on the biological tissues

</div>

4.1 Introduction

Simulations of ex vivo microwave hyperthermia which use the open ended coaxial cable as the applicator for different biological tissues have been carried out by using COMSOL Multiphysics software. The ex vivo microwave hyperthermia instrumentation is designed and constructed using a broad band amplifier (0.8 to 4.2GHz) with a maximum output power level of 10 Watts at 2.45GHz. The target temperature of microwave hyperthermia is a minimum 40°C. Above 40°C, the biological tissue will have irreversible changes. The hyperthermia simulations use 2D axisymmetrical finite–element method to simulate the temperature spatial variation in the biological tissue which is in contact with a coaxial cable assuming that all the boundary temperatures remain at ambient room temperature during the entire procedure.

4.2 Introduction of COMSOL Multiphysics

COMSOL Multiphysics (formerly FEMLAB) is a finite element analysis and solver software package for various physics and engineering applications, especially coupled phenomena, or multiphysics. This Multiphysics software also offers an extensive and well-managed interface to MATLAB and its toolboxes for a large variety of programming, preprocessing and post processing possibilities.

A similar interface is offered to COMSOL Script. The packages are cross-platform (Windows, Mac, Linux, and Unix). In addition to conventional physics-based user-interfaces, COMSOL Multiphysics also allows for entering coupled systems of partial differential equations (PDEs). The PDEs can be entered directly or using the weak form (see finite element method for a description of weak formulation). The development of COMSOL was started by graduate students from Germund Dahlquist based on codes developed for a graduate course at the Royal Institute of Technology (KTH) in Stockholm, Sweden.

Several application-specific modules are available for COMSOL Multiphysics:

- AC/DC Module: Simulates electrical components and devices that depend on electrostatics, magnetostatics and electromagnetic quasi-statics applications, particularly coupled to other physics. It consists of specific interfaces for rotating machinery applications and SPICE circuits' lists import.
- Acoustics Module: Contains built-in application modes and boundary settings for the modelling of acoustic propagation in solids and stationary fluids (also models for aeroacoustic applications in moving fluids).

- CAD Import Module: Facilitates the reading of most industry-standard CAD formats including add-in packages that support the file formats for specific CAD programs' geometry kernels.
- Chemical Engineering Module: Analyzes CFD and mass and energy balances coupled to chemical reaction kinetics. It incorporates a plethora of application models for the field of transport phenomena including ionic transport and multi component diffusion.
- Earth Science Module: Models single and coupled processes for geological and environmental phenomena particularly based around subsurface flow. Ideal for porous media flow coupled to other physics such as poro–elasticity applications.
- Heat Transfer Module: Consists of advanced application modes for the analysis of heat transfer by conduction, convection and radiation (specific for industrial applications such as electronics cooling and process engineering).
- Material Library: Internal material property database with more than 2500 materials and 20000 properties. The database contains temperature dependence of electrical, thermal, and structural properties of solid materials. The material library can also accept files generated by the MatWeb material property database which is searchable over 59,000 material data sheets, including property information on thermoplastic and thermoset polymers, metals, and other engineering materials.
- RF Module: Characterizes electromagnetic fields, currents and waves for RF, microwave, optical and other high-frequency devices. It allows for extensive post-processing such as S-parameter computations and far-field analyses.
- Structural Mechanics Module: Performs classical stress-strain analysis with full multiphysics capabilities. Comprises non-linear material models, large deformation and contact abilities; all able to be freely coupled to other physics.

4.3 Heating model for ex vivo microwave hyperthermia simulation

Three types of heat transfer within the tissue should be considered for the microwave hyperthermia simulations:

- The thermal conduction which automatically considers the value of the thermal conductivity k of the biological tissue.
- The convection is the transfer of internal energy into or out of an object by the physical movement of a surrounding fluid transferring the internal energy along with its mass. It is defined as "convective cooling" through the interface. The heat transfer coefficient of thermal convection h normally is 5W / m².K for ex vivo experiments. [59]
- Thermal radiation is parameterized through the "surface–to–ambient radiation" for interactions with the ambient.

Two methods in COMSOL Multiphysics are possible to use for simulating ex vivo microwave hyperthermia experiments:

- Using two models: electromagnetic waves (electromagnetism in the cable and in the tissues) and bioheat transfer (heat for biological tissue).
- Using only one model: microwave heating model which combines electromagnetism model together with heat transfer in solids model.

Therefore microwave heating model has been preferred. The simulations of microwave hyperthermia approximate all the biological tissues in contact with a thin cylinder coaxial cable assuming that its boundary conditions remain at ambient room temperature (~25°C) during the entire procedure. Microwave heating model includes four main conditions (figure 4.1):

$$\nabla \times \mu_r^{-1}(\nabla \times \mathbf{E}) - k_0^2\left(\epsilon_r - \frac{j\sigma}{\omega\epsilon_0}\right)\mathbf{E} = 0 \qquad\qquad \rho C_p\frac{\partial T}{\partial t} + \rho C_p\mathbf{u}_{trans}\cdot\nabla T = \nabla\cdot(k\nabla T) + Q$$

Wave Equation   **Heat transfer in solids**

Microwave Heating Model

Convective cooling   **Surface–to–ambient radiation**

$$-\mathbf{n}\cdot(-k\nabla T) = h\cdot(T_{ext} - T) \qquad\qquad -\mathbf{n}\cdot(-k\nabla T) = \epsilon\sigma(T^4_{amb} - T^4)$$
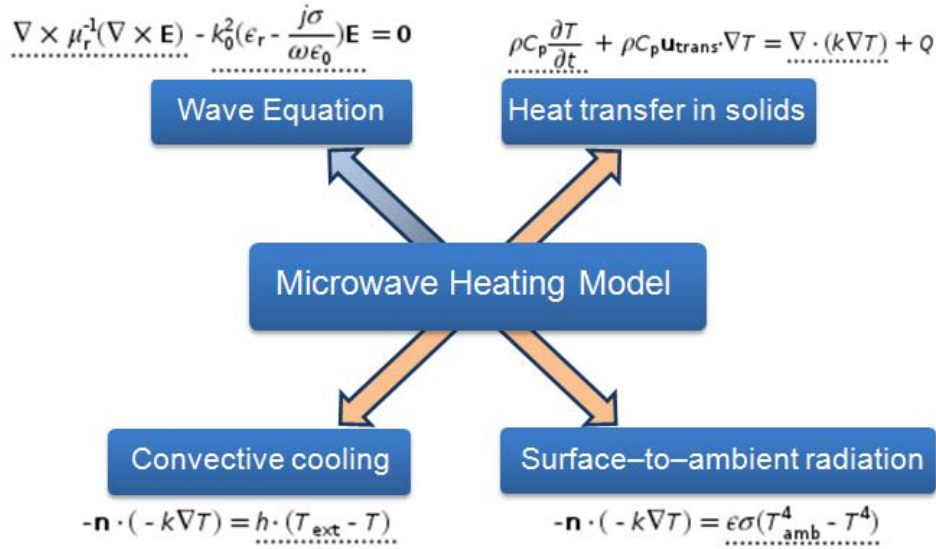
Figure 4.1: Conditions for microwave heating model
Involved for simulation of ex vivo microwave hyperthermia [60]

- Electromagnetic equation

$$\nabla \times \mu_r^{-1}(\nabla \times \mathbf{E}) - k_0^2\left(\varepsilon_r - \frac{j\sigma}{\omega\varepsilon_0}\right)\mathbf{E} = 0 \qquad [4.1]$$

μ_r: relative permeability, σ: conductivity [S/m],
k_0: wave number of free space ω: angular frequency [rad/s],
ε_r: relative permittivity, ε_0: permittivity of free space.

- Heat transfer in solid

$$\rho C_p\frac{\partial \boldsymbol{T}}{\partial t} + \rho C_p\boldsymbol{u}\cdot\nabla T = \nabla\cdot(k\nabla T) + Q \qquad [4.2]$$

ρ: body tissue density [kg/m^3], k: tissue's thermal conductivity [W/(m*K)],
C_p: tissue's specific heat [J/ (kg*K)], Q: heat from microwave heating [W/m^3].

- Convective cooling

$$-\mathbf{n}\cdot(-k)\nabla T = h\cdot(T_{ext} - T) \qquad [4.3]$$

h: heat transfer coefficient [W/(m^2*K)], T_{ext}: external temperature.

- Surface-to-ambient radiation

$$q = \varepsilon\sigma(T^4_{amb} - T^4) \qquad [4.4]$$

ε: surface emissivity, σ: Stefan-Boltzmann constant,
T_{amb}: ambient temperature

4.4 Design of microwave hyperthermia system

There are three parts for the simulations of microwave hyperthermia system using an open–ended coaxial applicator in contact with a biological tissue: coaxial cable (copper), dielectric part (Teflon) and biological tissue. Considering the symmetry of the cylinder coaxial cable and samples, 2D axisymmetric modelling is designed for the simulations.

- The diameter of inner conductor: 2*1.195mm;
- The diameter of dielectric part: 2*(1.195+2.425)mm;
- The outer diameter: 2*(1.195+2.425+0.735)mm;
- The diameter of sample: 2*10mm;
- The thickness of all simulated examples: 3mm.

Conductors

a = 1.195mm
b = 2.425mm
c = 0.735mm

Dielectric

Tissue

a b c
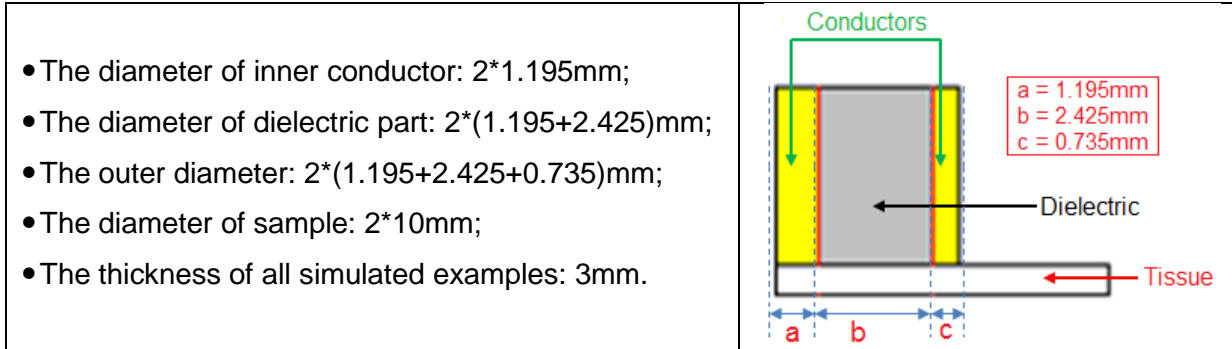
Table 4.1: Dimensions of coaxial cable applicator in contact with the biological tissues

Biological tissue
Thickness : 3mm
Diameter : 20mm

External copper conductor
Length : 100mm
Diameter : 8.71mm

Internal copper conductor
Length : 100mm
Diameter : 2.39mm

Dielectric (Teflon)
Length : 100mm
Diameter : 7.24mm
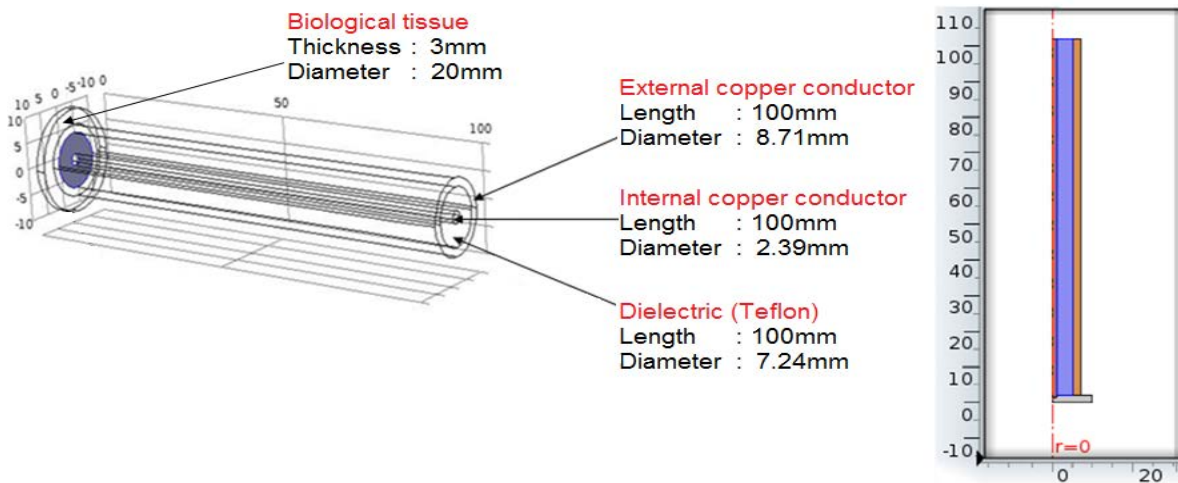
Figure 4.2: 3D and 2D axisymmetrical views of coaxial cable applicator
in contact with biological tissues

Property **Biological Tissue**	Name	Value	Unit
Density	rho	1047	kg/m^3
Electrical conductivity	sigma	1.74	S/m
Heat capacity at constant pressure	Cp	3700	J/(kg*K)
Relative permeability	mur	1	1
Relative permittivity	epsilonr	52.73	1
Thermal conductivity	k	0.6	W/(m*K)
Surface emissivity	epsilon_rad	1	1

Property **Teflon**	Name	Value	Unit
Electrical conductivity	sigma	0	S/m
Relative permeability	mur	1	1
Relative permittivity	epsilonr	2.21	1
Density	rho	2200	kg/m^3
Heat capacity at constant pressu...	Cp	1000	J/(kg*K)
Thermal conductivity	k	1.7	W/(m*K)

Property **Copper**	Name	Value	Unit
Relative permeability	mur	1	1
Electrical conductivity	sigma	5.998e7[S/m]	S/m
Relative permittivity	epsilonr	1	1
Coefficient of thermal expansion	alpha	17e-6[1/K]	1/K
Heat capacity at constant pressure	Cp	385[J/(kg*K)]	J/(kg*K)
Density	rho	8700[kg/m^3]	kg/m^3
Thermal conductivity	k	400[W/(m*K)]	W/(m*K)
Young's modulus	E	110e9[Pa]	Pa
Poisson's ratio	nu	0.35	1
Reference resistivity	rho0	1.72e-8[ohm*m]	Ω*m

Table 4.2: Properties of involved materials for the simulations

The properties of the materials of each part for the simulations of microwave hyperthermia are listed in table 4.2. Ambient temperature is fixed at T = 298.15 K which is equal to 25°C. The ex vivo microwave hyperthermia simulations were carried out on two types of biological tissues: muscle and liver. Their values of the dielectric and physical parameters of ambient temperature at frequency of 2.45GHz should be considered (table 4.3) for the simulations.

Tissue / Properties	Liver	Muscle
Relative Permittivity	43.0	52.7
Electric Conductivity (S/m)	1.69	1.74
Density (kg/m³)	1079	1090
Heat Capacity (J/kg/℃)	3540	3421
Thermal Conductivity (W/m/℃)	0.52	0.49
Heat Transfer Rate (ml/min/kg)	902	39

Table 4.3 Dielectric and physical parameters at ambient temperature of different biological tissue at f = 2.45GHz [62]

For practical ex vivo microwave hyperthermia experiments, five different biological tissues: pork, beef, chicken, pork liver, and calf's liver were used. For each simulation, the corresponding parameters for each tissue should be modified (table 4.4). Constant values of relative permittivity and electric conductivity are replaced by previously measured values of $\varepsilon'(T)$ and $\sigma(T)$ as a function of temperature (e.g. pork and calf's liver) in order to be as close as possible to the practical experiments (figure 4.3).

sample	Heat capacity at constant pressure [J/(kg*K)] (fresh)	thermal conductivity [W/(m*K)] (20°C)	Density [kg/m³]
pork	3590	0.453	1085
beef	3450	0.480	1060
chicken	3320	0.412	1121
pork liver	3540	0.482	1070
calf's liver	3470	0.488	1079

Table 4.4: Properties of five different biological tissues [63] [64] [65] [66]
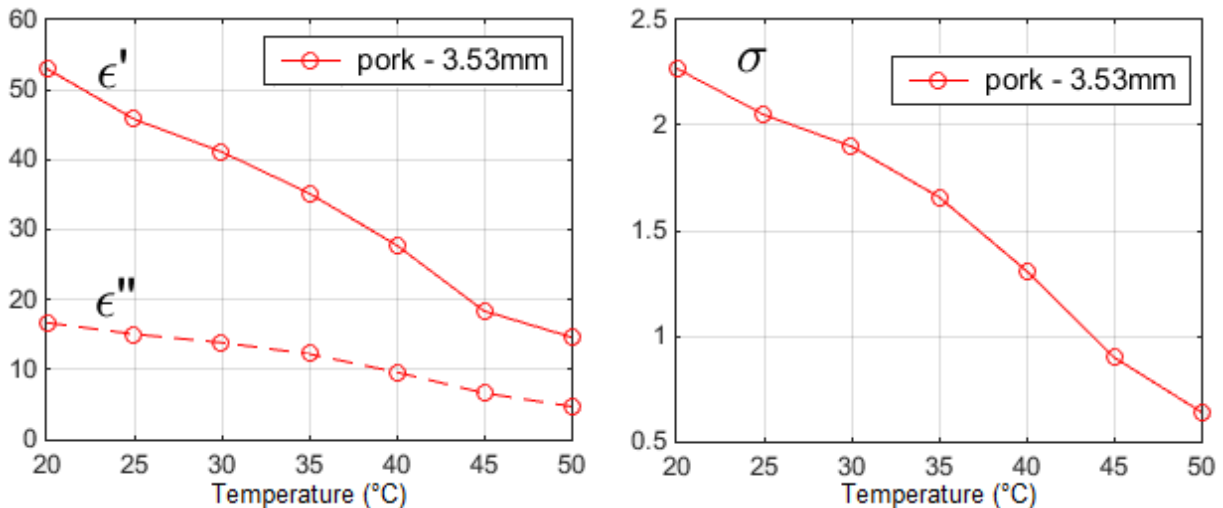
Figure 4.3: $\varepsilon'(T)$ and $\sigma(T)$ of pork (see Chapter 3)
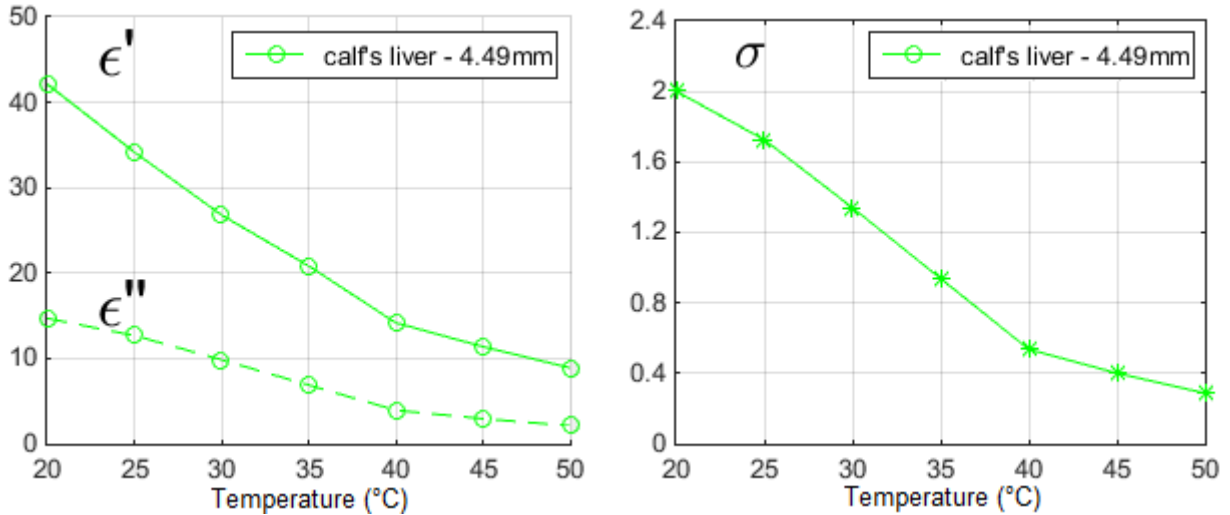
Figure 4.4: $\varepsilon'(T)$ and $\sigma(T)$ of calf's liver (see Chapter 3)

4.5 Microwave hyperthermia simulation protocol

There are also **two protocols** to simulate ex vivo microwave hyperthermia experiment:

1st: Applying a constant microwave power for a period of 210 seconds: the emitted microwave power keeps a constant value during the whole heating period (e.g. P=1, 2, or 3W) for 210 seconds. At the following 210 seconds, there is no delivered microwave power applied to the biological tissue (figure 4.5). For practical experiment, at least one second is needed to change power, so the relative size of transition zone is set to be 0.001 which is equal to 1s (figure 4.6).
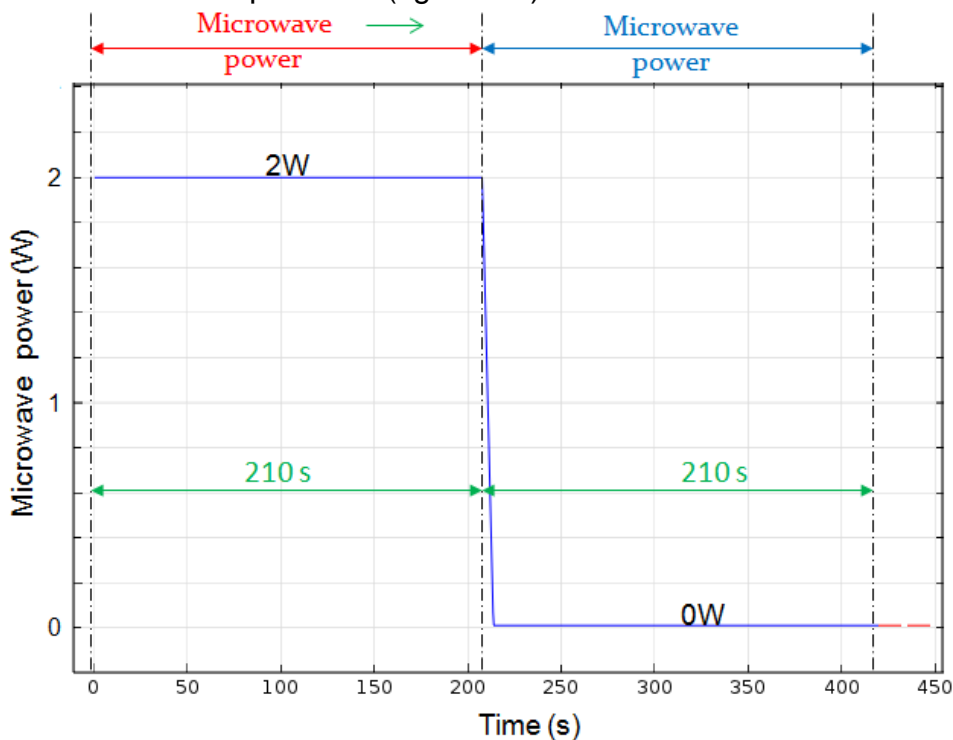
Figure 4.5: Applied constant microwave power protocol

2nd: Applying a step microwave power: the emitted incident microwave power increases progressively from 1W to 3W every 120 seconds, and then decreases from 3W to 0W every 60 seconds (figure 4.6).
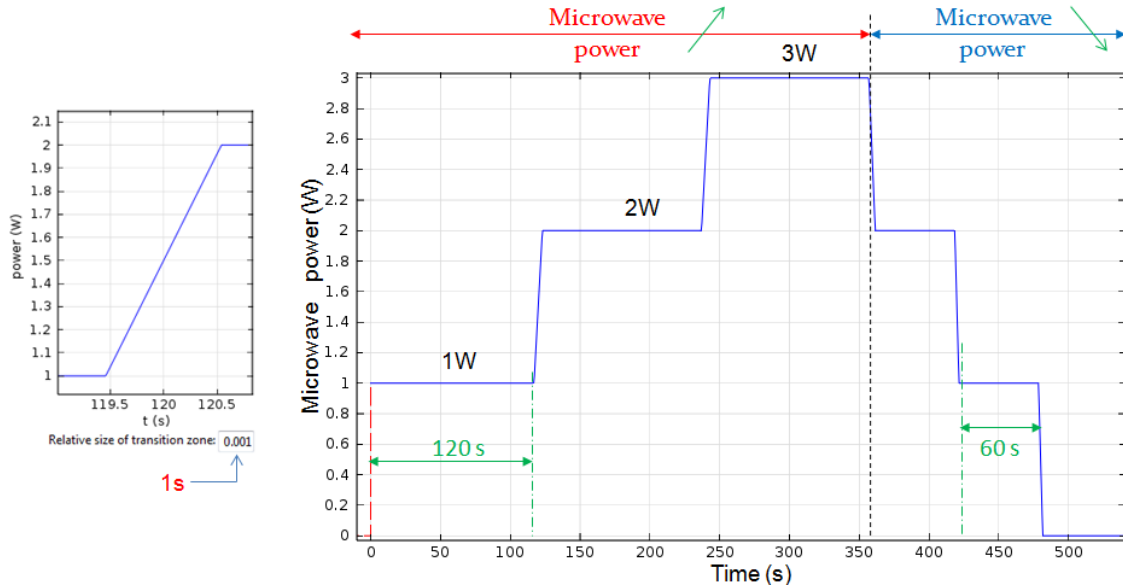
Figure 4.6: Progressively changing step microwave power

For practical ex vivo microwave hyperthermia experiments, the applicator side of tissue is in contact directly with the applicator and the other side of the sample is the sensor side which is in front of the infrared sensor. Infrared sensor measures the real–time temperature variation of the tissue, so the point where the tissue faces infrared sensor has been chosen as the considering point for the simulations (figure 4.7).
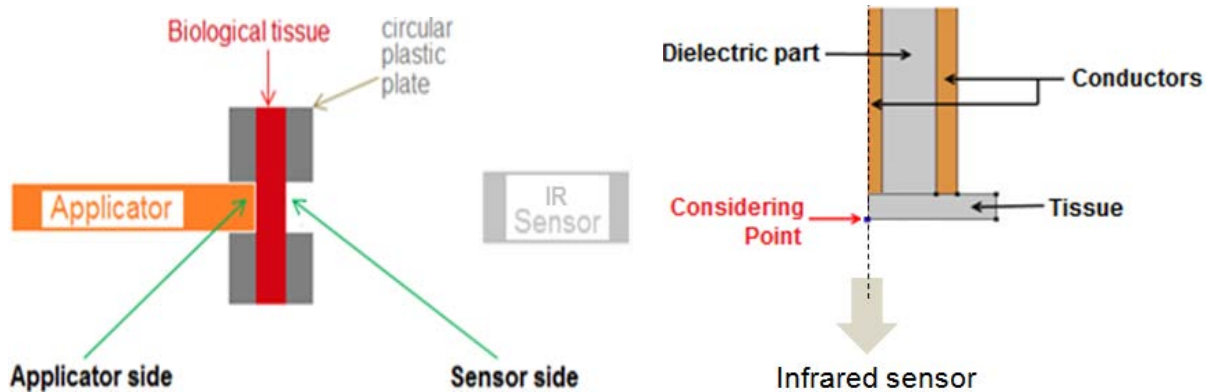
Figure 4.7: chose of sensor side temperature of tissue as considering point for simulation

4.6 Ex vivo microwave hyperthermia simulation results

Distributions of electric and magnetic field norms in the coaxial cable applicator and biological tissue are shown in the figure 4.8. Spatial distribution of temperature inside the tissue is shown in figure 4.9. In fact, the highest temperature (T_{max}) is inside of the tissue. The temperature of sensor side is lower than T_{max}. For example: the temperature of sensor side of 3mm thick pork with P=2W is 44.09°C and T_{max}=48.46°C. The difference between two temperatures is 4.37°C (figure 4.9).
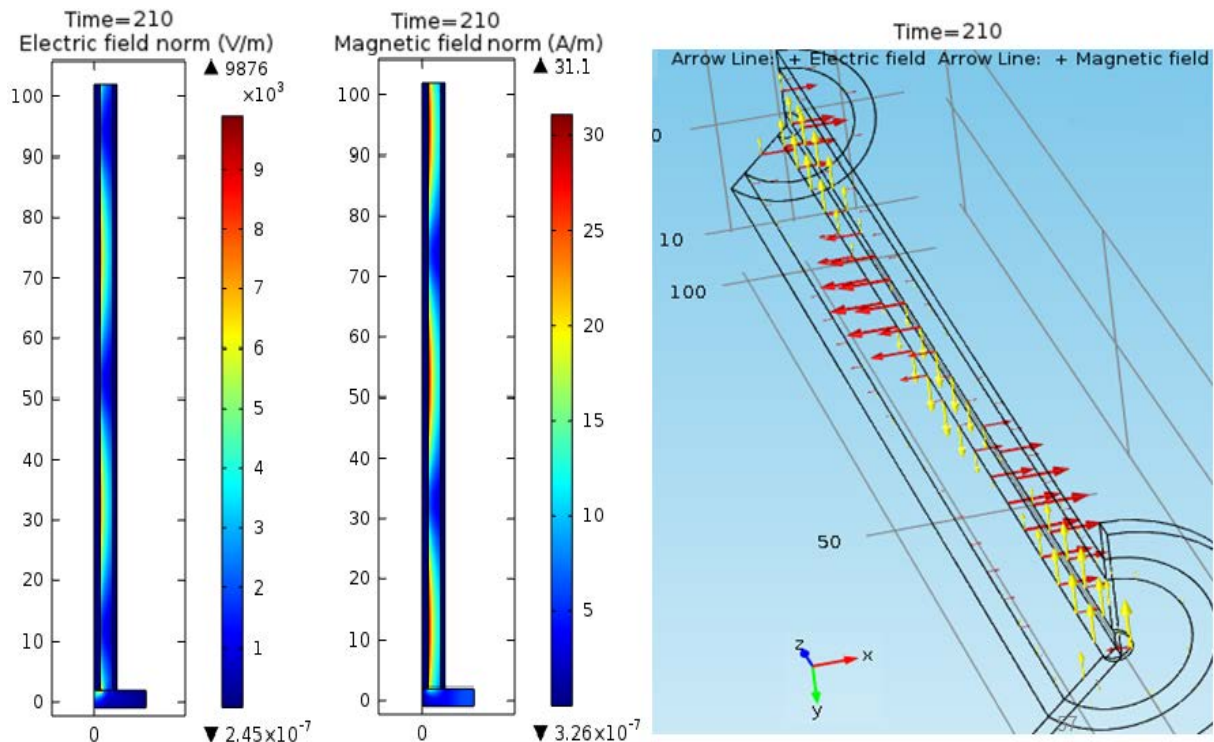
Figure 4.8 Distributions of electric and magnetic field norms
in the coaxial cable applicator and the biological tissue
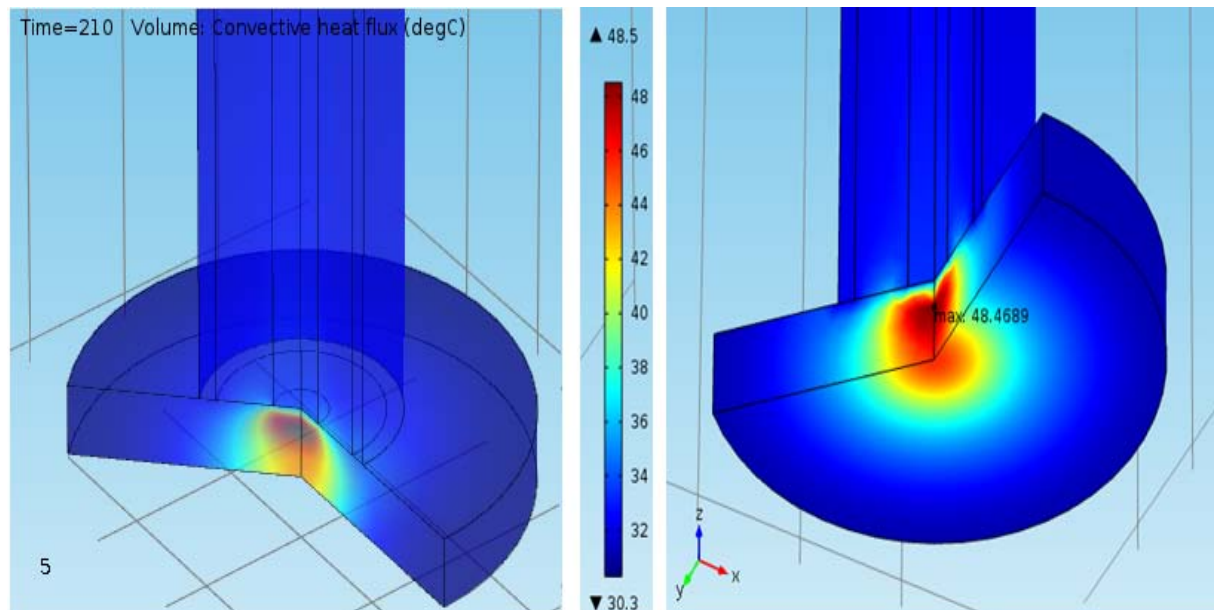
Figure 4.9: Spatial distribution of temperature inside the biological tissue

For five different biological tissues: muscle (pork, beef, and chicken) and liver (pork liver and calf's liver), we considered two protocols: constant applied microwave power (P=2W or 3W) and progressively changing step microwave power (P=1 to 3W). For ex vivo microwave hyperthermia experiments, only the temperature of sensor side of the tissue can be measured, so the simulated temperature of sensor side is considered. The simulated results will be shown in the following part according to different types of tissue and different simulated protocols.

a) Tissue: muscle

1st protocol: constant microwave power

Figure 4.10: Simulated temperature variations for the pork samples of different thicknesses
with an applied constant microwave power P=2W

Figure 4.11: Simulated temperature variations for the pork samples of different thicknesses
with an applied constant microwave power P=3W

With the same constant microwave power level, for muscles of different thicknesses (e.g. pork), similar tendencies of increase and decrease of simulated temperature variations have been obtained. Thinner sample leads to higher simulated temperature as observed also in the ex vivo experiments. Thinner sample is heated more quickly than mother thicker samples. For 2mm thick pork sample with P=2W, its temperature increases fastest and attains the highest value for T_{max} = 79.36°C and for 4.5mm thick sample, it attains the lowest value for T_{max} =45.54°C (figure 4.11)

<u>2nd protocol: step microwave power</u>

2nd protocol: step microwave power

Figure 4.12: Simulated temperature variations for the pork samples of different thicknesses
with applied step microwave power

With step microwave power, for muscle (e.g. pork), we obtain similar tendencies of
increase and decrease on simulated temperature variations. The temperature
variations on thinner sample are most observable than other thicker samples
corresponding to each power level. At the 360th second, T_{max} = 80.14°C for 2mm
thick sample and T_{max} =45.21°C for 4.5mm thick sample.

b) Tissue: liver

1st protocol: constant microwave power
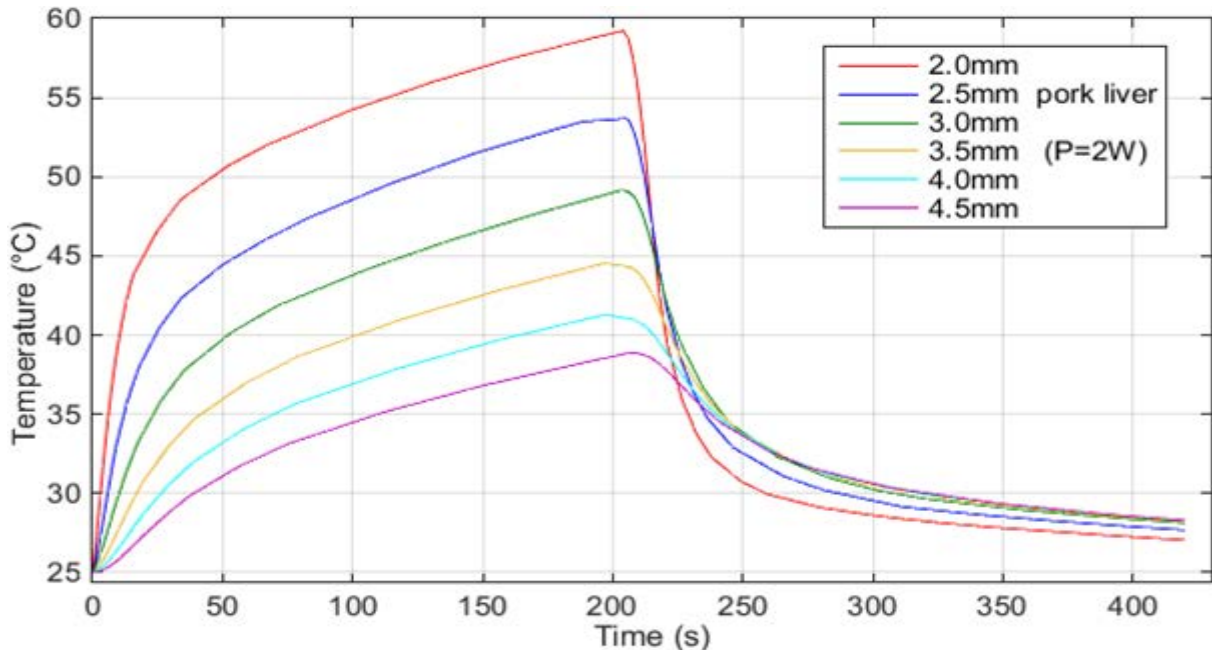
Figure 4.13: Simulated temperature variations for the pork liver samples of different thicknesses
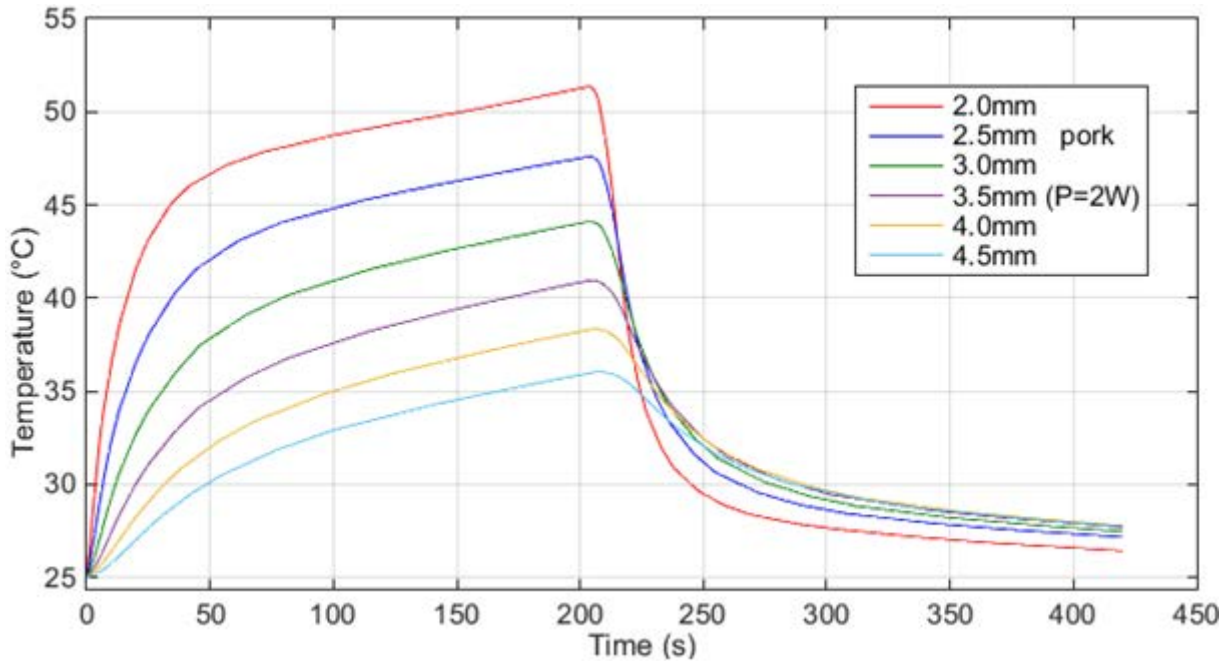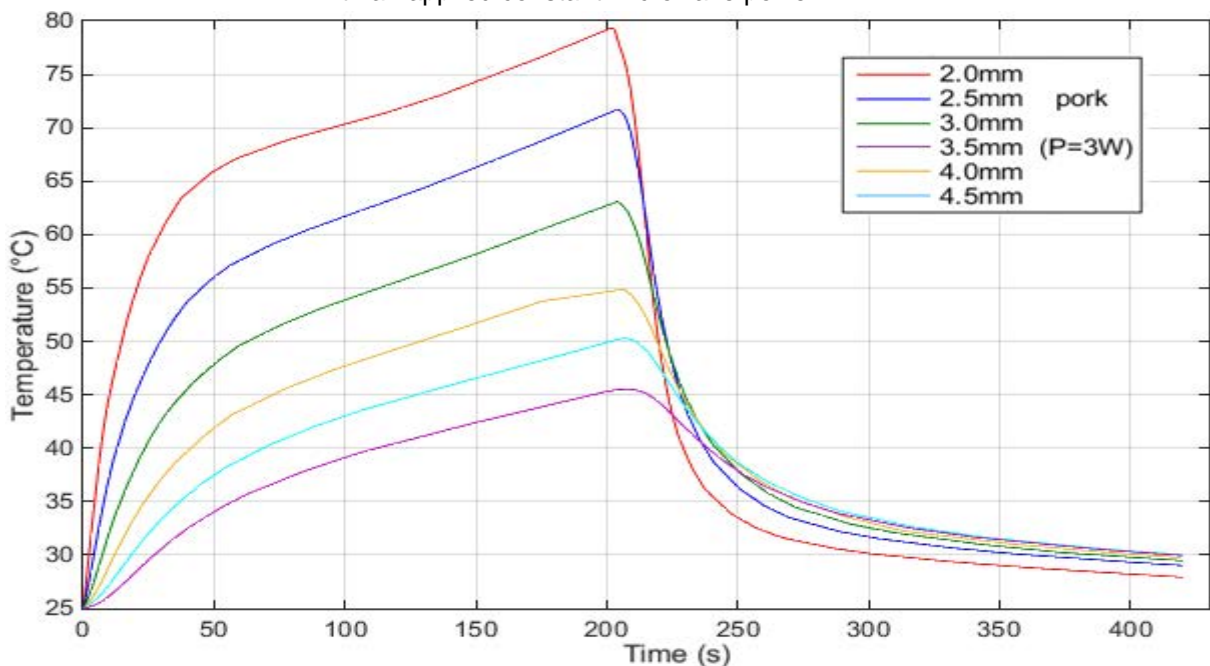with an applied constant microwave power P=2W
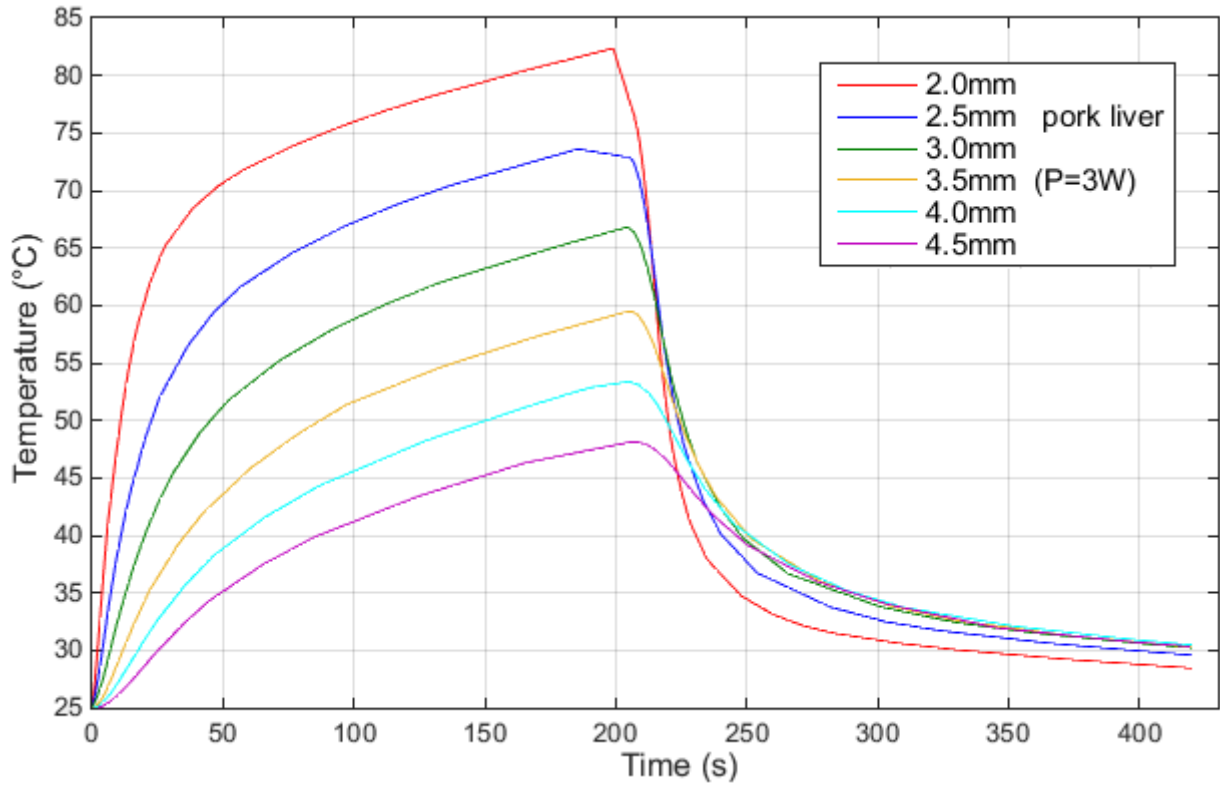
Figure 4.14: Simulated temperature variations for the pork liver samples of different thicknesses with an applied constant microwave power P=3W

2nd protocol: step microwave power
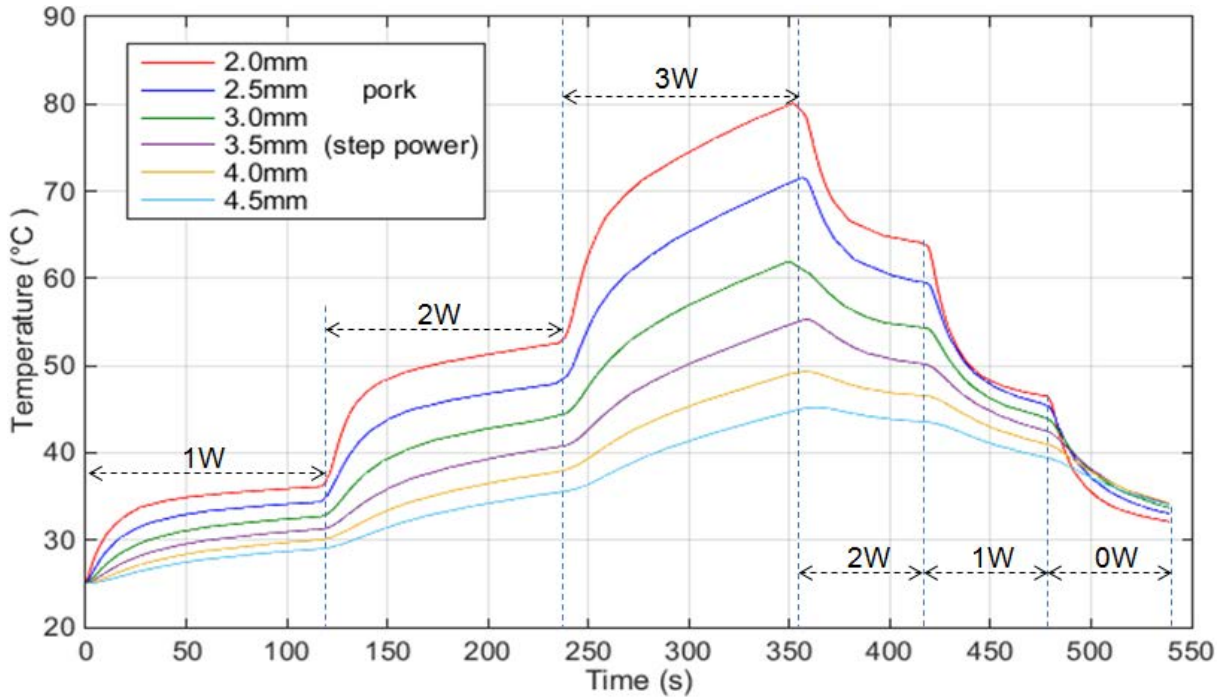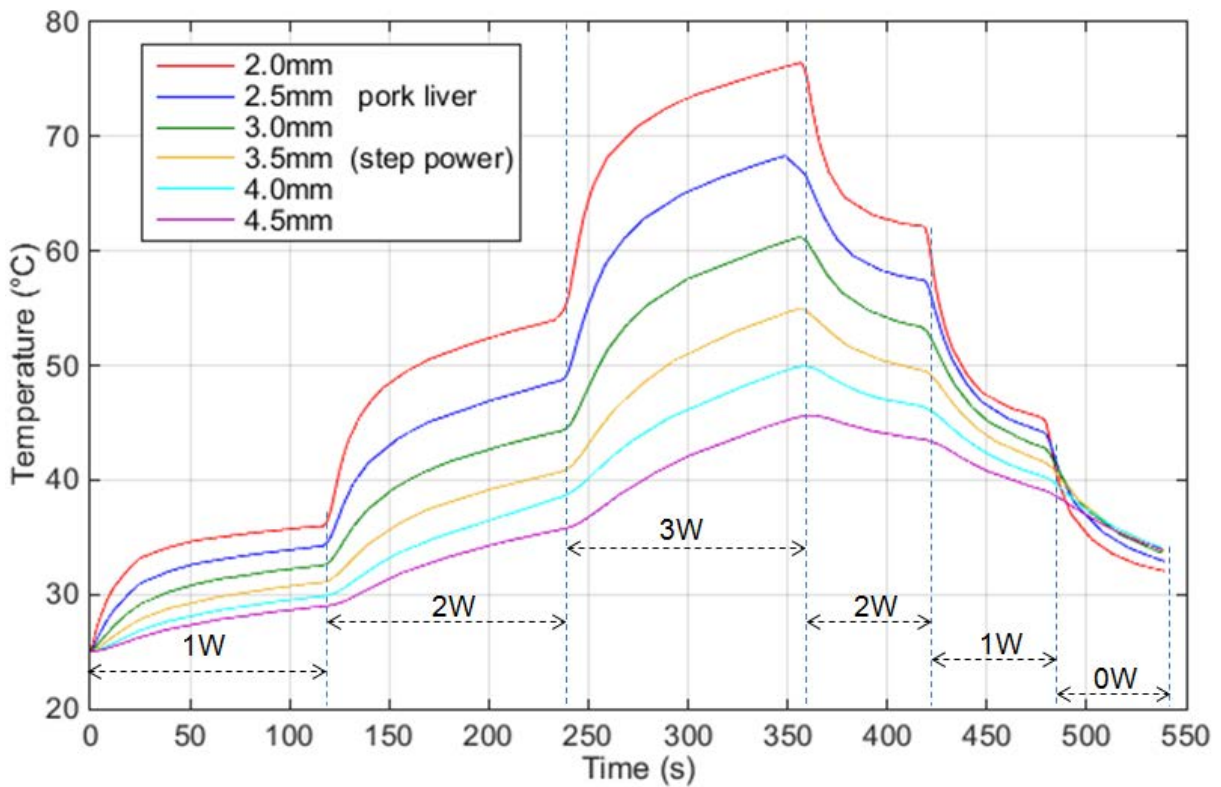

Figure 4.15: Simulated temperature variations for the pork liver samples of different thicknesses with applied step microwave power

For pork liver samples, they have similar tendencies of increase and decrease on simulated temperature variation like pork muscle samples. The thinnest sample is heated fastest and it attains the highest maximum temperature among all samples for both protocols. With an applied constant microwave power P=2W, for a 2mm thick sample, the T_{max} = 59.23°C and for 4.5mm thick sample, the T_{max} = 38.88°C. With an applied step microwave power, all samples have similar tendencies of increase and decrease on simulated temperature variations. The changes of temperature on the thinnest sample are most observable among all samples. It responds or follows the best with applied progressively changing microwave power.

4.7 Parameters' Influences on the simulation

When biological tissues are heated by microwave power, many intrinsic characteristic parameters of irradiated tissue change such as permittivity, electrical conductivity, density, thermal conductivity and specific heat capacity. [66] Simulations become more difficult with the variations of these parameters as the function of temperature. Some other extrinsic parameters such as the thickness of tissue, applied power level, and heat transfer coefficient can also affect the temperature simulation results.

a) Thickness of tissue

The thickness of tissue affects the temperature variation. Higher temperature can be obtained for thinner sample. In fact, it is quite logical as there is less volume of material to heat up. For example, pork samples of different thicknesses irradiated by a constant power level P=2W, the thinnest sample of 2.5mm pork attained the highest T_{max} = 47.61°C and 4mm pork attained the lowest T_{max} = 38.33°C (figure 4.16). The difference of temperature (ΔT) between each two neighboring samples decreases from thinner sample to thicker sample (table 4.5).
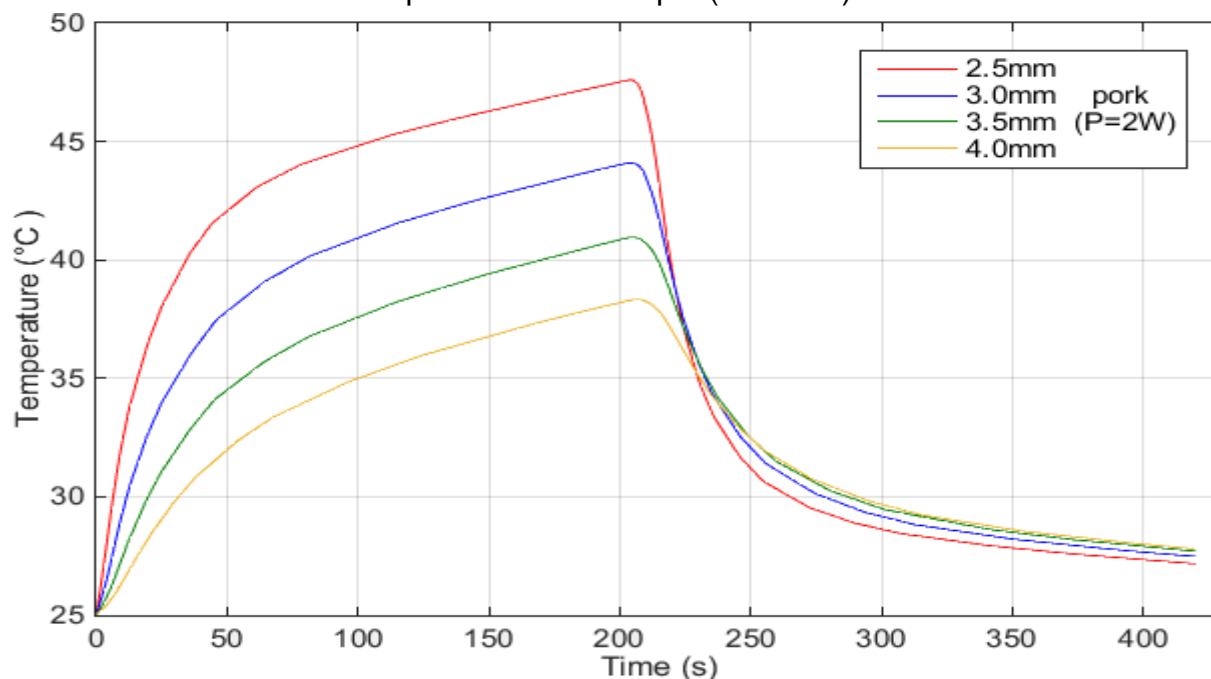
Figure 4.16: Simulated temperature variations for the pork samples of different thicknesses with P=2W showing the non linear decrease of the maximum temperature.

Pork (P=2W)		
Thickness	T_{max}	$\Delta T_{difference}$
2.5mm	47.61°C	3.51°C
3.0mm	44.10°C	3.15°C
3.5mm	40.95°C	2.62°C
4.0mm	38.33°C	
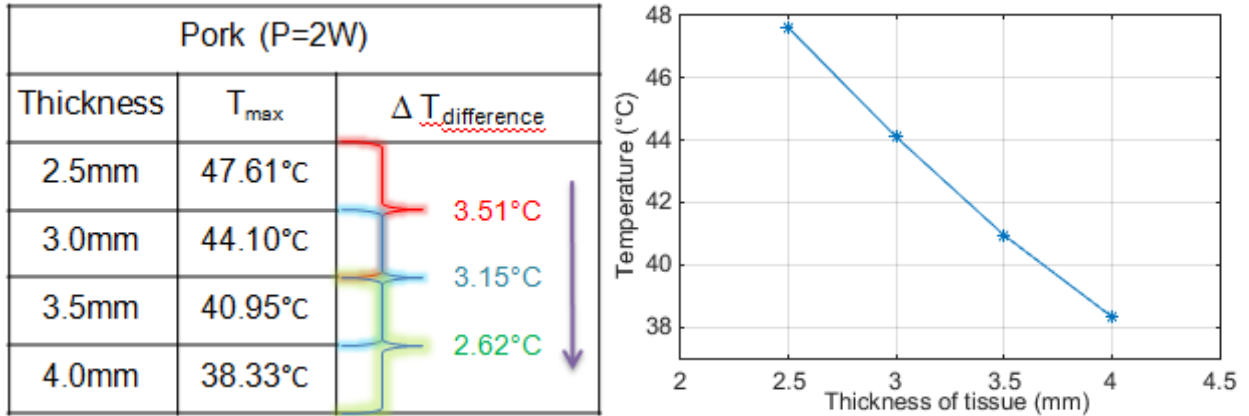
Table 4.5: Temperature variation of changed thickness for pork with P=2W

b) Applied power level

The level of applied microwave power affects the simulated temperature variation of the tissue. The higher applied power to the tissue leads to a higher temperature. The 3mm thick pork sample is heated by different power from 1W to 1.5W. The highest temperatures at the 210th second change from 39.35°C to 33.72°C (figure 4.17). The difference of temperature had been 1°C even with only 0.1W difference between 1W and 1.1W. The difference of temperature (ΔT) between each two neighboring power levels decreases from higher power to lower power (table 4.6).
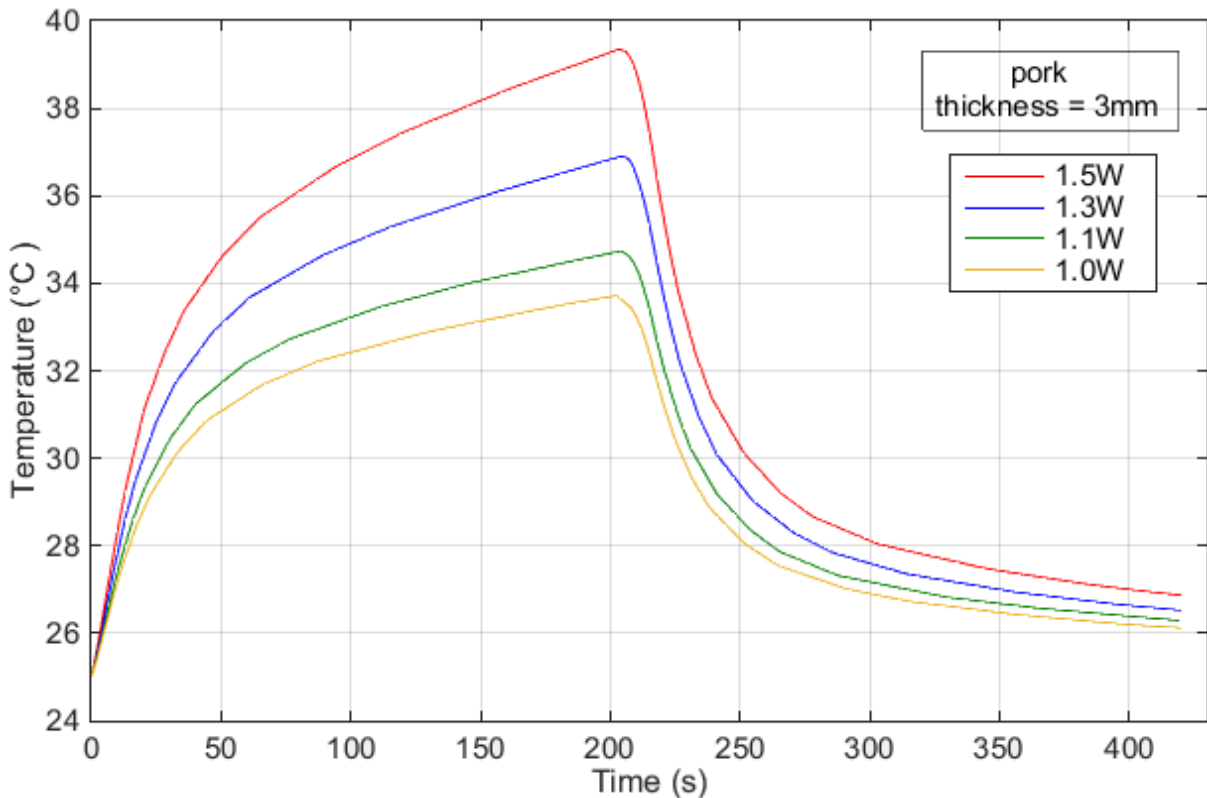
Figure 4.17: Simulated temperature variations for the 3mm thick pork samples with different applied constant microwave power levels

Pork (thickness = 3mm)		
constant power	T_{max}	$\Delta T_{difference}$
1.0W	33.72°C	
1.1W	34.73°C	1.01°C
1.3W	36.90°C	2.17°C
1.5W	39.35°C	2.45°C
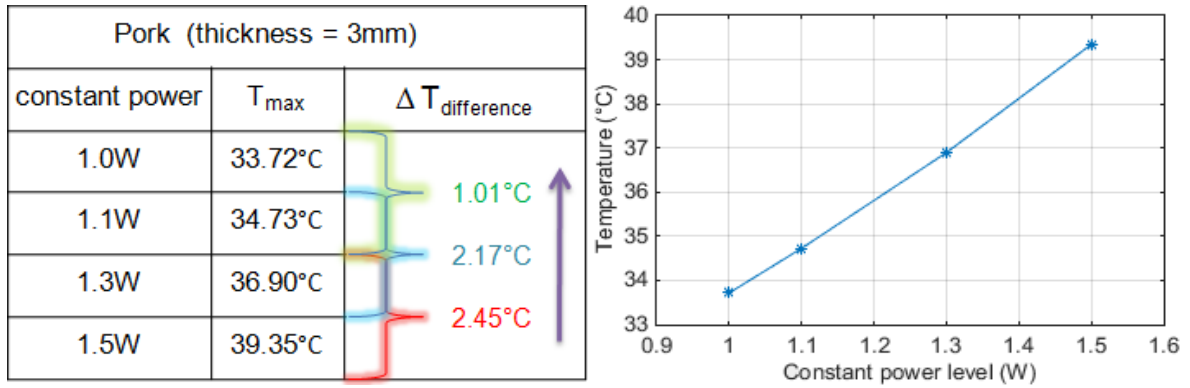
Table 4.6: Temperature variation of changed constant power level for pork with thickness=3mm

c) Permittivity and conductivity

When biological tissue is heated by the microwave power, many original properties of tissue change with temperature. Above ~45°C, some irreversible changes will happen. Values of dielectric properties ($\varepsilon'(T)$ and $\sigma(T)$) of raw biological tissues have been previously measured by the coaxial probe method (see chapter 2). They influence the temperature variation of the tissue. When the permittivity is considered as $\varepsilon' = f(T)$ (figure 4.3) for the simulations, the difference of simulated temperatures ($\Delta T_{\varepsilon'(T)}$) between the cases of σ = constant and $\sigma(T)$ is about 6.43°C. When ε = constant is used for the simulations, the difference of simulated temperatures ($\Delta T_{\varepsilon = constant}$) between σ = constant and $\sigma(T)$ is about 0.87°C (table 4.7). $\Delta T_{\varepsilon'(T)} > \Delta T_{\varepsilon = constant}$ means that when ε is constant, the variable value of electrical conductivity has a relatively small influence on the simulated temperature variation. When $\varepsilon' = f(T)$, the influence of electrical conductivity on the simulated temperature becomes bigger (figure 4.18).
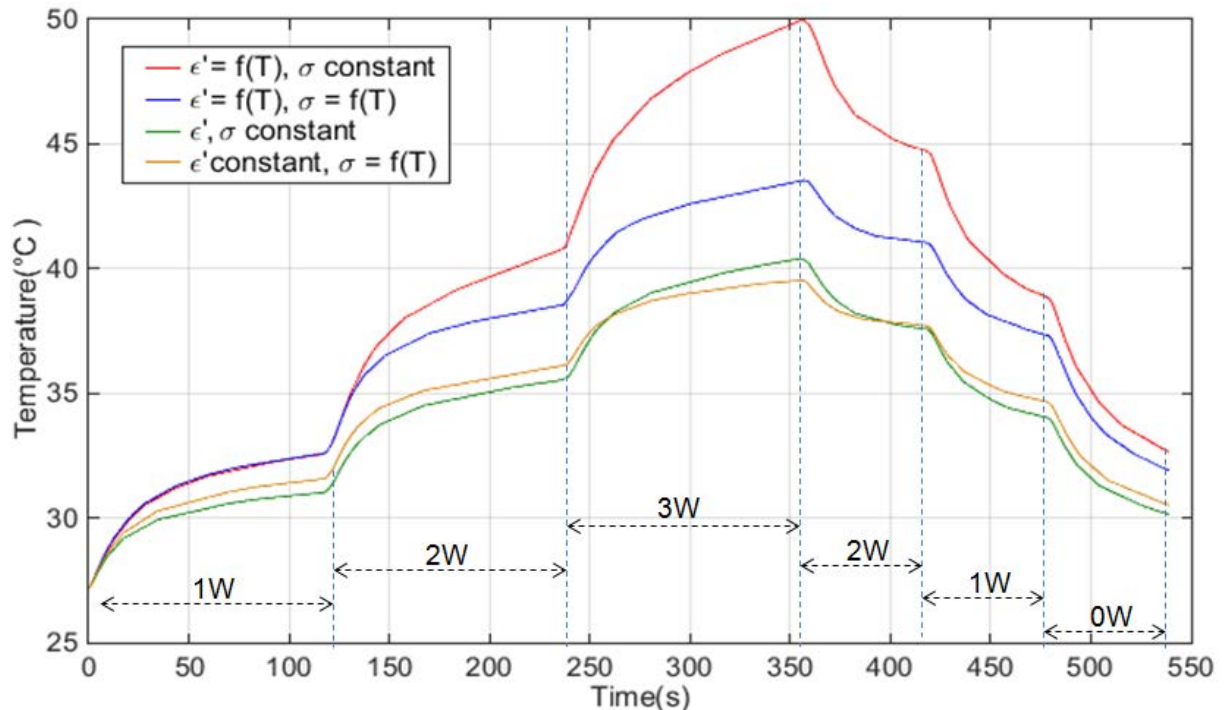
Figure 4.18: Temperature variations of for 3mm thick pork sample with influence of $\varepsilon'(T)$ and $\sigma(T)$ for progressively changing step microwave power.

Pork (thickness = 3mm) with step power			
$\varepsilon'(T)$		$\varepsilon' = constant$	
$\sigma = constant$	$\sigma(T)$	$\sigma = constant$	$\sigma(T)$
49.98°C	43.55°C	40.40°C	39.53°C

Table 4.7: Influence of dielectric properties on simulated temperature result

d) Heat transfer Coefficient

Heat transfer coefficient, *h* for thermal convection also has an influence on the simulated temperature variations. In fact, it determines the cooling of the tissue by convection. Figure 4.19 shows the temperature variations of pork muscle (thickness= 3mm and P=2W) with several values of heat transfer coefficient values (*h*=5, 10, 15). Greater value of heat transfer coefficient leads to lower maximum temperature. Under ambient condition, influences of *h* on the simulated temperatures are slight (table 4.8).
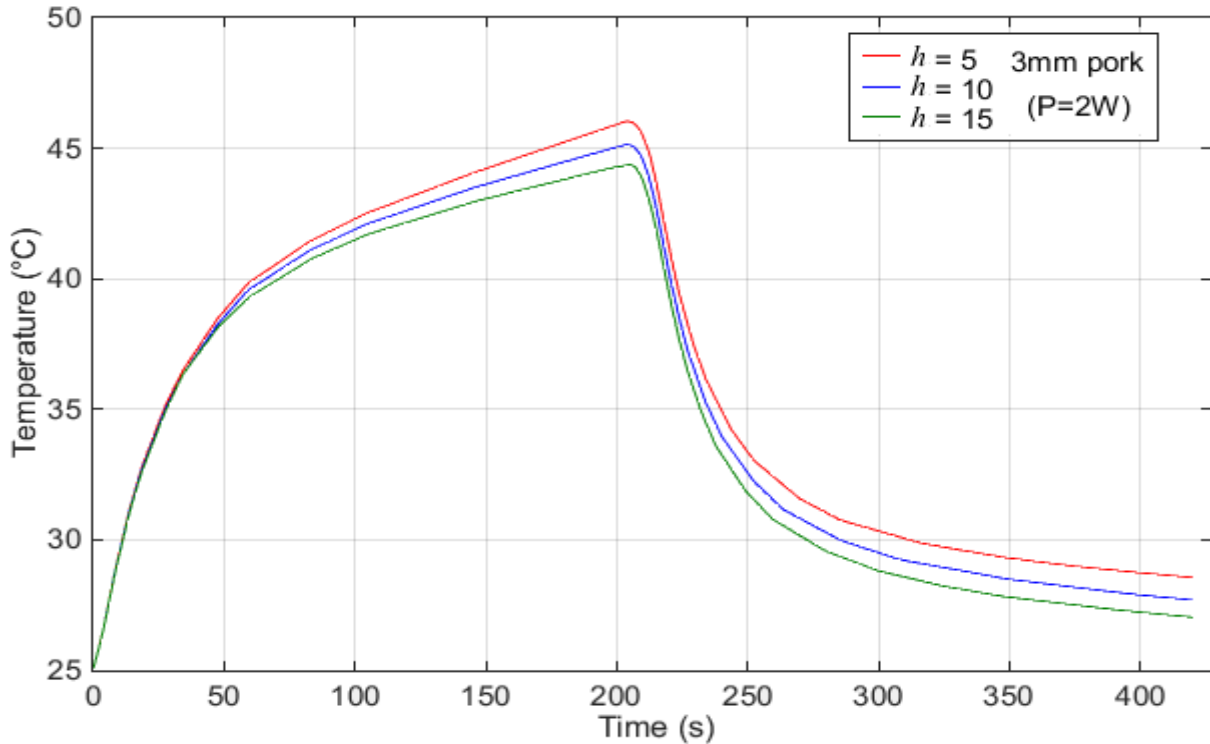
Figure 4.19: Temperature variations on the pork sample with influence of the heat transfer coefficient–*h*

pork (thickness: 3mm and P=2W)		
h [W/(m²K)]	T_{max}	$\Delta T_{difference}$
5	46.04°C	0.9°C
10	45.14°C	0.77°C
15	44.37°C	

Table 4.8: Influence of heat transfer coefficient on the simulated maximum temperature
(3mm thick pork sample and P=2W)

4.8 Discussions

It is important to compare simulated and experimental temperature variation results for each tissue and several following aspects influence on the comparisons.

- **Impedance matching**

  The Impedance matching for the microwave hyperthermia experiments is controlled manually by using a double stub tuner. The incident microwave power cannot be delivered totally (100%) to the biological tissue under test. For the ex vivo microwave hyperthermia experiments, the applied power level is small and the reflecting power is controlled by the double stub tuner below about –30dBm: But the simulation considers that there is no reflecting power going back, the applied power is 100% delivered to the tissue. Therefore, the simulated temperature can be a little higher than experimental temperature.

- **Thickness of tissue**

  The thickness of tissue is difficult to be measured precisely as it is a soft material. When the tissue sample is fixed by the two plastic sample holders on the test bench, the measured thickness can also be changed because of the fixture error by the operator. This fact increases the difficulties to compare the simulated and experimental temperatures. Thickness of tissue can affect the simulated results (figure 4.16)

- **Amplifier**

  The amplifier (25S1G4A) has 10 gain levels. Under control, it can provide a theoretical maximum value of 10 watts. The control knob for changing the gain level is continuous but not discrete. For example, when the knob is put on the position of 3, from a point view of overlook, it looks that the knob is exactly put in the middle of 3. But in fact, from the point view of horizon, the knob is not put centrally, so the output power can be a little more than 3W (figure 4.20). The power level can strongly affect the simulated temperature. Even for 0.1W power variation, 1°C difference of temperature has been achieved (figure 5.15).

Figure 4.20: Different point views of amplifier control knob
which may introduce power level adjustment error.

- **Permittivity and conductivity**

  $\varepsilon'(T)$ and $\sigma(T)$ are measured by open–ended coaxial probe, but the obtained values might not be very precise. When their values are used for the parameters of tissue, they can lead to the differences of both increase and decrease tendencies of temperature between simulations and experiments. Besides, the temperature of microwave hyperthermia experiments can exceed 50°C and the

dielectric properties have been measured up to 50°C. For the unmeasured values of both $\varepsilon'(T)$ and $\sigma(T)$ over 50°C also lead errors between simulations and experiments. For ex vivo microwave hyperthermia simulations, when the temperature dependent $\varepsilon'(T)$ and $\sigma(T)$ are used, COMSOL can only allow to put their values as a function of temperature but not parallel as a function of time. This can also lead to the errors of value and tendency of temperature between simulations and experiments. For example, when P=2W is applied during the first 210 seconds for heating, $\varepsilon'(T)$ and $\sigma(T)$ only consider the temperature variation of tissue but not its irreversible change after irradiation.

4.9 Comparisons between experimental and simulation results

Different types of biological tissues have been considered such as muscle (pork, beef, and chicken) and liver (pork liver, and calf's liver). Their simulated temperature variations have been compared to experimental results.

a) Pork muscle

For pork muscle samples with different microwave powers, simulated temperature variations correspond well with the experimental results. Both simulated and experimental temperatures change with, respond to or follow the applied microwave power. For all comparisons, there are small gaps between simulated and experimental temperatures, because of the several errors of impedance matching, thickness, amplifier, $\varepsilon'(T)$ and $\sigma(T)$ which are talked about in the discussion part. For P=2W, it is normally that simulated temperature is a little larger than experimental one in the heating part. Simulated temperatures $T_{s\text{-}max}$ and experimental temperatures $T_{e\text{-}max}$ are compared (table 4.9).

Figure 4.21: Comparison between experimental and simulated temperature variations of 2.97mm thick pork muscle sample with P=2W

Figure 4.22: Comparison between experimental and simulated temperature variations
of 2.99mm thick pork muscle sample with P=3W

Figure 4.23: Comparison between experimental and simulated temperature variations
of 2.81mm thick pork muscle sample with step microwave power

pork			
Thickness	2.97mm	2.99mm	2.81mm
Type of power	P = 2W	P = 3W	P = step power
T_{s-max}	44.34°C	62.11°C	68.51°C
T_{e-max}	44.20°C	62.80°C	68.20°C
ΔT	0.14°C	-0.69°C	0.31°C

Table 4.9: Comparison between simulated maximum temperatures (T_{s-max})
and experimental results (T_{e-max}) of pork muscle samples

b) Beef muscle

Figure 4.24: Comparison between experimental and simulated temperature variations
of 2.80mm thick beef muscle sample with P=2W

Figure 4.25: Comparison between experimental and simulated temperature variations
of 3.45mm thick beef muscle sample with P=3W

Figure 4.26: Comparison between experimental and simulated temperature variations
of 3.40mm thick beef muscle sample with step microwave power

For beef samples with different microwave powers, simulated temperatures correspond well with the experimental results. Both simulated and experimental temperatures follow the applied microwave power. For all comparisons, there are tolerable gaps between simulated and experimental temperatures. For P=2W, there is an obvious big difference from the 80th to the 110th second because of poor control of impedance matching by double stub tuner (figure 4.24). For step microwave power, at the beginning (P=1W), the experimental temperature is a little higher than the simulated temperature. The real applied microwave power level might be slightly higher than 1W and be the cause of the difference. At the end of the curve (P=0W), there is a big gap of temperature decrease tendency between simulation and experimental results because of the values of $\varepsilon'(T)$ and $\sigma(T)$ considered for the simulations. The simulated maximum temperature ($T_{s\text{-}max}$) and experimental maximum temperature ($T_{e\text{-}max}$) are compared in table 4.10.

beef			
Thickness	2.80mm	3.45mm	3.40mm
Type of power	P = 2W	P = 3W	P = step power
$T_{s\text{-}max}$	43.27°C	49.02°C	61.93°C
$T_{e\text{-}max}$	43.40°C	49.10°C	61.20°C
ΔT	-0.13°C	-0.08°C	0.73°C

Table 4.10: Comparison between simulated maximum temperatures ($T_{s\text{-}max}$)
and experimental results ($T_{e\text{-}max}$) of beef muscle samples
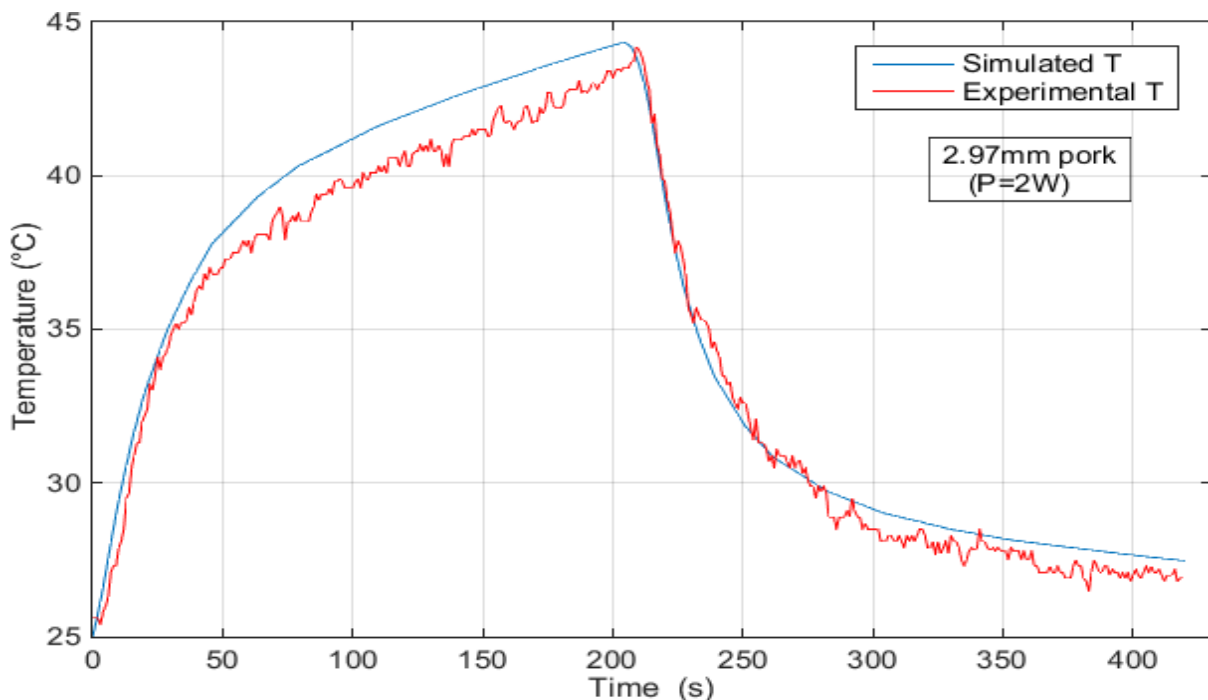
c) Chicken muscle

Figure 4.27: Comparison between experimental and simulated temperature variations
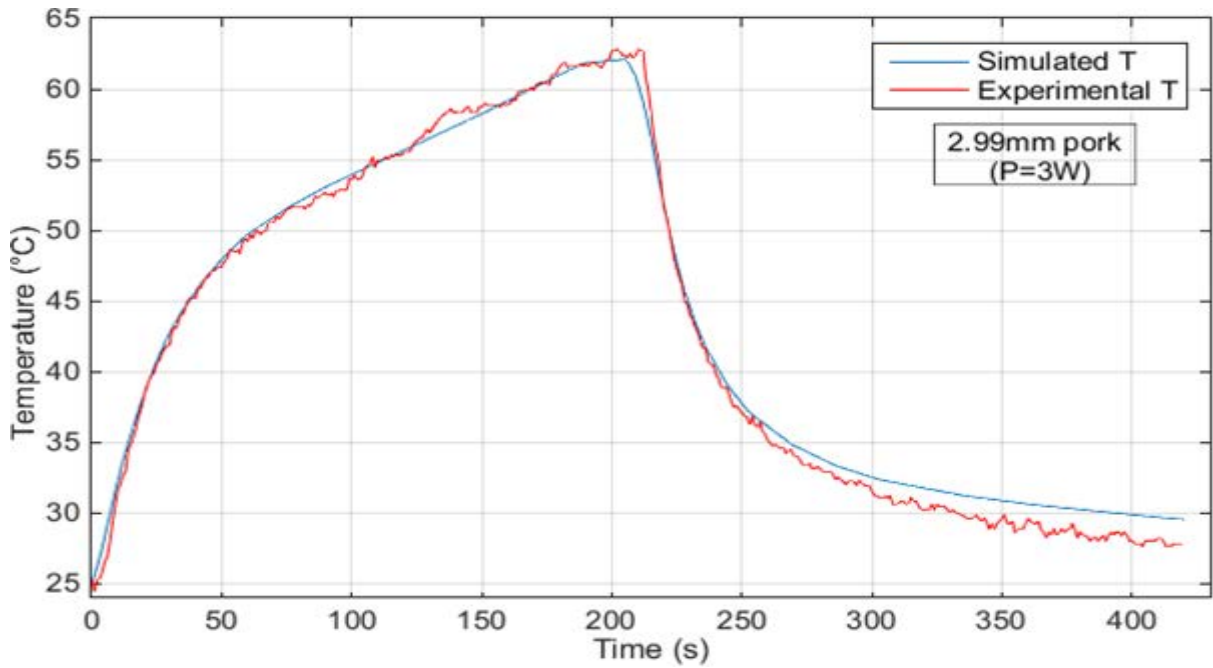of 3.28mm thick chicken muscle sample with P=2W

Figure 4.28: Comparison between experimental and simulated temperature variations
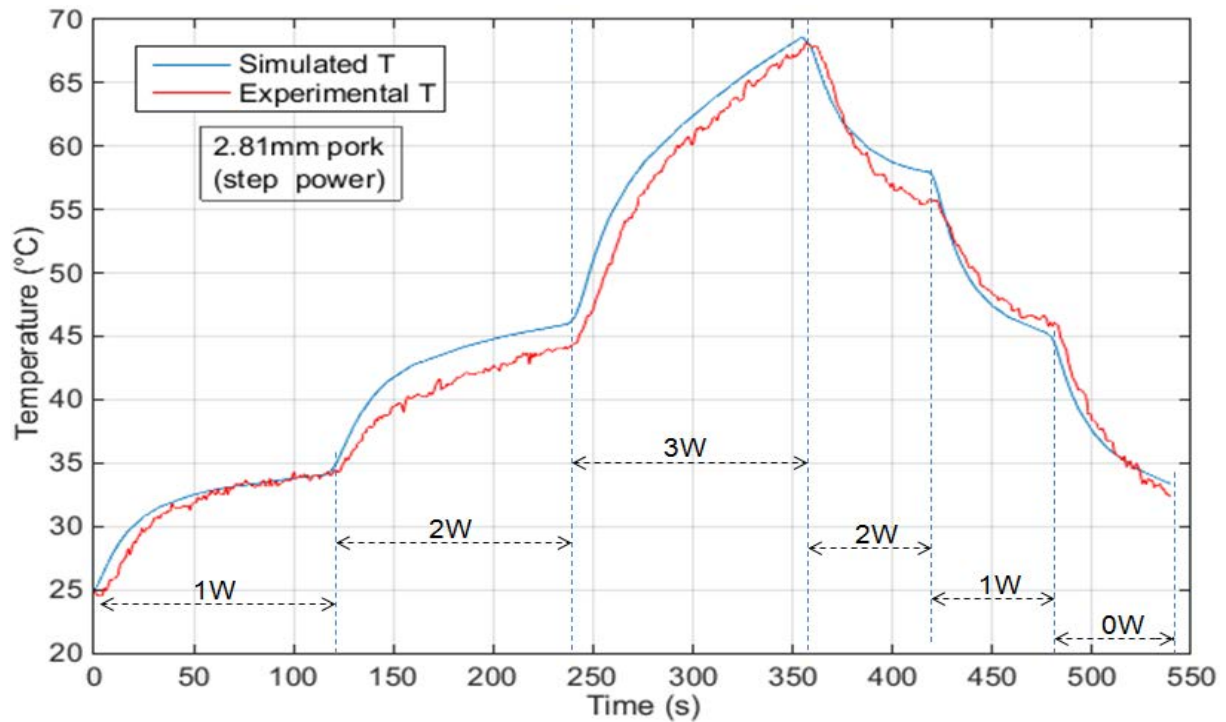of 3.27mm thick chicken muscle sample with P=3W

Figure 4.29: Comparison between experimental and simulated temperature variations
of 3.57mm thick chicken muscle sample with step microwave power

For all comparisons, there are tolerable gaps between simulated and experimental results. Both results respond to the applied microwave power. But the tendency for P=3W corresponds less well between simulation and experiment for the heating section (figure 4.28). The real applied power is less than 3W might be the reason for the difference. For P=2W, simulated temperature corresponds well with the experimental result (figure 4.27). For step microwave power, at the beginning (P=1W), the experimental temperature is a bit higher than the simulated temperature, because the real applied power level might be slightly higher than 1W. Around the 360th second, experimental result is a bit higher than simulated temperature. Generally, for all chicken samples with different microwave powers, simulated temperatures correspond well with the experimental results. The simulated maximum temperatures ($T_{s\text{-}max}$) and experimental maximum temperatures ($T_{e\text{-}max}$) are compared table 4.11.

chicken			
Thickness	3.28mm	3.27mm	3.57mm
Type of power	P = 2W	P = 3W	P = step power
$T_{s\text{-}max}$	44.22°C	67.19°C	73.51°C
$T_{e\text{-}max}$	44.50°C	67.30°C	76.20°C
ΔT	-0.28°C	-0.11°C	-2.69°C

Table 4.11: Comparison between simulated maximum temperatures ($T_{s\text{-}max}$)
and experimental results ($T_{e\text{-}max}$) of chicken muscle samples
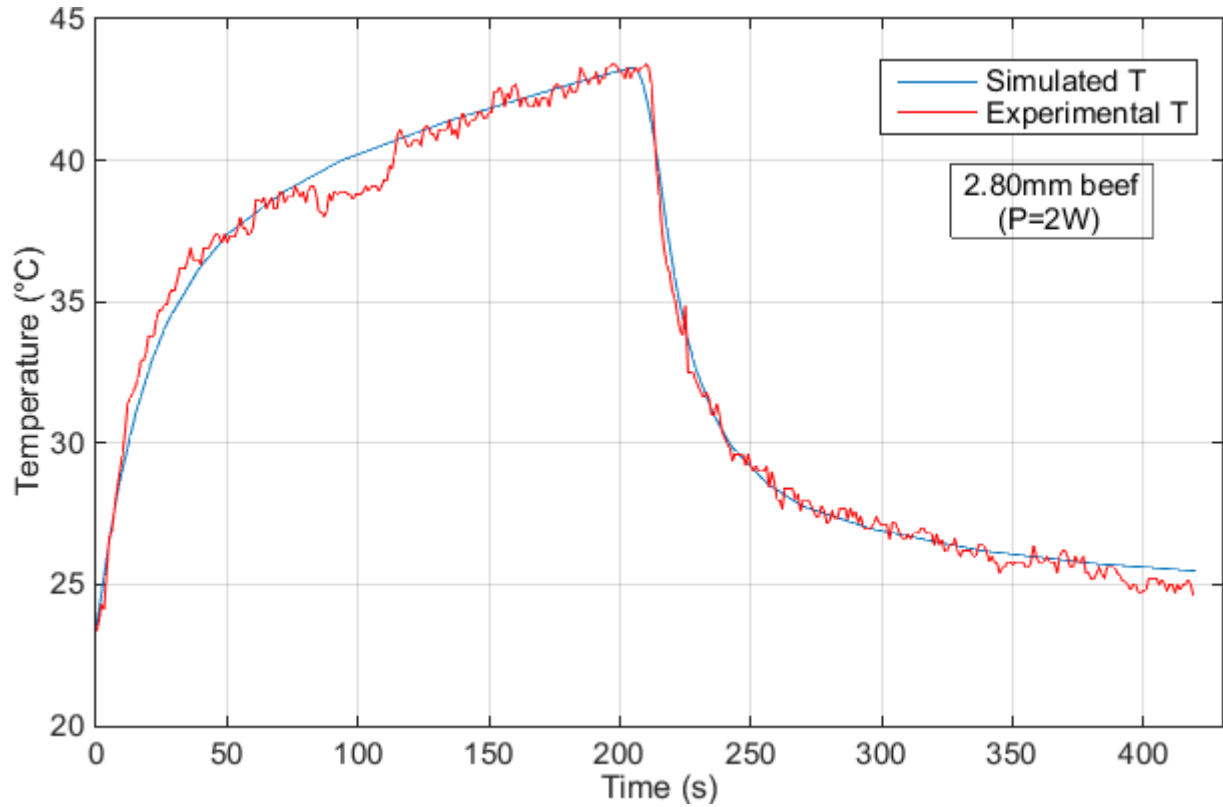
d) Pork liver

Figure 4.30: Comparison between experimental and simulated temperature variations
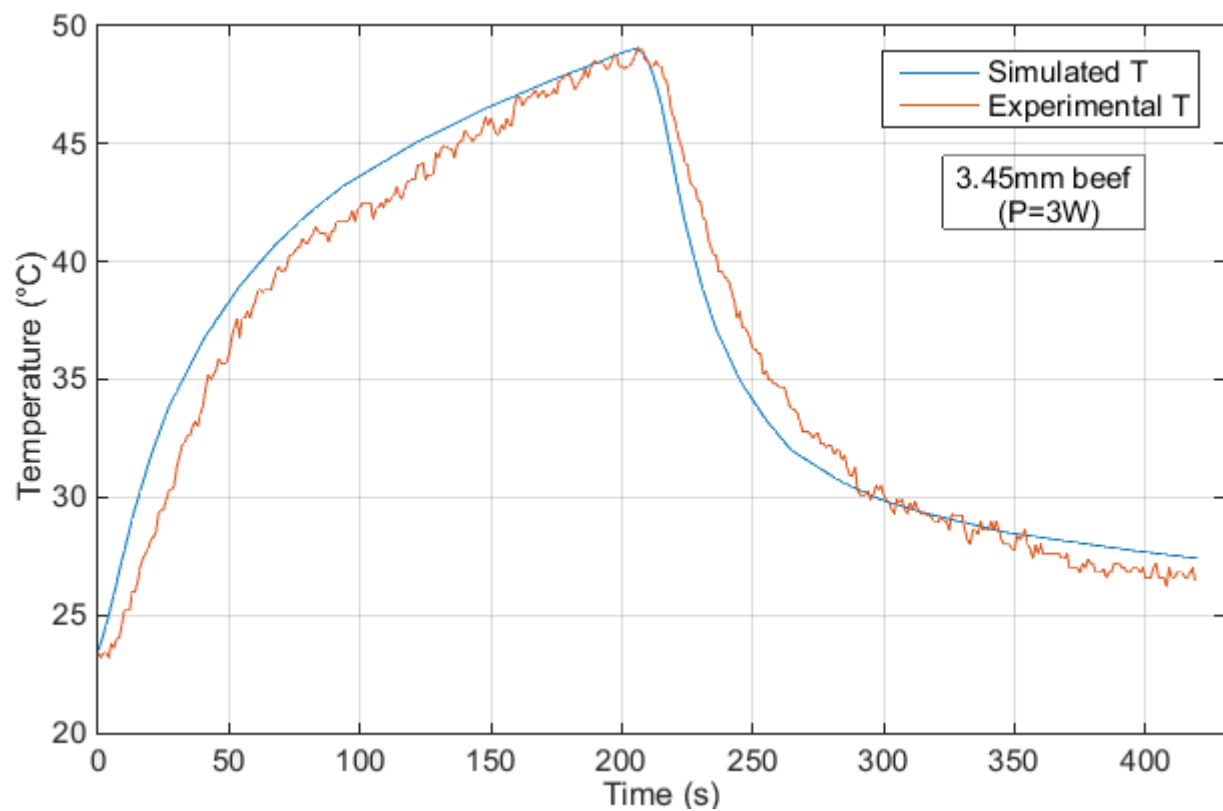of 2.84mm thick pork liver sample with P=2W

Figure 4.31: Comparison between experimental and simulated temperature variations
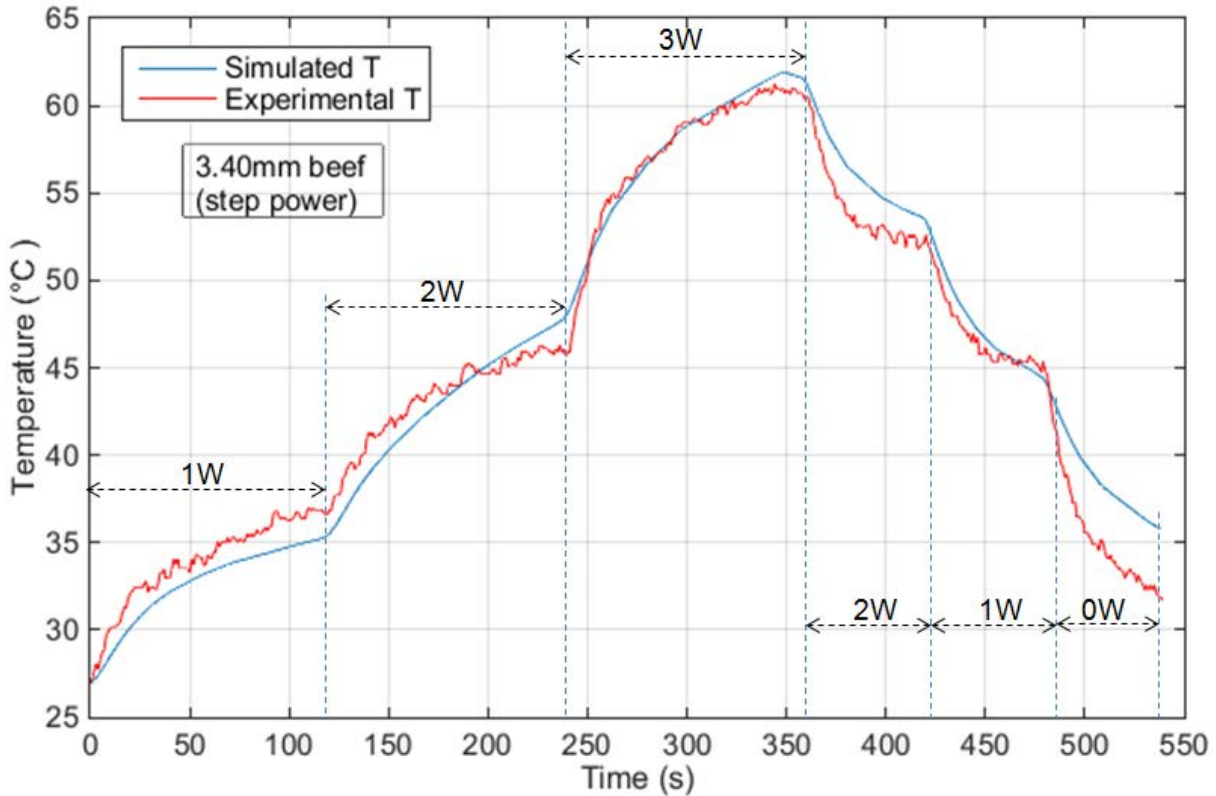of 3.49mm thick pork liver sample with P=3W

Figure 4.32: Comparison between experimental and simulated temperature variations
of 3.60mm thick pork liver sample with step microwave power

For pork liver samples irradiated by a constant microwave power, simulated temperatures correspond well with the experimental temperatures, but the tolerable gaps between simulated and experimental results are larger comparing with muscle samples. Both simulated and experimental temperatures respond to the applied microwave power (figures 4.30, 4.31 and 4.32). The values of temperature dependent $\varepsilon'(T)$ and $\sigma(T)$ of liver are more difficult to measure comparing with muscle samples. The errors of $\varepsilon'(T)$ and $\sigma(T)$ can lead to a difference of tendency between simulated and experimental data. For the progressively changing step microwave power, at the heating section, the difference is tolerable. But for the section without applying the microwave power, the difference between simulation and experiment becomes larger because of dielectric and physical changes in the liver samples during heating. Nevertheless the values of $T_{s\text{-}max}$ and $T_{e\text{-}max}$ are close to each other (table 4.12).

pork liver			
Thickness	2.84mm	3.49mm	3.60mm
Type of power	P = 2W	P = 3W	P = step power
$T_{s\text{-}max}$	50.45°C	59.13°C	51.06°C
$T_{e\text{-}max}$	50.70°C	59.10°C	51.30°C
ΔT	-0.25°C	-0.03°C	-0.24°C

Table 4.12: Comparison between simulated maximum temperatures ($T_{s\text{-}max}$)
and experimental results ($T_{e\text{-}max}$) of pork liver samples

e) calf's liver
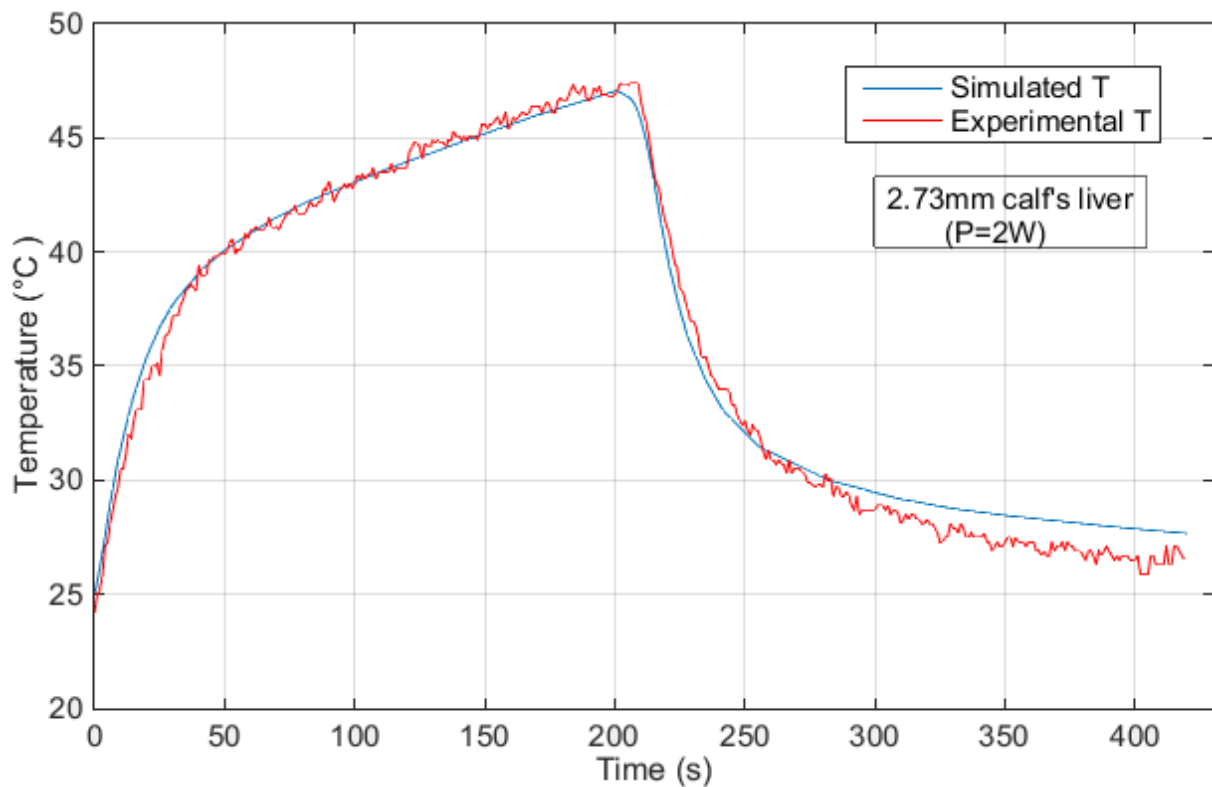
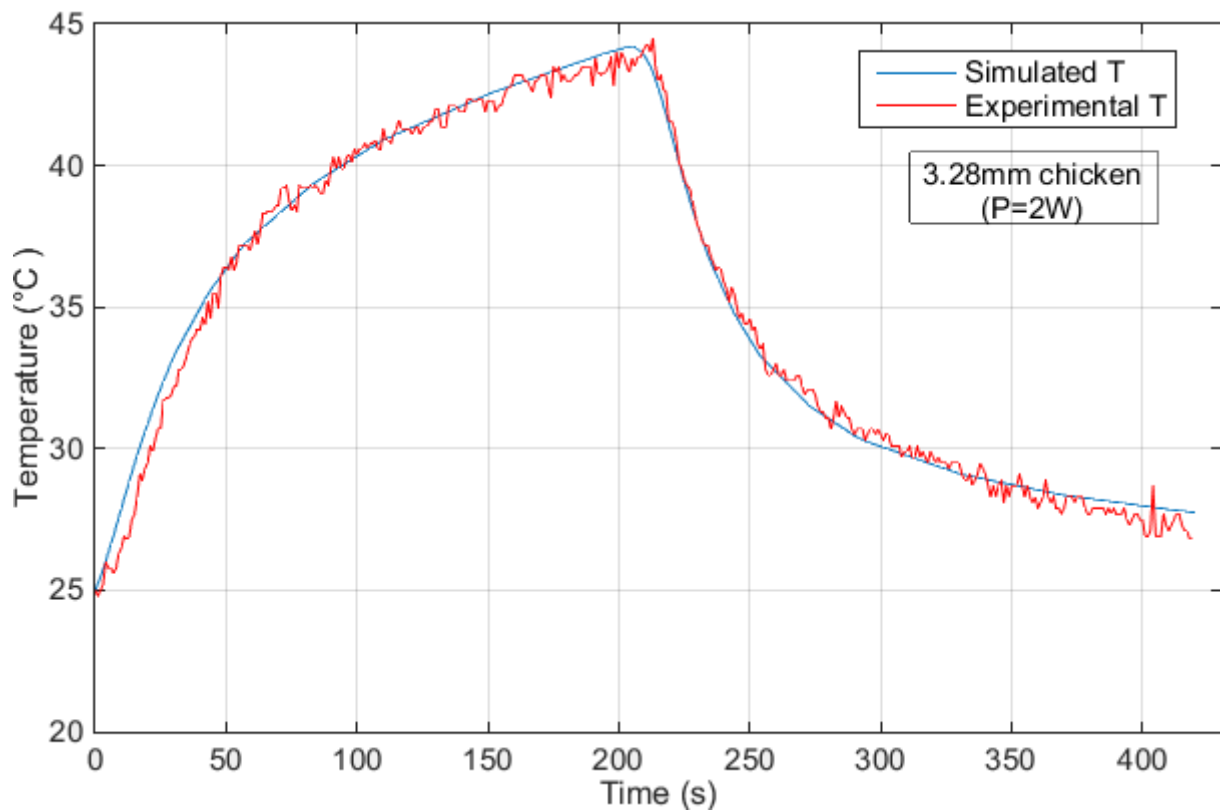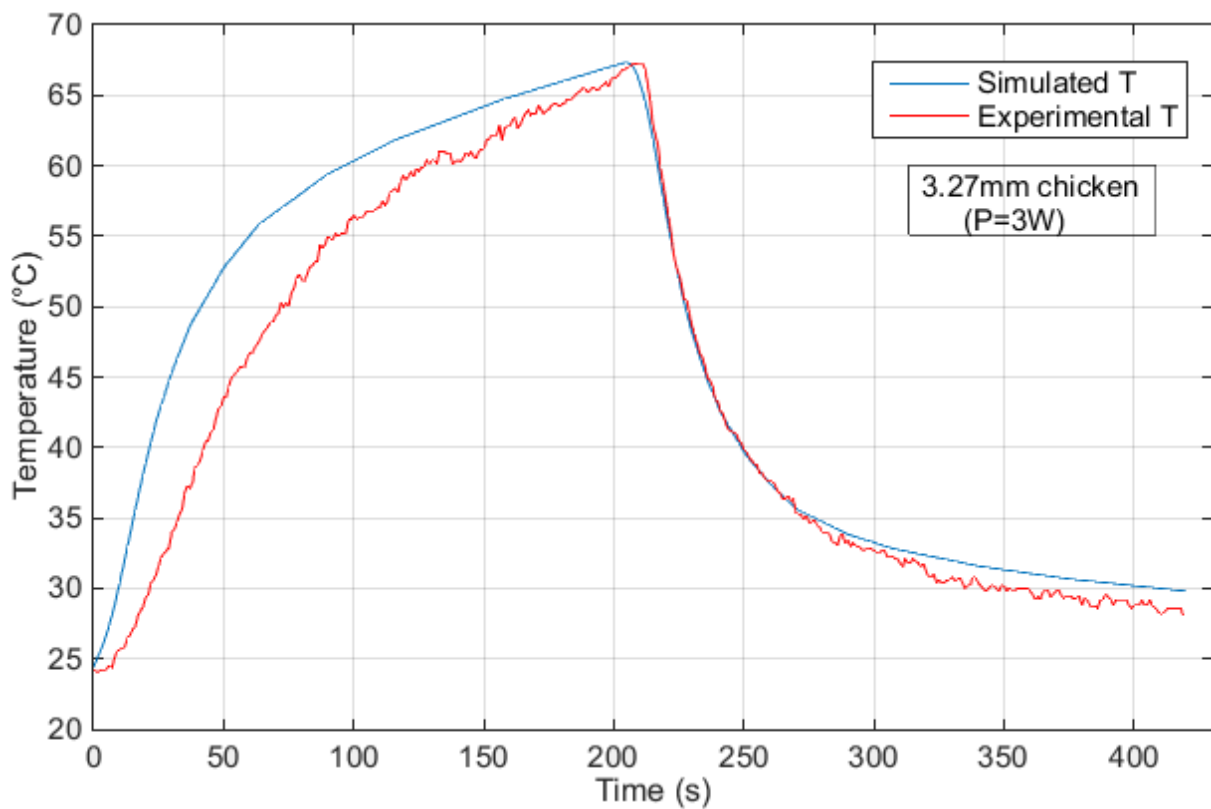Figure 4.33: Comparison between experimental and simulated temperature variations
of 2.73mm thick calf's liver sample with P=2W
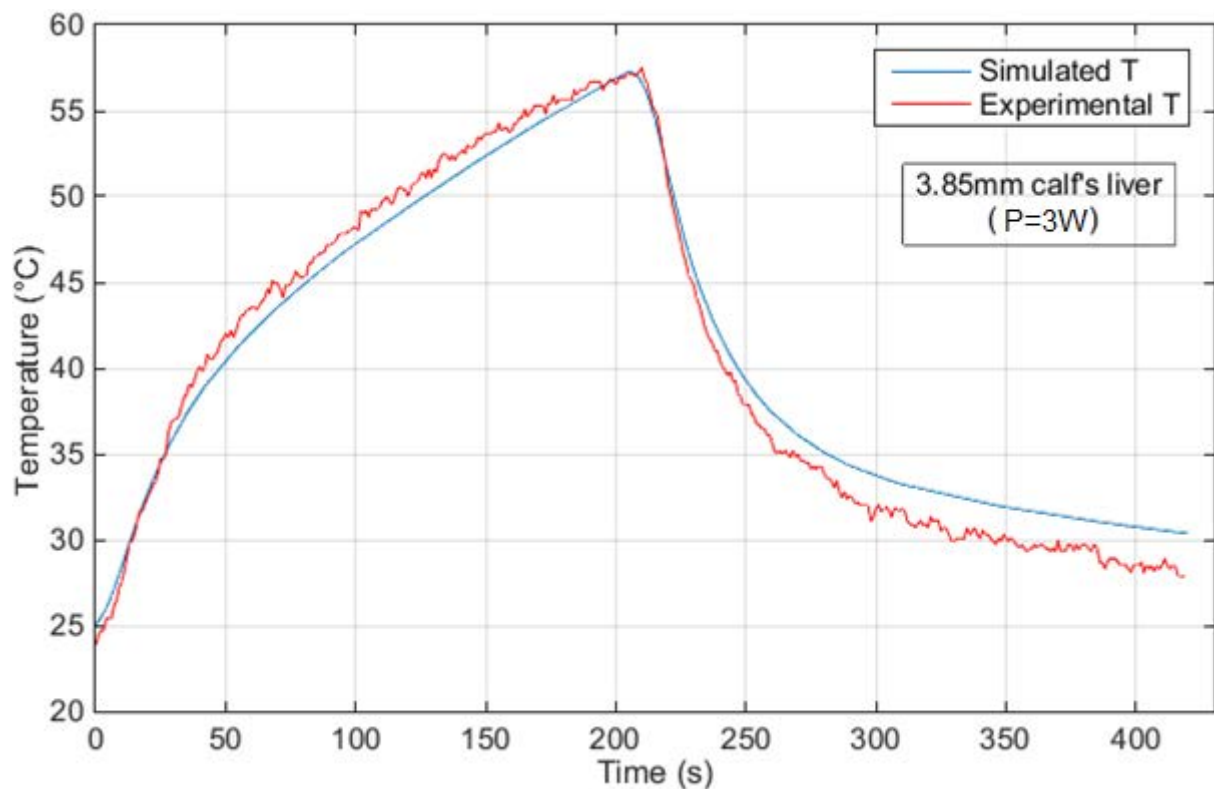
Figure 4.34: Comparison betwen experimental and simulated temperature variations
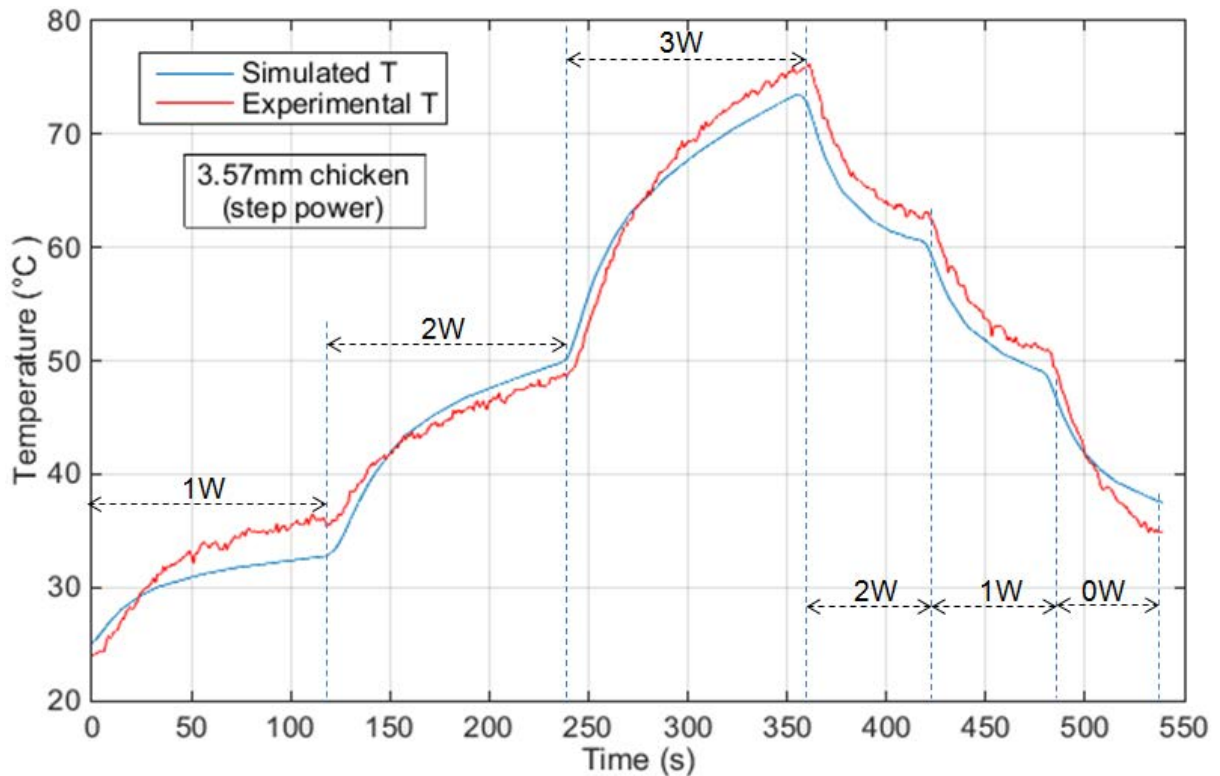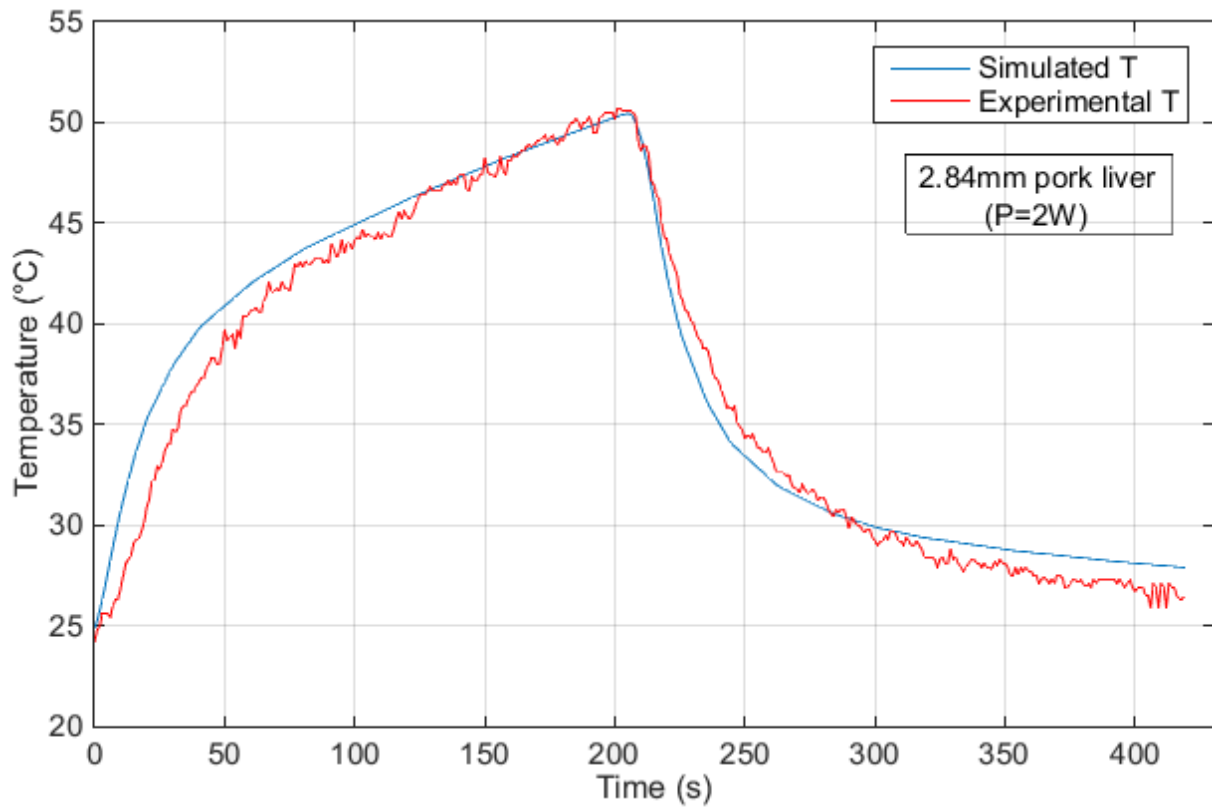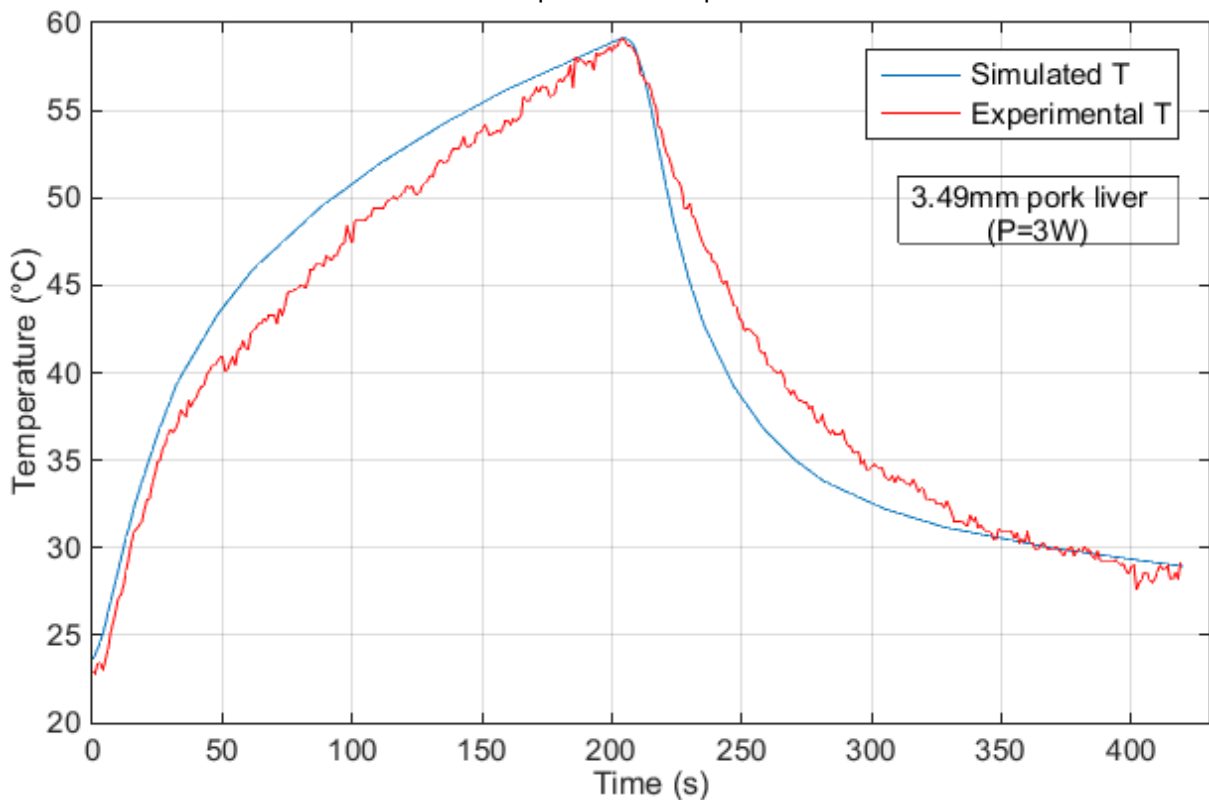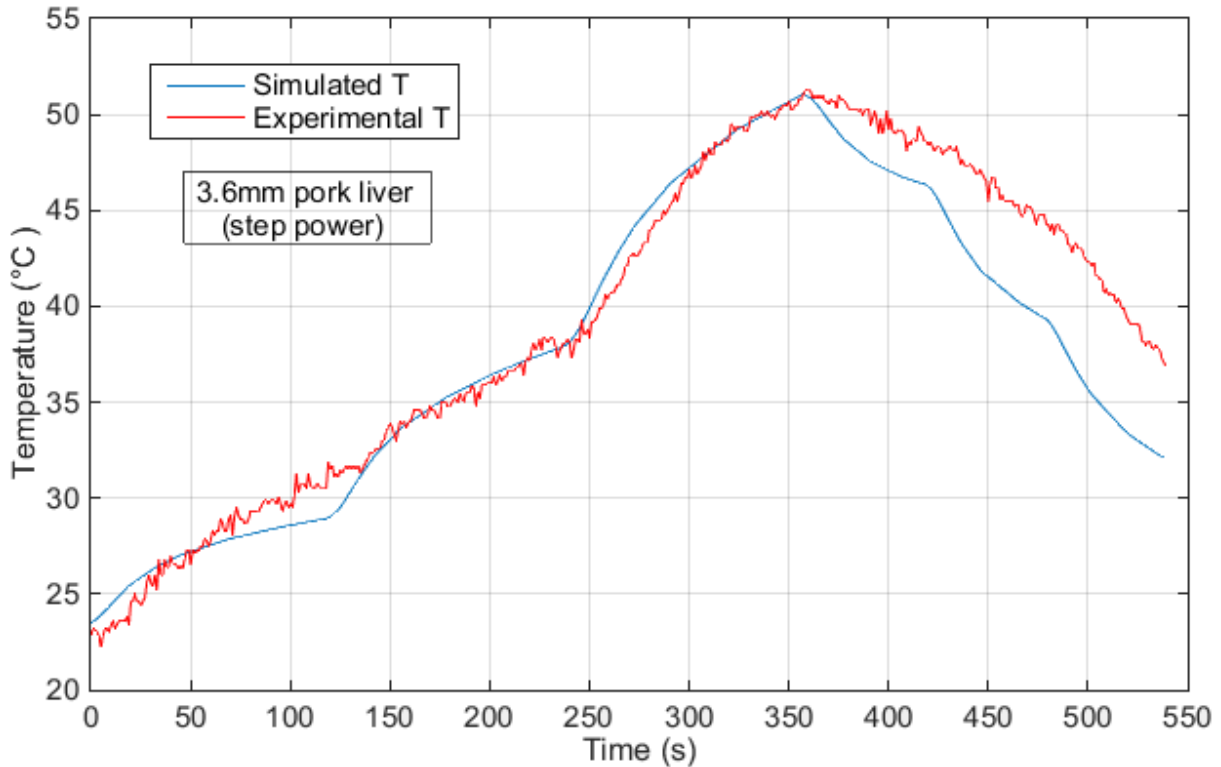of 3.85mm thick calf's liver sample with P=3W
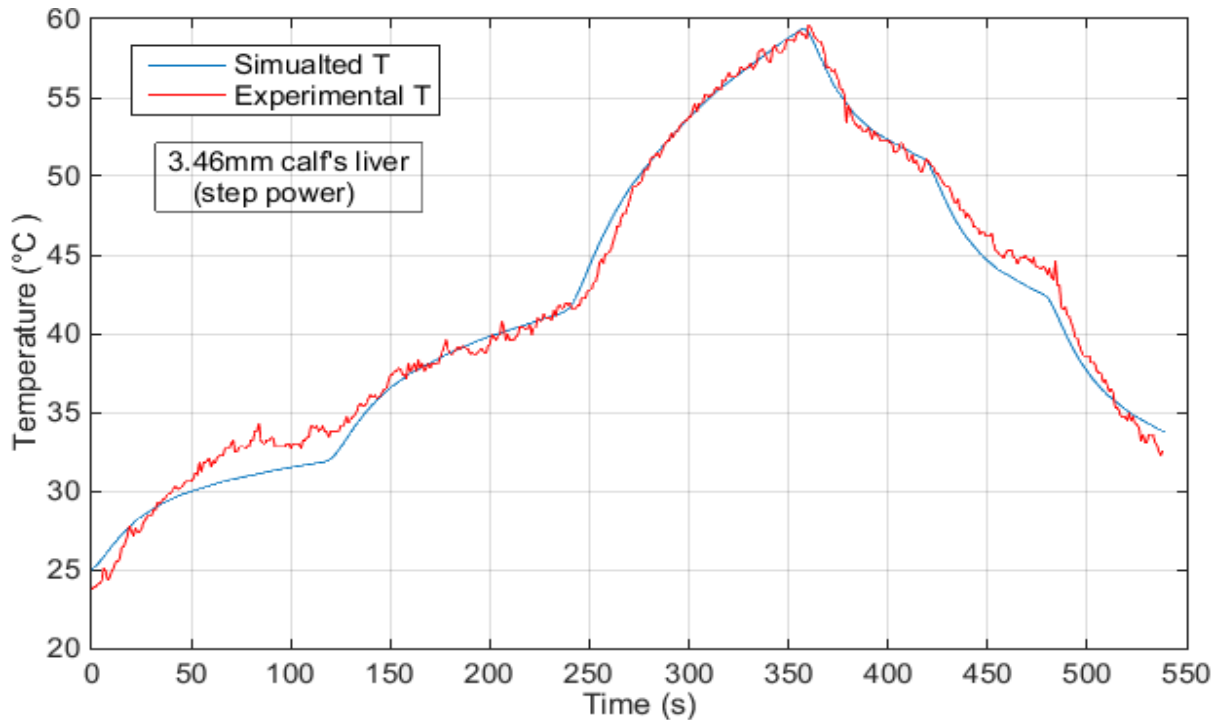
Figure 4.35: Comparison between experimental and simulated temperature variations
of 3.46mm thick pork liver sample with step microwave power

For all calf's liver samples with different applied microwave powers, simulated temperatures correspond well with the experimental results. For all comparisons, the differences between simulated and experimental results are tolerable. The correspondence of variation tendencies and values are better comparing with pork liver. Both simulated and experimental temperature variations respond to the applied microwave power, although there are still some small gaps between them. For a constant microwave power, the decreasing tendencies of temperature show less correspondence between simulation and experiment at the section without applying microwave power (figure 4.33 and 4.34). This might be due to the errors of $\varepsilon'(T)$ and $\sigma(T)$. For step microwave power, at the beginning (P=1W), the experimental temperature is a little higher than the simulated temperature, the real applied power level might be higher than 1W. For the section of P=3W, experimental temperature corresponds well with simulated temperature. Simulated maximum temperatures $T_{s\text{-}max}$ and experimental maximum temperatures $T_{e\text{-}max}$ are compared in table 4.13. The correspondence of simulated and experimental results of calf's liver is better comparing with the pork liver.

calf's liver			
Thickness	2.73mm	3.85mm	3.46mm
Type of power	P = 2W	P = 3W	P = step power
$T_{s\text{-}max}$	47.08°C	57.26°C	59.37°C
$T_{e\text{-}max}$	47.40°C	57.50°C	59.60°C
ΔT	-0.32°C	-0.24°C	-0.23°C

Table 4.13: Comparison between simulated maximum temperatures ($T_{s\text{-}max}$)
and experimental results ($T_{e\text{-}max}$) of pork liver samples

f) Comparison among different muscle samples
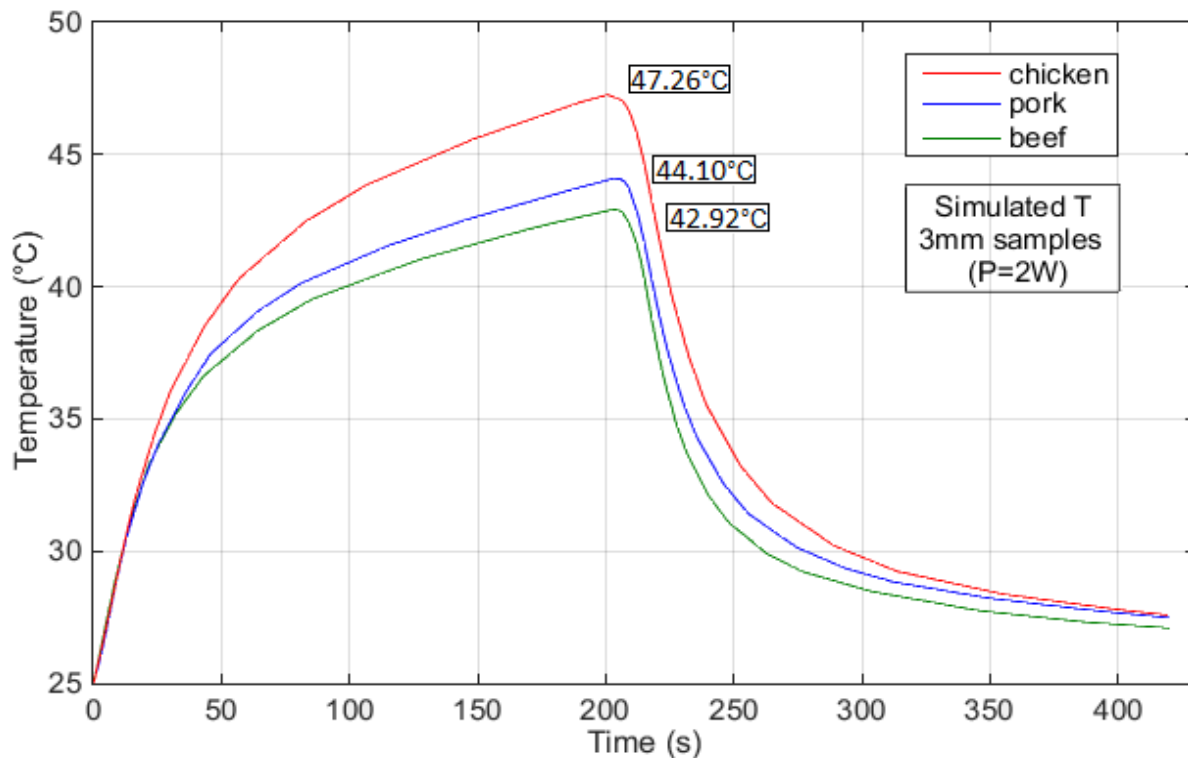
Figure 4.36: Simulated temperature variations for different muscle samples of same thickness (3mm) and an applied constant microwave power (P=2W)
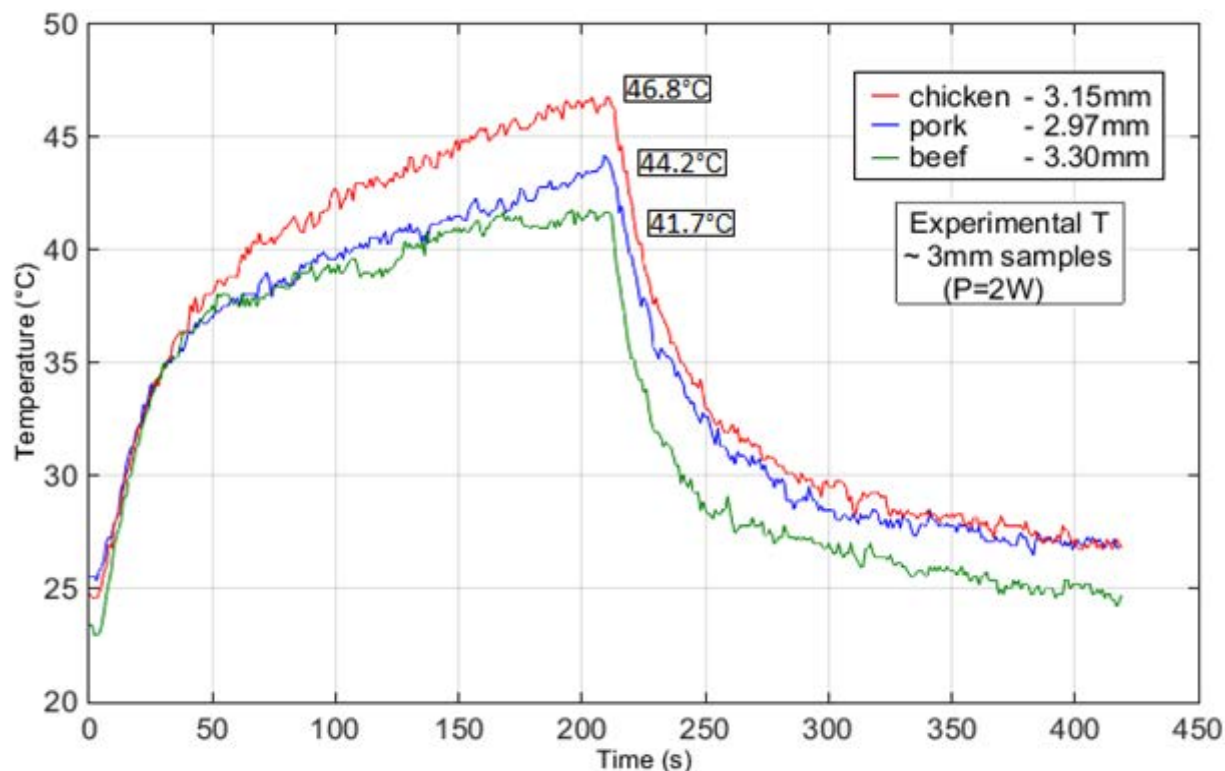
Figure 4.37: Experimental temperature variations for different muscle samples of similar thickness (about 3.15mm +/– 0,15mm) with a constant microwave power (P=2W)

Simulated and experimental temperature tendencies of all muscle samples correspond well with each other. Their highest temperatures are quite close to each other (figure 4.36 and 4.37).

g) Comparison between two different liver samples
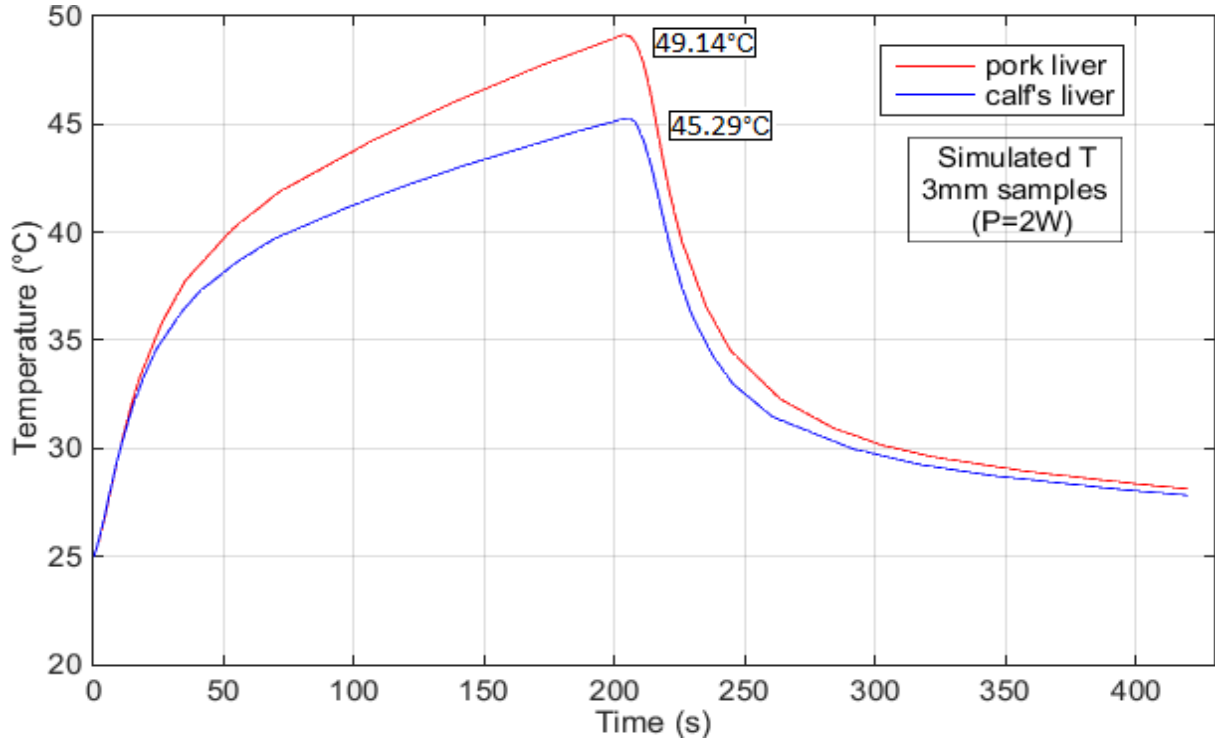
Figure 4.38: Simulated temperature variations for different liver samples of same thickness (3mm) and an applied constant microwave power (P=2W)
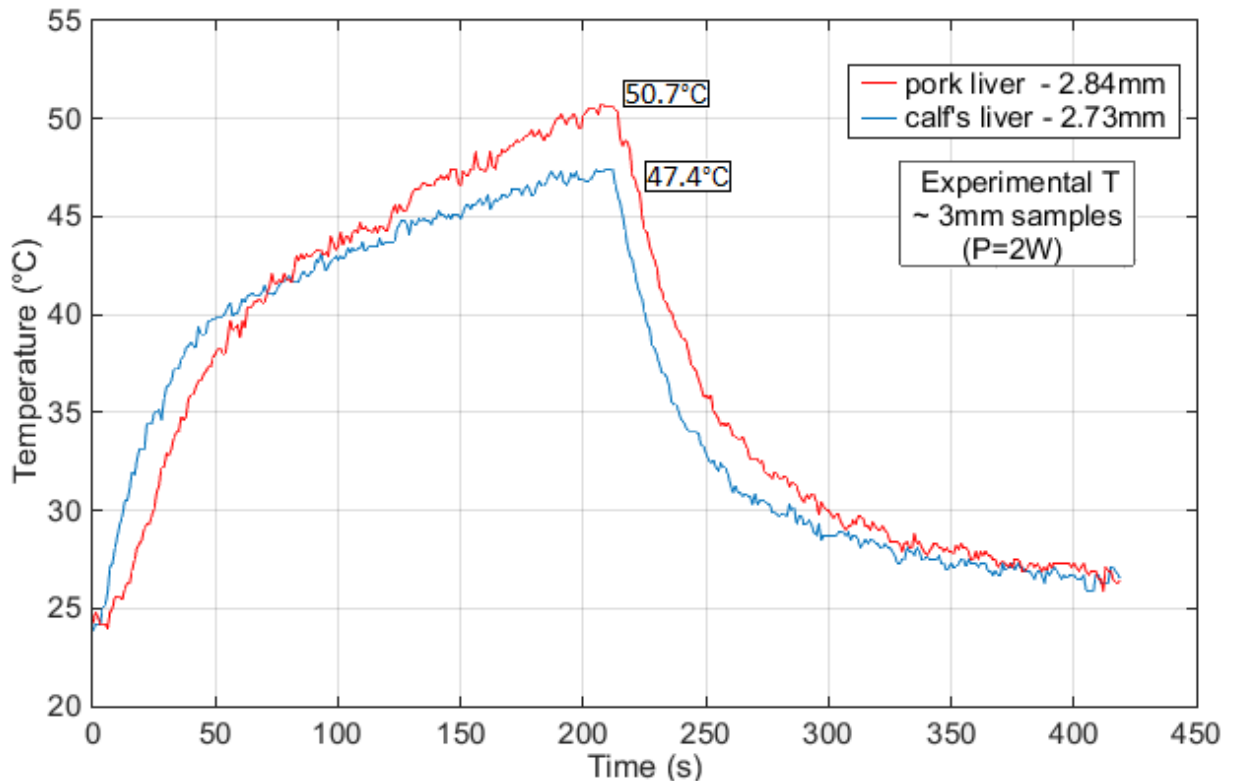
Figure 4.39: Experimental temperature variations for different liver samples of similar thickness with a constant microwave power (P=2W)

Simulated and experimental temperature variations of all liver samples correspond with each other. Their highest temperatures are quite close to each other (figure 4.38and 4.39).

4.10 Conclusion

Two protocols are applied for simulations with respect to experiments: constant microwave power and progressively changing step microwave power. Five different tissues have been simulated: pork, beef, chicken (muscle tissues), pork liver, and calf's liver (liver tissues). The proper values of dielectric and physical parameters of different tissues should be modified for each simulation. In order to be closer to the practical experiments, previously measured temperature dependent values of $\varepsilon'(\text{T})$ and $\sigma(T)$ (presented in chapter 2) are used for the ex vivo microwave hyperthermia simulations.

When biological tissues are irradiated by microwave power, many intrinsic characteristic parameters of tissue change such as their permittivity, electrical conductivity, density, thermal conductivity, and specific heat capacity. Simulations become more challenging with these parameters that change as a function of temperature. Some other extrinsic parameters such as the thickness of the tissues, applied power level, and heat transfer coefficient also affect the temperature simulation results. The increase of the thickness of tissue will lead to the decrease of temperature. The increase of thermal convection coefficient (*h*) allows the decrease of temperature and the increase of applied power level will lead to the increase of temperature.

When ε is considered as a constant, the variable value of electrical conductivity has a relatively small influence on the simulated temperature variation. When ε' is temperature dependent $(\varepsilon' = \text{f}(T))$, the influence of electrical conductivity on the simulated temperature variation becomes quite bigger.

Ex vivo microwave hyperthermia simulation results correspond well with the real experimental results. Both simulated and experimental temperatures follow the applied microwave power on the sample. For the comparisons between simulations and experiments, there might be some small gaps of temperature or difference of increasing and decreasing temperature tendencies. Several errors such as impedance matching, thickness of the tissue, amplifier gain level, temperature dependent values of $\varepsilon'(T)$ and $\sigma(T)$, have been identified to explain the small tolerable differences between simulations and experiments. For having better simulation results, other thermal dependences of physical properties of the biological tissues during the irradiation procedure should be considered such as density, the thermal conductivity and the specific heat capacity. Multiphysics Models built with LiveLink™ for MATLAB® should be also studied for better simulation, because temperature dependent values of $\varepsilon'(T)$ and $\sigma(T)$ can be properly used for all simulation conditions.

Conclusions and perspectives

The current existing commercial microwave hyperthermia systems cannot use only one single antenna or applicator for both diagnosis and therapeutic treatment at the same time. All of them can just offer high power microwave hyperthermia treatment. In our project, a new microwave hyperemia system is designed and researched which could have both diagnostic and therapeutic functions. It means that: first, using one single applicator with harmless microwave power level to do the diagnosis and verify if the tissue is pathological or not. If the tissue has been found abnormal, then the therapeutic treatment will be carried out on the pathological part by using the same applicator with higher microwave power.

For microwave diagnostic and hyperthermia therapy, research on the dielectric characterization of biological tissue at microwave frequency is an important issue. Normal and pathological tissues have different dielectric properties such as dielectric permittivity and electrical conductivity. Dielectric characterizations of biological tissues (muscles and livers) on microwave frequencies as a function of temperature have been achieved. Two methods of virtual line model: open–ended semi–rigid coaxial probe and flexible coaxial Warrior cable with two protocols have been carried out for dielectric measurements on five animal biological tissues: pork, beef, chicken, pork liver and calf's liver. Obtained values of dielectric parameters ($\varepsilon'(f)$, $\varepsilon''(f)$ and $\sigma(f)$) of known liquids (24°C) and fresh biological tissues (20°C) measured by coaxial probe and coaxial Warrior cable correspond well with their literature values. For dielectric characterizations of biological tissue as a function of temperature, all the measured dielectric parameters $\varepsilon'(T)$, $\varepsilon''(T)$ and $\sigma(T)$ showed decrease with increase of temperature. Dielectric properties of all biological tissues after heating are changed. The obtained values of dielectric properties are used for simulation of ex vivo experiment of microwave hyperthermia.

Ex vivo microwave hyperthermia experiments have been carried out on five biological tissue samples of two types: muscle (pork, beef, and chicken) and liver (pork liver, and calf's liver). Two open–ended coaxial applicators: RG393 and Warrior cables with two experimental protocols: constant (P=1, 2 or 3W) and variable step microwave powers (P=1 to 3W) at 2.45GHz have been used. The temperature variations of tissue were measured by using the infrared sensor. Heated above 40°C, a biological tissue may have the irreversible changes. After comparing the experimental results of different tissues, more detailed information has been obtained. For all samples, higher power level allows obtaining higher temperature and thinner thickness of the sample leads to higher temperature. The curve of temperature variation has a sharp slope of increase at the beginning, and later it increases slowly. The experimental results have shown the relations of maximum attained temperature (T_{max}) among three type of muscles (T_{max} of chicken $>$ T_{max} of pork $>$ T_{max} of beef) and between two types of livers (T_{max} of pork liver $>$ T_{max} of calf's liver).

2D axisymmetrical and finite–element method simulations of ex vivo microwave hyperthermia experiment have been achieved by using COMSOL Multiphysics with microwave heating model. The simulations allowed determining the temperature spatial variation in the biological tissues submitted to an open ended coaxial cable as the microwave applicator. Two protocols have been applied for simulations like for experiments: constant power level and variable power level have been applied to five different biological tissues: pork, beef, chicken, pork liver, and calf's liver. In order to achieve or be closer to the practical experiments, previously measured values of $\varepsilon^{'}(\mathrm{T})$ and $\sigma(T)$ as a function of (20 to 50°C with a step of 5°C) have been for the ex vivo microwave hyperthermia experiment simulation. Both simulated and experimental temperatures respond to applied microwave power on the sample. For the comparisons between simulation and experimental results, there have been some tolerable small gaps of temperature or difference of increasing and decreasing temperature tendency. In fact, there are several possible experimental errors such as impedance matching for reflected power, thickness of tissue, output power of microwave amplifier, temperature variations of $\varepsilon'(T)$ and $\sigma(T)$. Ex vivo microwave hyperthermia experiment simulation results are in good coincidence with the real experimental results. By comparing the simulated and experimental results, more researches should be developed for further requirements of microwave hyperthermia therapy.

By carrying out the dielectric characterization and microwave hyperthermia experiments, the existing inadequacies should be improved or studied in order to optimize the existing system like: for ex vivo dielectric characterization, APC7 connector could replace the coaxial line to reduce the resonance at the high frequency; a unique thinner and more flexible cable can be considered being tested for the in vitro microwave hyperthermia experiments; optimization of output power of the microwave amplifier and its remote control to deliver precise microwave power to the irradiated tissue; the manual double stub tuner can be replaced by an automatic impedance matching device which can offer more precise and better real time impedance matching and reduce energy loss; the smaller temperature sensor for the future real operational requirement could also be considered; Normalization or optimization of measuring the dimensions of tissue samples to obtain better and more precise experimental results; consideration of the simulation of the physical parameters with thermal influences on the biological tissue during the microwave hyperthermia procedure; Multiphysics Models Built with LiveLink™ for MATLAB® should also be studied for better and further simulation. It seems certainly that there can be a flexible and suitable coaxial cable to be used for both diagnosis and treatment. For the further researches, human healthy and pathological tissues should be used for experiments.

Microwave hyperthermia therapy–minimally invasive techniques which could make patients suffer less pain and reduce the risks of the surgical operation, may become the better choices for the patients in the future. The final aim of the research is to achieve that the pathological biological tissue can be examined for diagnosis and heated or irradiated for hyperthermia by using a single microwave applicator.

Annex 1
Measurement of dielectric complex permittivity by Matlab program

```matlab
%*************************** Calculation of permittivity of materials ********************

clear all

% **** declaration, initialization and loading measurement data ****

L0 = 0.3;                               % Initializing the length of virtual transmission line of 30 cm

F = load ('frequency.m');               % Loading values of frequency in file frequency.m to the matrix F
real_air = load ('real_air.m');         % Loading values of real part of reflection coefficient of air in the
                                          file real_air.m to the matrix real_air.
imag_air = load ('imag_air.m');         % Loading values of imaginary part of reflection coefficient of air
                                          in the file imag_air.m to the matrix imag_air
real_water = load ('real_water.m');     % Loading values of real part of reflection coefficient of bidistilled
                                          water in the file real_water.m to the matrix real_water
imag_water = load ('imag_water.m');     % Loading values of imaginary part of reflection coefficient of
                                          bidistilled water in the file imag_water.m to the matrix
                                          imag_water

real_test = load ('real_isopropanol.m'); % Loading values of real part of reflection coefficient of the
                                          sample in the real_test file to matrix real_test
imag_test = load ('imag_isopropanol.m'); % Loading values of imaginary part of reflection coefficient of
                                          the sample in the imag_test file to matrix real_test

epsilon_t = complex (2.1,-0.04);        % Complex permittivity of Teflon
epsilon_d_0 = complex (1,-1e-6);        % Complex permittivity of air

ro_0 = (sqrt(epsilon_t)-sqrt(epsilon_d_0)) / (sqrt(epsilon_t)+sqrt(epsilon_d_0));


%***** Parameters of dielectric dispersion of bidistilled water corresponding to the experimental
temperature *****

epsilon_infini = 4.6;                   % dielectric constant of distilled water at high frequency
epsilon_s = 78.3;                       % static dielectric constant of distilled water
taux = 8.08e-12;                        % characteristic relaxation time of distilled water
alpha = 0.014;                          % distribution parameter of distilled water
c = 3e8;                                % velocity of propagation in free space [m / s]

%***** Parameters of dielectric dispersion of test material corresponding to the experimental
temperature *****

cepsilon_infini = 3.23;                 % dielectric constant of test material at high frequency
cepsilon_s = 20.1;                      % static dielectric constant of test material
ctaux = 0.7/(2*pi*c);                   % characteristic relaxation time of test material
calpha = 0.03;                          % distribution parameter of test material
%****** Deletion of points which are not converged ******
```

```matlab
u=[];                              %*** Declaration of the matrix which will contain converged points

for k=[1:201]                      % Number of global points in the measure file

  f = F(k,1);                      % Frequency f corresponding to the point of order k

   ohmega = 2*pi*f;                        % Angular frequency (pulsatance)
   z0 = real_air(k,1) + j*imag_air(k,1);   % Reflection coefficient of the air at frequency f
   z1 = real_water(k,1) + j*imag_water(k,1);  % Reflection coefficient of distilled water at frequency f
   z = real_test(k,1) + j*imag_test(k,1);  % Reflection coefficient of test material at frequency f
   gama_m_0 = abs(z0) * exp(j*angle(z0));  % Reflection coefficient of the air in the other form
   gama_m_1 = abs(z1) * exp(j*angle(z1));  % Reflection coefficient of distilled water air in the other
                                            form
   gama_m = abs(z) * exp(j*angle(z));      % Reflection coefficient of test material in the other form

    % literature permittivity of water
    epsilon_d_1 = epsilon_infini + (epsilon_s - epsilon_infini) / (1 + (j*ohmega*taux).^(1-alpha));

   % literature permittivity of test material
    cole = cepsilon_infini + (cepsilon_s - cepsilon_infini) / (1 + (j*ohmega*ctaux).^(1-calpha));

    beta_0 = ohmega/c; % Propagation constant in air
    beta_t = beta_0*sqrt(epsilon_t) ; % Propagation constant in the coaxial probe

    % x0 = D0*beta_t
    x0 = (j/2) * log(gama_m_0 * (1+ro_0*exp(-2*beta_0*L0*j))/(ro_0+exp(-2*beta_0*L0*j)));

    erreurReel1=10000;
    erreurImaginaire1=10000;
    Lpred = L0; % Lpred equals to Li et Lsuivant equals to Li+1
    X=x0; % Di*beta_t
    lap=0; % Initialization the loop number of executions

    while((erreurReel1>1e-4)&(erreurImaginaire1>1e-4)&(lap<100))
        Lsuivant = (c/(ohmega*sqrt(epsilon_d_1))) * atan( (-sqrt(epsilon_t)*j/sqrt(epsilon_d_1)) * (1-
gama_m_1*exp(2*X*j))/(1+gama_m_1*exp(2*X*j)));
        erreurReel1 = abs((real(Lsuivant)-real(Lpred)) /real( Lpred));
        %erreurImaginaire1 = abs((imag(Lsuivant)-imag(Lpred)) / imag(Lpred));
 X = (j/2) * log(gama_m_0 * (1+ro_0*exp(-2*beta_0*Lsuivant*j))/(ro_0+exp(-2*beta_0*Lsuivant*j)));
        Lpred=Lsuivant;
        lap=lap+1;
    end

    if lap<100
      u=[u k];
    else
      k
    end
end
fs=0;
```

```matlab
% ****** Execution of the algorithm on the converged points******
for k=u
    fs=fs+1;
    f = F(k,1);                          % Frequency f corresponding to the point of order k
    ohmega = 2*pi*f;                     % Angular frequency (pulsatance)
    z0 = real_air(k,1) + j*imag_air(k,1);        % Reflection coefficient of the air at frequency f
    z1 = real_water(k,1) + j*imag_water(k,1);    % Reflection coefficient of distilled water at frequency f
    z = real_test(k,1) + j*imag_test(k,1);       % Reflection coefficient of test material at frequency f
    gama_m_0 = abs(z0) * exp(j*angle(z0));       % Reflection coefficient of the air in the other form
    gama_m_1 = abs(z1) * exp(j*angle(z1));       % Reflection coefficient of distilled water air in the other
                                                   form
    gama_m = abs(z) * exp(j*angle(z));           % Reflection coefficient of test material in the other form

    % literature permittivity of water
    epsilon_d_1 = epsilon_infini + (epsilon_s - epsilon_infini) / (1 + (j*ohmega*taux).^(1-alpha));

    % literature permittivity of test material
    cole = cepsilon_infini + (cepsilon_s - cepsilon_infini) / (1 + (j*ohmega*ctaux).^(1-calpha));

    beta_0 = ohmega/c;                   % Propagation constant in air
    beta_t = beta_0*sqrt(epsilon_t) ;    % Constante de propagation dans la sonde coaxiale

    % x0 = D0*beta_t
    x0 = (j/2) * log(gama_m_0 * (1+ro_0*exp(-2*beta_0*L0*j))/(ro_0+exp(-2*beta_0*L0*j)));
    erreurReel1=10000;
    erreurImaginaire1=10000;
    Lpred = L0; % Lpred equals to a Li et Lsuivant equals to Li+1
    X=x0; % Di*beta_t

     while((erreurReel1>1e-4)&(erreurImaginaire1>1e-4))
         Lsuivant = (c/(ohmega*sqrt(epsilon_d_1))) * atan( (-sqrt(epsilon_t)*j/sqrt(epsilon_d_1)) * (1-
gama_m_1*exp(2*X*j))/(1+gama_m_1*exp(2*X*j)));
        erreurReel1 = abs((real(Lsuivant)-real(Lpred)) /real( Lpred));
       %erreurImaginaire1 = abs((imag(Lsuivant)-imag(Lpred)) / imag(Lpred));
X = (j/2) * log(gama_m_0 * (1+ro_0*exp(-2*beta_0*Lsuivant*j))/(ro_0+exp(-2*beta_0*Lsuivant*j)));
Lpred=Lsuivant;
    end

    %X=D*beta_t
    %Lpred=L;
    L = abs(Lpred); % The length of the virtual line
    a = X; % the value of D*beta_t

    gama = gama_m*exp(2*X*j);
    epsilon_0 = (sqrt(epsilon_t)/j) * (c/(ohmega*L)) * ((1-gama)/(1+gama));
    x0=((ohmega*L)/c) * sqrt(epsilon_0);
    epsilon_1= (sqrt(epsilon_t)/j) * (c/(ohmega*L)) * ((1-gama)/(1+gama)) *x0* cot(x0);
    erreurReel = abs((real(epsilon_1)-real(epsilon_0)) / real(epsilon_0));
    erreurImaginaire =abs( (imag(epsilon_1)-imag(epsilon_0)) / imag(epsilon_0));
```

```
    epsilonPred = epsilon_1; % epsilonPred equals to epsilon1
    xNow = x0;

    while((erreurReel>1e-10) & (erreurImaginaire>1e-10))
        epsilonSuivant = (sqrt(epsilon_t)/j) * (c/(ohmega*L)) * ((1-gama)/(1+gama)) *xNow* cot(xNow);
        % epsilonSuivant equals to epsilonI+1
        xNow = ((ohmega*L)/c) * sqrt(epsilonSuivant);
        erreurReel = abs((real(epsilonSuivant)-real(epsilonPred)) / real(epsilonPred));
        erreurImaginaire = abs((imag(epsilonSuivant)-imag(epsilonPred)) / imag(epsilonPred));
        epsilonPred = epsilonSuivant;
        %epsilon_d_0 = complex(1,-1e-6); % Complex permittivity of air
        %%ro_0 = (sqrt(epsilon_t)-sqrt(epsilon_d_0)) / (sqrt(epsilon_t)+sqrt(epsilon_d_0));
    end

    s(fs,1) = f;
    E(fs,1) = epsilonPred; % Measured permittivity of test material
    Col(fs,1)=cole; % literature permittivity of test material
    conductivite = imag(E(fs,1))*f*10.^-9/18;
    cconductivite = imag(Col(fs,1))*f*10.^-9/18;
    A(fs,1) = conductivite; % Measured conductivity of test material
    cA(fs,1) = cconductivite; % literature conductivity of test material
end

figure(1)
subplot(2,2,1);semilogx(s,abs(real(E)),'+',s,abs(real(Col)),'r');zoom on;grid on;xlabel('f[Hz]');
ylabel('real part of epsilon [F/m]');
subplot(2,2,3);semilogx(s,abs(imag(E)),'+',s,abs(imag(Col)),'r');zoom on;grid on;xlabel('f[Hz]');
ylabel(' imaginary part of epsilon[F/m]');
subplot(2,2,2);semilogx(s,abs(A),'+',s,abs(cA),'r');zoom on;grid on;xlabel('f[Hz]'); ylabel('Conductivity
[S/m]');
subplot(2,2,4);plot(abs(real(E)),abs(imag(E)),'+',abs(real(Col)),abs(imag(Col)),'r');zoom on;grid
on; xlabel(''real part of epsilon de epsilon'); ylabel(' imaginary part of epsilon ');
```

Annex 2
MICRO Heat gun MH 550

PROXXON MICROMOT System

For shrinking sleeves (many devices are simply too large) and 1000 kinds of other applications.

DM 073123
Design Patent
All rights by PROXXON

Spot nozzle

Flat nozzle

Reflector nozzle

MICRO Heat gun MH 550

Small, robust and powerful. Complete with 3 additional nozzles.

For shrinking sleeves, shaping and welding plastics, soldering and de-soldering of electronic components. For removing layers of paint and varnish without aggressive chemicals (pickling agents). For drying and accelerating curing processes (adhesives, paints). For applying and removing films (stickers). For browning wood.

Housing of glass fibre reinforced POLYAMIDE with soft components in the grip area and footprints for stationary use. A powerful heating element ensures a consistent temperature in 2 stages with an air flow of approx. 180l/min. Installed thermostat as security against overheating. Main nozzle and spare nozzles of rust-proof steel.

Technical data:
220 - 240V. 500W. Air temperature in Stage 1: 350 °C. Stage 2: 550 °C. Air volume approx. 180l/min. Weight approx. 500g.

NO 27 130

Annex 3
Warrior cable

Rugged, Cost-effective RF Cable Assemblies - When Down-time is *Not* an Option

The Warrior cable, with internally armored GrooveTube® technology, is a field proven design having seen reliable operation in modern combat zones. The cable will provide long term repeatable performance in the extreme operating conditions associated with electronic countermeasures, electronic warfare and multiple types of field deployed communication systems. In addition to withstanding rugged field handling it provides lasting stability under vibration and flexure, and features excellent shielding effectiveness to avoid conflict with adjacent signals. Warrior cables are also employed in commercial factories where tough handling or other factory conditions demand dependable long term performance. These cables offer many commercial benefits in rugged test and measurement applications where failures can lead to costly and untimely consequences.

Electrical Data

Maximum Frequency:
520: 50.0 GHz
539: 12.4 GHz

Impedence: 50 Ω nominal

Propagation Velocity: 69% nominal

Time Delay: 1.47 ns/ft (4.82 ns/m)

Shielding Effectiveness:
-110 dB minimum (cable only)

Dielectric Withstanding Voltage:
520: 10 kV at 60 Hz
539: 15 kV at 60 Hz

Capacitance: 29.0 pF/ft (95.1 pF/m)

Mechanical Data

Finished Outer Diameter:
520: 0.330 in (0.838 cm)
539: 0.485 in (1.232 cm)

Static Bend Radius:
520: 1.5 in (3.81 cm)
539: 3.0 in (7.62 cm)

Weight with Standard Jacket/Armor:
520: 0.05 lbs/ft (0.067 kg/m)
539: 0.10 lbs/ft (0.149 kg/m)

Crush Resistance:
250 lbs/linear in (44.6 kg/linear cm)

Operating Temp. Range:
-67 to 275° F (-55 to 135° C)
Above 185° F (85° C) use "T" designation

Cable Construction

Inner Conductor: Solid Ag-plated Cu

Dielectric: PTFE

Outer Conductor: GrooveTube® Cu

Standard Finish:
Neoprene over Metallic Braid

(a wide variety of other protective finishes and armors available)

Available Connectors

520: 1.85mm, 2.4mm, 2.92mm, 3.5mm, 7mm, 7-16 DIN, BNC, SMA, TNC, Type N, ZMA, ZN

539: 7-16 DIN, SMA, TNC, Type N

(maximum frequency dependent on cable; other connectors available)

Additional Information

All Warrior cable assemblies are tested 100% for S-Parameters and each assembly is serialized. Standard test data includes VSWR and insertion loss. Additional testing options will be quoted upon request. Full traceability is available for each cable assembly.

Specifications

For attenuation data and additional specifications refer to PDF datasheet.

Annex 4
HP 8340A Synthesized sweeper (10MHz–26.5GHz)

The 8340A synthesized sweepers deliver the combined high–performance of a broadband sweep oscillator in one instrument that is completely controllable via the interface bus. This efficient combination of performance and versatility is ideal for manual or automatic test systems and in many cases enables the HP 8340A to replace a sweep oscillator, a frequency counter, an RF synthesizer, and a microwave synthesizer.

The synthesized broadband frequency coverage 10MHz to 26.5GHz and the precise 1 to 4Hz frequency resolution are generated by indirect synthesis techniques. With these techniques, the complete analog 8340A synthesized sweeper can achieve low single–sideband phase–noise performance. A "fast phase-lock" programming command can be used to reduce typical CW switching times to between 11ms and 22 ms.

Specification of HP 8340A
Frequency range: 10 MHz - 26.5 GHz
Frequency resolution: 1 to 4 Hz
Calibrated output range: +10 dBm to -110 dBm
Output level resolution: 0.1 dB
Output impedance: 50 ohms nominal
Internal level accuracy: ±0.9 dB
Internal flatness: ±0.6 dB to ±3.6 dB depending on output level range
Phase noise: -52 dBc to -107 dBc / 1 Hz noise bw
Pulse, AM modulation
Stability with Temperature: typically ±0.01dB/℃
Output connector: APC-3.5(m)
Power: 100, 120/220, 240 Vac ±10%; 48-66 Hz operation

Annex 5
Amplifier (25S1G4A) of amplifier research

The amplifier of model 25S1G4A produced by Amplifier Research is a solid state, self-contained, air-cooled, broadband amplifier designed for applications where instantaneous bandwidth, high gain and linearity are required. The 25S1G4A, when used with a sweep generator, will provide a minimum of 25 watts of RF power. Included is a front panel gain control which permits the operator to conveniently set the desired output level.

SPECIFICATIONS
Model 25S1G4A

RATED POWER OUTPUT .... 25 WATTS MINIMUM

INPUT FOR RATED OUTPUT .... 1.0 MILLIWATT MAXIMUM

POWER OUTPUT @ 3dB COMPRESSSION
Nominal .... 32 watts
Minimum .... 25 watts

POWER OUTPUT @ 1dB COMPRESSION
Nominal .... 27 watts
Minimum .... 20 watts

FLATNESS ....±1.5 dB typical
...±2.0 dB maximum

FREQUENCY RESPONSE .... 0.8 – 4.2 GHz
..instantaneously

GAIN (at maximum setting) .... 44 dB minimum

GAIN ADJUSTMENT.........................(Continuous Range)
..10 dB minimum
..(4096 steps remote)

INPUT IMPEDANCE .... 50 ohms
...VSWR 2.0:1 maximum

OUTPUT IMPEDANCE .... 50 ohms, nominal

MISMATCH TOLERANCE

100% of rated power without foldback. Will operate without damage or oscillation with any magnitude and phase of source and load impedance. (See Application Note #27)

MODULATION CAPABILITY

Will faithfully reproduce AM, FM, or pulse Modulation appearing on the input signal

THIRD ORDER INTERCEPT
See chart. The third order intercept points for this chart have been determined using two tones spaced 1 MHz apart. This is typical for W-CDMA systems. Closer tone spacing such as 60 kHz generally provides about a 1db to 3db improvement in the IP.

HARMONIC DISTORTION ....Minus 20 dbc
...max at 20 watts

SPURIOUS ....Minus 73 dbc Typ.

PHASE LINEARITY.................... ±1.0 deg/100 MHz, Typ

PRIMARY POWER.......................(Selected Automatically)
..90-132, 180-264 VAC
..50/60 Hz, single phase
..340 watts maximum

CONNECTORS
RF.. Type N female
REMOTE INTERFACES
IEEE-488 ....24 pin female
RS-232.................9 pin Subminiature D (female)

SAFETY INTERLOCK .... 15 pin Subminiature D

COOLING .... Forced air (self contained fans)

Annex 6
HP 437B Power meter

Electrical Characteristics	Performance Limits	Conditions
Frequency range	100 kHz to 50 GHz	Sensor dependent
Power range	−70 dBm to +44 dBm	Sensor dependent
	(100 pW to 25W)	
Dynamic range	50 dB total range	5 ranges of 10 dB steps for 50 dB total
Display units	Watts or dBm	Absolute measurement mode
	Percent or dB	Relative measurement mode
Resolution		
Low	1.0% full scale (0.1 dB)	
Mid	0.1% full scale (0.01 dB)	
High	0.01% full scale (0.001 dB)	
Accuracy:		
Instrumentation, includes sensor linearity[1]		
	Absolute mode:	
	±0.02 dB or ±0.5%	
	Relative mode:	
	±0.02 dB or ±0.5%	Within measurement range.
	±0.04 dB or ±1%	Outside measurement range.
Zero set (digital settability of zero)	±0.5% full scale	Most sensitive range. Decrease percentage by a factor of 10 for each higher range ± one count.
	±2.0% of full scale	If using the HP 8484A, 8481D, 8485D, 8486D, or 8487D Power Sensors.
EMI	Radiated and Conducted Emissions and Radiated and Conducted Susceptibility are within the requirements of RE02, CE03, RS01/03 and CS01/02 called out in MIL-STD-461C, and within the requirements of VDE 0871 and CISPR Publication 11.	
Power reference	1.00 mW	Internal 50 MHz oscillator factory set to ±0.7% traceable to National Institute of Standards and Technology (NIST).
Power reference accuracy	±1.2%	Worst case
	±0.9%	RSS for one year.

Table 1-1. Specifications

Electrical Characteristics	Performance Limits	Conditions
Operating Temperature		
Range	0° C to 55° C	
Power Requirements		
Line Voltage	100, 120, 220, or 240 Vac, +5% to −10%	
Line Frequency	48 to 66 Hz	All specified line voltages may be used.
	360 to 440 Hz	Limited to line voltages of 100 or 120 Vac.
Power Dissipation	<10 VA (8 watts max)	
Remote Operation	HP-IB	All functions except LINE switch, HP-IB address, self test, SPECIAL status, and INIT (initialize)
Compatibility	HP-IB interface	SH1, AH1, T5, TE0, L3, LE0, SR1, RL1, PP1, DC1, DT1, C0
Memory	Non-volatile	
Operating and non-operating environment	Temperature, humidity, shock, and vibration type tested to MIL-T-28800B Class V requirements.	
Safety	Meets requirements of IEC 348	
Net weight	2.6 kg (5.9 lbs.)	
Shipping weight	4.5 kg (10 lbs.)	
Dimensions	88 mm H x 212 mm W	EIA and IEC racking standards:
Height x Width x Depth	x 273 mm D	3.5 H x .5 MW x 11 D
	(3.46 H x 8.35 W x 10.75 inches D)	

**Table 1-1. Specifications (continued)**

Annex 7
Double stub tuner–impedance matching device (DS–109L)

Double Stub Tuner MODEL DS-109 is used for the microwave instrumentation for of pathological heart valves. It is produced by Weinschel Associates Ltd in USA which designs and manufactures high-quality RF and Microwave products for commercial and military markets both domestic and international. The double stub tuner has some features:

- Precision Operation: Stub Tuners allows precision matching within RF systems and subsystems to ensure optimum power transmission from source to load.

- Broadband Operation: The tuner is design to operate over a wide range of frequencies.

- Mechanical Locking: Rugged mechanical locking mechanisms are employed to secure the tuner in the optimal configuration.
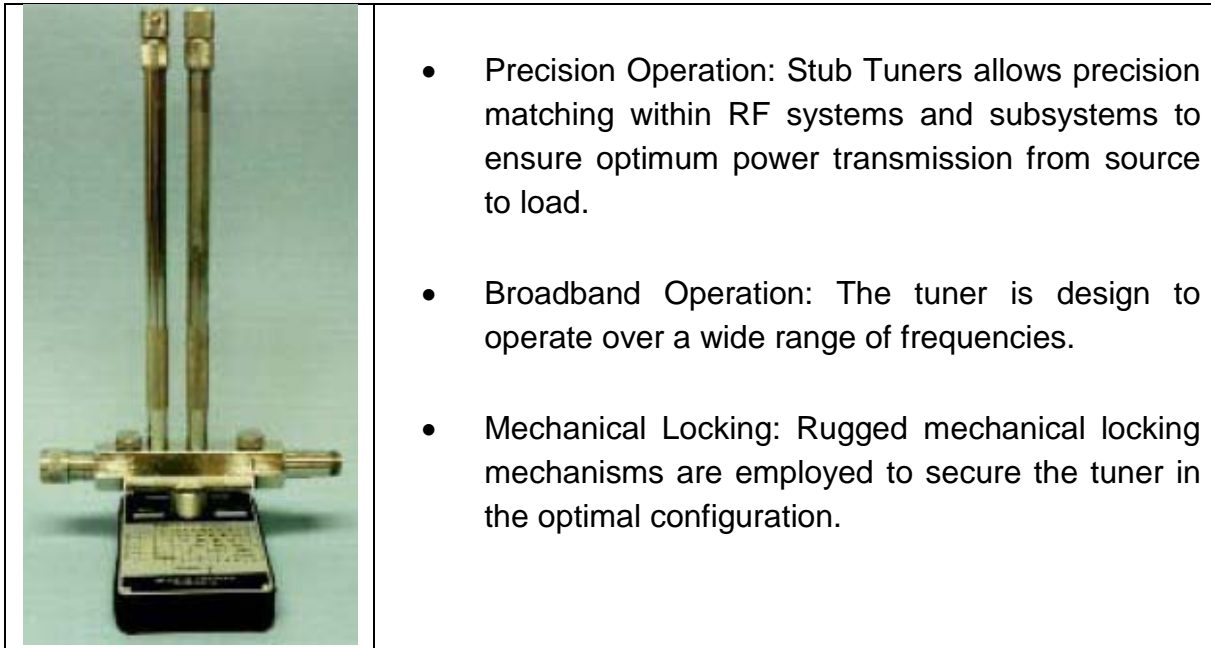
Model No.	DS-109L	*Specifications*
Frequency	0.4 – 4.0 GHz	**Nominal Impedance:** 50 ohms
Length of Stub	38cm.	
Net Weight	6 lbs. (2.73 kg)	**Matching Range:** From 7:1 to 1.00 within tuner frequency range.
Shipping Weight	9 lbs. (4.38 kg)	
Dimensions: mm (inched)		**Connectors:** Tuners are equipped with close toler-ance, stainless steel Type N, one male, one female, for long life with minimum wear.
DIM "A" *	32.50 (82.55)	**Construction:**
DIM "B"	7.38 (18.75)	* Stub height is adjustable, maximum value given ** Two pedestals are used for DS-109LL

Dimensional Drawing
mm(inched)
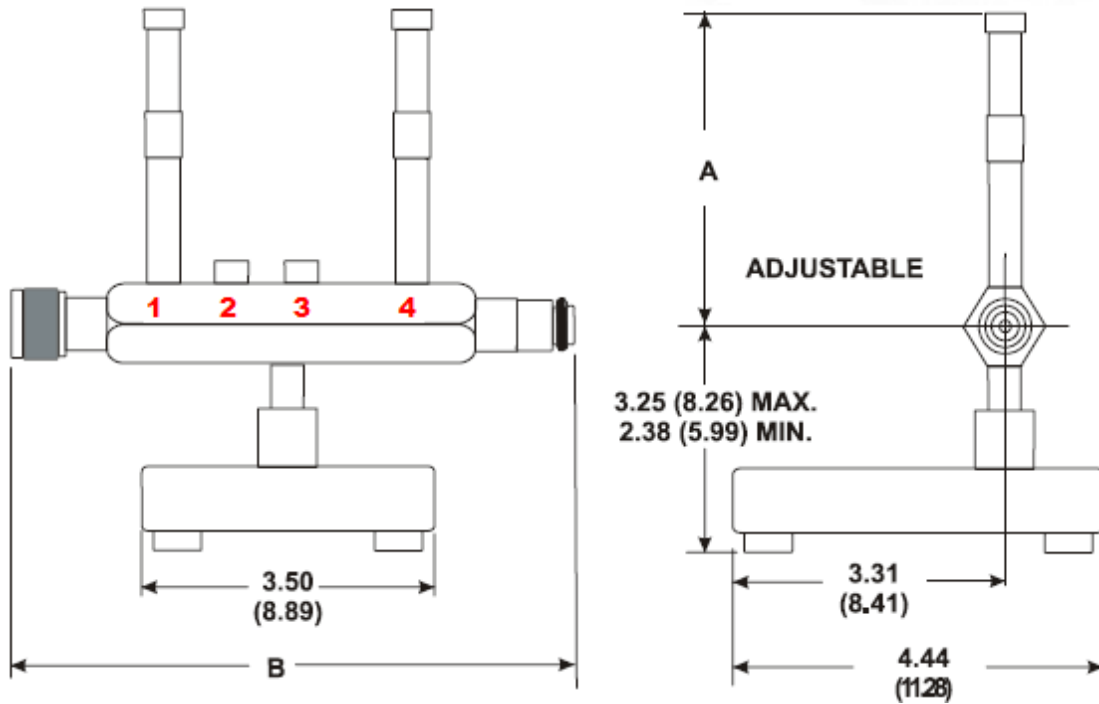
Different installed stub positions are correspondent to different using frequencies. The figure below shows how to choose and install the correct stubs' positions. For this microwave instrumentation, the frequency of microwave being used is 2.45GHz, so the stubs are separately put in the 1st and 3rd position.
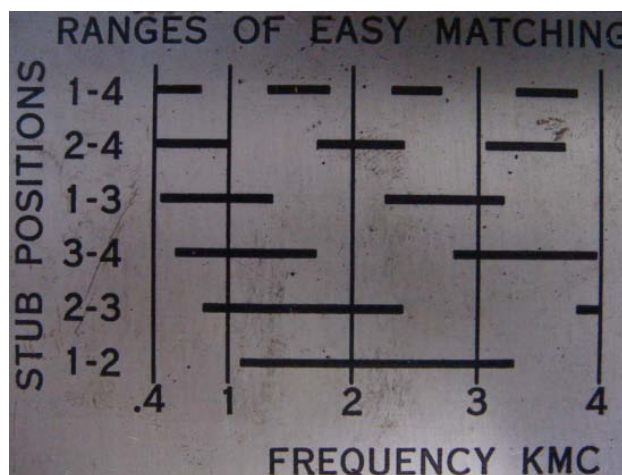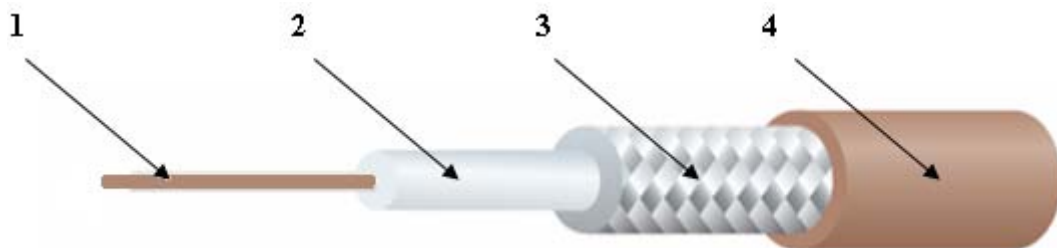
Annex 8
Coaxial cable

Detailed Description

RG393 Coaxial Cable,Communication Cable

M17/127-RG393 Microwave Coaxial Cable with Double Shielded and 9.91mm FEP Jacket

Key Specifications/Special Features:

- Physical properties(as shown in the illustration)

  o Inner conductor: 7/0.79 stranded silver plated copper-clad steel (1)
  o Insulation: 7.24mm solid PTFE (2)
  o Outer conductor: 8.71mm silver plated copper double braid (3)
  o Jacket: 9.91mm FEP (4)

- Electrical properties:

  o Nominal capacitance conductor to shield: 96.5pF/m
  o Nominal characteristic impedance: 50Ω
  o Nominal velocity of propagation: 69.5%
  o Minimum bend radius(install): 51mm
  o Voltage rating: 2,500VMS
  o Maximum operating frequency: 11,000MHz
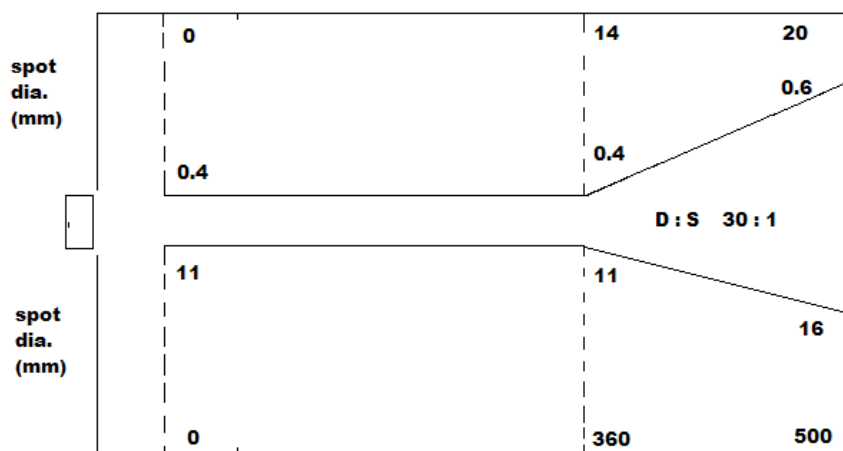 o Operating temperature: -55 to +200°C

Structure of coaxial cable: 1–inner conductor, 2–dielectric, 3–outer conductor, 4–jacket.

Annex 9
Technical specification of infra–red Sensor
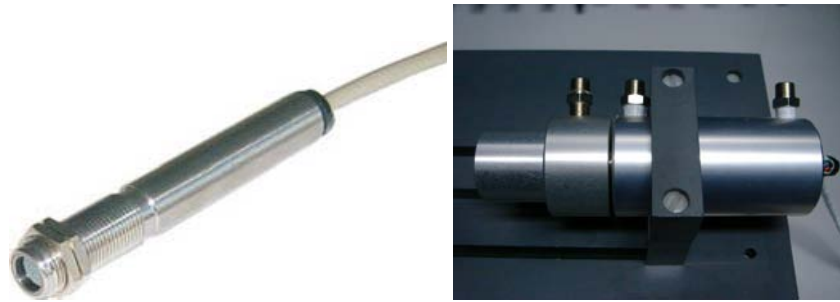
General Specifications	Temperature range	–20℃ to 500℃
	Output	4 to 20 mA
	Precision	±1.0%
	Accuracy	±0.5%
	Emissivity	Adjustable 0.1~1
	Response Time	150 ms (95%)
	Optical Field of View:	10 :1 ; 30 :1
	Spectral range	8 – 14 µm
	Power supply	24Vp-p (max 28Vp-p)
	Detector voltage	9Vp-p (min)
	Maximum loop impedance	750 Ohms
Mechanical Specifications	Structure	Stainless Steel
	Dimensions	Diameter : 25mm Length : 105.5 mm
	Cable length	1 m
	Weight with cable	175 g
Environmental Specifications	Environmental rating	IP65
	Ambient Operating Range	0℃ to 50℃
	Relative Humidity	Maximum 95% non-condensing

Distance : Sensor to object (Inches)

spot dia. (mm)

0   14   20
                      0.6
                 0.4
0.4

D : S   30 : 1

spot dia. (mm)

11   11
                 16

0   360   500

Distance : Sensor to object (mm)

## Annex 10
Absorbing foam wall (APM12)

The absorbing foam wall is made of carbon black powder and polyurethane foam. It is often used in the anechoic chamber which is originally designed to attenuate sound or electromagnetic energy and recently used to provide a shielded environment for radio frequency (RF) and microwaves. The absorbing foam wall, which has arrays of pyramid shaped pieces, can offer an effective protection in a large band of frequency. The absorbing foam wall which is used for the experiments is shown in the below figure.

A = 115 mm
B = 90 mm
C = 38.125 mm
D = 25 mm
E = 610 mm
N = 16
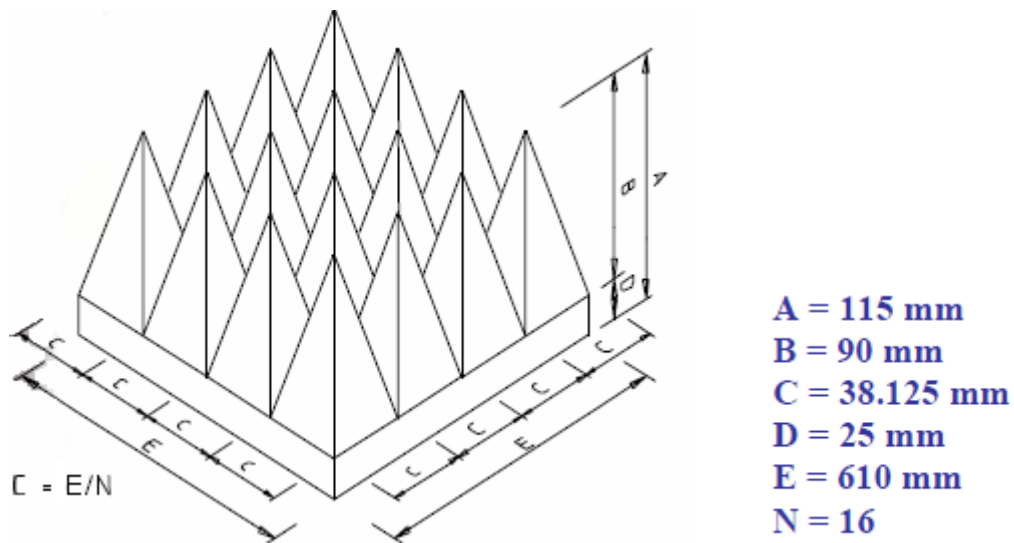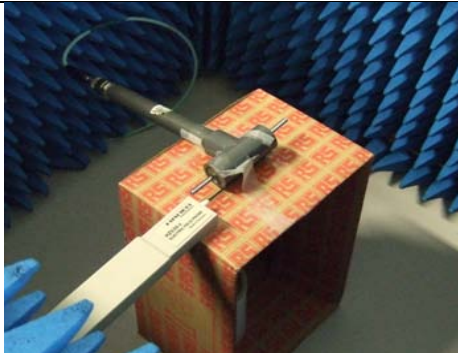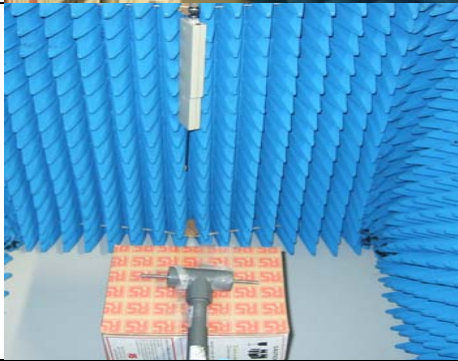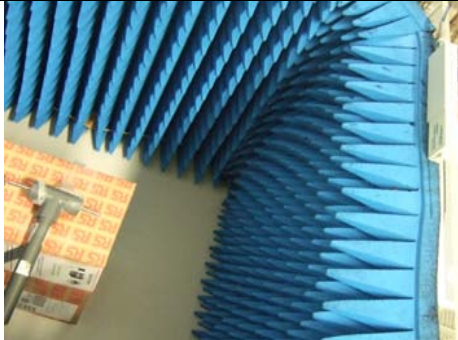
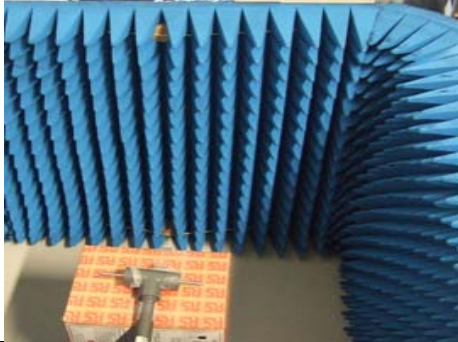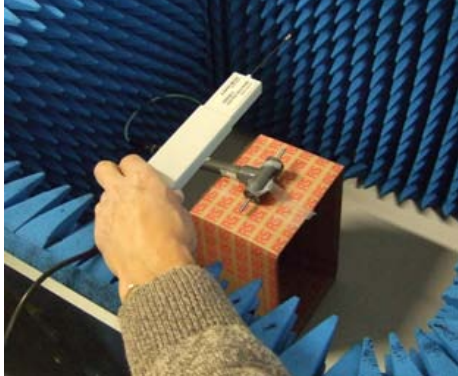| Absorbing Foam APM 12	Frequency (GHz)	1	2	4	8	12
	reflectivity (dB)	-18	-29	-35	-42	-50
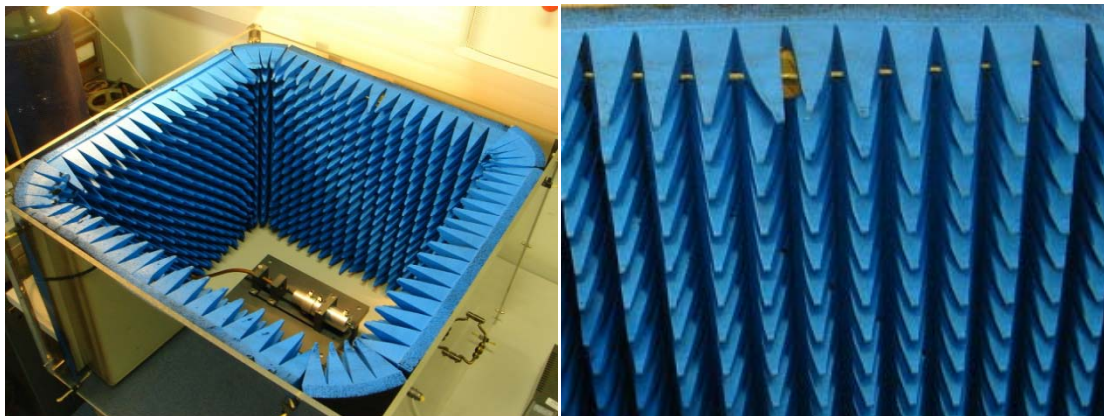
The characterization of anechoic chamber was carried out in order to test the shielded environment for microwave hyperthermia instrumentation. Signal generator (8340A synthesized sweeper) generates a signal at 2.45GHz with power level of –8.7dBm. A tuned dipole antenna (FCC-4) is connected with the signal generator 8340A. The near field probe is connected with a spectrum analyzer (Agilent PSA E44446A). The measured results are shown in the following table. The microwave hyperthermia instrumentation is very safe for the operator and it is harmless.
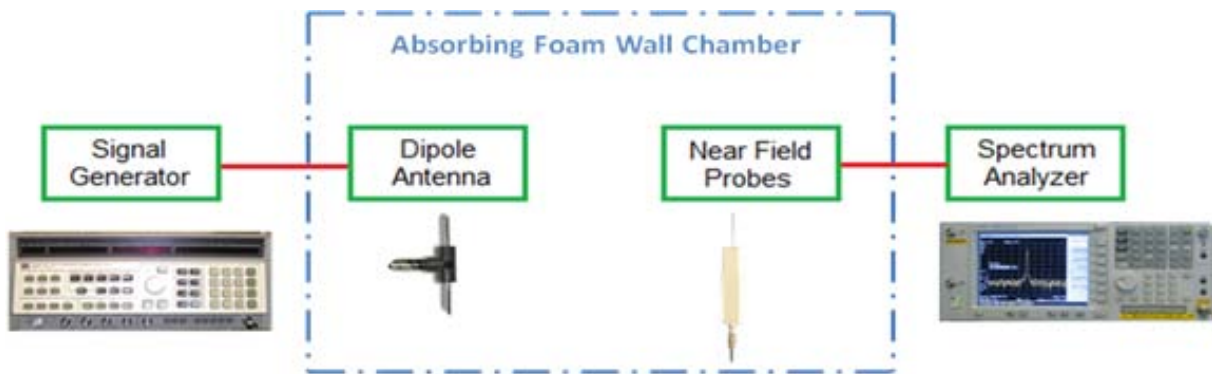
		Unit : dBm	
	Near filed probe was positioned horizontally in the center of the chamber and near the tuned dipole antenna	- 17.72	
		Right	Left
	Probe was positioned horizontally on the right or left side of the antenna. Probe and antenna are on the same horizontal plane,	- 42.58	- 40
		Right	Left
	Probe was positioned horizontally on the right or left side of the antenna and it is at the bottom of the chamber.	- 45.08	- 42.13

		Right	Left
	Probe was positioned horizontally on the right or left side of the antenna and it is in the upper part of the chamber.	- 48.17	- 48.05
	Probe was positioned horizontally in front of the antenna. They are on the same horizontal plane	- 60.05	
	Probe was positioned vertically in front of the antenna	- 65.12	

		Right	Left
	Probe was positioned vertically on the right or left side of the antenna	- 70.03	- 72.14

		Front	Back
	Probe was positioned horizontally in front or at back of the antenna and on the upper edge of chamber without foam cover.	- 72.08	- 75.15

		Right	Left
	Probe was positioned horizontally on the right or left of the antenna and on the upper edge of chamber without absorbing foam cover.	- 66.01	- 62.22
	Probe was positioned horizontally outside of chamber without foam cover and in front of the antenna.	- 60.65	
	Probe was positioned horizontally on the top of antenna without foam cover	- 50.07	
	Probe was positioned horizontally on the top of antenna with foam cover	- 50.38	

Annex 11
Technical specification of test bench
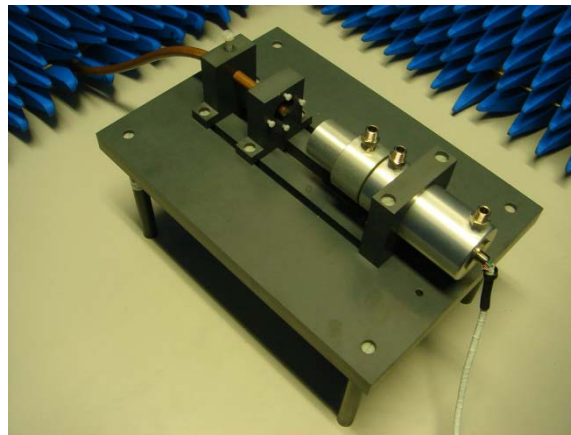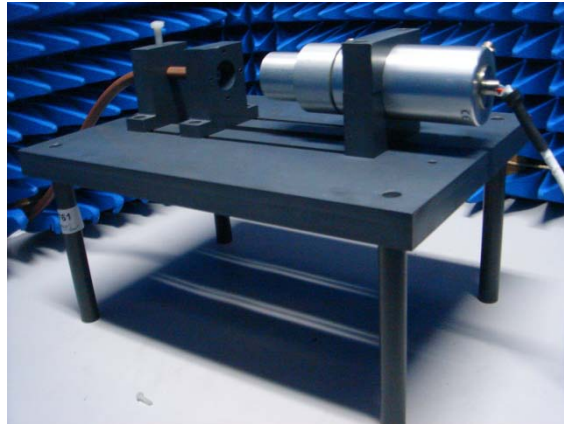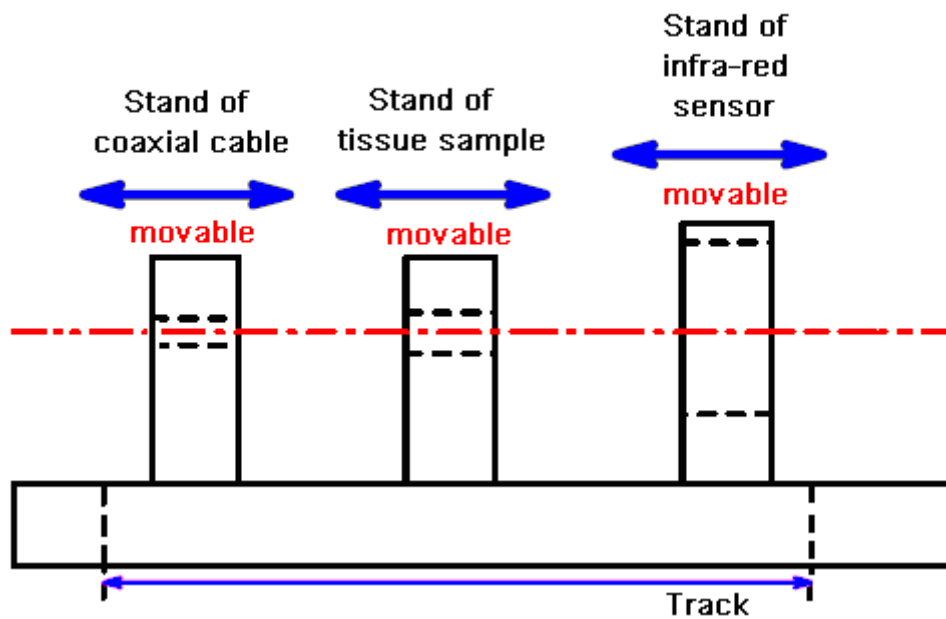
Dimensional Drawings

Annex 12
Mitutoyo ABSOLUTE Digimatic Caliper

500-151-30
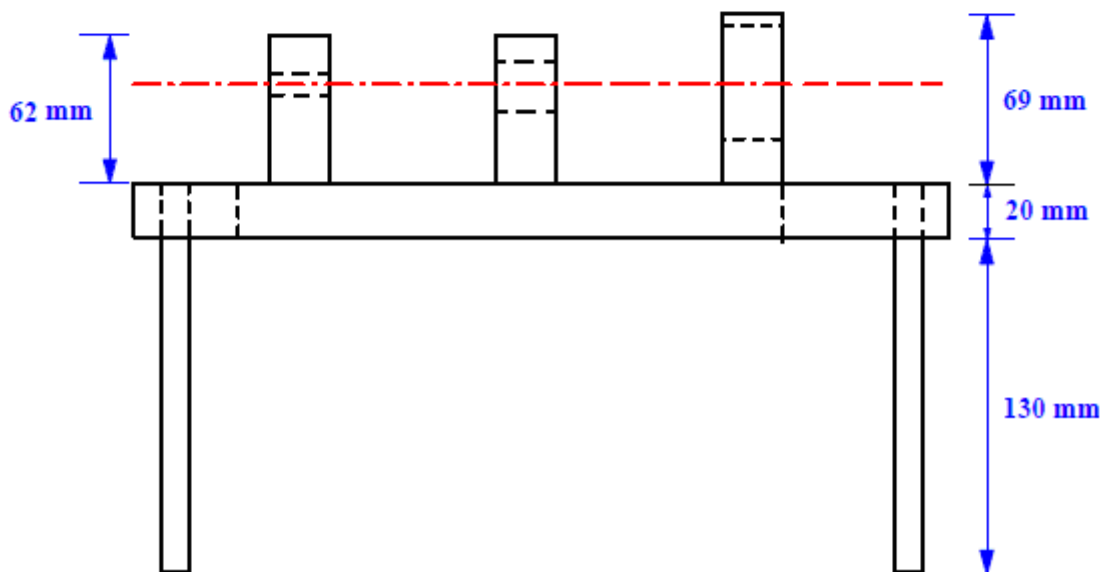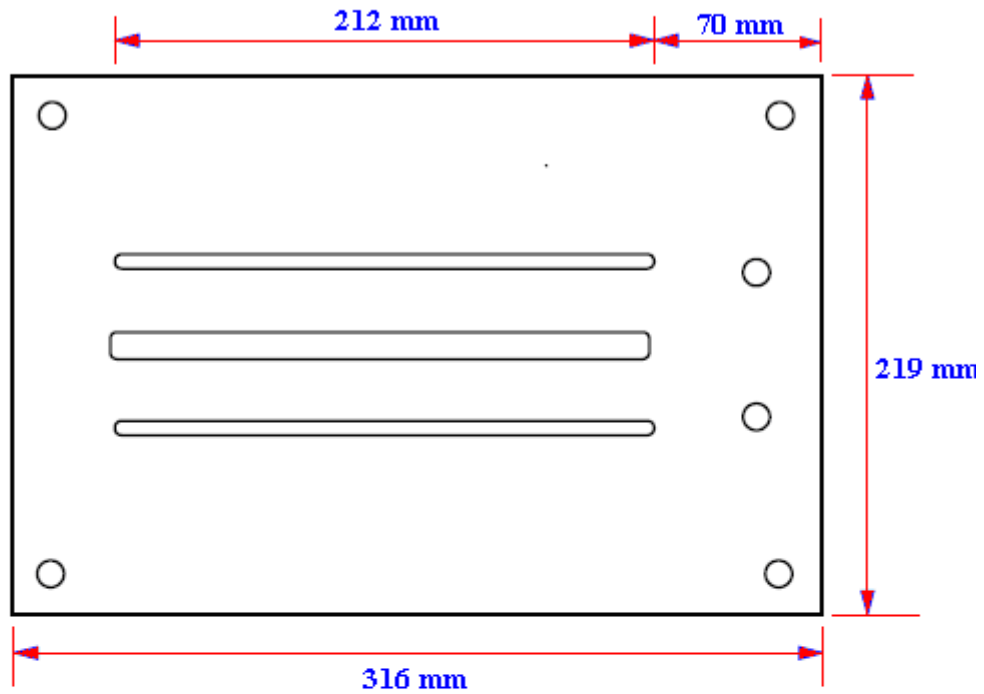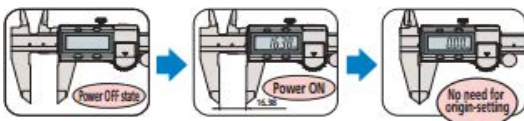Slider with measurement data output port and thumb roller

The slider provides **smooth**, **stable and comfortable** operation.

The ABS (absolute) scale **requires no origin setting** after power-on and **also has no limit to response speed.**

Power OFF state → Power ON → No need for origin-setting

The quality of the slider working surface has improved with the latest machining technology.
Ra:0.071µm
Longitudinal direction
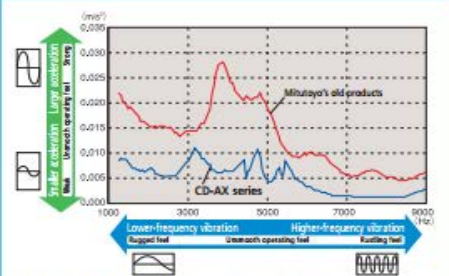
Assessment of slider operating 'feel'
This assessment is obtained from FFT analysis of vibrations during sliding with acceleration sensors mounted on the slider.

ABSOLUTE™

Common Specifications
- Resolution: 0.01mm
- Repeatability: 0.01mm
- Power supply: Button-type silver oxide battery SR44 (No. 938882), 1 piece supplied as standard (The standard supplied battery is for the monitor.)
- Battery life: Approx. 3.5 years under normal use
- Maximum response speed: Unlimited

Functions
ABS (absolute) measurement function:
Enables absolute-mode measurement to be started without any zero-setting after switch-on. The absolute origin position can be set, or reset, with the ORIGIN switch at any time.
INC (incremental) measurement function:
Enables the display value to be set to zero, temporarily, at the current slider position to enable easy incremental-mode measurement.

Low battery alarm:
Indicates (with a 'B' symbol in the display) that the battery needs replacing. This allows timely battery replacement before the caliper becomes unusable.
External output function:
Allows measurement data to be exported using the optional data cable.
Hold function:
Allows a display value to be held using the optional Data Hold unit. (This function cannot be used along with the external output function.)

SPECIFICATIONS

Metric

Order No.	Range	Accuracy	Mass	Measurement data output port	Thumb roller	Remarks
500-150-30	0-100mm		143 g	✔	✔	Depth bar ø1.9mm rod
500-180-30				–	–	
500-151-30	0-150mm	±0.02mm	168 g	✔	✔	–
500-154-30						Carbide-tipped jaws for outside measurement
500-155-30						Carbide-tipped jaws for outside and inside measurement
500-158-30						Depth bar ø1.9mm rod
500-181-30				–	–	–
500-152-30	0-200mm		198 g	✔	✔	–
500-156-30						Carbide-tipped jaws for outside measurement
500-157-30						Carbide-tipped jaws for outside and inside measurement
500-182-30				–	–	–

Inch

Order No.	Range	Accuracy	Mass	Measurement data output port	Thumb roller	Remarks
500-170-30	0-4"		143 g	✔		Depth bar ø3/40" rod
500-195-30				–		
500-171-30	0-6"	±0.001"	168 g	✔	✔	–
500-174-30						Carbide-tipped jaws for outside measurement
500-175-30						Carbide-tipped jaws for outside and inside measurement
500-178-30						Depth bar ø3/40" rod
500-196-30				–		–
500-159-30						Carbide-tipped jaws for outside measurement
500-160-30						Carbide-tipped jaws for outside and inside measurement
500-172-30	0-8"		198 g	✔		–
500-176-30						Carbide-tipped jaws for outside measurement
500-177-30						Carbide-tipped jaws for outside and inside measurement
500-197-30				–		–
500-163-30						Carbide-tipped jaws for outside measurement
500-164-30						Carbide-tipped jaws for outside and inside measurement

References

[1] H. Lodish, A.Berk, Chris A. Kaiser, M.Krieger, and M.Scott, Molecular Cell Biology, 6e. W.H.Freeman and Company. New York: WH Freeman, 2007.

[2] J. Cook, "Cell Structure and Function," Sam Houston State University, 2005.

[3] M. Kent, Advanced biology. Oxford University Press, 2000, p. 56.

[4] B. Rubinsky, "Cryosurgery", *Annual Review of Biomedical Engineering*, vol.2, pp. 157-187, August 2000.

[5] "Cell Structure and Function", Youtube, Nov.23, 2012 [video file]. Available: https://www.youtube.com/watch?v=g4L_QO4WKtM: Cell Structure and Function. [Accessed: Jan. 15, 2015].

[6] "CECB: capturing dynamic changes in chromatin." U.S. Department of health and human services, National Institutes of Health, *CCR (center for cancer research) connections*, vol. 7, No.1, p. 10, 2013.

[7] F. Martini. Anatomy and Physiology' 2007, Rex Bookstore, Inc., 2005, pp. 107-108.

[8] [Online]. Available: http://www.mhhe.com/biosci/ap/histology_mh/muscfs.html. [Accessed: Feb. 10, 2015].

[9] [Online]. Available:http://www.medicinenet.com/script/main/art.asp?articlekey=2667. [Accessed: June. 10, 2015].

[10] [Online]. Available: http://apps.who.int/classifications/icd10/browse/2010/en#/II. [Accessed: June. 10, 2015].

[11] G.M. Cooper, Elements of human cancer. Boston: Jones and Bartlett Publishers, 1992, p. 16.

[12] J.T. Elizabeth, Dorland's illustrated medical dictionary, 29th ed., Philadelphia: Saunders, 2000, p. 1184.

[13] World Health Organization (WHO), Cancer Fact sheet N°297", Feb 2015. [Online]. Available: http://www.who.int/mediacentre/factsheets/fs297/en/. [Accessed: May. 12, 2015].

[14] [Online]. Available: http://www.cancer.gov/about-cancer/what-is-cancer. [Accessed: June. 13, 2015].

[15] [Online]. Available: http://www.cancer.gov/about-cancer/what-is-cancer#tissue-changes-not-cancer. [Accessed: Feb. 13, 2015].

[16] M.D. Ralph Hruban, "What is cancer?", The Sol Goldman Pancreatic Cancer Research Center, Aug. 20, 2013, [video file]. Available: http://pathology.jhu.edu/pc/BasicTypes1.php?area=ba . [Accessed: Feb. 13, 2015].

[17] [Online]. Available: http//www.celsius42.de. [Accessed: Jan. 20, 2013].

[18] [Online]. Available: http://lungcancer.about.com/od/Biology-of-Cancer/a/Cancer-Cells-Normal-Cells.htm. [Accessed: Jan. 20, 2015].

[19] [Online]. http://sciencelearn.org.nz/Contexts/See-through-Body/Teaching-and-Learning-Approaches/Characteristics-of-normal-and-cancerous-cells. [Accessed: June. 20, 2015].

[20] [Online]. http://lungcancer.about.com/od/Biology-of-Cancer/a/Cancer-Cells-Normal-Cells.htm. [Accessed: June. 20, 2015].

[21] R. Habash, *Bioeffects and therapeutic applications of electromagnetic energy*. New York: CRC Press, 2008, pp. 201-291.

[22] M. Nikfarjam, C. Malcontenti-Wilson, and C.Christophi, "Focal hyperthermia produces progressive tumor necrosis independent of the initial thermal effects." *Journal of gastrointestinal surgery*, vol. 9, pp. 410-417, March 2005.

[23] van der Zee and Jill, "Heating the patient: a promising approach?." *Annals of oncology*, vol. 13, pp. 1173-1184, 2002.

[24] B. Hildebrandt, P. Wust, O. Ahlers, A. Dieing, G. Sreenivasa, T. Kerner, R. Felix, and H. Riess, "The cellular and molecular basis of hyperthermia." *Critical Reviews in Oncology/Hematology*. vol. 43, pp. 33-56, 2002.

[25] R. W. Habash, R. Bansal, D. Krewski, and H. T. Alhafid, "Thermal therapy, part 2: hyperthermia Techniques." *Critical Reviews™ in Biomedical Engineering*, p. 496, 2006.

[26] P. Wust, B. Hildebrandt, G. Sreenivasa, B. Rau, J. Gellermann, H. Riess, R. Felix, and P.M. Schlag, "Hyperthermia in combined treatment of cancer." *lancet oncology*, vol. 3, pp. 487–97, 2002.

[27] T. Kotnik and D. Miklavcic, "Theoretical evaluation of the distributed power dissipation in biological cells exposed to electric field." *Bioelectromagnetics*, vol. 21, pp. 385–94, 2000.

[28] K. Hynynen, D. Shimm, D. Anhalt, B. Stea, H. Sykes, J.R. Cassady, and R.B. Roemer, "Temperature distributions during clinical scanned, focused ultrasound hyperthermia treatments." *International journal hyperthermia*, vol. 6, pp. 891–908, 1990.

[29] A.K. Singh, E.G. Moros, P. Novak, W. Straube, A. Zeug, J.E. Locke, and R.J. Myerson, "MicroPET–compatible, small animal hyperthermia ultrasound system (SAHUS) for sustainable, collimated and controlled hyperthermia of subcutaneously implanted tumours." *International journal hyperthermia*, vol. 20, pp. 32–44, 2004.

[30] K. Lindsley, P.R. Stauffer, P. Sneed, R. Chin, T.L. Phillips, E. Seppi, E. Shapiro, and S. Henderson, "Heating patterns of the Helios ultrasound hyperthermia system." *International journal hyperthermia*, vol. 9, pp. 675–84, 1993.

[31] X.Q. Lu, E.C. Burdette, B.A. Bornstein, J.L. Hansen, and G.K. Svensson, "Design of an ultrasonic therapy system for breast cancer treatment." *International journal hyperthermia*, vol. 12, pp. 375–99, 1996.

[32] R.J. Lee, M. Buchanan, L.J. Kleine, and K. Hynynen. "Arrays of multielement ultrasound applicators for interstitial hyperthermia." *IEEE Transactions on Biomedical Engineering*, vol. 46, pp. 880–90, 1999.

[33] R.J. Lee and H. Suh, "Design and characterization of an intracavitary ultrasound hyperthermia applicator for recurrent or residual lesions in the vaginal cuff." *International journal hyperthermia*, vol. 19, pp. 563–74, 2003.

[34] K.M. Sekins, D.B. Leeper, J.K. Hoffman, G.W. Keilman, M.C. Ziskin, M.R. Wolfson, and T.H. Shaffer, "Feasibility of lung cancer hyperthermia using breathable perfluorochemical (PFC) liquids. Part II: Ultrasound hyperthermia." *International journal hyperthermia*, vol. 20, pp. 278–99, 2004.

[35] M.A. d'Arsonval, "Action physiologique des courants alternatifs". *CR Soc Biol* vol. 43, pp. 283–286, 1891.

[36] P.R. Stauffer, "Evolving technology for thermal therapy of cancer." *International journal hyperthermia*, vol. 21, pp. 731–44, 2005.

[37] K.Bt Lias, N. Buniyamin, and A. Narihan, "An overview of cancer thermal therapy technology based on different types of antenna exposure." *International Conference on Electrical, Electronics and System Engineering (ICEESE),* Kuala Lumpur, Malaysia. 2013. pp. 96–101.

[38] [Online]. Available: http://en.wikipedia.org/wiki/Electromagnetic_radiation. [Accessed: Sep. 13, 2014].

[39] [Online]. Available: http://surgical.covidien.com/products/ablation-systems/microwave-ablation/evident-mwa-system. [Accessed: Sep. 13, 2014].

[40] [Online]. Available: http://www.ablatech.fr/technique/micro-ondes/. [Accessed: Sep. 20, 2014].

[41] [Online]. Available: http://www.terumo–europe.com/endovascular/_pdf/microthermx.pdf. [Accessed: Sep. 15, 2014].

[42] [Online]. Available: http://www.covidien.com/surgical/products/ablation-systems/evident–mwa–system. [Accessed: Aug. 13, 2014].

[43] [Online]. Available: http://www.doitpoms.ac.uk/tlplib/dielectrics/printall.php. [Accessed: Aug. 13, 2014].

[44] Application Note, Agilent Application. "Agilent basics of measuring the dielectric properties of materials." *Agilent Literature Number*, pp. 4–12, 2006. [Online]. Available: http://www3.imperial.ac.uk/pls/portallive/docs/1/11949698.PDF. [Accessed: Feb. 13, 2015].

[45] O.V.Tereshchenko, F.J.K.Buesink, and F.B.J. Leferink, "An overview of the techniques for measuring the dielectric properties of materials" *The XXXth URSI General Assembly and Scientific Symposium, Istanbul, Turkey, August 13–20,* 2011. pp. 13–20.

[46] D. V. Blackham and R. D. Pollard, "A comparative study of four open–ended coaxial probe models for permittivity measurements of lossy dielectric/biological materials at microwave frequencies." *IEEE transactions on instrument and measurement*, vol. 44, pp. 1928–1934, 1996.

[47] M.A. Stuchly and S.S. Stuchly, "Coaxial line reflection method for measuring dielectric properties of biological substances at radio and microwave frequencies–A review," *IEEE transactions on instrument and measurement*, vol. 29, pp. 176–183, 1980.

[48] T. Whit Athey, M.A. Stuchly, and S.S. Stuchly, "Measurement of radio frequency permittivity of biological tissues with an open–ended coaxial line: Part I, "*IEEE transactions on microwave theory and techniques*, vol. 30, pp. 82–86, 1982

[49] M. A. Stuchly, T. Whit Athey, C. M. Samaras, and G. E. Taylor, " Measurement of radio frequency permittivity of biological tissues with an open-ended coaxial Line: Part II–Experimental results "*IEEE transactions on microwave theory and techniques*, vol. 30, pp. 87–92, 1982.

[50] T. P. Marsland and S. Evans, "Dielectric measurements with an open-ended coaxial probe ." *Proceedings of the IEEE*, vol 134, pp. 341–349, 1987.

[51] D. Misra, M. Chabbra, B. R. Epstein, M. Mirotznik, and K. R. Foster, " Non-invasive electrical characterisation of materials at microwave frequencies using aan openended coaxial line: Test of an improved calibration technique." *IEEE transactions on microwave theory and techniques*, vol. 38, pp. 8–14, 1990.

[52] K. Folgero, T. Friiso, J. Hilland, and T. Tjomsland, "A broad–band and highsensitivity dielectric spectroscopy measurement system for quality determination of low–permittivity fluids." *Measurement Science and Technology*, vol. 6, pp. 995–1008, 1995.

[53] J. Hilland, "Simple sensor system for measuring the dielectric properties of saline solutions ." *Measurement Science and Technology*, vol. 8, pp. 901–910, 1997.

[54] D. Bérubé, F. M. Ghannouchi, and P. Savard. "A Comparative Study of Four Open-Ended Coaxial Probe Models for Permittivity Measurements of Lossy Dielectric/Biological Materials at Microwave Frequencies." *IEEE Transactions on Microwave Theory and Techniques*, vol. 44, pp. 1928–1934, 1996.

[55] F.M. Ghannouchi and R.G. Bosisio "Measurement of microwave permittivity using a six-port reflectometer with an open-ended coaxial line." *IEEE Transactions on Instrumentation and Measurement*, vol. 38, pp. 505–508, 1989.

[56] F.Buckley, and A.A. Maryott. *Tables of dielectric dispersion data for pure liquids and dilute solutions* (vol. 589). United States: Department of Commerce, National Bureau of Standards; 1958.

[57] S. Gabriel, R.W. Lau, and C. Gabriel. "The dielectric properties of biological tissues: II. Measurements in the frequency range 10 Hz to 20 GHz." *Physics in medicine and biology*, vol. 41, pp. 2251–2269, 1996.

[58] J. Vrba, M. Lapeš, and L. Oppl, "Technical aspects of microwave thermotherapy." *Bioelectrochemistry and bioenergetics*, vol.48, pp. 305-309, 1999.

[59] [Online]. Available: http://www.engineeringtoolbox.com/convective-heat-transfer-d_430.html. [Accessed: Feb. 05, 2014].

[60] Multiphysics Comsol. "Heat Transfer Module User's Guide." *Comsol AB Group*, 2006: pp. 1-268. [Online]. Available: http://www.ewp.rpi.edu/hartford/~collir5/MP/OTHER/Reference/HeatTransferModule UsersGuide.pdf [Accessed: May. 20, 2014].

[61] [Online]. Available: http://www.itis.ethz.ch/itis-for-health/tissue-properties/database/ [Accessed: May. 25, 2014].

[62] [Online]. Available: http://www.engineeringtoolbox.com/specific-heat-capacity-food-d_295.html. [Accessed: Sep. 28, 2014].

[63] S.G. Sumnu, and S. Sahin, *Advances in deep-fat frying of foods*. CRC Press, 2008, p. 120,

[64] [Online]. Available:

http://go.key.net/rs/key/images/Bulk%20Density%20Averages%20100630.pdf.

[Accessed: Sep. 28, 2014].

[65] W.F. Stoecker, *Industrial refrigeration handbook* (Vol. 10). New York: McGraw-Hill, 1998, p. 10.

[66] M. Marcotte, A.R. Taherian, and Y. Karimi, "Thermophysical properties of processed meat and poultry products." *Journal of Food Engineering*, vol. 88, pp. 315–322, 2008.

Papers in preparation

1)   G. CHEN, H. KOKABI, N. BELHADJ-TAHAR, "Microwave hyperthermia of different   biological tissues, comparison between multi-physics simulations and ex-vivo experimental   results"

2)   G. CHEN, H. KOKABI, N. BELHADJ-TAHAR, "Microwave dielectric characterizations of   different biological tissues as a function of temperature"

International conferences

1)   G. CHEN, I. MOUNSI, N. MOGES, N. BELHADJ-TAHAR and H. KOKABI, "Microwave hyperthermia of biological tissues, multi-physics simulations and ex-vivo experimental results", International Symposium on Biomaterials and Smart Systems, Cergy-Pontoise, (**Octobre 2014**).

2)   G. CHEN, J. LO, N. BELHADJ-TAHAR and H. KOKABI, "Microwave Broad Band Measurement of Dielectric Permittivity of biological tissues as a function of temperature", International Symposium on Biomaterials and Smart Systems, Cergy-Pontoise, (**Octobre 2014**).

3)   G. CHEN, H. KOKABI, N. BELHADJ-TAHAR, P. LEPRINCE, "Electromagnetic and Thermal Simulation of Microwave Percutaneous ablation of Human Biological Tissues", Advanced Electromagnetics Symposium (AES), Paris, (**Avril 2012**).

National conferences

1)   G. CHEN, N. BELHADJ-TAHAR, H. KOKABI, " Modélisations multiphysiques d'hyperthermie micro-ondes des tissus biologiques, comparasion avec les résuluats expérimentaux ex-vivo", Journées Nationales Micro-ondes (JNM), Bordeaux, (**Juin 2015**).

2)   G. CHEN, N. BELHADJ-TAHAR, H. KOKABI, "Microwave broad band measurement of dielectric permittivity of biological tissues as a function of temperature", Journée Nationale du Réseau Doctoral en Microélectronique, Lille, (**Mai 2014**).

3)   G. CHEN, H. KOKABI, N. BELHADJ-TAHAR, C. BOUE "Modélisations multiphysiques et expérimentations pour l'hyperthermie micro-ondes des tissus biologiques", Journées Club EEA et GDR SoC-SIP "Electronique et Santé", Limoges (**Nov. 2013**).